Traffic Synchronization with Controlled Time of Arrival for Cost-Efficient Trajectories in High-Density Terminal Airspace

RAÚL SÁEZ GARCÍA
Aeronautical Engineer

Advisor
DR. XAVIER PRATS I MENÉNDEZ

Doctorate program in Aerospace Science and Technology
Department of Physics - Aerospace Engineering Division
Technical University of Catalonia - BarcelonaTech

A dissertation submitted for the degree of
International Doctor of Philosophy
September 2021

Traffic Synchronization with Controlled Time of Arrival for Cost-Efficient Trajectories in High-Density Terminal Airspace

Author
Raúl Sáez García

Advisor
Dr. Xavier Prats i Menéndez

Reviewers
Dr. Eri Itoh
Dr. Michael Schultz

Thesis committee
Dr. Eri Itoh
Dr. Michael Schultz
Dr. Karim Zeghal

Doctorate program in Aerospace Science and Technology
Technical University of Catalonia - BarcelonaTech
September 2021

PhD. Thesis made in:
Department of Physics - Aerospace Engineering Division
Esteve Terradas, 5
08860 Castelldefels (Barcelona), Spain

We keep learning,

Contents

List of Figures

Figures in Appendices

List of Tables

List of Publications

The list of publications resulting from this PhD. work is given in inverse chronological order as follows:

Journal Papers

- SÁEZ, RAÚL & PRATS, XAVIER. 2021. Achieving RTAs outside the Energy-Neutral Time Window of Nominal Aircraft Descents - Fuel Consumption of Powered Descents along Published Routes vs. Neutral CDOs along Pre-Defined Routes. Submitted to *Transportation Research Part C: Emerging Technologies*.

- SÁEZ, RAÚL, POLISHCHUK, TATIANA, SCHMIDT, CHRISTIANE, HARDELL, HENRIK, SMETANOVÁ, LUCIE, POLISHCHUK, VALENTIN & PRATS, XAVIER. 2021. Automated Sequencing and Merging with Dynamic Aircraft Arrival Routes and Speed Management for Continuous Descent Operations. Submitted to *Transportation Research Part C: Emerging Technologies*.

- SÁEZ, RAÚL, PRATS, XAVIER, POLISHCHUK, TATIANA & POLISHCHUK, VALENTIN. 2020. Traffic synchronization in terminal airspace to enable continuous descent operations in trombone sequencing and merging procedures: An implementation study for Frankfurt airport. *Transportation Research Part C: Emerging Technologies*. D.O.I: 10.1016/j.trc.2020.102875. **121**.

- SÁEZ, RAÚL, PRATS, XAVIER, POLISHCHUK, TATIANA, POLISHCHUK, VALENTIN & SCHMIDT, CHRISTIANE. 2020. Automation for separation with continuous descent operations: dynamic aircraft arrival routes. *Journal of Air Transportation*. D.O.I: 10.2514/1.D0176. **28(4)**, 144–154.

Conference Proceedings

- POLISHCHUK, TATIANA, POLISHCHUK, VALENTIN, SCHMIDT, CHRISTIANE, SÁEZ, RAÚL, PRATS, XAVIER, HARDELL, HENRIK & SMETANOVÁ, LUCIE. 2020 (Dec.). How to achieve CDOs for all aircraft: automated separation in TMAs - enabling flexible entry times and accounting for wake turbulence categories. *In: 10th SESAR Innovation Days (SIDS)*. Virtual event: SESAR JU.

- SÁEZ, RAÚL & PRATS, XAVIER. 2020 (Jun.). Comparison of Fuel Consumption of Continuous Descent Operations with Required Times of Arrival: Path Stretching vs. Powered Descents. *In: 9th International Conference on Research in Air Transportation (ICRAT)*. Virtual Event: EUROCONTROL/FAA.

- LEMETTI, ANASTASIA, POLISHCHUK, TATIANA, POLISHCHUK, VALENTIN, SÁEZ, RAÚL & PRATS, XAVIER. 2020 (Jun.). Identification of significant impact factors on Arrival Flight Efficiency within TMA. *In: 9th International Conference on Research in Air Transportation (ICRAT)*. Virtual Event: EUROCONTROL/FAA.

- LEMETTI, ANASTASIA, POLISHCHUK, TATIANA & SÁEZ, RAÚL. 2019 (Nov.). Evaluation of flight efficiency for Stockholm Arlanda Airport using OpenSky Network data. *In: 7th OpenSky Workshop*. Zurich, Switzerland: EasyChair.

- LEMETTI, ANASTASIA, POLISHCHUK, TATIANA, SÁEZ, RAÚL & PRATS, XAVIER. 2019 (Oct.). Analysis of weather impact on flight efficiency for Stockholm Arlanda Airport arrivals. *In: 6th ENRI International Workshop on ATM/CNS (EIWAC)*. Tokyo, Japan: ENRI.

- SÁEZ, RAÚL, PRATS, XAVIER, POLISHCHUK, TATIANA, POLISHCHUK, VALENTIN & SCHMIDT, CHRISTIANE. 2019 (Jun). Automation for separation with continuous descent operations: dynamic aircraft arrival routes. *In: 13th USA/Europe Air Traffic Management Research & Development Seminar*. Vienna, Austria: FAA/EUROCONTROL. **Best paper in track award.**

- SÁEZ, RAÚL, DALMAU, RAMON & PRATS, XAVIER. 2018 (Sept.). Optimal assignment of 4D close-loop instructions to enable CDOs in dense TMAs. *In: IEEE/AIAA 37th Digital Avionics Systems Conference (DASC)*. London, UK: IEEE.

Book Chapters

- LEMETTI, ANASTASIA, POLISHCHUK, TATIANA, SÁEZ, RAÚL & PRATS, XAVIER. 2021 (Feb.). Analysis of weather impact on flight efficiency for Stockholm Arlanda Airport arrivals. *Lecture Notes in Electrical Engineering (LNEE) - Air Traffic Management and Systems IV: Selected Papers of the 6th ENRI International Workshop on ATM/CNS*. Springer. ISBN: 1876-1100.

Acknowledgements

Siempre he pensado que la palabra “gracias” ha perdido todo el significado en la mayoría de las lenguas que se hablan actualmente. Se ha vuelto meramente una palabra vacía que se usa rutinariamente sin pensar realmente lo que significa en realidad. Y es por eso que yo no la suelo usar muy a menudo. Sin embargo, durante estos 4 años de doctorado sí que han habido personas a las que tengo que dar las “gracias” con todo su significado, ya que de una manera u otra han ayudado a que pueda acabar esta tesis satisfactoriamente.

Els meus primers i possiblement els més importants agraïments són pel Dr. Xavier Prats. Gràcies Xevi per la confiança, l’entusiasme i les teves idees. Tot i tenir mil coses entre mans sempre has trobat temps durant aquests 4 anys per guiar-me de manera impecable durant el doctorat. Mereixes jubilar-te als 40!

I would like to thank as well the guys from Linköping University in Norrköping, Sweden, where I lived for 4 months. Thank you Tatiana and Valentin for your kindness, and of course for helping me out with new ideas for my PhD. I hope we will carry on working together in the future! Thanks also to Christiane, Leonid, Anastasia, Henrik and Lucie. I believe we have succeeded in writing very nice papers together over these years, and I hope we can meet soon in some conference!

I would also like to thank Dr. Eri Itoh from The University of Tokyo and Priv.-Doz. Dr.-Ing. habil. Michael Shcultz from Dresden University of Technology (TU Dresden) for agreeing to review this PhD dissertation and being members of the committee. I really appreciate your time and commitment, which resulted in valuable comments to improve the quality of the final document. I must also acknowledge Dr. Karim Zeghal, from the European Organisation For The Safety Of Air Navigation (Eurocontrol), for agreeing to be part of the committee and for reviewing some chapters of the thesis.

Òbviament, no m’oblido dels companys de la universitat. Gràcies al Ramon Dalmau per la seva ajuda en els primers mesos de doctorat, ets un crack! Gràcies també al Marc Melgosa, que ha estat present des que vaig arribar, sempre disposat a ajudar. A veure si podem repetir una conferència com la de San Diego ben aviat! També al Yan i al Leo, que tot i que ja estaven acabant els seus doctorats quan vaig arribar, vam compartir molt bons moments. I would also like to thank Homeyra, my officemate and guardian of the castle during COVID times! And of course Jovana, for being always very positive and being always there to give me a hand. I no m’oblido de les noves incorporacions a l’equip, que han fet la vida a la uni molt més interessant aquests últims

mesos: Júlia, Martí, Antoni, David i Jordi.

Per últim, agraïr a la meva família i amics... o potser no... en veritat, puc pensar en moltes més coses que van abans del doctorat que agraïr-los a ells, no creieu? Però clar, els agraïments sempre solen acabar així. Suposo que el més adient seria dir simplement "gràcies per ser-hi".

Castelldefels, September 2021
Raúl Sáez García

Abstract

The growth in air traffic has led to a continuously growing environmental sensitivity in aviation, encouraging the research into methods for achieving a greener air transportation. In this context, continuous descent operations (CDOs) allow aircraft to follow an optimum flight path that delivers major environmental and economic benefits, giving as a result engine-idle descents from the cruise altitude to right before landing that reduce fuel consumption, pollutant emissions and noise nuisance. However, this type of operations suffers from a well-known drawback: the loss of predictability from the air traffic control (ATC) point of view in terms of overfly times at the different waypoints of the route. In consequence, ATC requires large separation buffers, thus reducing the capacity of the airport.

Previous works investigating this issue showed that the ability to meet a controlled time of arrival (CTA) at a metering fix could enable CDOs while simultaneously maintaining airport throughput. In this context, more research is needed focusing on how modern arrival managers (AMANs)—and extended arrival managers (E-AMANs)—could provide support to select the appropriate CTA. ATC would be in charge to provide the CTA to the pilot, who would then use four-dimensional (4D) flight management system (FMS) trajectory management capabilities to satisfy it. A key transformation to achieve a more efficient aircraft scheduling is the use of new air traffic management (ATM) paradigms, such as the trajectory based operations (TBO) concept. This concept aims at completely removing open-loop vectoring and strategic constraints on the trajectories by efficiently implementing a 4D trajectory negotiation process to synchronize airborne and ground equipment with the aim of maximizing both flight efficiency and throughput.

The main objective of this PhD thesis is to develop methods to efficiently schedule arrival aircraft in terminal airspace, together with concepts of operations compliant with the TBO concept. The simulated arrival trajectories generated for all the experiments conducted in this PhD thesis, to the maximum possible extent, are considered to be energy-neutral CDOs, seeking to reduce the overall environmental impact of aircraft operations in the ATM system. Ultimately, the objective of this PhD is to achieve a more efficient arrival management of traffic, in which higher levels of predictability and similar levels of capacity are achieved, while the safety of the operations is kept. The designed experiments consider a TBO environment, involving a high synchronization between all the involved actors of the ATM system. Higher levels of automation and information sharing are expected, together with a modernization of both current ATC ground-support tools and aircraft FMSs to comply with the new TBO paradigm.

First, a trajectory optimization framework is defined in order to generate the simulated trajectories for the experiments conducted in this PhD thesis. Then, the benefits of flying energy-neutral CDOs are assessed by comparing them with real trajectories, which are obtained from historical flight data. Two sources of data are compared, concluding which is more suitable for efficiency assessments in terminal airspace. Energy-neutral CDOs are the preferred type of trajectories from an environmental point of view but, depending on the amount of traffic, it might be impossible for the ATC to assign a CTA achievable by the arriving aircraft when flying this kind of descents along the published route. In this PhD thesis, two strategies are compared in order to achieve the assigned CTA: flying energy-neutral CDOs along longer/shorter routes vs. flying powered descents along the published route. The sensitivity of the fuel consumption of both strategies to several parameters, such as the initial cruise altitude or wind speed, is analyzed. Finally, two strategies are analyzed in this PhD in order to efficiently schedule arriving aircraft in terminal airspace. First, an interim strategy between full 4D negotiated trajectories and open-loop vectoring is used: a methodology is proposed to effectively schedule arrival traffic flying energy-neutral CDOs along a trombone area navigation (RNAV) procedure. Then, a novel methodology is proposed to generate dynamic arrival routes that automatically adapt to the current air traffic demand. Once again, energy-neutral CDOs are enforced for all arrival traffic.

There are several factors to be considered that may limit the benefits of the proposed solutions. The arrival traffic amount and distribution greatly affect the results obtained, limiting in some cases the successful scheduling of all the arrival aircraft. Furthermore, some of the solutions proposed involve high computational loads that may limit their applicability in operational practice, encouraging future research in order to optimize the models and methodologies involved. Finally, allowing some aircraft to fly powered descents might ease the scheduling of the arrival aircraft in the experiments focusing on the trombone procedure and on the dynamic generation of arrival routes.

Resumen

El incremento de tráfico aéreo ha llevado a una mayor sensibilidad medioambiental en la aviación, motivando la investigación de métodos para conseguir un transporte aéreo más ecológico. En este contexto, las operaciones de descenso continuo (CDOs) permiten a las aeronaves seguir una trayectoria que aporta grandes beneficios económicos y ambientales, dando como resultado descensos con los motores al ralentí desde la altitud de crucero hasta justo antes de aterrizar. Estas trayectorias reducen el consumo de combustible, las emisiones contaminantes y el ruido generado por las aeronaves. No obstante, este tipo de operaciones tiene una gran desventaja: la pérdida de predictibilidad desde el punto de vista del controlador aéreo (ATC) en términos de tiempos de paso en los diferentes puntos de la ruta. Como consecuencia, el ATC necesita asignar una mayor separación entre las aeronaves, lo cual comporta una reducción en la capacidad del aeropuerto.

Estudios previos investigando este problema han demostrado que la capacidad de cumplir con un tiempo controlado de llegada (CTA) en un punto de la ruta (utilizado para secuenciar las aeronaves) podría habilitar las CDOs manteniendo al mismo tiempo la capacidad del aeropuerto. En este contexto, es necesario investigar más en cómo los gestores de llegadas (AMANs)—y los gestores de llegadas extendidos (E-AMANs)—podrían dar soporte en la selección de la CTA más adecuada. El ATC sería el encargado de enviar la CTA al piloto, el cual, para cumplir con la CTA, usaría la capacidad de gestión de trayectorias de un sistema de gestión de vuelo (FMS) de cuatro dimensiones (4D). Una transformación clave para conseguir una gestión más eficiente del tráfico de llegada es el uso de nuevos paradigmas de gestión del tráfico aéreo (ATM), como por ejemplo el concepto de operaciones basadas en trayectorias (TBO). Este concepto tiene como objetivo eliminar completamente de las trayectorias la vectorización en "bucle abierto" y las restricciones estratégicas. Para conseguirlo, se propone implementar de manera eficiente una negociación de la trayectoria 4D, con el objetivo de sincronizar el equipamiento de tierra con el de la aeronave, maximizando de esta manera la eficiencia de los vuelos y la capacidad del sistema.

El principal objetivo de este doctorado es desarrollar métodos para gestionar aeronaves de manera eficiente en espacio aéreo terminal, junto con conceptos de operaciones que cumplan con el concepto de TBO. Las trayectorias de llegada simuladas para todos los experimentos definidos en esta tesis doctoral, en la medida de lo posible, son CDOs de energía neutra. De esta manera, la idea es reducir lo máximo posible el impacto medioambiental de las operaciones aéreas en el sistema ATM. En definitiva, el objetivo de este doctorado es conseguir una gestión del tráfico de llegada más eficiente, obteniendo una mayor predictibilidad y capacidad, y asegurando que la seguridad de las operaciones se mantiene. Los experimentos diseñados consideran una situación

donde el concepto de TBO está presente, lo que comporta una sincronización elevada entre todos los actores implicados en el sistema ATM. Asimismo, se esperan mayores niveles de automatización y de compartición de información, junto con una modernización de las herramientas de soporte en tierra al ATC y de los FMSs de las aeronaves, todo con el objetivo de cumplir con el nuevo paradigma de TBO.

Primero de todo, se define un marco para la optimización de trayectorias utilizado para generar las trayectorias simuladas para los experimentos definidos en esta tesis doctoral. A continuación, se evalúan los beneficios de volar CDOs de energía neutra comparándolas con trayectorias reales obtenidas de datos de vuelo históricos. Se comparan dos fuentes de datos, concluyendo cuál es la más adecuada para estudios de eficiencia en espacio aéreo terminal. Las CDOs de energía neutra son el tipo preferido de trayectorias desde un punto de vista medioambiental pero, dependiendo de la cantidad de tráfico, podría ser imposible para el ATC asignar una CTA que pueda ser cumplida por las aeronaves mientras vuelan la ruta de llegada publicada. En esta tesis doctoral, se comparan dos estrategias con el objetivo de cumplir con la CTA asignada: volar CDOs de energía neutra por rutas más largas/cortas o volar descensos con el motor accionado por la ruta publicada. Para ambas estrategias, se analiza la sensibilidad del consumo de combustible a diferentes parámetros, como la altitud inicial de crucero o la velocidad del viento. Finalmente, en esta tesis doctoral se analizan dos estrategias para gestionar de manera eficiente el tráfico de llegada en espacio aéreo terminal. Primero, se utiliza una estrategia provisional a medio camino entre la negociación completa de trayectorias 4D y la vectorización en "bucle abierto": se propone una metodología para gestionar de manera eficaz tráfico de llegada donde las aeronaves vuelan CDOs de energía neutra en un procedimiento de navegación de área (RNAV) conocido como trombón. A continuación, se propone una nueva metodología para generar rutas de llegada dinámicas que se adaptan automáticamente a la demanda actual de tráfico. De igual manera, se aplican CDOs de energía neutra a todo el tráfico de llegada.

Hay diferentes factores a considerar que podrían limitar los beneficios de las soluciones propuestas. La cantidad y distribución del tráfico de llegada tiene un gran efecto sobre los resultados obtenidos, limitando en algunos casos una gestión eficiente de las aeronaves de llegada. Además, algunas de las soluciones propuestas comportan elevadas cargas computacionales que podrían limitar su aplicación operacional, motivando mayor investigación en el futuro con el fin de optimizar los modelos y metodologías utilizados. Finalmente, permitir a algunos aviones volar descensos con el motor accionado podría facilitar la gestión de las aeronaves de llegada en los experimentos que se centran en el procedimiento de trombón y en la generación de rutas de llegada dinámicas.

Resum

L'increment de trànsit aeri ha portat a una major sensibilitat mediambiental en l'aviació, motivant la recerca en mètodes per aconseguir un transport aeri més ecològic. En aquest context, les operacions de descens continu (CDOs) permeten a les aeronaus seguir una trajectòria que aporta grans beneficis econòmics i ambientals, donant com a resultat descensos amb els motors al ralentí des de l'altitud de creuer fins just abans d'aterrar. Aquestes trajectòries redueixen el consum de combustible, les emissions contaminants i el soroll generat per les aeronaus. No obstant això, aquest tipus d'operacions té un gran desavantatge: la pèrdua de predictibilitat des del punt de vista del controlador aeri (ATC) en termes de temps de pas als diferents punts de la ruta. Com a conseqüència, l'ATC necessita assignar una major separació entre les aeronaus, la qual cosa comporta una reducció en la capacitat de l'aeroport.

Estudis previs investigant aquest problema han demostrat que la capacitat de complir amb un temps controlat d'arribada (CTA) a un punt de la ruta (utilitzat per seqüenciar les aeronaus) podria habilitar les CDOs tot mantenint la capacitat de l'aeroport. En aquest context, es necessita investigar més en com els gestors d'arribades (AMANs)—i els gestors d'arribades extesos (E-AMANs)—podrien donar suport en la selecció de la CTA més adequada. L'ATC seria l'encarregat d'enviar la CTA al pilot, el qual, per tal de complir amb la CTA, faria servir la capacitat de gestió de trajectòries d'un sistema de gestió de vol (FMS) de quatre dimensions (4D). Una transformació clau per aconseguir una gestió més eficient del trànsit d'arribada és l'ús de nous paradigmes de gestió del trànsit aeri (ATM), com per exemple el concepte d'operacions basades en trajectòries (TBO). Aquest concepte té com a objectiu eliminar completament de les trajectòries la vectorització en "bucle obert" i les restriccions estratègiques. Per aconseguir-ho, es proposa implementar de manera eficient una negociació de la trajectòria 4D, amb l'objectiu de sincronitzar l'equipament de terra amb el de l'aeronau, maximitzant d'aquesta manera l'eficiència dels vols i la capacitat del sistema.

El principal objectiu d'aquest doctorat és desenvolupar mètodes per gestionar aeronaus de manera eficient en espai aeri terminal, juntament amb conceptes d'operacions que compleixin amb el concepte de TBO. Les trajectòries d'arribada simulades per tots els experiments definits en aquesta tesi doctoral, en la mesura que s'ha pogut, són CDOs d'energia neutra. D'aquesta manera, la idea és reduir el màxim possible l'impacte mediambiental de les operacions aèries al sistema ATM. En definitiva, l'objectiu d'aquest doctorat és aconseguir una gestió del trànsit d'arribada més eficient, obtenint una major predictibilitat i capacitat, i assegurant que la seguretat de les operacions es manté. Els experiments dissenyats consideren una situació on el concepte de TBO és

present, el que comporta una sincronització elevada entre tots els actors implicats en el sistema ATM. Així mateix, s'esperen nivells majors d'automatització i de compartició d'informació, juntament amb una modernització de les eines de suport en terra a l'ATC i dels FMSs de les aeronaus, tot amb l'objectiu de complir amb el nou paradigma de TBO.

Primer de tot, es defineix un marc per l'optimització de trajectòries utilitzat per generar les trajectòries simulades pels experiments definits en aquesta tesi doctoral. A continuació, s'avaluen els beneficis de volar CDOs d'energia neutra comparant-les amb trajectòries reals obtingudes de dades de vol històriques. Es comparen dues fonts de dades, concloent quina és la més adequada per estudis d'eficiència en espai aeri terminal. Les CDOs d'energia neutra són el tipus preferit de trajectòries des d'un punt de vista mediambiental però, depenent de la quantitat de trànsit, podria ser impossible per l'ATC assignar una CTA que pugui ser complida per les aeronaus mentre volen la ruta d'arribada publicada. En aquesta tesi doctoral, es comparen dues estratègies amb l'objectiu de complir amb la CTA assignada: volar CDOs d'energia neutra per rutes més llargues/curtes o volar descensos amb el motor accionat per la ruta publicada. Per les dues estratègies, s'analitza la sensibilitat del consum de combustible a diferents paràmetres, com l'altitud inicial de creuer o la velocitat del vent. Finalment, en aquest doctorat s'analitzen dues estratègies per gestionar de manera eficient trànsit d'arribada en espai aeri terminal. Primer, s'utilitza una estratègia provisional a mig camí entre la negociació completa de trajectòries 4D i la vectorització en "bucle obert": es proposa una metodologia per gestionar de manera eficaç trànsit d'arribada on les aeronaus volen CDOs d'energia neutra en un procediment de navegació d'àrea (RNAV) conegut com a trombó. A continuació, es proposa una nova metodologia per generar rutes d'arribada dinàmiques que s'adapten automàticament a la demanda actual de trànsit. D'igual manera, s'apliquen CDOs d'energia neutra per tot el trànsit d'arribada.

Hi ha diversos factors a considerar que podrien limitar els beneficis de les solucions proposades. La quantitat i distribució del trànsit d'arribada afecta en gran mesura els resultats obtinguts, limitant en alguns casos una gestió eficient de les aeronaus d'arribada. A més, algunes de les solucions proposades comporten elevades càrregues computacionals que podrien limitar la seva aplicació operacional, motivant una major recerca en el futur per tal d'optimitzar els models i metodologies emprats. Finalment, permetre a alguns avions volar descensos amb el motor accionat podria facilitar la gestió de les aeronaus d'arribada en els experiments que es centren en el procediment de trombó i en la generació de rutes d'arribada dinàmiques.

Notation

Throughout this PhD thesis and as a general rule, scalars and vectors are denoted either with lower or upper case letters. Vectors are noted with the conventional overhead arrow, like for example $\vec{a}$ or $\vec{\psi}$. Sets are denoted using calligraphic fonts, like for example $\mathcal{A}$, $\mathcal{B}$ or $\mathcal{X}$, while matrices use the same font but in bold series, like $\boldsymbol{\mathcal{R}}$. The time derivative of magnitude $a(t)$ with respect to t is expressed by $\frac{\mathrm{d}a(t)}{\mathrm{d}t} = \dot{a}$. Furthermore, if not otherwise noted, all vectors are column vectors and a transposed vector is denoted by $[\cdot]^T$. In the notation , $(\cdot)^*$ indicates *optimal*. Next, the principal symbols that are used throughout this dissertation are shown along with their meaning. The reader should note that this list is not exhaustive.

B B-Spline basis function

C_D drag coefficient

C_L lift coefficient

C_{D0} parasite drag coefficient

C_{D2} induced drag coefficient

D aerodynamic drag

E_k kinetic energy of the aircraft

E_p potential energy of the aircraft

E_s specific energy of the aircraft

E_t total energy of the aircraft

J cost function of the optimal control problem

L aerodynamic lift force

M Mach number

N number of discretisation intervals in the whole time horizon

N_j number of discretisation intervals in the j^{th} phase

P number of phases of the optimal control problem

R perfect gas constant

S wing surface area

T engine thrust

T_{idle} idle thrust

T_{max} maximum thrust

$\Delta\tau$ discretisation step

$\Delta\tau_j$ discretisation step in the j^{th} phase

Π quadrature function of the running cost

Ξ penalty cost function

α Hellman exponent

β speed brakes deflection

χ_a aerodynamic heading angle

χ_g ground track angle

δ normalised pressure of the air

δ_{11} normalised pressure of the air at the tropopause

η landing gear status

γ aerodynamic flight path angle

γ_g ground flight path angle

γ_{min} minimum aerodynamic flight path angle

λ_h standard temperature lapse rate

$\mathbb{R}$ set of real numbers

$\mathcal{E}$ set associating the index of the last time sample to its corresponding phase

$\mathcal{I}$ set associating the index of each time sample to its corresponding phase, excluding the last time sample of each phase

$\mathcal{L}$ lagrangian of the nonlinear programming optimisation problem

$\mathcal{P}$ algorithm that solves the nonlinear programming optimisation problem

$\mathcal{Q}$ algorithm that solves the quadratic programming optimisation problem

$\mathcal{T}$ set associating the index of each time sample to its corresponding phase

ϕ end cost or Mayer term

π running cost or Lagrange term

ρ density of the air

σ normalised density of the air

τ_{SSL} temperature of the air at standard sea level

θ normalised temperature of the air

θ_{11} normalised temperature of the air at the tropopause

$\vec{F}$ evolution function of the state vector

$\vec{\chi}$ current states vector

$\vec{\lambda}$ dual variables associated with inequality constraints

$\vec{\mu}$ dual variables associated with equality constraints

$\vec{\psi}$ terminal constraints

$\vec{\varphi}$ equality algebraic path constraints

$\vec{\vartheta}^{eq}$ equality interior-point constraints

$\vec{\vartheta}^{in}$ inequality interior-point constraints

$\vec{b}$ path constraints

$\vec{d}$ fixed parameters of the model

$\vec{e}$ vector of slack variables

$\vec{f}$ dynamics of the state vector

$\vec{g}$ inequality constraints of the nonlinear programming problem

$\vec{h}$ equality constraints of the nonlinear programming problem

$\vec{p}$ vector of parameters of the nonlinear programming problem

$\vec{u}$ controls vector

$\vec{w}$ wind vector

$\vec{x}$ states vector

ζ aerodynamic configuration of the aircraft

f cost function of the nonlinear programming optimisation problem

g gravity acceleration

h geometric altitude

h_r reference altitude of the Hellman model

h_{11} standard altitude of the tropopause

k_j k^{th} discretisation time sample

m mass of the aircraft

n_z load factor

p_{SSL} pressure of the air at standard sea level

q nominal fuel flow

q_{idle} idle fuel flow

s distance to go

t time

t_F final time of the time horizon

t_I initial time of the time horizon

t_j initial time of the j^{th} phase

v true airspeed

v_{CAS} calibrated airspeed

w_e east wind component

w_h vertical wind component

w_n north wind component

w_r reference speed of the Hellman model

w_s longitudinal wind component

w_x cross wind component

List of Acronyms

2D	two-dimensional
3D	three-dimensional
3D-PAM	3D-path arrival management
4D	four-dimensional
AAL	above aerodrome level
ADS-B	automatic dependent surveillance-broadcast
ADS-C	automatic dependent surveillance-contract
AGL	above ground level
AIP	aeronautical information publication
AMAN	arrival manager
ANSP	air navigation service provider
APM	aircraft performance model
ATC	air traffic control
ATCO	air traffic control officer
ATFM	air traffic flow management
ATM	air traffic management
ATS	air traffic services
BADA	base of aircraft data
CARATS	collaborative actions for renovation of air traffic systems
CAS	callibrated airspeed
CDO	continuous descent operation
CI	cost index
CONOP	concept of operation
CPR	correlated position report
CTA	controlled time of arrival
DAE	differential algebraic equation
DCB	demand and capacity balance
DDR	demand data repository
E-AMAN	extended arrival manager
E-TMA	extended terminal maneuvering area
ECAC	european civil aviation conference
ECMWF	european centre for medium-range weather forecasts
EDA	efficient descent advisor
EPP	extended projected profile
ETA	estimated time of arrival

FAA	federal aviation administration
FAB	functional airspace block
FAP	final approach point
FAS	final approach speed
FCOM	flight crew operating manual
FIM	flight-deck interval management
FL	flight level
FMS	flight management system
GAMS	general algebraic modelling system
GD	green dot speed
GFS	global forecast system
GRIB	gridded binary
GS	glide slope
i4D	initial four-dimensional
IAF	initial approach fix
ICAO	international civil aviation organization
IF	intermediate fix
ILS	instrumental landing system
IM	interval management
INAP	integrated network ATC planning
ISA	international standard atmosphere
KKT	Karush-Kuhn-Tucker conditions
KPI	key performance indicator
MILP	mixed integer linear programming
MIP	mixed integer programming
MLW	maximum landing weight
MMO	maximum operative Mach
NASA	national aeronautics and space administration
NextGen	next generation air transportation system
NLP	non-linear programming
NMOC	network manager operations centre
NOAA	national oceanic and atmospheric administration
NWP	numerical weather prediction
ODE	ordinary differential equation
OEM	original equipment manufacturer
OPTIMAL	optimised procedures and techniques for improvement of approach and landing
PARTNER	partnership for air transportation noise and emission reduction
PI	performance indicator
PRU	performance review unit
RAP	rapid refresh
RBT	reference business trajectory
RMSE	root-mean-square error
RNAV	area navigation
RNP	required navigation performance
RTA	required time of arrival
SESAR	single european sky ATM research
SLQP	sequential linear-quadratic programming
SNOPT	sparse nonlinear optimiser
SQP	sequential quadratic programming
SSL	standard sea level
STAM	short-term air traffic flow capacity measure
STAR	standard terminal arrival route
STATFOR	statistics and forecast service
SWIM	system-wide information management
TA	tailored arrival

TAAM	total airport and airspace model
TAS	true airspeed
TBO	trajectory based operations
TDDA	three-degrees deceleration approach
TMA	terminal maneuvering area
TOD	top of descent
TRL	technology readiness level
UPC	technical university of Catalonia
UPS	united parcel service
VFE	vertical flight efficiency
VLS	lowest selectable speed
VMO	maximum operative CAS

現実を見る角度、置き換える場所。これらが少し違うだけで、心の中は大きく変わるわ。
[Any new position from which you view your reality will change your perception of its nature. It's all literally a matter of perspective.]

— 伊吹マヤ (新世紀エヴァンゲリオン) [Maya Ibuki (*Neon Genesis Evangelion*)]

I

Introduction

Air transportation has been experiencing a continuous growth over the last decades and, although the 2020 setback might slow down this upward trend, high levels of air traffic are still projected for the future (Iacus *et al.*, 2020). Despite the desirable growth of the global economy, the higher volume of traffic has also increased the environmental impact of aviation and the workload faced by air traffic control officers (ATCOs). This is especially evident in terminal maneuvering areas (TMAs), which are areas of controlled traffic surrounding one or more aerodromes. Specifically in large airports, TMAs are very congested and experience large levels of noise and emissions produced by aircraft. This leads to the need for research into methods for achieving a greener air transportation and for lessening the ATCO workload, which would allow for an increase in capacity.

Numerous ongoing air traffic management (ATM) improvement programs are being undertaken by a number of international civil aviation organization (ICAO) member states, like the single european sky ATM research (SESAR) in Europe, the next generation air transportation system (NextGen) in the United States, the collaborative actions for renovation of air traffic systems (CARATS) in Japan or SIRIUS in Brazil, among others. Through these programs, organizations like the SESAR Joint Undertaking and the federal aviation administration (FAA)—in charge of SESAR and NextGen programs, respectively—are addressing the impact of air traffic growth by developing new or improved procedures and technologies that aim to increase the capacity and efficiency of the ATM system, while simultaneously improving safety and reducing the environmental impact.

In Europe, SESAR aims at increasing the capacity of the whole ATM system by 80-100% (SESAR JU, 2020) by 2035. Enhancements to conflict and separation management processes and increased automation for both on-board and ground systems will help to safely handle the

increasing traffic demand in the TMA and en-route environments. At airspace and air traffic flow management (ATFM) level, more dynamic optimization and allocation of airspace (see for instance Sergeeva *et al.* (2017)) is foreseen to enable airspace users to access required airspace with minimum constraints. Finally, airport throughput is expected to increase by improving the traffic sequencing and merging techniques and by reducing separation requirements for both arrivals and departures, which would lead to a 5-10% capacity improvement in highly congested airports (SESAR JU, 2020).

Another SESAR ambition is to achieve a total reduction of between 4% and 10% in fuel burn per flight (SESAR JU, 2020). In this context, improvements to the design of engines over the past years have greatly reduced fuel consumption and gaseous emissions. Promising procedural solutions, which have the advantage to provide fuel benefits without modifying aircraft engines or airframe, have been also proposed. For instance, in the en-route environment, a fuel reduction of around 2.5% is expected due to more direct routes and more efficient vertical profiles (altitude and speed). Optimal vertical profiles for en-route operations were investigated, for instance, by Betts & Cramer (1995) and Soler *et al.* (2012), and the actual quantitative benefits in terms of fuel and time savings with respect to current profiles were assessed by Dalmau & Prats (2015) and Dalmau & Prats (2017a). In the TMA environment, the SESAR target is to enable an average reduction of around 10% in fuel burn by enabling continuous climb and descent profiles with fewer tactical interventions from air traffic control (ATC). The introduction of more fuel-efficient profiles, however, could be achieved at the cost of a reduction of capacity, provided new concepts of operation are not implemented. Major challenges involved with the implementation of new concepts of operation include the upgrade of current flight management systems (FMSs) planning and guidance capabilities; changes in airspace and procedure design; and modernization of current ATC separation, sequencing and merging techniques and their ground decision support tools.

I.1 Environmental Impact of Descents

One of the strategies to achieve a greener air transportation system is the use of continuous descent operations (CDOs), which allow aircraft to follow an optimum flight path that delivers major environmental and economic benefits, giving as a result engine-idle continuous descents that reduce fuel consumption, pollutant emissions and noise nuisance (Erkelens, 2000; Warren & Tong, 2002; Clarke *et al.*, 2004). A CDO is understood as a trajectory executed with the engines at idle during the whole descent, no matter how many level-offs are performed. In the case of a level-off at idle thrust, the aircraft will rapidly reduce the kinetic energy without requiring additional drag devices. In addition, a CDO could also be executed with the engines at non-idle, but with no level-offs. In this PhD thesis, the concept of energy-neutral CDO (or simply neutral CDO) is introduced. This concept refers to a descent in which the total energy is not increased by means of thrust higher than idle nor removed by using active drag devices (e.g. speed brakes).

Figure I-1 shows an illustrative comparison between the altitude profile of a conventional descent and that of a CDO for an aircraft planning to land at Barcelona airport (LEBL). A conventional descent leaves the cruise altitude earlier, typically as a result of an ATC clearance. The aircraft descends by performing a series of level-offs caused by tactical ATC instructions (as discussed in Section I.2.1) or constraints defined at the waypoints of the particular procedure being flown. During these segments at constant altitude, additional thrust is typically required to maintain the altitude without decelerating too much.

During a CDO, the aircraft remains at the cruise altitude for a longer distance, thus, consuming a lower quantity of fuel. Then, at the optimal top of descent (TOD), the point at which the aircraft starts the descent, the engines are set to idle and the aircraft starts a continuous descent towards the interception of the instrumental landing system (ILS) glide slope (GS). A short

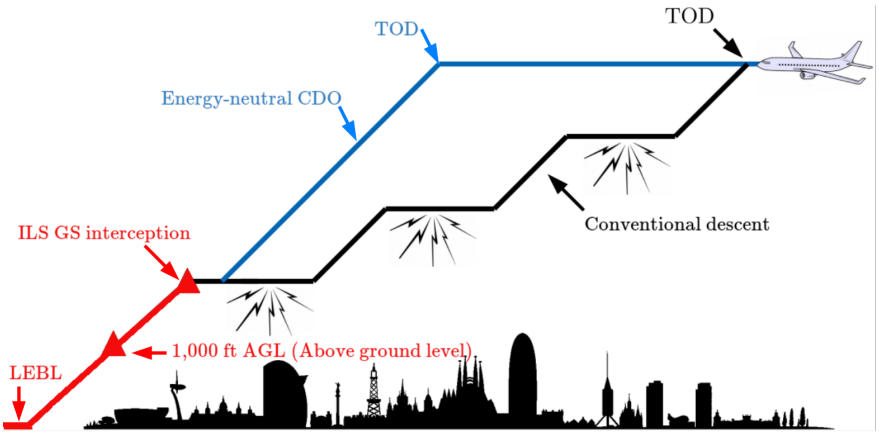

Figure I-1: *Illustrative comparison of a CDO and a conventional descent operation*

level-off is required in order to properly intercept the GS. In general, a CDO is performed (as far as possible) at higher altitudes, lower thrust settings and lower drag configurations all along the descent.

Extensive research has been conducted to assess the environmental benefits of CDOs. For instance, a series of simulations and field tests were performed within the optimised procedures and techniques for improvement of approach and landing (OPTIMAL) program initiated by the European Commission in 2004 (European Comission, 2020) and the partnership for air transportation noise and emission reduction (PARTNER) program established by the FAA in support of the NextGen initiative in 2003 (Massachusetts Institute of Technology, 2020). It is worth mentioning that these programs are only two of the many research activities that have been performed to quantify the benefits and to identify the limitations of CDOs.

In the OPTIMAL program, field tests were performed at two major European airports to assess the trade-off between environmental benefits and operational flexibility of CDOs, including predictability of the descent trajectories, ATC coordination procedures and workload of the flight crew. The results obtained from field tests at London Heathrow airport (LHR) were reported by Reynolds *et al.* (2005), while the main findings obtained at Amsterdam Schiphol airport (AMS) were presented by Wat *et al.* (2006). Similar experiments were performed within the PARTNER project at Louisville international airport (SDF) (Clarke *et al.*, 2004, 2006), Atlanta international airport (ATL) (Clarke *et al.*, 2007) and Los Angeles international airport (LAX) (Clarke *et al.*, 2013).

With no exception, all the aforementioned experiments concluded that CDOs lead to fuel savings, noise nuisance and gaseous emission reduction if compared to conventional descents. For instance, results from united parcel service (UPS) flight tests during night-time operation at SDF reported fuel savings of about 200 kg per flight for B767 models (Clarke *et al.*, 2004, 2006), while results from flight tests at ATL, which considered flights from two airlines, suggested fuel savings of around 460 kg and 600 kg per flight for B757 and B767 models, respectively (Clarke *et al.*, 2007). Finally, an analysis over more than 480,000 flights at 25 airports in the US national airspace system during a four-month period concluded that fuel savings of CDOs were lower than 25 kg for 45% of the flights, and less than 100 kg for 87% of the flights (Robinson & Kamgarpour, 2010).

Based on this diversity of fuel savings figures, it can be concluded that comparison of results across different experiments is difficult due to the substantial differences in assumptions, types of data, models, and methods being used. Nevertheless, Thompson *et al.* (2013) quantified the benefits of CDOs in Paris and New York regions using similar sources of data, analytical methods and models, and concluded that discrepancies in fuel saving figures across different experiments are also caused by the differences in traffic intensity, as well as the distribution of level-off segments in

the conventional descent trajectories due to the dissimilar ATC practices, procedure designs, traffic patterns and meteorological conditions. These results manifest the tangible trade-off between environmental impact and capacity, which will be further discussed in the next section.

Different from previous works, Jin *et al.* (2013) aimed at explaining the fuel savings observed in field tests found in the literature from an analytical point of view. In this work, the relationship between speed, altitude, and fuel consumption during a CDO were analytically derived. Based on their findings, several helpful design guidelines for CDOs were proposed.

I.2 CDO Adherence in the Current Air Transportation System: Efficiency vs. Capacity

This section focuses on the viability of applying CDOs in the current air traffic system. Section I.2.1 presents a discussion regarding the low predictability of CDOs, and how the predicted increase in traffic demand in the future could negatively impact their application in high-traffic-demand scenarios. In order to face these issues, several ATM concepts have been proposed to enable CDOs in busy TMAs, which are detailed in Sections I.2.2 to I.2.7.

I.2.1 Predictability of CDOs

CDOs are optimized to the operating capability of the aircraft, resulting in different optimum trajectories for aircraft with different characteristics. Even more, each aircraft is *unique*, and presents variations in performance data with respect to the same aircraft type when issued from the assembly line. In this context, aircraft performance, as discussed in Airbus (2002), changes with aging, since the aerodynamic and engine characteristics typically deteriorate over time (and with maintenance actions). Furthermore, weather conditions have also an impact on the descent trajectory, since different wind, air temperature and/or pressure conditions will lead to different idle descent trajectories. Consequently, in practical terms, each individual flight performs a different CDO, which leads to a significant decrease of the vertical and temporal predictability of incoming traffic flows, with the resulting increase of ATCO workload. Consequently, ATCOs would increase separation buffers leading to airspace and runway capacity losses that are not desirable in major TMAs, especially during peak hours.

For the reasons stated above, in busy TMAs CDOs hardly take place, except for off-peak hours, when the traffic demand is low (Robinson & Kamgarpour, 2010). Firstly, and at a strategic level, altitude and speed constraints published in standard terminal arrival route (STAR) charts do not take into account the particular operating capability of each aircraft, thus, limiting the possibility of performing optimum descent trajectories. Moreover, in the tactical level, ATCOs use instructions such as altitude assignments, speed adjustments and path stretching (i.e. radar vectoring, also called *open-loop* instructions) so as to maintain safe separation between aircraft and maximize the throughput. These techniques, however, tend to degrade the performance of descent operations, leading to a higher environmental impact. Furthermore, the duration of such open-loop vector instructions is not known by the aircraft crew, nor how the aircraft will re-join its initial route. This is indeed one of the disadvantages of flying CDOs with the current ATC sequencing and merging techniques because, once a CDO is already initiated, it is very hard to react to ATC instructions while maintaining the engines at idle for the remainder of the descent. The main reason is that it is impossible for state-of-the-art FMSs to predict the remaining distance to go and, therefore, to optimize the trajectory to achieve the most environmentally-friendly descent profile. This would be only possible through the use of closed-loop instructions, issued by the ATC before the aircraft arrives at the TOD, as discussed in Section I.2.4.

Figure I-2 depicts a simplified diagram focusing on open-loop and closed-loop instructions: if the ATC assigns the aircraft any of the green routes (R_{CL1} and R_{CL2}) before the aircraft's TOD, the aircraft FMS will receive the remaining distance to go and, thus, will be able to generate the optimal descent trajectory following the assigned route. However, this will not be possible if an open-loop instruction is issued by the ATC. Let us assume the aircraft was assigned the R_{CL1} route. However, at some point in this route, the ATC assigns the aircraft the R_{OL1} route, without any additional information regarding the distance to go. In such a case, the aircraft FMS will not be able to compute an optimal descent unless the ATC communicates to the aircraft which route will be assigned to rejoin the initially planned route (R_{OL2}, R_{OL3} or R_{OL4}).

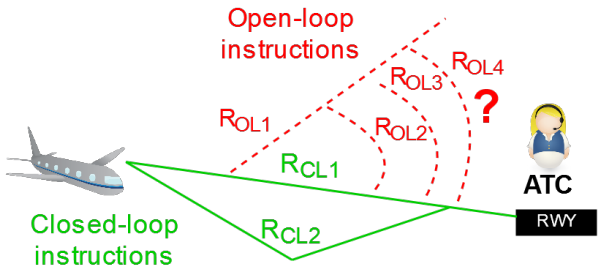

Figure I-2: *Open-loop vs. closed-loop instructions (lateral view)*

As illustrative example, Figure I-3 shows the vectoring instructions used by the ATC of Barcelona-El Prat airport during a typical day of operations. These trajectories were obtained from automatic dependent surveillance-broadcast (ADS-B) data gathered with an antenna installed in technical university of Catalonia (UPC).

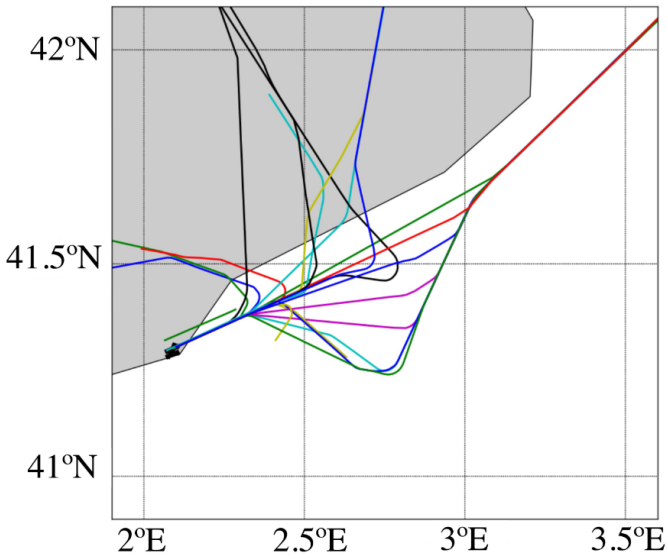

Figure I-3: *Vectoring instructions used by the ATC at Barcelona-El Prat airport during a typical day (Dalmau, 2019)*

The relationship between target spacing, probability of uninterrupted CDO execution, and airport capacity was investigated by Ren & Clarke (2007) by means of Monte-Carlo simulations. The simulations were used to estimate the number of possible CDOs that could be performed without ATC intervention and thereby determine the minimum target spacing at a metering fix, such that there was a high probability of no separation violations thereafter. Later on, the tool was used to determine the target spacing for CDOs at SDF airport. Results showed that CDOs could be efficiently implemented in TMAs under low to moderate traffic conditions (Ren & Clarke, 2008).

Most of the field tests presented in Section I.1 were performed in low-traffic-demand scenarios. Nevertheless, some studies indicated that the fuel savings expected to result from CDOs could be potentially neutralized by the need to provide separation assurance modifying the aircraft speed, altitude and/or by using vector instructions (Cao *et al.*, 2014). The extent of this reduction on the benefits of CDOs would depend on the target spacing, the traffic demand level and the types of ATC instructions used to absorb the delays due to the additional separation buffers.

Since field tests of CDOs in high-traffic scenarios are difficult to conduct, Wilson & Hafner (2005) presented a simulation-based approach to quantify the benefits of CDOs in busy TMAs taking into consideration spacing and sequencing issues. Fast-time simulations at ATL airport were performed with the total airport and airspace model (TAAM) software by removing altitude constraints of the original procedures and allowing aircraft to directly fly from the initial approach fix (IAF) to the base-leg of the landing runway. Promising results showed significant fuel and time savings with minimum increase on ATC workload. Aiming at assessing safety aspects of CDOs, Park *et al.* (2016) proposed a trajectory-based methodology to estimate the encounter rate of CDOs in high-traffic scenarios. The proposed method was validated by comparing it with Monte-Carlo simulation results. Khan *et al.* (2009) also performed fast-time simulations in high-traffic scenarios to compare current ATC procedures with ATC assisted with various systems of ground automation in terms of CDO success rate and throughput at the metering fix.

Statistical analysis from the fast-time experiment performed by Robinson & Kamgarpour (2010) revealed that fuel savings of CDOs are marginal for high-traffic scenarios due to the tactical instructions required to provide separation assurance, which have negative effects on the fuel-efficiency of CDOs. In particular, fuel savings due to CDOs were reduced by 70-85% if compared to the low-traffic scenarios. This work also reported a reduction of 45 kg per CDO due to traffic congestion at ATL airport. A similar experiment at ATL airport reported a sightly different reduction of 23 to 36 kg per CDO (Cao *et al.*, 2014).

In addition to fast-time simulations, human-in-the-loop studies with ATC showed that CDOs would not be feasible at ATL airport during the busiest traffic periods, since too much efficiency would be lost to accommodate the traffic demand (Johnson *et al.*, 2009). In such traffic conditions, few flights would be issued the CDO clearance and even some flights would likely need to be removed from CDO procedures after being cleared in order to manage the demand, which would reduce the benefits associated with CDOs. Nevertheless, results also showed that at least 15% of the total environmental benefit would still be achievable for CDOs that are terminated earlier.

The following sections present several approaches to cope with the low predictability (and subsequent loss of capacity) of CDOs, with the aim of enabling them in high-traffic scenarios.

I.2.2 Fixed Flight-Path Angle Descents

The three-degrees deceleration approach (TDDA) (De Prins *et al.*, 2007; Sopjes *et al.*, 2011; De Leege *et al.*, 2009) is a concept in which the descent is performed all along a 3° path from the TOD to the runway threshold. To perform the spacing task, two controls are given to the pilot: the first one is the thrust cutback altitude, in which the throttle is set to idle and, consequently, the aircraft starts to decelerate; and the second one is the flaps/slats and gear setting, which allows to manage the deceleration after the thrust cutback altitude.

Pradeep & Wei (2017) investigated the variability and operational feasibility aspect of CDOs with fixed flight-path angle descents, and concluded that this kind of flight operation has higher degree of vertical predictability and lesser variability in terms of altitude and speed profiles if compared to the CDOs performed at idle thrust. However, this is achieved at the cost of thrust settings different from idle and with higher drag configurations, which implies more environmental impact.

More recently, Itoh *et al.* (2018a) and Itoh *et al.* (2018b) also studied the operational feasibility of CDOs from the point of view of pilots when flying fixed flight-path angle descents. Results showed that this technique improves the efficiency of the flight and, according to the pilots, operationally stable flights for B777-200 aircraft could be achieved providing the flight path angle is around 2.5 degrees. However, steeper angles led to slow speed reductions not controlled by the thrust and speed brakes as the pilots expected. Finally, the level of pilot workload was acceptable for all the experiments conducted in the simulations.

I.2.3 CDOs in Vertical Corridors

The ICAO has published some CDO guidance material (ICAO, 2010) to support air navigation service providers (ANSPs) to design vertical corridors in which all descent trajectories must be contained, helping to strategically separate them from other procedures in the vicinity. However, as reported by Fricke *et al.* (2015), these criteria have been established without explicitly considering the aircraft type, assuming international standard atmosphere (ISA) conditions and with coarse assumptions regarding the aircraft gross mass and aircraft performance models. This leads, in the majority of cases, to too restrictive corridors that limit the potential CDO adherence in real operations.

I.2.4 3D-Path Arrival Management

In the 3D-path arrival management (3D-PAM) concept (Nagle *et al.*, 2011; Coppenbarger *et al.*, 2010; Scharl *et al.*, 2007), a ground system computes the arrival schedule of flights at a metering fix. Then, for each flight, it strategically assigns the best route to a metering fix in combination of cruise and speed advisories and (eventually) a path adjustment in the form of point-bearing-distance to meet the schedule. These instructions, which are designed to facilitate the delivery by voice using standard phraseology, are cleared prior the TOD and given to the pilot for manual entry into the FMS. This negotiation prior the TOD allows the FMS to know the remaining distance to go, compute the optimal trajectory plan complying with the cleared instructions, and uninterruptedly execute it.

A system for the integration of this concept is the efficient descent advisor (EDA), developed by the national aeronautics and space administration (NASA) (Coppenbarger *et al.*, 2004). Figure I-4 shows a scheme of the 3D-PAM concept.

It should be noted that, even if when implementing 3D-PAM some flights are actually travelling a longer distance due to the point-bearing-distance instruction (see blue segment in Fig. I-4), the descent to the metering fix is typically flown at a lower power setting.

I.2.5 Tailored Arrivals

The EDA tool could be also used to implement the concept of tailored arrivals (TAs) (Coppenbarger *et al.*, 2009; Elmer, 2008), which are a step further of 3D-PAM to enable CDOs. In the TA concept, a customized, dynamic and conflict-free descent trajectory, tailored by ATC through use of a list of fixes with associated speed and altitude constraints, is uplinked via data-link to the FMS before starting the descent, given as a single clearance well prior to TOD. The clearances provide sufficient information for the FMS to compute the trajectory plan from the current aircraft state to the runway threshold. When possible, the clearances should allow to generate a near-idle descent trajectory. It should be noted that even for ATC without data-link support, TAs could be implemented by using a pre-negotiated set of standard terminal arrival routes (STARs) stored in the FMS.

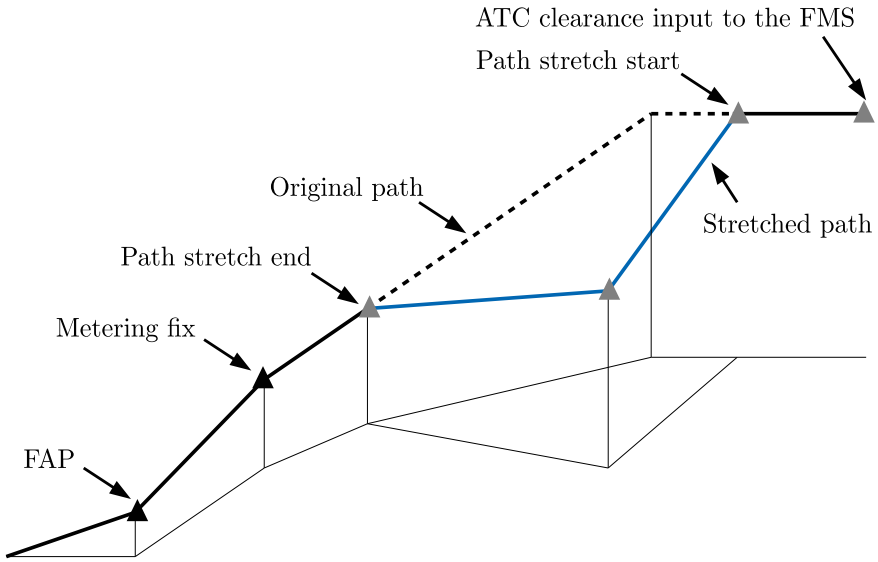

Figure I-4: *Scheme of the 3D-path arrival management concept (Coppenbarger et al., 2010)*

A primary challenge of 3D-PAMs and TAs is the design of the route and constraints that are issued to the FMS, which shall be chosen to allow the FMS to generate a trajectory plan that can be flown at idle thrust, using only elevator control and minimizing the use of speed brakes. Ground systems in charge of computing these constraints, use trajectory predictors configured with simplified models to represent the dynamics and performance of the aircraft. However, these models will rarely reproduce the behavior of all aircraft types without errors. Any discrepancy between the models used by the on-board and ground-based trajectory predictors might result in clearances selected by the 3D-PAM or TA ground-automation system that, even if supporting an idle descent according to the ground trajectory predictor, might require the use of additional thrust and/or speed brakes according to the more accurate FMS trajectory planner.

I.2.6 CDOs with Controlled Times of Arrival and Fixed Routes

Another promising concept to enable CDOs in busy TMAs consists of enforcing controlled times of arrival (CTAs) at one or several metering fixes while keeping the aircraft on a lateral route cleared before the TOD (Muynch *et al.*, 2012). Note that this route could be either a published STAR or a sequence of waypoints uplinked to the FMS by the ground system prior the descent. With this type of flight operations, ATC would assign (using data-link, for instance) at least one CTA to each aircraft, ideally before they reach their TOD, to sequence and merge arrival traffic at a metering fix. Figure I-5 presents a simplified diagram with aircraft A, B and C, for each of which the ATC assigns a series of CTAs at different waypoints along their respective fixed routes.

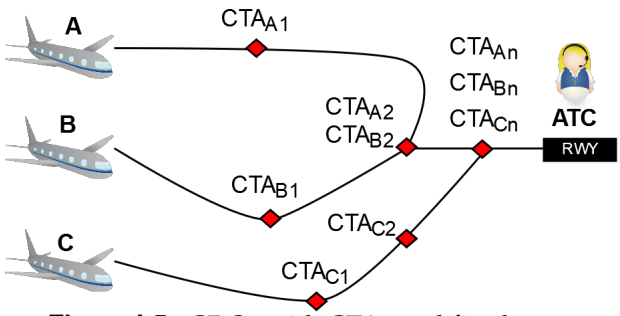

Figure I-5: *CDOs with CTAs and fixed routes*

A negotiation process of CTAs via data-link between ATC and FMS provided with four-dimensional (4D) capabilities was proposed by Uebbing-Rumke & Temme (2011) and Oberheid *et al.* (2008). The negotiation process includes the on-board computation (i.e., using accurate models bundled into the FMS) of the earliest and latest achievable CTAs at the metering fix (in other words, the feasible CTA window) for the known lateral route that is to be flown, and the subsequent down-link of this information to the ground automation system. Based on the feasible CTA window and the surrounding traffic, the ground system replies with the CTA. The received CTA would be entered as a required time of arrival (RTA) into the FMS and, then, the on-board trajectory planner would compute a new (optimal) trajectory plan starting at the current state, while satisfying the RTA and other operational constraints (e.g., altitude and speed constraints) (De Prins *et al.*, 2007). Finally, the resulting trajectory plan would be executed by an on-board guidance system with 4D capabilities.

Note that, unlike TAs and 3D-PAM, the constraints are not in form of altitude and speed instructions at the different waypoints, but purely CTAs. The on-board trajectory planner is who selects the optimal altitude and speed profile such that the applicable CTAs are satisfied. Accordingly, this kind of flight operations are expected to increase the likelihood of generating a trajectory plan at idle thrust, while still satisfying the time constraints requested by ATC that are supposed to sequence and merge arrival traffic with acceptable throughout at the metering fix.

Although assigning CTAs at one or several fixes to manage incoming traffic might suffice for low to medium traffic loads, it might not be enough for higher traffic demands, as shown by Pawelek *et al.* (2019). In those situations, the aircraft route should also be stretched to absorb even more delay.

I.2.7 Interval Management

Interval management (IM) consists of a set of ground and flight-deck capabilities and procedures that are used in combination by ATCOs and flight crews to more efficiently and precisely manage spacing between aircraft in a stream of traffic (Federal Aviation Administration, 2021a). During an IM operation, the ATCO will share an objective to the flight crew (to achieve and maintain a spacing goal relative to a target aircraft), and the flight crew will use the avionics to execute the spacing objective. The avionics and automation systems will support IM operations to the same runway, parallel runways, and crossing and converging runways, enabling increased throughput over today's operations.

IM uses ADS-B capabilities to precisely manage spacing between aircraft. IM is a component of the future trajectory based operations (TBO) vision (described in Section I.3.2), where ATCOs may opt to provide clearances to flights to manage their spacing intervals relative to other aircraft. Flight-deck applications, like IM, can provide more precise spacing than ground-based decision support tools alone, providing greater TBO benefits.

Several authors have studied the use of IM together with CDOs. Itoh & Uejima (2013) studied the application of CDOs in a high-density traffic scenario, in Tokyo international airport. After performing a fast-time simulation, it was concluded that IM has the potential to achieve a safe separation between aircraft, achieving at the same time fuel savings for arrival traffic as a whole, not just for individual aircraft. Similarly, Callantine *et al.* (2013) also assessed the benefits of IM in a sustained high-demand scenario, identifying a variety of factors that could impact the safety and viability of the concept from an ATC perspective. Some of these factors are, for instance, en-route preconditioning of arrival flows and the characteristics of airspace, routes, and traffic-management methods in use at a particular site. More recently, Riedel *et al.* (2020) applied a novel technology known as flight-deck interval management (FIM) (which is an aircraft self-spacing technology to improve the efficiency and safety of flight) during CDOs using a fixed flight-path angle. In this work, pilots were invited to evaluate the system in an Airbus A320 simulator. Results

indicated that the new changes implemented in the control logic of FIM—mainly involving a reduction in the amount of IM speed commands and reversals—was well accepted by the pilots.

I.3 Motivation of this PhD

This section outlines the main future needs for the efficient scheduling of arrival traffic flying CDOs and subject to RTAs. These future needs are aligned with the goals defined by the SESAR and NextGen programs, and drive the motivation of this PhD thesis.

I.3.1 Ground Automation

Arrival managers (AMANs) were developed in the late 1990s to provide automated sequencing support for ATC to achieve a smooth, predictable and optimized arrival stream to perform as few tactical interventions as possible. State-of-the-art AMANs use information from the flight plans, radar tracks, weather data, local airspace structure information, and aircraft performance models to predict trajectories and provide the predicted time of arrival at the different fixes for every flight. Research is currently ongoing into how modern AMANs could also provide support to select appropriate CTAs (Muynch *et al.*, 2012). ATC would be in charge to provide the CTA to the pilot, who would then use 4D FMS trajectory management capabilities to satisfy it. In this context, Bronsvoort (2014) proposed a novel two-stage trajectory prediction system to synchronize airborne and ground-based trajectory computation processes, which was used in an AMAN proposed by the authors. A framework was developed supporting different levels of aircraft equipage, where instructions by the ATC were either given by speed and route advisories or through the use of the RTA capability of more modern FMSs.

More recently, an extended version of the AMAN, known as extended arrival manager (E-AMAN) was proposed by SESAR (SESAR JU, 2019b). In short, the aim of E-AMAN is to alleviate pressure in the terminal airspace by allowing to sequence arrival traffic much earlier than is currently the case. The current AMAN horizon is extended from the airspace close to the airport to further upstream, thus, allowing a smoother traffic management. Controllers in the upstream sectors (e.g., en-route sectors), which may be in a different control centre or even in a different functional airspace block (FAB), obtain system advisories to support an earlier pre-sequencing of aircraft. E-AMAN is supported by sharing the airport's arrival management information with upstream sectors in real time. All parties share the same information using a system-wide information management (SWIM) service. Toratani *et al.* (2018) and Toratani (2019) recently considered aircraft scheduling and E-AMAN algorithms, where they proposed a method to simultaneously optimize the arrival sequence and trajectories of the arrival traffic, known as the merging optimization method. Research is still ongoing into methods to further optimize the arrival trajectories considered by E-AMAN and its application in the current ATM system.

I.3.2 Trajectory Based Operations

A key transformation to achieve the goals defined by SESAR and NextGen is the use of new ATM paradigms, such as the TBO concept (Federal Aviation Administration, 2021b). TBO aims at completely removing open-loop vectoring and strategic constraints on the trajectories by efficiently implementing a 4D trajectory negotiation process to synchronize airborne and ground equipment with the aim of maximizing both flight efficiency and throughput. In this scenario, there would be no need for vectoring except for unforeseen or contingency situations.

Current ATM is based on a filed flight plan and tactical interventions by ATC as the flight

progresses. The idea behind TBO is to enable the ATM system to know and, where appropriate, modify the flight's planned and actual trajectory, before or during flight, based on accurate information that has been shared by all stakeholders. This will lead to efficiency gains for both individual aircraft and for the network as a whole.

TBO involves a full integration of flight information in order to create a synchronized view of flight data by all actors involved in the ATM system. This shared information also includes any constraints imposed by the various ATM stakeholders. SESAR and NextGen are addressing the operational and technical procedures needed to manage this shared information, and the scenarios where a stakeholder is allowed to update a trajectory.

TBO is a broad topic, and extensive research has been done in the recent years in several of the initiatives needed to efficiently implement TBO in the current ATM environment. Subramanian *et al.* (2013) proposed a series of trajectory computation algorithms for a next generation flight management system (NG-FMS), compliant with the TBO concept, where a series of 4D intents were generated and downlinked to the ATC. Similarly, Benavides *et al.* (2014) proposed a trajectory prediction function for tactical flight management to continuously update the 4D flight path that will be flown by the FMS. Finally, Lopez-Leones *et al.* (2007) proposed a formal language in order to facilitate the exchange of predicted trajectories within a TBO environment. Research is still ongoing into methods to further optimize the 4D trajectory flown by the arrival aircraft within a TBO environment, improving the situational awareness of all the involved actors and the overall efficiency of operations.

I.3.2.1 Traffic Synchronization

Within TBO, one remarkable concept is traffic synchronization (SESAR JU, 2019a), which refers to the establishment and maintenance of a safe, orderly and efficient flow of air traffic. It concerns the management and execution of 4D trajectories based on constraints combined with integrated queue management and handling, aiming to develop a sequence, both in the air and on the ground. It operates on individual flights but for the overall ATM network benefit, aiming to facilitate the highest achievable capacity of the ATM system and to manage delays in a fuel-efficient and environmentally acceptable manner.

Where required to *smooth* the arrival flow at the destination airport, target times are applied in the planning stage over a metering point associated with the runway, with the reference business trajectory (RBT) defined to respect that constraint. In order to efficiently manage the subsequent inbound traffic flow, an E-AMAN allocates a time to begin to establish a sequence.

The arrival management systems use enhanced trajectory prediction capabilities, integrating and updating ground prediction, where appropriate, with available airborne data from suitably equipped flights. This data could be exchanged via the extended projected profile (EPP), which contains trajectory information–e.g. predicted aircraft weight, as well as the predicted horizontal and vertical speed—of up to 128 waypoints. Information from multiple arrival management systems operating out to extended range is integrated with local traffic/sector information within the en-route sectors, and allows balancing of the workload and needs of the TMA and en-route. Trajectory negotiation between en-route and TMA air traffic services (ATS) providers and airspace users is enabled through SWIM.

Where appropriate, the AMAN allocated time can be uplinked to the affected flight as a CTA, providing the advantage of high levels of accuracy where there is sufficient stability of the traffic sample. The use of the aircraft estimated time of arrival (ETA) by the ground system in determining the CTA and the accurate management of flights subject to this CTA improves the performance and reliability of the arrival sequencing. Together with the airspace design and overall traffic management, this has the potential to enable the use of more closed-loop procedures in high-density-traffic situations, thereby allowing a high proportion of traffic to fly an optimum

profile, ideally from the cruise phase.

Gwiggner *et al.* (2011) presented a trade-off analysis of the traffic synchronization problem, focusing on the pre-sequencing of arrival traffic. They concluded that it is critical that FMSs are equipped with the RTA functionality in order to enable a smoother arrival management; in addition, they highlight the need for accurate trajectory prediction algorithms to minimize uncertainty. In this context, Casado Magaña (2016) identified the main sources of uncertainties in trajectory prediction: i) **initial conditions**, corresponding to the deviation between the true and assumed initial states, for instance the initial weight of the aircraft; ii) **aircraft motion modeling**, linked to the intrinsic simplifications on the dynamic aircraft model; iii) **aircraft performance model**, related to the aircraft type which determine the aircraft behavior during the flight; iv) **weather models and forecasts**, which are recognized as one of the most influential sources of uncertainty; and v) **aircraft intents**, which refer to the lack of knowledge about the user's operational strategy (unless for ownship trajectory prediction).

More recently, Mondoloni & Rozen (2020) did a review of current research applicable to trajectory prediction throughout the trajectory prediction process, addressed the differences in decision-making structures, and considered trajectory synchronization research applicable to TBO. They recognized the need for further research in the topic, in order to enable an efficient synchronization of the many involved actors in the ATM system.

I.3.3 Dynamic and Enhanced Routes and Operations

Currently, during the arrival phase, flights tend to follow static STARs which do not take into account the particular operating capability of each aircraft, thus, leading to a reduction of the efficiency of the operation. In this context, one of the recommendations of SESAR (SESAR JU, 2019a) and NextGen programs is the dynamic use of the terminal airspace, including its routes and transitions with the en-route sectors.

Dynamic terminal airspace would accommodate the transition between the TMA and both free-route airspace and fixed-route airspace. This would ensure, as much as possible, the facilitation of a broad range of descent profiles which are fuel-efficient for the specific flight, where aircraft follow CDOs. New controller tools using enhanced knowledge of the predicted vertical behavior of the aircraft would help to ensure CDOs, as well as trajectory management together with traffic synchronization. Enhanced airborne functionalities would be used to optimize descent paths and support the crew in the management of aircraft energy. CDOs could be planned as part of the trajectory and would represent the nominal case of operations. The TOD may need to be revised during the execution phase of the flight, for example to take into account sequencing requirements, e.g. CTA, and/or the dynamic use of lateral routes for the TMA.

The interface between TMA and en-route would see dynamic use of lateral routes and the application of 4D trajectory constraints when required; making use of high accuracy and high reliability required navigation performance (RNP) capability, speed and various descent profiles in order to provide the optimal link between the two environments. Under nominal conditions, all traffic would be delivered to the final approach phase via closed-loop procedures, which are designed to provide reduced track miles wherever possible and to provide good predictability to all involved actors.

Utilization of RNP procedures provides an additional level of assurance in aircraft adherence to the trajectory, which is important in an environment where constraints are dynamically managed. Civil aircraft not certified or approved for RNP operations could still be accommodated on traditional procedures which may not offer individual flights the full efficiency benefits associated with the concept. However, such flights are expected to represent the exception.

Recently, some authors have dealt with the generation of dynamic arrival routes within TMA.

For instance, Dahlberg *et al.* (2018) proposed a MIP-based approach for automation of aircraft separation along optimal dynamic arrival routes. The authors took the arrival times at the TMA entry points of all aircraft during a day as an input, and computed arrival routes that ensured safe separation from the entry points to the runway along the entire routes. However, they used the simplifying assumptions that all aircraft (independently of the type) flew with the same speed. Similarly, Krozel *et al.* (2007) proposed a methodology to generate weather avoidance arrival routes, where the problem was modeled in a two-dimensional (2D) horizontal plane. The authors succeeded to generate alternate routes around hazardous weather using the current STARs as a baseline. Still, for all the experiments conducted, they assumed a very simple aircraft dynamics model.

I.4 Objectives of this PhD Thesis

The main objective of this PhD thesis is to develop methods to efficiently schedule arrival aircraft in terminal airspace, proposing as well concept of operations (CONOPs) aligned with the TBO paradigm. The simulated arrival trajectories generated for all the experiments conducted in this PhD thesis, to the maximum possible extent, are considered to be energy-neutral CDOs, seeking to reduce the overall environmental impact of aircraft operations in the ATM system. Ultimately, the objective of this PhD is to achieve a more efficient arrival management of traffic, in which higher levels of predictability and similar levels of capacity are achieved, while the safety of the operations is kept.

The designed experiments consider a TBO paradigm, involving a high synchronization between all the involved actors of the ATM system. Higher levels of automation and information sharing are expected, together with a modernization of both current ATC ground-support tools and aircraft FMSs.

The specific objectives of this PhD thesis can be outlined as follows:

- Develop a trajectory optimization framework for the generation of efficient aircraft descent trajectories, with the aim of using it to generate all the simulated trajectories for the experiments conducted in this PhD thesis. This framework is built on top of the trajectory management framework developed by Dalmau (2019).
- Assess the efficiency of current arrival operations in a major European airport. More specifically, the objective is to analyze the benefits of flying energy-neutral CDOs by comparing them with actual flown trajectories, which can be obtained from several databases containing historical flight data. Analyzing the suitableness of each database for carrying out efficiency assessments, pointing out their strengths and weaknesses, is another goal of this PhD thesis.
- For high loads of traffic, ATCOs might not be able to assign to the arrival aircraft CTAs that could be achieved by flying energy-neutral CDOs along the published route. In such a case, aircraft would need to follow a different strategy in order to meet the RTA that will be input to the FMS. One strategy would be to still fly energy-neutral CDOs but along shorter/longer routes, while the other strategy would involve flying powered descents along the published route. In this context, another objective of this PhD thesis is to compare—in terms of fuel consumption and for different conditions—the two aforementioned strategies so that aircraft could achieve the assigned RTA in such a scenario.
- Propose a CONOPs and develop a methodology to schedule arrival traffic flying energy-neutral CDOs in terminal airspace. The aim is to improve the predictability and efficiency of the ATM system, thus, reducing the environmental impact of aircraft operations and the workload of ATCOs. For that purpose, two solutions were identified:

  - A short-term solution, seeking to maximize the number of energy-neutral CDOs flown by arrival aircraft by taking advantage of the most advanced arrival and approach procedures currently in operation. More specifically, the aim is to schedule arrival traffic in a trombone area navigation (RNAV) procedure.
  - A long-term solution in which, by assuming a more futuristic scenario with TBO deployed to its limits, arrival traffic is scheduled by means of dynamic arrival routes within terminal airspace, thus, shifting away from the current STAR paradigm. The aim is to develop a framework to generate arrival routes automatically adapting to the current traffic demand and enabling arrival traffic to fly energy-neutral CDOs.

I.5 Scope and Limitations of this PhD Thesis

In order to accomplish the objectives of this PhD thesis, the research is subject to several assumptions and limitations that define its scope:

- All the results in this PhD were obtained via fast-time simulations, without involving any human-in-the-loop studies.
- In this PhD thesis, all the proposed solutions correspond to a low technology readiness level (TRL)[1], between 2 and 3 depending on the solution. Therefore, many of the solutions proposed are not still mature enough for being applied in operational practice, and more research should be done in order to rise the TRL. More specifically, the computational times obtained in many experiments are very high, which may limit the application of the proposed solutions in the current air traffic system. In addition, many experiments were performed with a medium-range laptop, which will not be the case in many of the real applications proposed in this PhD. Furthermore, neither safety assessments nor human-in-the-loop simulations were performed.
- ATFM is out of the scope of this PhD. Although demand and capacity balance (DCB) initiatives performed at a pre-tactical level could have an effect on some of the solutions proposed in this PhD, only tactical operations in the terminal area and the scheduling of traffic in this region are considered. Still, the solutions proposed in this PhD thesis could help to develop initiatives such as integrated network ATC planning (INAP) and short-term air traffic flow capacity measure (STAM), seeking to extend the ATS planning to improve the synchronization between DCB and ATC (SESAR JU, 2021).
- An aircraft performance model (APM) widely accepted by the ATM community, known as base of aircraft data (BADA) (Mouillet *et al.*, 2018), was used for the experiments conducted in this PhD. Thus, the results obtained in this PhD may differ from those that could be obtained with a performance model provided by the manufacturer, which would reflect with a higher accuracy the actual behavior of the aircraft. Still, all the proposed solutions could work with any other performance model, providing it is available.
- The guidance system of the FMS is out of the scope of this PhD. Thus, only the optimal trajectory plan generated by the FMS is considered, but not how this plan will be actually flown. Dalmau *et al.* (2019a) did extensive research on several guidance strategies, which could be applied in the experiments conducted in this PhD to execute the generated trajectory plans.

[1]TRLs are a method for estimating the maturity of technologies during the acquisition phase of a program, developed at NASA during the 1970s (NASA, 2021)

- The concept of operations investigated assumes a closed-loop path from the TOD to the runway threshold, as the route and CTA are pre-negotiated before the aircraft starts to descend. Therefore, updates of the optimal trajectory plan due to route changes are not contemplated. Changes of the lateral route, however, could be eventually translated to changes in the distance to go and use the proposed algorithms with minimum modifications.
- The only environmental impact metric considered for the optimization of aircraft trajectories in this PhD thesis is the fuel consumption. Still, carbon dioxide (CO_2) emissions could be easily considered too, as they are proportional to fuel consumption. On the other hand, other aircraft emissions, which consist primarily of nitrogen oxides (NO_x) and methane, are not considered. Of additional concern are the generation of contrails, sulphur oxides (SO_x) and the particulate matter. Furthermore, airframe noise is not directly taken into account either. However, the trajectory optimization framework is indirectly considering noise as energy-neutral CDOs are generated. In such descents, aircraft usually stay at higher altitudes and they perform idle-engine descents with no speed brakes usage, which lead to a reduction of noise in the vertical domain. However, differently from other works (Ho-Huu *et al.*, 2020), the sequencing and merging techniques proposed in this PhD thesis do not minimize the effect of noise in the lateral domain, and focus only on the maximization of the number of energy-neutral CDOs flown.
- The trajectory optimization problem tackled in this PhD involves nonlinear constraints and/or cost function and is, in consequence, a non-convex optimization problem. This means that several local minima may exist. Since global optimization algorithms require a high computational burden, they are prohibited for real-time applications. Thus, the proposed trajectory optimization techniques involve the use of local optimization algorithms.
- Contingencies, such as engine failure, are not considered in the experiments. That is, nominal operations are assumed in all the experiments.

I.6 Outline of this PhD Thesis

The present document is organized in seven chapters, which are summarized as follows. It is worth noting that a broad state of the art of the main topics addressed in this PhD thesis has been presented before. A deeper and more specific state of the art for each individual topic is included at the beginning of each chapter.

- **Chapter II** presents the framework for trajectory optimization used in this PhD, involving the several models and trajectory optimization techniques used for generating optimal trajectory plans.
- **Chapter III** presents an efficiency assessment for arrival traffic in a major European airport. A series of key performance indicators (KPIs) are analyzed, where actual flown trajectories are compared with the submitted flight plans, as well as with CDOs. The required historical-trajectory data required to do this study was obtained from different databases, which are compared in terms of suitableness for efficiency assessments within TMAs.
- **Chapter IV** compares two strategies to effectively sequence arrival traffic when not all aircraft can achieve the assigned RTA by flying energy-neutral CDOs along the published route. The sensitivity of the fuel consumption to several parameters, such as the aircraft model and the wind speed, is analyzed.

- **Chapter V** focuses on the interim strategy between full 4D negotiated trajectories and open-loop vectoring: a methodology to effectively schedule arrival traffic flying energy-neutral CDOs along a trombone RNAV procedure.
- **Chapter VI** proposes a methodology to generate dynamic arrival routes that automatically adapt to the current air traffic demand. Energy-neutral CDOs are enforced for all arrival traffic.
- **Chapter VII** gives the conclusions that are drawn from this work and points out some future work that could be done in the direction of the presented research.
- **Appendix A** presents the mixed integer programming (MIP) formulation used in Chapter VI to generate the dynamic arrival routes.

Tu es blanche, et je suis noir; mais le jour a besoin de s'unir à la nuit pour enfanter l'aurore et le couchant qui sont plus beaux que lui!
[You are white, and I am black; but the day needs to unite with the night to give birth to the dawn and the setting sun, which are more beautiful than it!]

— Victor Hugo

II

Framework on Trajectory Optimization

Flight management systems (FMSs) emerged as a part of the standard avionics suite on Boeing 757 and 767 aircraft in the early 1980s (Liden, 1994). From that point on, FMSs became a standard in all new aircraft. FMSs represented a revolutionary advance in the management of a flight, reducing both workload of the flight crew and cost of flight for the airline due to its capability to generate and automatically execute trajectory plans minimizing fuel and time costs according to certain optimization criteria. The birth of FMSs also allowed high flexibility in the avionics functionalities and opened the door to design new operational concepts, such as those addressed in this PhD thesis.

One of the main tasks of a FMS is to generate the trajectory plan that is to be subsequently flown. The trajectory plan is decomposed in a lateral route (sequence of waypoints) and a vertical profile (time histories of the altitude and speed). Since this PhD thesis assumes an operational concept in which the lateral route is fixed and only the vertical profile is managed to satisfy required times of arrival (RTAs), the concept of *trajectory plan* will refer only to the vertical profile.

In current FMSs, the trajectory plan is usually constructed by numerical integration of the differential equations of the model describing the dynamics of the aircraft. This numerical integration starts at the current state of the aircraft, applying the appropriate flight intents or controls, using certain aircraft performance and weather models, and satisfying the operational constraints entered at the different waypoints of the lateral route. In order to be optimal, the trajectory plan is generated by using optimal speeds and altitudes stored in pre-computed look-up tables as a

function of the cost index (CI)[1] and other flight parameters. Even if some modern FMSs are also able to satisfy RTAs by using brute force (they iterate with the CI to obtain different speed profiles, and therefore times of arrival, until the RTA is satisfied), the trajectory plan for the descent is typically computed and frozen before the top of descent (TOD), meaning that re-plans of the optimal trajectory plan are not allowed once the descent has started. The initial trajectory plan, however, will be actually optimal and its time prediction will be correct only if the models used by the FMS to represent the aircraft dynamics, aircraft performance, and weather are accurate enough. In practice, these models will rarely reproduce the *real world* and are not exempted from errors.

FMSs suitable for continuous descent operations (CDOs) subject to RTAs not only require on-board trajectory planning algorithms capable to rapidly generate, in real-time, the optimal trajectory plan complying with entered RTAs and typical operational constraints (e.g., altitude and speed); but also a guidance system capable to nullify time deviations in such a way the RTAs are satisfied in the most efficient way in terms of environmental impact, even in presence of modelling errors during the trajectory planning process (Dalmau, 2019). However, the guidance system is out of the scope of this PhD thesis, as all the experiments presented in the following chapters are dealing solely with the trajectory planning functionality of the FMS.

In this PhD thesis, the trajectory optimization framework is built on top of the trajectory management framework developed by Dalmau (2019). Section II.1 presents the models considered in the formulation of the trajectory optimization problem. Note that, depending on the specific goal of each particular experiment conducted in this PhD thesis, these models will be adapted in the following chapters according to appropriate assumptions. Then, Section II.2 formulates the generic optimal control problem, whose objective function and constraints will be also particularized later on for each experiment. Furthermore, a semi-analytic method to solve simpler optimization problems and a numerical method to solve non-linear programming (NLP) problems are presented.

II.1 Models

This section describes the models used in this PhD thesis to generate optimal trajectory plans. An aircraft can be represented as a system composed by several states, which evolve according to a set of nonlinear ordinary differential equations (ODEs) given some control inputs or, more generally, flight intents in the form of algebraic constraints, which transform the ODEs system into a system of differential algebraic equations (DAEs). In turn, this model for the aircraft dynamics must be particularized with certain models for the aircraft performance and the weather, respectively. These models are thoroughly described in the following sections.

II.1.1 Aircraft Dynamics Model

The motion of an aircraft can be accurately described with a six degrees of freedom model (Nelson, 1997), where the derivative equations of the three translations and the three rotations of the aircraft can be integrated along the time. Although this methodology results in the most accurate planning of the aircraft trajectory, it requires an extensive aerodynamic and propulsive model and the knowledge of the inertia tensor of the aircraft. Due to the complexity of this model, many trajectory prediction tools used in some air traffic management (ATM) applications use basic kinematic models that directly model the path characteristics of the aircraft, without attempting to model the underlying physics (Bilimoria *et al.*, 2000). Somewhere in between these two approaches lie

[1]The CI is a parameter chosen by the airspace user that reflects the relative importance of the cost of time with respect to fuel costs (Airbus, 1998)

the aircraft point-mass model (Hull, 2007), a kinetic approach that is considered accurate enough for on-board trajectory planning systems and the majority of ground-based ATM applications.

In a point-mass model, the aircraft motion is reduced to three degrees of freedom (the three translations), assuming that all forces are applied to the center of gravity of the aircraft. Thus, there is no need to model its inertia tensor or stability control loops (considered as higher order dynamics) and only the aerodynamic, propulsive, and external forces (e.g., due to the gravity) must be modeled.

It should be noted that a flat, non-rotating earth with a constant gravity acceleration has been assumed when modeling the aircraft dynamics. Moreover, the sideslip angle and angle of attack have been neglected, being the sum of all propulsive forces a single thrust vector along the longitudinal axis of the aircraft. Finally, the vertical component of the wind—a local phenomenon caused, for example, by convective weather—is typically not considered in weather models used for ATM purposes on a large scale. In addition, the effects of the wind derivatives are much lower than those of the wind itself, and can be deprecated for the purposes of this PhD thesis. Accordingly, both vertical wind and wind derivatives have been neglected (i.e. $\dot{w}_v = w_h = 0$). Moreover, the vertical component of the wind is typically orders of magnitude below that of the horizontal component. These assumptions are most common in the literature dealing with similar topics (Slattery & Zhao, 1997).

In this PhD, the point-mass model was reduced to a γ-*command* model, which could be considered accurate enough for all the experiments conducted in this PhD thesis. This model is described by the following set of equations:

$$\frac{\mathrm{d}v}{\mathrm{d}t} = \dot{v} = \frac{T - D(v, h, s, C_L, \beta)}{m} - g \sin\gamma \tag{II.1a}$$

$$\frac{\mathrm{d}h}{\mathrm{d}t} = \dot{h} = v \sin\gamma \tag{II.1b}$$

$$\frac{\mathrm{d}s}{\mathrm{d}t} = \dot{s} = \sqrt{v^2 \cos^2\gamma - w_x^2(h, s)} + w_s(h, s) \tag{II.1c}$$

$$\frac{\mathrm{d}m}{\mathrm{d}t} = \dot{m} = -q(v, h, s, T). \tag{II.1d}$$

where the state vector $\vec{x} = [v, h, s, m]^T$ is composed, respectively, by the true airspeed (TAS), the geometric altitude, the distance to go and the mass of the aircraft; the control vector $\vec{u} = [T, \beta, \gamma]^T$ is composed, respectively, by the total thrust force of the engines, the speed brakes deflection and the aerodynamic flight path angle; D is the aerodynamic drag force; L is the aerodynamic lift force; C_L is the lift coefficient; q is the nominal fuel flow; w_x and w_s are, respectively, the cross and longitudinal wind components; and g is the local gravity acceleration. In the notation adopted in this PhD thesis, $(\cdot)^T$ represents the transpose of vector $(\cdot)$.

The γ-*command* model assumes continuous vertical equilibrium thorough the flight (i.e., lift balances weight):

$$\dot{\gamma} = 0 \rightarrow L = mg \cos\gamma. \tag{II.2}$$

As a result, the aerodynamic flight path angle becomes an input control variable that can change instantaneously. Finally, the aerodynamic forces (lift and drag) in Eq. (II.1) are commonly modeled as:

$$L(v,h,s,C_L) = \frac{1}{2}\sigma(s,h)\rho_{SSL}v^2SC_L \tag{II.3a}$$

$$D(v,h,s,C_L,\beta) = \frac{1}{2}\sigma(s,h)\rho_{SSL}v^2SC_D(v,h,s,C_L,\beta), \tag{II.3b}$$

where σ is the normalized density of the air, ρ_{SSL} is the density of the air at standard sea level (SSL), S is the wing surface area, and C_D is the drag coefficient.

For practical reasons (such as requirements to speed up the algorithms) several simplifications can be done in the mathematical representation of the equations describing the aircraft dynamics (Eq. (II.1)). In general, the more complex (and typically accurate) the model is, the larger the number of nonlinearities in the model and the more execution time of the optimization problem. As a result, the trade-off between accuracy and execution time must be considered when selecting an appropriate aircraft dynamics model for real-time trajectory optimization purposes. For this reason, the chapters of this PhD thesis consider different variants of Eq. (II.1).

The thrust control is typically bounded by the idle (or minimum) thrust (T_{idle}), and maximum thrust (T_{max}) of the particular aircraft type. Similarly, bounds on the remaining controls, C_L and γ, are also enforced to ensure that the aircraft remains within its operational limits. Generally speaking, the drag coefficient, the maximum and minimum thrust, the nominal fuel flow, and the fuel flow when the engines operate at idle (q_{idle}) are functions of the state and/or control variables. The complexity of these mathematical expressions depends on the adopted aircraft performance model (APM).

Finally, it should be noted that operational speeds are typically given in terms of Mach number or callibrated airspeed (CAS), which depend on the TAS but also on certain atmospheric conditions. In this PhD, the expressions used to compute the Mach number and the CAS—$M : \mathbb{R}^{n_x} \to \mathbb{R}$ and $v_{CAS} : \mathbb{R}^{n_x} \to \mathbb{R}$, respectively—are the following:

$$M = \frac{v}{\sqrt{\gamma_a \tau R}} \tag{II.4}$$

$$v_{CAS} = \sqrt{\frac{2p_0}{\mu\rho_0}\left(\left(\frac{p}{p_0}\left(\left(\frac{\mu v^2}{2R\tau}+1\right)^{\frac{1}{\mu}}-1\right)+1\right)^{\mu}-1\right)}, \tag{II.5}$$

where $R = 287.058$ Jkg K^{-1} is the specific gas constant for dry air, τ is the air temperature, γ_a is the specific heat ratio of the air, $\mu = (\gamma_a - 1)/\gamma_a$; and p_{SSL} is the standard pressure at SSL.

II.1.2 Aircraft Performance Model

An APM particularizes the expressions for C_D, T_{max}, T_{idle}, q and q_{idle} as a function of $\vec{x}$ and/or $\vec{u}$. The accuracy of the APM is of crucial importance if one aims at computing realistic trajectories and, thus, obtain representative results. Without going any further, the fuel flow function will be used to determine the total fuel consumption, which will be used, in turn, to support investment decisions in many assessments of new ATM systems and concept of operations (CONOPs).

Generally speaking, the drag coefficient depends on C_L (induced drag); Mach number (M) (effects of air compressibility); and, to a lesser extent, the altitude (effects of air temperature on the Reynolds Number). The drag coefficient will also change if speed brakes are applied, the gear ($\eta \in \{0,1\}$) is deployed or the aircraft is configured with flaps/slats (ζ). These gear status and flaps/slats configurations could be either considered as additional controls (i.e., $\vec{u} = [T, \beta, \gamma, \eta, \zeta]$) or modeled as a function of the state vector.

Another alternative widely used to reduce the non-linearities of the model consists in splitting the descent in several phases, where each phase is particularized with a different model for the C_D, q, T_{min} and T_{max}. The formulation of multi-phase optimal control problems, where each phase could have a different aircraft dynamics and/or performance model, will be described in Section II.2.3.

For low subsonic flight (Mach approximately below 0.6) the effects of Mach and altitude in the drag coefficient can be neglected, leading to the well known drag polar, which is composed by a constant term plus a quadratic term function of the square of the lift coefficient:

$$C_D(C_L, \beta, \eta, \zeta) = C_{D0}(\beta, \eta, \zeta) + C_{D2}(\beta, \eta, \zeta)C_L^2, \tag{II.6}$$

where C_{D0} and C_{D2} are the parasite and induced drag coefficients, respectively, which depend on the status of the landing gear, the flaps/slats configuration and the speed brakes deflection. Typical airliners, however, operate in the range between approximately Mach 0.60-0.85 for most of the flight. Thus, compressibility effects on drag coefficient cannot be neglected and models more elaborated than Eq. (II.6) need to be considered to generate realistic trajectories.

Regarding the idle and maximum thrust, these functions essentially depend on the Mach number and the outside temperature and pressure conditions. Similarly, nominal fuel flow depends on thrust, Mach number and outside temperature and pressure.

Several APMs can be used to model these aerodynamic and propulsive functions, from simple linear interpolations with look-up tables coming directly from experimental data, to more or less sophisticated mathematical approximations that fit these data. To give a couple of examples, Dalmau & Prats (2015) approximated aerodynamic and propulsive tabular data from the manufacturer with polynomial functions; while Betts (2010) approximated similar kinds of data with tensor product B-spline functions (de Boor, 1972).

Another example of APM used in many ATM applications, such as air traffic control (ATC) simulation purposes, is the Eurocontrols's base of aircraft data (BADA) v3. In BADA v3, the drag coefficient is modeled with Eq. (II.6), thus, neglecting compressibility effects. In addition, the thrust limits are only given as a function of altitude and the fuel flow depends on the TAS and thrust. It is well known that BADA v3 was designed to model aircraft performance and fuel consumption in nominal flight conditions, and several studies have already revealed that is not accurate enough to derive correct fuel consumption figures in the terminal maneuvering area (TMA) (Senzig *et al.*, 2009; Senzig & Fleming, 2009). In particular, it has been reported that BADA v3 model tends to underestimate fuel flow in idle conditions.

BADA v4 (currently version 4.2) was designed as a realistic, accurate, and complete APM that overcomes the main limitations of BADA v3, being the preferred model to use for trajectory optimization purposes (Poles *et al.*, 2010). Indeed, this model will be the main APM used in this PhD thesis. It covers 80% of aircraft types in the european civil aviation conference (ECAC) area, and it provides increased levels of precision in aircraft performance parameters over the entire flight envelope to enable modelling and simulation of advanced systems and future concepts. Mouillet *et al.* (2018) assessed the viability of BADA v4 for trajectory optimization purposes. The results obtained with BADA v4 were compared with those obtained with original equipment manufacturer (OEM) reference performance data from certain Boeing aircraft types. Several metrics were analyzed (mainly errors in trip fuel and trip time, in absolute and relative terms), concluding in the end that BADA v4 would be suitable for ATM simulations and environmental impact assessments. However, the authors do not recommend to use this model in on-board applications and business economic studies, which look into the operating costs of an airline.

It is out of the scope of this PhD thesis to review and assess the accuracy of existing APMs. Yet, it is worth noting the importance of having representative APMs when aiming to compute

accurate trajectory plans and time predictions. For instance, Slater (2009) showed the importance to accurately model idle thrust and drag coefficient functions when generating trajectory plans for the descent phase. In the same context, Casado *et al.* (2013) proposed a methodology to assess the impact of uncertainties in the coefficients of parametric models such as BADA (i.e. models defined by mathematical functions which depend on several coefficients) and its effect on the accuracy of the computed trajectory plan.

II.1.3 Weather Model

The ground speed of the aircraft is greatly influenced by the wind field. Moreover, the performance of the aircraft notably depends on the temperature and pressure of the air. For instance, during a 20 minutes climb, temperature errors of 1.5 Kelvin throughout the climb would produce an altitude prediction error around 500 ft (Forester & Dharssi, 1992); and a difference of 12 kt in the ground speed would result in an estimated time of arrival deviation of 5%, assuming an original ground speed of 250 kt (Robert & De Smedt, 2013). The ground speed not only depends on the longitudinal and cross winds, but also on temperature if the aircraft is flying at a constant Mach number, or on temperature and pressure if it is following a constant CAS, as shown in Eqs. (II.4) and (II.5), respectively. As shown by Chatterji *et al.* (1996), ground speed sensitivity is around 1.1 knot per Kelvin for typical cruise conditions, where aircraft operate at constant Mach number.

Therefore, an accurate weather model will definitely reduce the number of corrective actions required to nullify altitude, time and/or speed deviations when executing the trajectory plan. Furthermore, the trajectory plan is optimal only for the weather conditions considered in the weather model. Thus, if the model does not accurately reproduce the actual wind, temperature and pressure, the executed trajectory will not be optimal.

Typically, trajectory planning tools assume the international standard atmosphere (ISA) model (ICAO, 1993), which is representative of an ideal atmosphere based on the thermodynamic equation, as defined by the international civil aviation organization (ICAO). In the ISA model, the normalized temperature of the air (θ) decreases at a constant lapse rate of $\lambda_h = 6.5$ K/km^{-1} from SSL (where the ISA temperature is $\tau_{SSL} = 288.15$ K) up to the altitude of the tropopause, whose ISA value is $h_{11} = 36,000$ ft. Above the tropopause, the temperature is considered constant with a value of $\theta_{11} = 0.732$ up to 65,600 ft (well above the typical altitudes where commercial aircraft operate):

$$\theta(h) = \begin{cases} 1 - \frac{\lambda_h}{\tau_{SSL}} h & \text{if } h \leq h_{11} \\ \theta_{11} & \text{if } h > h_{11}. \end{cases} \tag{II.7}$$

By combining this linear model with the hydrostatic equation, the expression of the normalized pressure (δ) as a function of the altitude can be obtained:

$$\delta(h) = \begin{cases} \theta(h)^{\frac{g}{\lambda_h R}} & \text{if } h \leq h_{11} \\ \delta_{11} e^{\frac{g\tau_{SSL}}{R\theta_{11}}(h_{11}-h)} & \text{if } h > h_{11}, \end{cases} \tag{II.8}$$

where $\delta_{11} = 0.224$ is the normalized pressure of the air at the tropopause and $p_{SSL} = 1013.25$ hPa is the pressure at SSL. Finally, given the normalized temperature and pressure values, the air density can be obtained by using the perfect gas law relationship:

$$\sigma(h) = \frac{\delta(h)}{\theta(h)}. \tag{II.9}$$

The ISA model is just a theoretical representation of the atmosphere. In practice, due to temperature inversions, as well as additions or decrease of moisture, the actual atmosphere will have lapse rates and standard conditions at sea level different from those of ISA. Non-standard conditions are often modeled by adding a specified temperature offset to the standard temperature at SSL (so called ISA+ΔT). However, pressure is not recalculated at the non-standard temperature because temperature effects on it are considered to be much less important than the effect of altitude. In spite of that, non-standard conditions for the pressure can be also modeled by considering a p_{SSL} different from 1013.25 hPa.

It should be noted that the ISA model is not the only existing reference for temperature and pressure profiles. The United States department of defense standard MIL-STD-210C and its successor standard MIL-HDBK-310, also define temperature models for use as references of hot day, cold day, tropical, and polar temperature profiles. Figure II-1(a) compares these temperature profiles.

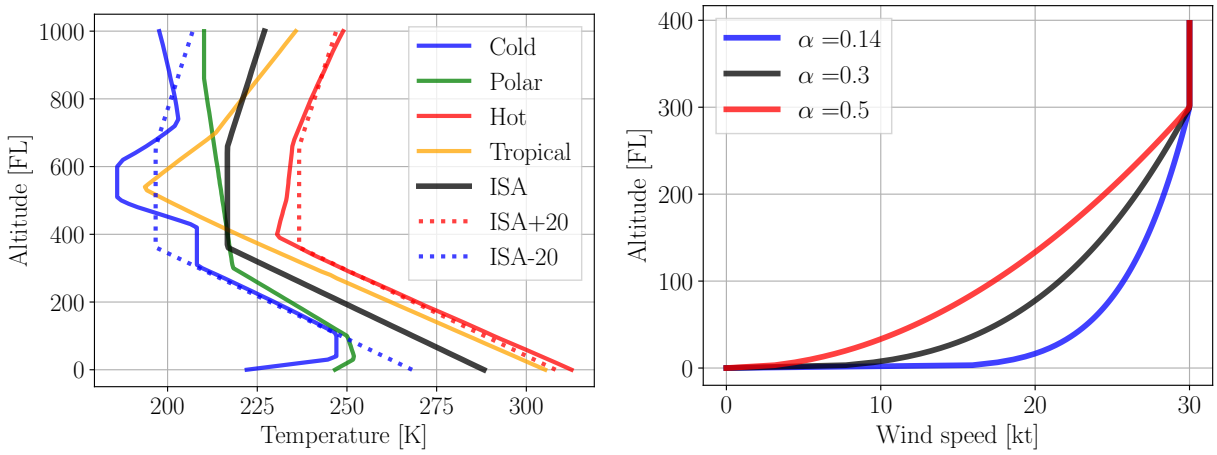

(a) Standard temperature profile models (b) Empirical wind models (Hellmann model)

Figure II-1: *Theoretical and empirical weather models (Dalmau, 2019)*

Realistic temperature and pressure data, as a function of the geopotential altitude[2] and geographical location (latitude and longitude) for different time stamps, can be obtained from weather forecasts and analysis generated by numerical weather prediction (NWP) models. Currently, there are several available NWP which provide weather forecasts and analysis with a variety of resolutions, accuracies and look-ahead times. For instance, the global forecast system (GFS) (NOAA, 2021) is a NWP developed and maintained by the national oceanic and atmospheric administration (NOAA) that covers the entire globe with an horizontal resolution of 28 km and look-ahead forecast times up to 192 hours; while the rapid refresh (RAP) covers a limited region (North America), but has an horizontal resolution of 13 km and forecast look-ahead times going up to 18 hours. Another example of NWP models is ERA5 (ECMWF, 2021), developed and maintained by the european centre for medium-range weather forecasts (ECMWF). ERA5 provides hourly estimates of a large number of atmospheric, land and oceanic climate variables. The data cover the Earth on a 30km grid and resolve the atmosphere using 137 levels from the surface up to a height of 80km. In addition, ERA5 includes information about uncertainties for all variables at reduced spatial and temporal resolutions. This data in gridded format can be interpolated to obtain the weather information at specific geographical coordinates and altitudes or approximated with continuous functions of various complexity such as polynomials or splines.

[2]For typical aircraft altitudes, the gravity variations at different altitudes can be neglected. Thus, geopotential altitudes—which are typically used in weather models—and geometric altitudes are assumed to be the same.

Note that since in the CONOPs tackled in this PhD thesis the lateral route (sequence of waypoints) is known before generating the optimal vertical profile, realistic air temperature and pressure models will be essentially functions of the altitude and distance to go.

A similar rationale is adopted to model the wind field. Simple models used for academic purposes assume constant wind speed and direction throughout the descent, independently of the geographical location and altitude. In practice, however, wind speed tends to increase with the altitude. This typical behavior can be represented using various empirical and theoretical models, from linear functions to more or less complex mathematical expressions. An example of empirical model for the total wind speed ($|\vec{w}|$), which assumes constant longitudinal wind above a reference altitude (h_r) is the well known Hellmann power law (Hellmann, 1916):

$$|\vec{w}|(h) = \begin{cases} w_r & \text{if } h > h_r \\ w_r \left(\frac{h}{h_r}\right)^{\alpha} & \text{if } h \leq h_r, \end{cases} \tag{II.10}$$

where w_r is a known wind speed at h_r. The Hellman exponent (α) depends on many factors, such as the coastal location, the shape of the terrain on the ground, and the stability of the air. Figure II-1(b) shows the Hellmann power law for different values of α, fixing w_r at 30 kt and h_r at FL300.

State-of-the-art weather forecasts obtained from NWPs typically provide the wind vector at different altitudes and geographical locations. These forecasts decompose the wind vector in north component (w_n), east component (w_e) and vertical component. Again, since the route is known beforehand in this PhD thesis, the bearing between consecutive waypoints of the route is also known, and the wind field can be projected to along-track and cross-track wind components as a function of the altitude and distance to go:

$$w_s(h,s) = w_n(h)\cos\chi_g(s) + w_e(h)\sin\chi_g(s) \tag{II.11a}$$
$$w_x(h,s) = -w_n(h)\sin\chi_g(s) + w_e(h)\cos\chi_g(s), \tag{II.11b}$$

where χ_g is the track angle, a known function of the distance to go.

It should be noted that the temporal variations of temperature, pressure and wind components are neglected in this PhD thesis because the duration of a descent is small if compared with the time scale of typical atmosphere dynamics. In addition, the trade-off between additional complexity (involving a longer execution time) of the model and accuracy of the resulting trajectories is not appealing.

For each of the experiments conducted in this PhD thesis, the expressions for δ, θ, w_s and w_x will be particularized as a function of h and s, either with mathematical expressions approximating realistic weather data from NWP forecasts or using empirical or theoretical models. However, w_n and w_e will be only computed as a function of h, as the variation of wind with respect to s is negligible during a descent.

II.2 Optimal Trajectory Planning

As mentioned before, the optimization of the vertical profile of an aircraft trajectory can be formulated as a multi-phase, constrained optimal control problem (Soler *et al.*, 2015), in which it is desired to determine the controls of the aircraft such that a given objective function is maximized (or minimized) while satisfying a set of constraints, including those describing the dynamics of the aircraft, ATM operational constraints, and aircraft envelope. This optimization process should also consider realistic weather conditions.

The formulation of a generic optimal control problem is presented in Section II.2.1. In general, the aircraft trajectory optimization problem cannot be solved analytically due to the complexity and non-linearity of the constraints and cost function. However, there are some approaches designed to tackle simpler trajectory optimization problems. In Section II.2.2, an example of these approaches is presented, consisting in a semi-analytic method which was used in some of the experiments designed in this PhD thesis. For more complex problems, the numerical approach explained in Section II.2.3 was used. Finally, in Section II.2.4, the NLP is presented, while in Section II.2.5, some implementation considerations that should be taken into account when dealing with NLP optimization problems are detailed.

II.2.1 Optimal Control Problem Formulation

An optimal control problem for a generic system during a fixed or variable continuous time horizon $[t_I, t_F]$ for a single phase can be formulated as follows (Bryson & Ho, 1975):

$$\begin{aligned} \min_{\vec{u}(t)} \quad & J := \phi\left(\vec{x}(t_F), \vec{d}\right) + \int_{t_I}^{t_F} \pi\left(\vec{x}(t), \vec{u}(t), \vec{d}\right) \mathrm{d}t \\ \text{s.t} \quad & \vec{x}(t_I) = \vec{X} \\ & \dot{\vec{x}} = \vec{f}\left(\vec{x}(t), \vec{u}(t), \vec{d}\right) \\ & \vec{b}^{in}\left(\vec{x}(t), \vec{u}(t), \vec{d}\right) \leq 0 \\ & \vec{b}^{eq}\left(\vec{x}(t), \vec{u}(t), \vec{d}\right) = 0 \\ & \vec{\psi}\left(\vec{x}(t_F), \vec{d}\right) = 0 \end{aligned} \tag{II.12}$$

where $\vec{x} \in \mathbb{R}^{n_x}$ is the vector of differential states; $\vec{u} \in \mathbb{R}^{n_u}$ is the vector of controls; and $\vec{d} \in \mathbb{R}^{n_d}$ is the vector of fixed parameters of the model. The cost function $J : \mathbb{R}^{n_x} \times \mathbb{R}^{n_u} \times \mathbb{R}^{n_d} \to \mathbb{R}$, which is composed by a running cost (or Lagrange term) $\pi : \mathbb{R}^{n_x} \times \mathbb{R}^{n_u} \times \mathbb{R}^{n_d} \to \mathbb{R}$ and an end cost (or Mayer term) $\phi : \mathbb{R}^{n_x} \times \mathbb{R}^{n_d} \to \mathbb{R}$, is to be minimized subject to: dynamic constraints $\vec{f} : \mathbb{R}^{n_x} \times \mathbb{R}^{n_u} \times \mathbb{R}^{n_d} \to \mathbb{R}^{n_x}$ in the form of ODE with initial conditions $\vec{X} \in \mathbb{R}^{n_x}$; algebraic constraints $\vec{b}^{eq} : \mathbb{R}^{n_x} \times \mathbb{R}^{n_u} \times \mathbb{R}^{n_d} \to \mathbb{R}^{n_\varphi}$; inequality path constraints $\vec{b}^{in} : \mathbb{R}^{n_x} \times \mathbb{R}^{n_u} \times \mathbb{R}^{n_d} \to \mathbb{R}^{n_b}$; and terminal constraints $\vec{\psi} : \mathbb{R}^{n_x} \times \mathbb{R}^{n_d} \to \mathbb{R}^{n_\psi}$ enforced only at the end of the time horizon.

II.2.2 Solving Optimization Problems Semi-Analytically

This section presents a methodology designed to tackle simpler trajectory optimization problems, where some assumptions are made in order to compute a trajectory by solving semi-analytically the optimization problem. The proposed methodology builds up on the recent work developed by Park *et al.* (2017).

Let us assume that the trajectory considered covers the latter part of the cruise phase and all the descent down to a metering fix, where an RTA is assigned. In addition, the original cruise speed is maintained (and therefore, not subject to optimization). Yet, the fuel consumption in cruise is considered in the objective function, since the location of the TOD is indeed subject to optimization. Under these conditions, this problem can be modeled as a single-phase optimal control problem that minimizes a compound function that takes into account both fuel and time costs, relating them with the CI.

The flight path angle (γ), which appears linearly in the equations describing the dynamics of the aircraft as well as in the cost function, is the only control considered in this problem. Consequently, the Hamiltonian of the system (Park *et al.*, 2017) is also linear with respect to this control,

leading to a singular optimal control problem which can be solved semi-analytically from the implicit formulation of optimal singular arcs.

Since the initial and final states of the trajectory are fixed, the optimal trajectory will be of a *bang-singular-bang* type. These solutions consist of three arcs: one non-singular arc with the control variable at its maximum or minimum value to go from $\vec{x}_0$ to the singular arc; a singular arc where the optimal control is given as a function of the states vector; and a final non-singular arc to go from the singular arc to the final state $\vec{x}_f$. The control input of the non-singular arcs is determined by the airspeed difference between the singular arc and the boundary points at the initial and final altitudes. At the initial altitude, if airspeed on the singular arc is larger than cruise speed, the aircraft must accelerate to meet the singular arc. In such a case, a maximum given flight path angle is selected for the non-singular arc generation. On the other hand, if the singular arc speed is less than the cruise speed, a minimum given flight path angle is selected. The first non-singular arc (i.e. from the initial state to the singular arc) is computed by forward integration and the second non-singular arc (i.e. from the singular arc to the final state) by backward integration. The integration is performed by using a Runge-Kutta numerical method of 4th order (RK-4). An example of the optimal speed profiles that can be generated with this methodology is shown in Figure II-2. In this particular case, it can be observed how the optimal speed profile lies in between the boundaries delimited by a given minimum CAS value (CAS_{min}) and MMO/VMO (maximum operative Mach/CAS). Also note that since these maximum and minimum speeds are given in terms of CAS and Mach, the corresponding TAS changes with altitude.

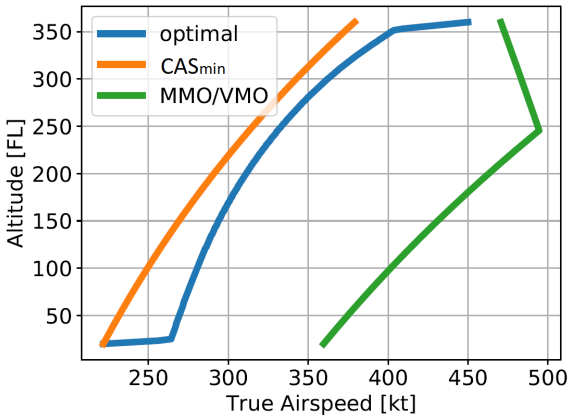

Figure II-2: *Optimal speed profile for a typical narrow-body jet aircraft in ISA and no-wind conditions*

This method, however, has some limitations. It can only be used to optimize the descent or climb vertical profiles, while the lateral profile is not optimized. However, this will not suppose a problem since this PhD thesis assumes an operational concept in which the lateral route is fixed. Furthermore, this semi-analytic optimizer can only achieve RTAs by brute force, iterating over several CIs. However, depending on the application, it is a very good choice given its robustness and speed. As the trajectory optimization technique used is not based on a non-linear solver, there are no convergence problems and a solution is always found. Finally, only one control variable can be considered in the optimal control formulation. Therefore, other control variables, such as the flap setting, thrust or speedbrakes could not be included in the optimization problem. The analytical expression of the optimal control in the singular arc for this method, and the steps to generate an optimal trajectory semi-analytically can be found in Park *et al.* (2017).

II.2.3 Direct Multiple-Shooting Formulation

Essentially, two different methods are available for solving Eq. (II.12): indirect methods, which involve the calculus of variations or the maximum principle of Pontryagin Bryson & Ho (1975); and direct methods, which transform the original infinite-dimensional optimal control problem into a finite-dimensional NLP optimization problem Betts (2010). In turn, indirect methods can be divided into single-shooting and multiple-shooting, while the direct methods can be divided into single-shooting, multiple-shooting and collocation. An excellent review of these methods was performed by Andersson (2013), illustrating the working principle of them by introducing a simple, yet industrially relevant optimal control problem. Prats (2010) also described the main features and the trade-offs of each method, in terms of complexity and computational burden, from a more practical perspective.

In this PhD, direct multiple-shooting methods are used. These methods discretize the time histories of the control and/or state variables at a set of time samples. The cost function and constraints of the optimal control problem can be expressed in terms of these discretized states and/or controls, which become the decision variables of a parametric NLP optimization problem that can be solved by means of standard solvers.

Let the continuous time horizon $[t_I, t_F]$ be discretized into $N+1$ equidistant time samples τ_k, with $k = 0, \ldots, N$. Note that $\tau_0 = t_I$, $\tau_N = t_F$ and the discretization step is $\Delta\tau = {}^{(\tau_N - \tau_0)}/_{N}$. The discrete optimal control problem minimizing the cost function J in a time horizon of N time intervals can be formulated as:

$$
\begin{aligned}
\min_{\substack{\vec{x}_k, k=0,\ldots,N \\ \vec{u}_k, k=0,\ldots,N-1}} \quad & J := \phi\left(\vec{x}_N, \vec{d}\right) + \sum_{k=0}^{N-1} \Pi\left(\vec{x}_k, \vec{u}_k, \vec{d}, \Delta\tau\right) \\
\text{s.t} \quad & \vec{x}_0 = \vec{X} \\
& \vec{x}_{k+1} = \vec{F}\left(\vec{x}_k, \vec{u}_k, \vec{d}, \Delta\tau\right);\ k = 0, \ldots, N-1 \\
& \vec{b}^{in}\left(\vec{x}_k, \vec{u}_k, \vec{d}\right) \leq 0;\ k = 0, \ldots, N-1 \\
& \vec{b}^{eq}\left(\vec{x}_k, \vec{u}_k, \vec{d}\right) = 0;\ k = 0, \ldots, N-1 \\
& \vec{\psi}\left(\vec{x}_N, \vec{d}\right) = 0,
\end{aligned}
\tag{II.13}
$$

where $\vec{x}_k \in \mathbb{R}^{n_x}$ and $\vec{u}_k \in \mathbb{R}^{n_u}$ are the state and control vectors discretized at τ_k, respectively, for $k = 0, \ldots, N$. While the algebraic, path and terminal constraints of the continuous optimal control problem (Eq. (II.12)) can be directly evaluated at the discretized states and controls, the states evolution function $\vec{F} : \mathbb{R}^{n_x} \times \mathbb{R}^{n_u} \times \mathbb{R}^{n_d} \times \mathbb{R} \to \mathbb{R}^{n_x}$ must be defined as the result of integrating $\vec{f}$ during a time interval of duration $\Delta\tau$ using an appropriate integration scheme with the discretized states and controls. Similarly, $\Pi : \mathbb{R}^{n_x} \times \mathbb{R}^{n_u} \times \mathbb{R}^{n_d} \times \mathbb{R} \to \mathbb{R}$ is a quadrature function resulting from a numerical integration of π during a time interval of duration $\Delta\tau$.

The optimal control problem described by Eq. (II.13) assumes that the same running cost, dynamic constraints and algebraic and path constraints apply during the whole time horizon. In addition, event constraints can be set only at the very end of the time horizon. Yet, many *real-life* processes can be divided into several phases (or stages), where the dynamics of the system, the running cost and the algebraic and path constraints might change. In addition, in some particular applications it is necessary to formulate interior-point constraints in between two consecutive phases.

Eq. (II.13) can be easily extended to such multi-phase problems. First, let the continuous time horizon $[t_I, t_F]$ be divided into P time intervals $[t_j, t_{j+1}]$ for $j = 0, \ldots, P-1$; each time interval corresponding to a different phase. Again, $t_0 = t_I$ and $t_P = t_F$. Then, each time interval (or phase)

is discretized into N_j equidistant time samples $\tau_k, \tau_{k+1}, \ldots, \tau_{k+N_j-1}$, where $\tau_k = t_j$, $\tau_{k+N_j-1} = t_{j+1}$ and $k = \sum_{i<j} N_i$, for all $j = 0, \ldots, P-1$. The discretization step of the j^{th} phase is denoted by $\Delta\tau_j$. As a result, the whole time horizon is discretized into $N+1 = \sum_{j=0}^{P-1} N_j$ time samples $\tau_0, \tau_1, \ldots, \tau_N$.

Let $\mathcal{T}$ be a multi-dimensional set that relates the index of each phase to the indexes of its corresponding time samples. The subset $\mathcal{E} \subseteq \mathcal{T}$ only includes the index corresponding to the last time sample of each phase; and $\mathcal{I}$ is defined as $\mathcal{T} \backslash \mathcal{E}$.

Based on the definitions stated above, the discrete multi-phase optimal control problem can be formulated as:

$$
\begin{aligned}
\min_{\substack{\vec{x}_k, k=0,\ldots,N \\ \vec{u}_k, \forall(j,k)\in\mathcal{I}}} \quad & J := \sum_{(j,k)\in\mathcal{E}} \phi_j\left(\vec{x}_k, \vec{d}\right) + \sum_{(j,k)\in\mathcal{I}} \Pi_j\left(\vec{x}_k, \vec{u}_k, \vec{d}, \Delta\tau_j\right) \\
\text{s.t} \quad & \vec{x}_0 = \vec{X} \\
& \vec{x}_{k+1} = \vec{F}_j\left(\vec{x}_k, \vec{u}_k, \vec{d}, \Delta\tau_j\right); \forall(j,k) \in \mathcal{I} \\
& \vec{b}_j^{in}\left(\vec{x}_k, \vec{u}_k, \vec{d}\right) \leq 0; \forall(j,k) \in \mathcal{I} \\
& \vec{b}_j^{eq}\left(\vec{x}_k, \vec{u}_k, \vec{d}\right) = 0; \forall(j,k) \in \mathcal{I} \\
& \vec{\vartheta}_j^{eq}\left(\vec{x}_k, \vec{d}\right) = 0; \forall(j,k) \in \mathcal{E}\backslash\{(P-1, N) \\
& \vec{\vartheta}_j^{in}\left(\vec{x}_k, \vec{d}\right) \leq 0; \forall(j,k) \in \mathcal{E}\backslash\{(P-1, N) \\
& \vec{\psi}\left(\vec{x}_N, \vec{d}\right) = 0 \\
& \vec{x}_k - \vec{x}_{k+1} = 0; \forall(j,k) \in \mathcal{E}\backslash\{(P-1, N)\}
\end{aligned}
\tag{II.14}
$$

In Eq. (II.14), $\Pi_j : \mathbb{R}^{n_x} \times \mathbb{R}^{n_u} \times \mathbb{R}^{n_d} \times \mathbb{R} \to \mathbb{R}$ and $\vec{F}_j : \mathbb{R}^{n_x} \times \mathbb{R}^{n_u} \times \mathbb{R}^{n_d} \times \mathbb{R} \to \mathbb{R}^{n_x}$ are the quadrature and states evolution functions for the j^{th} phase, respectively. Similarly, $\vec{b}_j^{eq} : \mathbb{R}^{n_x} \times \mathbb{R}^{n_u} \times \mathbb{R}^{n_d} \to \mathbb{R}^{n_{\varphi_j}}$ and $\vec{b}_j^{in} : \mathbb{R}^{n_x} \times \mathbb{R}^{n_u} \times \mathbb{R}^{n_d} \to \mathbb{R}^{n_{b_j}}$ are the algebraic and path constraints, respectively, of the j^{th} phase; and $\vec{\vartheta}_j^{eq} : \mathbb{R}^{n_x} \times \mathbb{R}^{n_d} \to \mathbb{R}^{n_{\vartheta_j^{eq}}}$, and $\vec{\vartheta}_j^{in} : \mathbb{R}^{n_x} \times \mathbb{R}^{n_d} \to \mathbb{R}^{n_{\vartheta_j^{in}}}$ represent applicable equality and inequality interior-point constraints, respectively, applying at the last time of the j^{th} phase. Note that in Eq. (II.14) a new set of constraints has been added to link the state variables across two consecutive phases and guarantee continuity in the solution.

Analogously to the single-phase optimal control problem, the discretization step of each individual phase could be considered either a known parameter or an unknown variable to be optimized, depending on the context. For instance, if the duration of the whole time horizon were fixed to a certain parameter, say a RTA, but the duration of each phase were flexible, $\Delta\tau_j$ for $j = 0, \ldots, P-1$ would become decision variables subject to the following constraint:

$$
\sum_{j=0}^{P-1} (N_j - 1)\,\Delta\tau_j - \text{RTA} = 0, \tag{II.15}
$$

which would be appended to Eq. (II.14).

II.2.4 Nonlinear Programming Problem

Direct methods for optimal control compute the optimal trajectory plan by formulating the generic multi-phase optimal control problem as a parametric NLP optimization problem. This optimiza-

tion problem has the following form:

$$\begin{aligned} \min_{\vec{z}} \quad & f\left(\vec{z},\vec{p}\right) \\ \text{s.t} \quad & \vec{h}\left(\vec{z},\vec{p}\right)=0 \\ & \vec{g}\left(\vec{z},\vec{p}\right)\leq 0 \end{aligned} \tag{II.16}$$

where $\vec{z}\in\mathbb{R}^{n_z}$ is the vector of primal variables; $\vec{h}:\mathbb{R}^{n_z}\times\mathbb{R}^{n_p}\rightarrow\mathbb{R}^{n_h}$ is the vector of equality constraints; $\vec{g}:\mathbb{R}^{n_z}\times\mathbb{R}^{n_p}\rightarrow\mathbb{R}^{n_g}$ is the vector of inequality constraints; and $\vec{p}\in\mathbb{R}^{n_p}$ is the vector of (fixed) parameters of the NLP optimization problem. In this PhD thesis, the following definitions have been considered:

$$\vec{z}:=\begin{bmatrix}\vec{z}_0\\ \vec{z}_1\\ \dots\\ \vec{z}_N\end{bmatrix},\ \vec{h}\left(\vec{z},\vec{p}\right)\ :=\begin{bmatrix}\vec{h}_0\left(\vec{z},\vec{p}\right)\\ \vec{h}_1\left(\vec{z},\vec{p}\right)\\ \dots\\ \vec{h}_N\left(\vec{z},\vec{p}\right)\end{bmatrix},\ \vec{g}\left(\vec{z},\vec{p}\right):=\begin{bmatrix}\vec{g}_0\left(\vec{z},\vec{p}\right)\\ \vec{g}_1\left(\vec{z},\vec{p}\right)\\ \dots\\ \vec{g}_N\left(\vec{z},\vec{p}\right)\end{bmatrix} \tag{II.17}$$

where:

$$\begin{aligned} \vec{z}_k &:= \begin{cases}\begin{bmatrix}\vec{u}_k\\ \vec{x}_k\end{bmatrix} & \text{if } (j,k)\in\mathcal{I}\\ \vec{x}_k & \text{if } (j,k)\in\mathcal{E}\end{cases}\\ \vec{h}_k &:= \begin{cases}\begin{bmatrix}\vec{x}_{k+1}-\vec{F}_j\left(\vec{x}_k,\vec{u}_k,\vec{d},\Delta\tau_j\right)\\ ,\vec{b}_j^{eq}\left(\vec{x}_k,\vec{u}_k,ved\right)\end{bmatrix} & \text{if } (j,k)\in\mathcal{I}\\ \begin{bmatrix}\vec{\vartheta}_j^{eq}\left(\vec{x}_k,\vec{d}\right)\\ \vec{x}_k-\vec{x}_{k+1}\end{bmatrix} & \text{if } (j,k)\in\mathcal{E}\backslash\{P-1,N\}\\ \vec{\psi}\left(\vec{x}_k,\vec{d}\right) & \text{if } k=N\end{cases}\\ \vec{g}_k &:= \begin{cases}\vec{b}_j^{in}\left(\vec{x}_k,\vec{u}_k,\vec{d}\right) & \text{if } (j,k)\in\mathcal{I}\\ \vec{\vartheta}_j^{in}\left(\vec{x}_k,\vec{d}\right) & \text{if } (j,k)\in\mathcal{E}\backslash\{P-1,N\}.\end{cases}\end{aligned} \tag{II.18}$$

According to Eq. (II.18), $\vec{z}_k$ includes both discretized states and controls at the time sample τ_k. Similarly, $\vec{g}_k$ and $\vec{h}_k$ include the inequality and equality constraints applied at τ_k, respectively.

In Eq. (II.16), f is the cost function of the original optimal control problem evaluated at the primal variables and NLP parameters, i.e., $f\left(\vec{z},\vec{p}\right)=J(\vec{z},\vec{p})$. In this PhD thesis, the vector of NLP parameters is composed of both current state of the aircraft and parameters of the model:

$$\vec{p}=\begin{bmatrix}\vec{X}\\ \vec{d}\end{bmatrix} \tag{II.19}$$

Furthermore, in order to reduce the number of NLP variables and constraints, the constraint that fix the initial conditions of the optimal control problem to the current state of the system is eliminated by substituting the variables $\vec{x}_0$ for the vector of fixed initial conditions $\vec{X}$ in the whole NLP optimization problem (i.e., equality constraints, inequality constraints and cost function). This allows to remove the redundant constraint $\vec{x}_0=\vec{X}$ and the variable $\vec{x}_0$ from the optimization problem.

The Lagrangian function associated to the NLP optimization problem (II.16) is:

$$\mathcal{L}\left(\vec{z},\vec{p},\vec{\lambda},\vec{\mu}\right) := f\left(\vec{z},\vec{p}\right) + \vec{\lambda}^T\vec{g}\left(\vec{z},\vec{p}\right) + \vec{\mu}^T\vec{h}\left(\vec{z},\vec{p}\right), \tag{II.20}$$

where $\vec{\lambda} \in \mathbb{R}^{n_g}$ and $\vec{\mu} \in \mathbb{R}^{n_h}$ are the Lagrange multipliers (dual variables) vectors paired up with the constraints $\vec{g}$ and $\vec{h}$, respectively. An optimal primal-dual pair $\left(\vec{z}^*,\vec{\lambda}^*,\vec{\mu}^*\right)$, where $(\cdot)^*$ indicates *optimal*, satisfies the first-order necessary conditions of optimality, also known as Karush-Kuhn-Tucker conditions (KKT) (Kuhn & Tucker, 1951):

$$\frac{\partial\mathcal{L}}{\partial\vec{z}}\left(\vec{z}^*,\vec{p},\vec{\lambda}^*,\vec{\mu}^*\right) = \frac{\partial f}{\partial\vec{z}}\left(\vec{z}^*,\vec{p}\right) + \vec{\lambda}^{*T}\frac{\partial\vec{g}}{\partial\vec{z}}\left(\vec{z}^*,\vec{p}\right) + \vec{\mu}^{*T}\frac{\partial\vec{h}}{\partial\vec{z}}\left(\vec{z}^*,\vec{p}\right) = 0 \tag{II.21a}$$

$$\vec{h}\left(\vec{z}^*,\vec{p}\right) = 0;\ \vec{\mu}^* > 0 \tag{II.21b}$$

$$g_i\left(\vec{z}^*,\vec{p}\right) = 0;\ \lambda_i^* > 0;\ \forall(g_i,\lambda_i^*) \in \mathcal{G}_{ac} \tag{II.21c}$$

$$g_i\left(\vec{z}^*,\vec{p}\right) < 0;\ \lambda_i^* = 0;\ \forall(g_i,\lambda_i^*) \in \mathcal{G}_{in} \tag{II.21d}$$

where the pairs of inequality constraints and associated dual variables have been divided into two complementary sets: the active set ($\mathcal{G}_{ac}$) and the inactive set ($\mathcal{G}_{in}$) (Würth *et al.*, 2009).

Newton methods suitable to solve this kind of optimization problems try to find a point satisfying Eq. (II.21) by using successive linearization of the cost function and constraints. The major differences between them are on how to achieve the conditions related with the inequality constraints Eqs. (II.21c) and (II.21d). The two big families are:

- **Interior-point methods**, which typically replace the original NLP optimization problem by a series of barrier sub-problems (Wächter & Biegler, 2006), which are controlled by a barrier parameter. Two representative interior-point methods are the primal-dual method and the trust-region method.
- **Active-set methods**, which solve in turn a sequence of sub-problems based on a quadratic approximation of the original NLP optimization problem. Representative active-set methods are the sequential quadratic programming (SQP) method (Gill *et al.*, 2005), the sequential linear-quadratic programming (SLQP) method (Byrd *et al.*, 2003) and the gradient projection method (Lin & Moré, 1999; Byrd *et al.*, 1995)

II.2.5 Implementation Considerations

Several common issues must be considered when dealing with NLP optimization problems. In particular, how to react in the face of an infeasible solution in which some constraints are not satisfied and how to handle discontinuities present in tabular data. The following sections give a couple of recommendations related to these two topics, respectively.

II.2.5.1 Recovering from Infeasible Solutions

In practical applications, the solution of the NLP optimization problem described by Eq. (II.16) may not always be feasible. Accumulated deviations caused by disturbances and modelling errors could eventually lead to the impossibility to satisfy one or several constraints to a given numerical precision. If this were the case, the NLP solver would not provide a valid solution and, consequently, the optimal trajectory plan could not be obtained. Yet, in some circumstances it may be reasonable to allow, to some extent, violations in certain constraints, so that a sub-optimal solution can still be obtained, as long as the application permits. With this aim, there exist several alternatives to recover the feasibility of the solution.

Constraint Relaxation Method

An attractive method consists of not defining the admissible range of the constraints to their actual operational limits but to more conservative values. Then, these limits will be systematically relaxed whenever an infeasible solution is obtained. This approach is commonly referred as the constraint relaxation method. It is not always obvious, however, which constraints to relax, nor the amount which they should be relaxed. In order to overcome this issue, some optimization techniques have been proposed, which determine the constraints that should be relaxed, according to some priority list, and the the minimum relaxation required to recover feasibility (Vada *et al.*, 2001). These techniques resort to optimization problems running in parallel to the original optimal control problem. Accordingly, their algorithmic complexity may be significant.

Transient Constraint Violation Method

A second alternative consists of allowing constraint violations only during a certain period of time, typically at the beginning of the new trajectory, which is to be minimized. In some cases, however, the time transient constraints violations could be large (Scokaert & Rawlings, 1999).

Soft-Constraint Method

Finally, the soft-constraint method consists of defining additional slack variables in the optimization problem, which allow to violate the path and/or terminal constraints in case of not obtaining a feasible solution to the optimal control problem (Scokaert & Rawlings, 1999). By using this method, the original NLP problem of Eq. (II.14) is re-formulated as follows:

$$\begin{aligned} \min_{\vec{z},\vec{e}^{eq},\vec{e}^{in}} \quad & f(\vec{z},\vec{p}) + \vec{e}^{in^T}\boldsymbol{\mathcal{W}}^{in}\vec{e}^{in} + \vec{e}^{eq^T}\boldsymbol{\mathcal{W}}^{eq}\vec{e}^{eq} \\ \text{s.t} \quad & \vec{h}(\vec{z},\vec{p}) = \vec{e}^{eq} \\ & \vec{g}(\vec{z},\vec{p}) \leq \vec{e}^{in} \\ & \vec{e}^{in} \geq 0 \end{aligned} \tag{II.22}$$

where $\vec{e}_{in} \in \mathbb{R}^{n_g}$ and $\vec{e}_{eq} \in \mathbb{R}^{n_h}$ are the vector of slack variables paired up with the inequality and equality constraints of the original NLP optimization problem. Additional constraints ensure that the slack variables do not make the associated constraints more restrictive than their original values.

The positive-definite weighting matrices $\boldsymbol{\mathcal{W}}^{in} \in \mathbb{R}^{n_g \times n_g}$ and $\boldsymbol{\mathcal{W}}^{eq} \in \mathbb{R}^{n_h \times n_h}$ determine how much the violation of inequality and equality constraints is penalized, respectively. By educatedly tuning these weights, it is expected that the optimization algorithm will violate constraints only if necessary. Otherwise, the result shall be equivalent to that obtained from solving (II.14). The rule of thumb known as *Bryson's rule* (Bryson & Ho, 1975) can be used as a guideline to determine these weighting matrices. This rule states that the weights should be chosen so that the contribution of each slack variable to the cost function is approximately the same. In order to accomplish that, the inverse square of the admissible range of each constraint could be used as weight for the associated slack variable.

Note that when using this technique not all the constraints need to be necessarily slacked. For those constraints which cannot be violated under any condition, the corresponding slack variable could be either removed from the set of decision variables, or the weight associated to the slack variable could be set to a very large value. Yet, the latter solution is not recommended for numerical stability reasons.

II.2.5.2 Handling Tabular Data in NLP Algorithms

When facing optimal control problems such as the one presented in Eq. (II.12), it is common to encounter a cost function and/or constraints given in tabular form, as a function of the states and/or controls. For instance, the drag coefficient of the aircraft, which depends on the lift coefficient and Mach number, could be given as a look-up table with performance data obtained from the manufacturer. Similarly, wind data from NWP forecasts, which are required to compute the ground speed, are typically given in tabular form as a function of the latitude, longitude and pressure level.

For use in simulations, the (linear) interpolation between discrete data points is an easy way to extract the desired information from these look-up tables. However, modern NLP solvers require the first and second derivatives of the cost functions and constraints with respect to the primal variables in order to work. The derivatives of a piece-wise linear function are undefined at the data points, where two linear functions with different slopes intercept. For this reason, state-of-the-art NLP solvers have difficulties when using tabular data. In this kind of optimization problems, the data must be approximated off-line in order to generate continuous and twice-differentiable curves by some smooth function fitting techniques.

The easiest way to approximate tabular data is perhaps to use polynomial fittings (Prats *et al.*, 2015). Although some of the aircraft performance data could be approximated quite well by polynomial functions, these expressions are not able to accurately approximate sharp change such as the drag rise region due to compressibility effects or complex functions such as the wind field. In such cases, high-order polynomials prone to oscillation due to the Runge's phenomenon would be required, potentially leading to poor convergence, local minima issues and large errors between data points.

In order to deal with tabular data in optimal control problems, Betts (2010) suggested to approximate the data points with tensor product splines. Splines are functions defined piece-wise by polynomials of any degree, which keep sufficiently continuity and differentiability at the places where the polynomial pieces connect, called knots (de Boor, 1972).

The simplest way to compute the splines coefficients is by ensuring interpolation to all data points (the interpolating spline). The resulting function provides the continuity and second-order differentiability required by NLP solvers to work. However, it is common for this kind of function to include *wiggles* that are not actually present in the data itself. A technique for eliminating these oscillations is to approximate the data rather than interpolating it. This can be achieved by using smoothing splines, which minimize the *curvature* of the spline whilst ensuring sufficient accuracy through the smoothing factor (Betts, 2010). By using smoothing splines, a small reduction on the accuracy of the resulting interpolation function could lead to significant benefits in terms of convergence and execution time, due to the smoother first and second derivatives.

Wer mit Ungeheuern kämpft, mag zusehn, dass er nicht dabei zum Ungeheuer wird. Und wenn du lange in einen Abgrund blickst, blickt der Abgrund auch in dich hinein.
[He who fights with monsters should look to it that he himself does not become a monster. And if you gaze long into an abyss, the abyss also gazes into you.]

— Friedrich Nietzsche

III

Evaluation of Historical-Flights Databases for Efficiency Assessments

Energy-neutral continuous descent operations (CDOs), as previously discussed (Section I), bring a lot of environmental benefits to the air traffic management (ATM) system. However, this kind of descents are not always performed in current operations, thus, leading to a higher environmental impact of aircraft descents. This efficiency loss is caused, to a great extend, by inefficiencies in the vertical profile, which are caused in turn by descents containing segments at constant altitude.

This chapter presents an evaluation of the vertical flight efficiency (VFE) of Stockholm-Arlanda airport arrivals via a use of a series of performance indicators (PIs). This includes the calculation of some key performance indicators (KPIs) proposed by the international civil aviation organization (ICAO) and, additionally, the computation of the fuel consumption impact caused by deviations from the flight plans and by inefficient vertical flight profiles within the terminal maneuvering area (TMA). Finally, this chapter compares different data sources—OpenSky Network automatic dependent surveillance-broadcast (ADS-B) data and Eurocontrol demand data reposi-

This chapter is based on the following publications:

- Lemetti, A., Polishchuk, T., Polishchuk, V., Sáez, R. & Prats, X.. 2020 (Jun.). Identification of significant impact factors on Arrival Flight Efficiency within TMA. *In: 9th International Conference on Research in Air Transportation (ICRAT)*. Virtual Event: EUROCONTROL/FAA.
- Lemetti, A., Polishchuk, T. & Sáez, R.. 2019 (Nov.). Evaluation of flight efficiency for Stockholm Arlanda Airport using OpenSky Network data. *In: 7th OpenSky Workshop*. Zurich, Switzerland: EasyChair.
- Lemetti, A., Polishchuk, T., Sáez, R. & Prats, X.. 2019 (Oct.). Analysis of weather impact on flight efficiency for Stockholm Arlanda Airport arrivals. *In: 6th ENRI International Workshop on ATM/CNS (EIWAC)*. Tokyo, Japan: ENRI.

tory (DDR)—used to obtain historical-flight trajectories, discussing their applicability for carrying out efficiency assessments within the TMA, outlining their strengths and weaknesses.

III.1 State of the Art

Eurocontrol developed the methodology used by its performance review unit (PRU) for the analysis of VFE during climb and descent (Peeters & Guastalla, 2017). The performance review commission of Eurocontrol made an assessment of the ATM state in Europe for the year 2018 where, among other indicators, reviewed air traffic punctuality and vertical flight inefficiency at the top 30 European airports, including Stockholm-Arlanda airport (Performance Review Comission, 2018). In addition, the PRU develops and maintains open-access-cloud-based data repositories to enable stakeholders to reproduce the performance review results (Spinielli *et al.*, 2018) including, among other data, correlated position report (CPR) data and ADS-B position reports from FlightRadar24 live feed over Europe. Other open sources of ADS-B include the OpenSky Network. Several authors have used this source of data to develop their research. For instance, Olive *et al.* (2018) developed a method to analyze flight trajectories from OpenSky data, in order to detect unusual flight behaviors and infer air traffic control (ATC) actions. In this work, the trajectory outlier detection method was based on auto-encoder machine learning models. It determined trajectory outliers and quantified a level of abnormality, therefore giving hints about the nature of the detected situations. The authors also claim that trajectories from the OpenSky Network are unequally sampled and subject to errors happening in different steps of the acquisition chain: errors before the emission of data (imprecision in the positioning, quantification artifacts) and errors in the receiving and decoding of the data by feeders. In their work, a cascade of basic median filters was first applied to filter out irrelevant values from each individual trajectory.

Ryerson *et al.* (2014) evaluated fuel consumption for TMAs with a terminal inefficiency metric based on the variation in TMA fuel consumed across flights, reported by a major US airline. By using this metric, the authors quantified the additional fuel burn caused by ATM delays and terminal inefficiencies. Furthermore, Fricke *et al.* (2015) and Wubben & Busink (2000) analyzed the fuel savings of CDOs with respect to conventional procedures. The authors reported a reduction in fuel consumption of around 25-40% by flying CDOs.

Estimation of flight inefficiencies in terms of extra fuel burn—calculated based on the algorithm proposed by Chatterji (2011)—was considered in the scope of the APACHE project, a single european sky ATM research (SESAR) 2020 exploratory research project (Prats *et al.*, 2018b,a, 2019) mainly focusing on the en-route phase of flight. Similar techniques were applied in this chapter to estimate the fuel consumption of the descent phase in the TMA.

Classification and analysis of causes of airport delays was a topic of interest for many years. In early works (Allan *et al.*, 2001; Beatty *et al.*, 1999), weather uncertainties were mentioned as the main contributor to deviations in airport schedules. Furthermore, the inability of the ATM system—which limits the airport capacity—to meet the ever raising demand is also one the most significant influencing factors resulting in airport delays, as reported by Bai (2006).

Finally, Correia (2017) presented a detailed analysis of VFE and additional fuel burn at Lisbon Airport for the years 2014-2017 and compared statistics for several European airports, including Stockholm Arlanda, for the year 2017.

III.2 Methodology

In this chapter, the following PIs to capture inefficiencies within Stockholm TMA—some of them corresponding to KPIs proposed by the ICAO (ICAO, 2020)—are used:

- VFE during the descent phase, which includes:
  - Average distance flown in level flight (KPI19.1).
  - Average time flown in level flight (KPI19.2).
  - Percent of aircraft flying in level flight.
- Fuel-based PIs.

Figure III-1 presents a block diagram illustrating the methodology followed to compute the different PIs from historical-flights data.

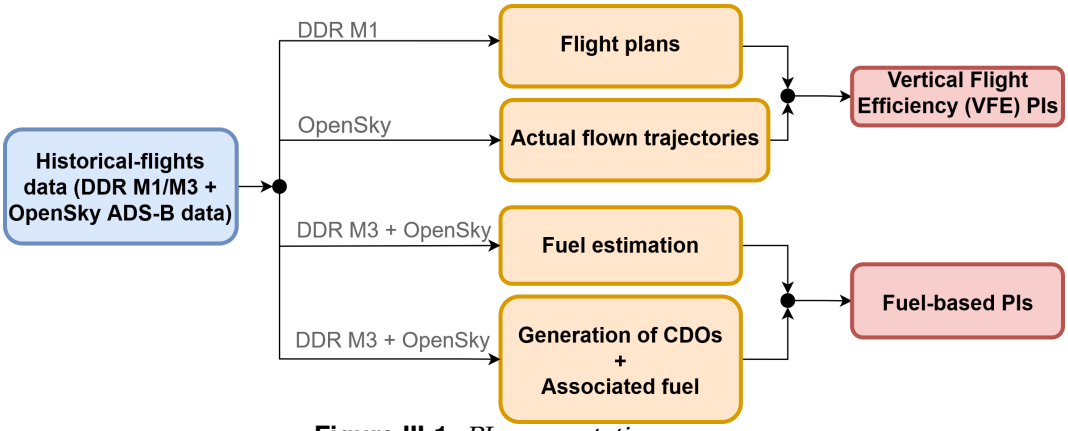

Figure III-1: *PIs computation process*

Two databases were used in this chapter in order to obtain historical-flights data: Eurocontrol's DDR (Eurocontrol, 2017) and the OpenSky Network (The OpenSky Network, 2019; Schäfer *et al.*, 2014). DDR contains flight-trajectory data in SO6 format, consisting of files with space-separated values. In this chapter, DDR data was used in two formats: SO6 M1 and SO6 M3. The M1 format is based on the last filed flight plan, while the M3 format corresponds to the actual flown trajectories. It is worth highlighting the fact that the actual flown trajectories that can be obtained from M3 files correspond to the M1 trajectories updated with available radar information whenever the flight deviates from its last filed flight plan by more than any of the pre-determined network manager operations centre (NMOC) thresholds (5 minutes, 7FL or 20NM) (Ivanov *et al.*, 2017). On the other hand, OpenSky contains historical ADS-B data and it supports two types of data: state vectors and tracks, being the latter a sub-set of the state vectors. The aircraft state vectors contain a summary of all tracking information at a series of points in different timestamps. OpenSky tracks do not contain all information about the flights the database keeps, but rather show the aircraft general movement pattern as a list of data samples, similar to Eurocontrol's DDR. OpenSky data also contains erroneous position records, as well as false altitude records, which were filtered out. For that purpose, similarly to what was proposed by Olive *et al.* (2018), a series of median filters were used.

In this chapter, the efficiency assessment was done only inside the Stockholm TMA. The point of the trajectory at which the aircraft entered the TMA was identified from the aforementioned historical-flights data, to be later used as the starting point for the PIs calculations—instead of the top of descent (TOD), which may lie outside of TMA. The several PIs were computed as follows:

- **VFE PIs**: data from DDR M1 files was used to obtain the last filed flight plans. Then, this data was compared with the data from actual flown trajectories, obtained from OpenSky (state vectors) ADS-B data. Aircraft in level flight inside the TMA were detected by using the techniques proposed by Eurocontrol (Peeters & Guastalla, 2017), with some minor changes. A segment in level flight was detected when a given aircraft was flying with a vertical speed below a certain threshold, which corresponded to 300 feet per minute in this experiment. In addition, the minimum time duration for a segment to be considered level flight was 30 seconds, amount of time which was subtracted from each level duration as suggested by Peeters & Guastalla (2017).
- **Fuel-based PIs**: these PIs capture inefficiencies on the tactical ATM layer in vertical domain, as discussed by Prats *et al.* (2019). In this chapter, the fuel consumption of CDOs—generated by solving the optimal control problem presented in Section III.3.2—was compared with the fuel consumption of actual flown trajectories, obtained from historical-flight data (DDR M3 and OpenSky tracks and state vectors ADS-B data). In order to generate the CDOs, the same route followed by the actual flown trajectories was used, which was different depending on the data source, and led to different distances to go. Finally, the computations followed to estimate the fuel consumption of actual flown trajectories are detailed in Section III.2.1.

III.2.1 Fuel Estimation

Fuel-based PIs are calculated by using the base of aircraft data (BADA) v4 aircraft performance model (APM). The first expression used, known as the total-energy model, equates the rate of work done by forces acting on the aircraft to the rate of increase in potential and kinetic energy, that is:

$$(T - D)v = mg\frac{\mathrm{d}h}{\mathrm{d}t} + mv\frac{\mathrm{d}v}{\mathrm{d}t}, \tag{III.1}$$

where T is the thrust acting parallel to the aircraft velocity vector, D is the aerodynamic drag, m is the aircraft mass, h is the geometric altitude, g is the gravitational acceleration and v is the true airspeed (TAS).

Three separate thrust models are proposed in BADA, depending on the engine type: turbofan, turboprop or piston. Each model includes the contribution from all engines and provides the thrust as a function of airspeed, throttle setting and atmospheric conditions. The general formula of the thrust force is:

$$T = \delta W_{mref} C_T, \tag{III.2}$$

where δ is the pressure ratio, m_{ref} is the reference mass—obtained from the Propulsive Forces Model (PFM)—W_{mref} is the weight force at m_{ref} and C_T is the thrust coefficient, which is a function of Mach number.

For the three engine types, BADA proposes different equations to compute C_T depending on the engine rating: maximum climb, maximum cruise, idle and no rating (direct throttle parameter input).

For estimation of the fuel consumption, BADA proposes once again a different model depending on the engine type, and also depending on the engine rating. Each model includes the contribution from all engines and provides the fuel consumption as a function of airspeed, throttle parameter and atmospheric conditions. The general formula for the fuel consumption, q, is:

$$q = \delta\theta^{\frac{1}{2}} W_{mref} a_0 L_{HV}^{-1} C_F, \tag{III.3}$$

where θ is the temperature ratio, a_0 is the speed of sound at standard sea level (SSL), L_{HV} is the fuel lower heating value (obtained from the PFM) and C_F is the fuel coefficient, which depends on T for non-idle ratings.

For each aircraft model, BADA provides an *xml* file with the corresponding aircraft performance data. For instance, the coefficients used to compute C_T are located in this file. With the equations stated above, and the *xml* files for each aircraft, it is possible to compute the fuel consumption of a trajectory. The process followed is detailed below:

- **Thrust computation**: if the aircraft is climbing, maximum climb rating is chosen and the corresponding thrust formula (depending on the engine type) is applied. If the aircraft is descending, an idle rating is assumed. In level-offs, the total-energy model (Eq. (III.1)) is used in order to compute the corresponding aircraft thrust.
- **Fuel consumption computation**: for non-idle ratings, the thrust computed in the previous step is used to obtain C_F. For descents, idle rating is assumed.

Furthermore, a 90% of the maximum landing weight (MLW) has been assumed at the final point of the trajectory for all aircraft.

III.3 Experimental Setup

The generic models introduced in Section II.1 are particularized in Section III.3.1. Analogously, the generic optimal control problem stated in Section II.2.1 is particularized in Section III.3.2 with specific cost function and constraints. Finally, Section III.3.3 presents the scenario and case studies considered in this chapter.

III.3.1 Models

The models required to formulate the optimization of the aircraft trajectory, which were presented in Section II.1, are particularized below for the experiment conducted in this chapter.

III.3.1.1 Aircraft Dynamics Model

The γ-*command* model described by Eq. (II.1) was used for the experiments conducted in this chapter. The following assumptions were also considered:

- The effect of the cross-wind on the ground speed is orders of magnitude below that of the longitudinal wind (i.e., $w_x = 0$).
- The longitudinal wind is a function of only the altitude (i.e., $w_s = w_s(h)$).
- The fuel consumption during an energy-neutral descent is a very small fraction of the total mass (Clarke *et al.*, 2004) and, consequently, the variations in mass m can be neglected (i.e., $\dot{m} = 0$). In spite of that, the idle fuel flow q_{idle} was indeed computed in the model to determine the amount of fuel consumption for each trajectory, which was used as a metric during the assessment of results.
- The aerodynamic flight path angle is assumed to be small (i.e., $\sin\gamma \simeq \gamma$ and $\cos\gamma \simeq 1$).

Under the aforementioned assumptions, Eq. (II.1) can be simplified to:

$$\begin{aligned}\frac{\mathrm{d}v}{\mathrm{d}t} &= \dot{v} = \frac{T_{idle}(v,h) - D(v,h,\gamma,\zeta)}{m} - g\gamma \\ \frac{\mathrm{d}s}{\mathrm{d}t} &= \dot{s} = v + w_s(h) \\ \frac{\mathrm{d}h}{\mathrm{d}t} &= \dot{h} = v\gamma,\end{aligned} \tag{III.4}$$

where ζ is the flaps/slats configuration. In this experiment, ζ is considered to be always *clean*.

In this widely known γ-*command* model, the state vector is $\vec{x} = [v, s, h]^T$. Furthermore, since neither additional thrust nor speed brakes use is allowed, the control vector is composed by only the aerodynamic flight path angle (i.e., $\vec{u} = [\gamma]$). Moreover, the thrust in Eq. (II.1a) is replaced by T_{idle}, which mathematical expression, function of $\vec{x}$, is particularized by the APM described in the next section.

III.3.1.2 Aircraft Performance Model

The BADA v4 APM was adopted for this experiment to model T_{idle}, T_{max}, C_D, q_{cr} and q_{idle}. As detailed in Section II.1.2, not all aircraft models are covered by BADA v4 so, in the experiment presented in this chapter, in the case the aircraft model considered did not correspond to any of the BADA models, a similar aircraft in terms of performance and dimensions was used.

III.3.1.3 Weather Model

In this experiment, the international standard atmosphere (ISA) model, established to provide a common reference for temperature and pressure, was considered to represent the normalized temperature θ and pressure δ as a function of h through Eqs. II.7 and II.8, respectively. Then, the normalized density was computed assuming the perfect gas law relationship with Eq. (II.9).

The longitudinal component of the wind (w_s) was modeled by a smoothing spline of the form:

$$w_s(h) = \sum_{i=1}^{n_c} c_i B_i(h) \tag{III.5}$$

where B_i, $i = 1, \ldots, n_c$, are B-spline basis functions and $\vec{c} = [c_1, \ldots, c_{n_c}]$ are control points of the spline (de Boor, 1972). It should be noted that the longitudinal wind has been modeled as a function of the altitude only, as done in similar works (de Jong *et al.*, 2014). The control points of the spline approximating the longitudinal wind profile are obtained by fitting historical weather data. In the experiment presented in this chapter, this data was obtained from gridded binary (GRIB) formatted files provided by the global forecast system (GFS) of the national oceanic and atmospheric administration (NOAA).

III.3.2 Optimal Control Problem Formulation

This section presents the optimization process followed in order to generate the (optimal) trajectories for the validation case studies of this chapter (simulated traffic). In real life, these trajectories would be generated by the flight management system (FMS). The adopted methodology is based on the semi-analytic approach described in Section II.2.2.

The dynamic constraints ($\vec{f}$) were particularized by the γ-*command* model given by Eq. (III.4):

$$\vec{f} = \begin{bmatrix} \dot{v} \\ \dot{s} \\ \dot{h} \end{bmatrix} = \begin{bmatrix} \frac{T_{idle}(v,h) - D(v,h,\gamma,\zeta)}{m} - g\gamma \\ v + w_s(h) \\ v\gamma \end{bmatrix}, \tag{III.6}$$

In this chapter, the trajectory considered covers the latter part of the cruise phase and the subsequent descent. It is assumed that the original cruise speed is maintained (and therefore, not subject to optimization). Yet, the fuel consumption in cruise is considered in the objective function, since the location of the TOD is indeed subject to optimization. This problem can be modeled as a single-phase optimal control problem that minimizes a compound function that takes into account both fuel and time costs, relating them with the cost index (CI). Expressing the cost function in Lagrange form:

$$J_a = \int_{t_0}^{t_f} -\left(\frac{q_{cr} + \text{CI}}{v_{cr}}\right)(v + w) + q_{idle} + \text{CI}\ \mathrm{d}t \tag{III.7}$$

where v_{cr} is the cruise speed (which is assumed to be constant), q_{cr} is the cruise fuel flow (which is assumed to be constant, since the cruise altitude and speed are also constant) and $q_{idle} : \mathbb{R}^{n_x} \to \mathbb{R}$ is the idle fuel flow in the descent (which depends on the speed and altitude).

In addition to the dynamic constraints $\vec{f}$, the following path constraints were enforced to ensure that the aircraft airspeed remains within operational limits; that the aircraft is not climbing and that a given minimum descent gradient is not exceeded:

$$\vec{h} = \begin{bmatrix} v_{CAS,min} - v_{CAS} \\ v_{CAS} - \text{VMO} \\ M - \text{MMO} \\ \gamma \\ \gamma_{min} - \gamma \end{bmatrix} \leq \begin{bmatrix} 0 \\ 0 \\ 0 \\ 0 \\ 0 \end{bmatrix} \tag{III.8}$$

where $v_{CAS} : \mathbb{R}^{n_x} \to \mathbb{R}$ is the callibrated airspeed (CAS) and $M : \mathbb{R}^{n_x} \to \mathbb{R}$ is the Mach number, both functions of the state vector and presented in Eqs. (II.5) and (II.4), respectively; $v_{CAS,min}$ and VMO are the minimum and maximum operative CAS, respectively; MMO is maximum operative Mach; and γ_{min} is the minimum descent gradient (recall it is a negative value).

For the optimization of the CDOs, the upper bounds on the speed limits (VMO and MMO), which are aircraft dependent, are obtained from the BADA v4 aircraft performance files; the minimum speed $v_{CAS,min}$ corresponds to the green dot speed[1]; and the maximum descent gradient (γ_{min}) was set to $-7°$, which represents a realistic operational value.

The initial state of the aircraft, consisting of the cruise altitude, cruise speed and distance to go at an hypothetical extended terminal maneuvering area (E-TMA) located at 250NM from the airport, is obtained directly from historical-flight databases, as mentioned in Section III.2. The final state corresponds to a speed equal to the green dot speed, an altitude equal to 2,000 feet and a distance to go equal to 0 NM.

III.3.3 Scenario and Case Studies

Stockholm-Arlanda airport was selected as the scenario for the experiments conducted in this chapter. Arlanda is the busiest airport in Sweden by number of passengers, ranked 17th among

[1]For aircraft in the Airbus family, the green dot speed is the minimum operating speed in managed mode and clean configuration, being approximately the best lift-to-drag ratio speed

all the European airports. In all the experiments performed in this chapter, the focus was made in the flights present in the Stockholm TMA, which is in charge of managing the arriving and departing traffic to Arlanda airport.

Arrival traffic to Stockholm-Arlanda airport for the year 2018 was used in order to conduct the experiments of this chapter. More specifically, all the aforementioned PIs were computed for the 2018 traffic, focusing only inside the Stockholm TMA. Regarding the fuel PIs, only the month of February of 2018 was considered.

III.4 Results

This section presents the results of the flight efficiency evaluation for the Stockholm-Arlanda airport arrivals during the year 2018. Section III.4.1 compares the two historical-flights databases used in the experiments of this chapter. Then, Section III.4.2 presents the results for the VFE evaluation. Finally, Section III.4.3 presents the results for the fuel-based PIs.

III.4.1 Eurocontrol's DDR vs. OpenSky Network ADS-B Data

The actual flown trajectories inside TMA for the VFE assessment were obtained from OpenSky states data. The OpenSky states data is very accurate as it provides data samples each second, while DDR has a lower data granularity. Figures III-2(a) and III-2(b) show an example of the vertical and lateral profiles of two randomly-chosen flights, obtained from DDR M3 data and OpenSky data (both tracks and states) for comparison.

The difference between OpenSky states and OpenSky tracks is clearly shown in Figure III-2(a). Although OpenSky tracks, as claimed by the OpenSky developer team, are a subset of OpenSky states, it was clearly not the case in this example.

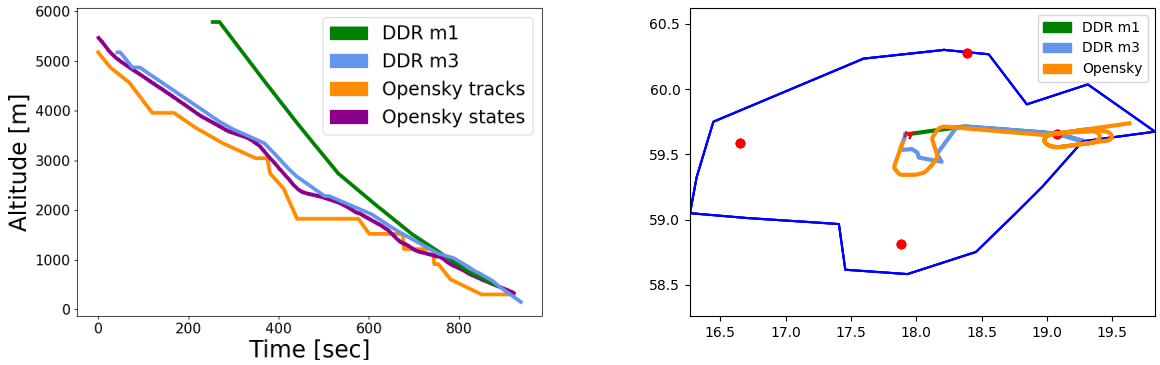

(a) Vertical profile for flight *SAS410* (January 01, 2018). (b) Lateral profile for flight *SAS964* (February 26, 2018).

Figure III-2: *Comparison of DDR and OpenSky data: vertical and lateral profiles for arrival flights in Stockholm-Arlanda-airport TMA*

Figure III-2(b) depicts a series of non-optimal paths within TMA during a day with bad weather in Arlanda airport. OpenSky reflects holding patterns, while DDR only sketches the resulting path. Finally, Figure III-3 clearly confirms that OpenSky provides more accurate aircraft tracking: while DDR shows the aircraft landed on one runway, the last segments of OpenSky data correspond to the other runway in Arlanda airport, with a higher number of data samples.

It can be concluded that OpenSky states data is more suitable for reconstruction of the flight

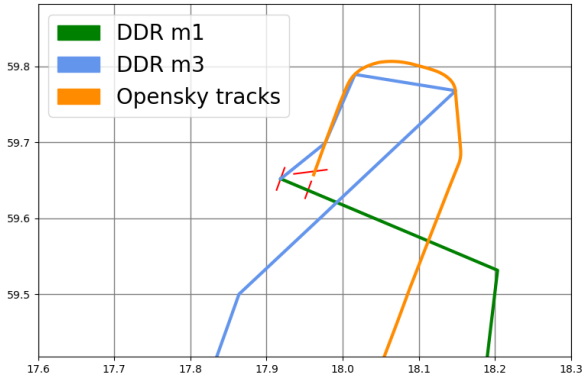

Figure III-3: *Lateral profile of the arrival flight with callsign SAS410 in Stockholm Arlanda airport TMA from DDR and OpenSky data on January 01, 2018.*

trajectories both in vertical and lateral domains. However, the computations based on such a dense data are very memory consuming; still, the computational times were manageable as only the portion of flight inside the TMA was considered when computing the VFE and fuel-based PIs. For tasks requiring a lower number of data samples, tracks would be a good data source, but current methods used for extracting tracks need to be refined.

III.4.2 Vertical Flight Efficiency (VFE)

Vertical inefficiencies during the descent phase are caused, in general, when aircraft do not fly CDOs, which allow aircraft to fly efficient descent trajectories that minimize fuel consumption, gaseous emissions and noise nuisance. For instance, air traffic control officers (ATCOs) could issue vector instructions that could cause aircraft to perform a level flight at intermediate altitudes before landing. In such a case, the fuel consumption would significantly increase, leading to a vertical-inefficient descent.

The results for the several PIs are summarized in Table III-1, where n_{arr} is the number of

Table III-1: *Vertical Efficiency of Stockholm Arlanda Airport Arrivals During the Year 2018*

Months in 2018	n_{arr}	P [%]	L_{avg}	$KPI19.1$ [NM]	$KPI19.1$ [%]	σ_D [NM]	$KPI19.2$ [min.]	$KPI19.2$ [%]	σ_T [min.]
01	7721	55	1.00	2.80	5	4.62	0.72	5	1.11
02	7419	52	0.87	2.72	4	4.90	0.70	5	1.18
03	8131	56	1.08	2.99	5	4.79	0.77	6	1.17
04	8944	54	1.00	2.77	4	4.97	0.69	5	1.16
05	9552	50	0.88	2.22	4	4.73	0.52	4	1.01
06	8923	51	0.90	2.68	4	4.61	0.69	5	1.12
07	8426	46	0.68	2.38	4	4.21	0.61	4	1.02
08	8915	47	0.73	2.25	3	3.95	0.56	4	0.94
09	8779	48	0.79	2.28	3	4.03	0.59	4	1.00
10	9162	51	0.80	2.40	4	4.10	0.64	4	1.04
11	8558	41	0.59	1.91	3	3.71	0.49	3	0.91
12	6954	49	0.73	2.68	4	5.21	0.71	5	1.25

arrival flights, P the percent of aircraft with at least one segment in level flight, L_{avg} the average number of segments in level flight per flight, *KPI19.1* ([NM]) the average distance flown in level flight, *KPI19.1* ([%]) the average percent of distance flown in level flight, σ_D the standard deviation of distance flown in level flight, *KPI19.2*[min.] the average time flown in level flight, *KPI19.2*[%] the average percent of time flown in level flight and σ_T the standard deviation of time flown in level flight.

According to Eurocontrol's performance review report for year 2018 (Performance Review Comission, 2018), the average time flown in level flight during descents was 1.1 minute at Arlanda in 2018, which does not contradict the results presented in this chapter. This report also stated that the VFE during climb and descent at the top 30 airports remained in 2018 at the same level as in 2017. Thus, it can be concluded that the share of CDOs during descent at Arlanda was approximately 50% (Performance Review Comission (2017)), which aligns with the results obtained in this chapter.

III.4.3 Fuel-based PIs

Additional fuel burn was computed per day for all Arlanda airport arrivals during the month of February, 2018. Figure III-4 illustrates the results.

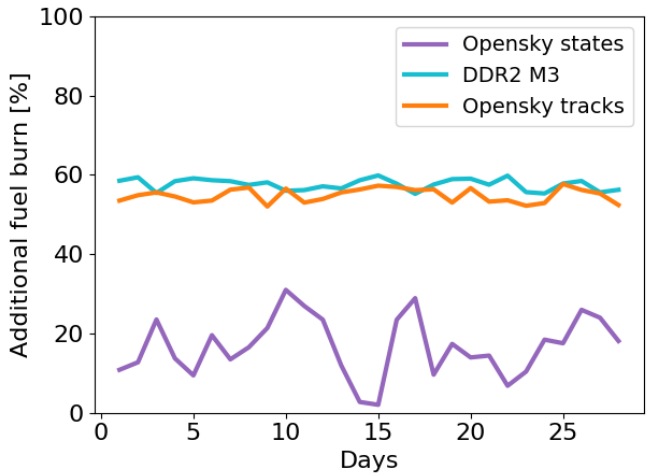

Figure III-4: *Additional fuel burn (in %) in the TMA of actual flown trajectories with respect to CDOs (values per day February 2018).*

While the fuel consumption obtained for the actual flown trajectories was higher in OpenSky tracks than in DDR M3 (usually the difference was between 1% and 10%), the additional fuel burn with respect to CDOs, depicted in Figure III-4, remains almost the same. Results demonstrate that CDOs may provide a reduction of fuel consumption between 55% and 60% if actual flown trajectories are obtained from DDR M3 or OpenSky tracks, which constitutes a significant inefficiency of the vertical profiles actually flown. It is important to recall that only fuel inside the TMA was considered; if the whole descent was compared, the difference would have been lower, as level-offs at lower altitudes are more detrimental for efficiency than those at higher altitudes.

Regarding OpenSky states, however, the reduction in fuel consumption was much less, from between 5% and 30% depending on the day, which is a more realistic result as the data obtained from OpenSky states is more accurate.

The absolute values for the fuel consumption for both actual flown trajectories (i.e., DDR M3 and OpenSky data) and CDOs are shown in Figure III-5.

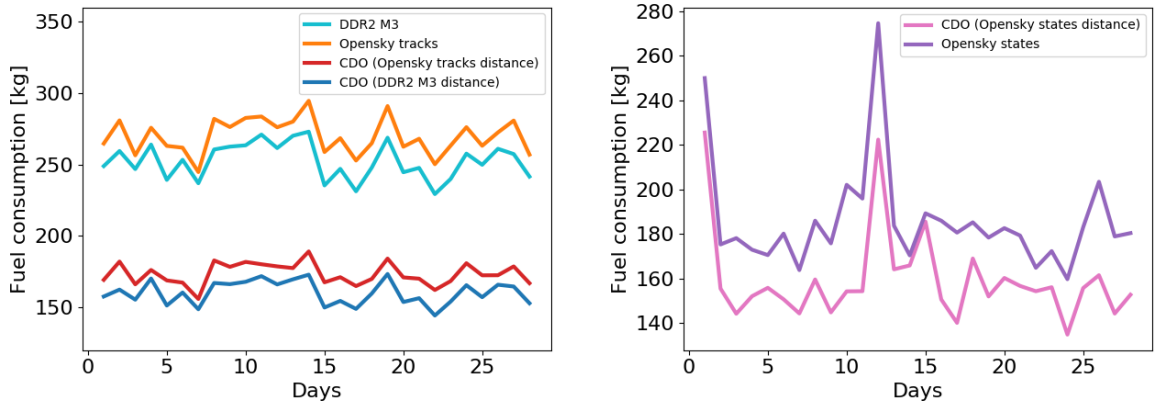

(a) DDR M3 and OpenSky tracks

(b) OpenSky states

Figure III-5: *Average fuel burn (in kg) in the TMA of actual flown trajectories and of CDOs (values per day of February 2018).*

Fuel consumption suffers significant changes throughout the month. The fuel calculation took into account wind components, which demonstrated the impact on the efficiency of vertical profiles. Indeed, the results confirm a decrease in fuel consumption during days with low wind gust values reported, and an increase in fuel consumption during the days with the highest wind gust measurements, as reported by Lemetti *et al.* (2019a).

Regarding the data being used as actual flown trajectories, DDR data, as expected, was not very accurate for fuel computations inside the TMA, as it tends to provide very few segments (around 10 to 15 data samples) if compared with OpenSky data. On the other hand, OpenSky tracks are not as accurate as OpenSky states. More levels can be found in tracks than in states (Figure III-2(a)), which increases the fuel consumption. However, tracks have a lower amount of data samples, which reduces significantly the computation time. While the fuel consumption computation time for tracks could be around 10 seconds for 1 trajectory, the computation time for states could reach up to 2 minutes in some cases.

Better data granularity of OpenSky makes it a better option to estimate fuel consumption inside TMA, as well as for VFE assessments. While DDR usually provides only 10 to 15 segments inside TMA, in OpenSky tracks there are about 60-80 data samples (depending on the trajectory), which makes it more reliable. However, there are also some errors in OpenSky data, which led to very high and unrealistic fuel consumption values. Several data outliers were found in OpenSky tracks. For instance, in some trajectories there were repeated data samples, even with the time advancing (which would mean the aircraft remained still, which is not possible). There were also data samples with erroneous values for latitude and longitude, and some of the speed values that could be extracted from OpenSky tracks were wrong too. Therefore, all those outliers need to be filtered.

Another drawback of the OpenSky data is the lack of flight identifier and aircraft type information, needed for the calculation of fuel consumption. This problem was solved by merging the data with DDR flight plans (obtained from M1 files). Regarding OpenSky states, there are even more data points, one each second, so the data is even more accurate. However, the time it takes to compute the fuel consumption was higher than in OpenSky tracks, up to 2 minutes in some cases. As it happens with OpenSky tracks, OpenSky states contain some outliers that need to be filtered.

III.5 Discussion

In this chapter, the flight efficiency of Stockholm-Arlanda airport arrivals was evaluated by using two different sources of flight trajectories historical data: OpenSky Network data and Eurocontrol's DDR. Although OpenSky has certain problems with data integrity and additional methods to detect and filter the different kinds of integrity breaches are needed, it provides data with high granularity in form of state vectors with accurate three-dimensional (3D) aircraft positions along with precise timestamps for aircraft trajectories. Thus, OpenSky state vectors—after a preprocessing—could be considered the preferred data source for efficiency assessments within TMA.

By using OpenSky states, fuel savings of up to 30% were obtained by flying energy-neutral CDOs. However, it is worth remarking the fact that sometimes, depending on the traffic demand, it is difficult to apply this kind of trajectories. The application of CDOs in the current ATM system will be assessed in the following chapters.

Further analysis of the performance of Stockholm-Arlanda airport arrivals, which are out of the scope of this PhD thesis, were presented in the following publications:

- Lemetti *et al.* (2019b) presented an evaluation of punctuality, vertical efficiency and additional fuel burn
- Lemetti *et al.* (2019a) analyzed the impact of different weather phenomena on arrival punctuality and VFE

La sapienza è figliola della sperienzia.
[Wisdom is the daughter of experience.]

— Leonardo da Vinci

IV

Achieving RTAs outside the Energy-Neutral Time Window: Energy-Neutral CDOs vs. Powered Descents

Given a merging fix, if the required time of arrival (RTA) is assigned close to the estimated time of arrival (ETA) of the original planned (idle-thrust) trajectory at that fix, the aircraft will be able to adapt the trajectory and still fly an energy-neutral continuous descent operation (CDO) (i.e. idle thrust and without using speed brakes). Moreover, as shown by Dalmau & Prats (2017b), aircraft would still be able to adapt their descent trajectory—in order to keep flying the energy-neutral CDO—even if the RTA is updated when the descent has been already initiated. Nevertheless, regardless of whether the aircraft has started the descent, there are certain aircraft energy states (i.e., altitude/speed conditions) that, depending on the assigned RTA, will not enable the execution of an energy-neutral CDO. Furthermore, depending on the terminal maneuvering area (TMA) size and the density of traffic, it might be necessary to assign RTAs significantly differing from the ETA. In such a case, it might not be always possible to build an aircraft arrival sequence by only

This chapter is based on the following publications:

- Sáez, R. & Prats, X.. 2021. Achieving RTAs outside the Energy-Neutral Time Window of Nominal Aircraft Descents - Fuel Consumption of Powered Descents along Published Routes vs. Neutral CDOs along Pre-Defined Routes. Submitted to *Transportation Research Part C: Emerging Technologies*.
- Sáez, R. & Prats, X.. 2020 (Jun.). Comparison of Fuel Consumption of Continuous Descent Operations with Required Times of Arrival: Path Stretching vs. Powered Descents. *In: 9th International Conference on Research in Air Transportation (ICRAT)*. Virtual Event: EUROCONTROL/FAA.

using RTAs that lead to energy-neutral CDOs, as reported for instance by Pawelek *et al.* (2019).

One of the recommendations of the single european sky ATM research (SESAR) and next generation air transportation system (NextGen) programs in order to improve the predictability and efficiency of TMA operations, is to limit the use of radar vectoring when sequencing and merging aircraft—i.e. heading instructions issued by the air traffic control officer (ATCO) to tactically stretch the path flown). Radar vectoring is detrimental for the efficiency of the flights, as the flight management system (FMS) of the arriving aircraft is not aware of the remaining distance to the landing runway and, thus, cannot compute the optimal descent profile. Therefore, in a trajectory based operations (TBO) environment, it is envisaged to fly the published arrival route in the TMA, or to up-link a new (closed) route to the FMS as part of the TBO tactical trajectory renegotiation process.

This chapter compares two strategies to effectively sequence arrival traffic when not all aircraft can fly energy-neutral CDOs following the published route: i) aircraft flying the published route but with descents requiring thrust or speed brake usage to comply with the RTA (i.e., powered descents); and ii) aircraft flying predefined (up-linked) shorter or longer arrival routes that enable energy-neutral CDOs, while meeting the same RTA.

A concept of operations (CONOPs) is formulated in order to better understand the applicability and impact of the concept presented in this chapter in a future TBO-enabled paradigm. Furthermore, the trajectory optimizer considered in this chapter—used to generate the (optimal) simulated trajectories for the validation scenarios—was designed in order to provide trajectories closer to those applied in real air traffic operations, where energy-neutral CDOs are computed beyond the metering fix, all the way down to the final approach point (FAP). Finally, this chapter analyzes the sensitivity of the fuel consumption for both strategies to different parameters, such as the wind speed, cruise altitude and aircraft characteristics.

The work presented in this chapter is expected to be valuable when designing future ground-support tools that will help ATCOs to efficiently manage arrival flows of traffic under the TBO paradigm, where advanced synchronization mechanisms between ground and airborne tools are expected. In addition, this chapter will help to better understand the behavior of aircraft in the arrival phase of the flight, as well as to provide a comprehensive explanation regarding some of the causes that could potentially improve or degrade the fuel consumption during this phase.

IV.1 State of the Art

To the best of our knowledge, no other works analyzed the trade-offs between the two strategies aforementioned to fulfill RTAs not enabling energy-neutral CDOs for the published route. Dalmau *et al.* (2017) dealt with the computation of fuel consumption for energy-neutral CDOs and powered descents, but without focusing on which strategy would be better for different RTAs. Similarly, Nikoleris *et al.* (2016) quantified fuel consumption for descent trajectories with an assigned RTA later than the ETA at the metering fix. However, they did not focus on CDOs specifically.

Other works dealt with time-based CDOs, but without considering sub-optimal trajectories that could be flown with an RTA assigned outside the energy-neutral time window. For instance, De Prins *et al.* (2011) proposed a methodology to implement time-based CDOs in high-density scenarios, where advanced four-dimensional (4D) guidance methods would be required to fly the generated trajectory plan by the FMS. Similarly, Helmke *et al.* (2009) also studied the concept of time-based arrival management; they successfully developed a new 4D arrival manager (AMAN) which could be used for managing time-based CDOs in terminal airspace.

Finally, Vilardaga & Prats (2015) did a similar study, but focusing on departures. The authors aimed at the quantification—in terms of fuel and time consumption—of implementing sub-

optimal trajectories in a 4D trajectory context where RTAs at specific navigation fixes were used.

IV.2 Concept of Operations

This section describes the CONOPs proposed in this chapter. Section IV.2.1 presents a general description of the CONOPs, while Section IV.2.2 focuses on the particular case where RTAs are notified to the aircraft when they are already descending.

IV.2.1 Concept of Operations: General Description

Let us assume an aircraft approaching its destination airport. Well before the top of descent (TOD), while still in cruise, the ATCO requests the aircraft to compute its arrival time window at a given metering fix. This time window is defined as the difference between the earliest and the latest time of arrival at that fix (RTA_E and RTA_L), which are assumed to be computed by the FMS of the incoming aircraft by considering the earliest and latest trajectories.

The width of this time window depends on several factors, e.g. the aircraft performance, weather conditions, etc. However, the aircraft can also manage the width of the time window by following different descent strategies. Energy-neutral CDOs (or simply neutral CDOs) are defined as idle thrust and no speed brakes descents, while non-neutral (or powered) descents allow the use of thrust and speed brakes. This translates into a higher flexibility with respect to neutral CDOs, which leads to wider time windows, but at the expense of increasing the fuel burnt and/or noise nuisance. As a result, in this chapter, two time windows are considered: the neutral and powered time windows, which are both downlinked by the aircraft to the ATCO. These windows are depicted in Figure IV-1 as the difference between the neutral/powered arrival times, i.e., $[RTA_{E_n}, RTA_{L_n}]$ and $[RTA_{E_p}, RTA_{L_p}]$, respectively.

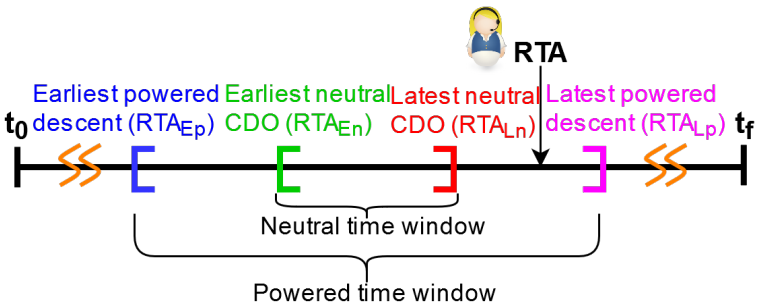

Figure IV-1: *Neutral and powered time windows if the published route is flown*

In addition to the neutral and powered time windows, the aircraft sends to the ATCO its ETA at the metering fix. While the earliest and latest times of arrival at the metering fix mainly depend on aircraft performance, flight envelope and weather conditions; the ETA at the same fix is also dependent to optimization considerations for that particular flight, including airline and flight crew policies, such as setting a cost index (CI) for that descent.

After receiving the two time windows and the ETA, ATCOs can assign an RTA at the metering fix to all arriving aircraft while they are still in cruise. Thus, each on-board FMS can compute the optimal CDO that complies with the RTA. Ideally, the RTA should lie inside the neutral time window, in order to minimize the environmental impact of the descent trajectory. As mentioned before, this chapter explicitly focuses on those cases that traffic congestion does not permit to fly neutral CDOs. Thus, as depicted in Figure IV-1, it is assumed the ATCO will assign an RTA outside the neutral time window, either before or later than RTA_{E_p} or RTA_{L_p}, respectively. In

order to comply with this RTA outside the neutral window, two strategies are considered:

- **Scenario 1 - Powered descents and published route**: aircraft fly the descent published route. In addition, the trajectory can be controlled by means of either additional thrust or speed brakes.
- **Scenario 2 - Neutral CDOs and predefined routes with a variable distance**: aircraft can fly a shorter or longer descent route (i.e. distances to go different than the published route) while keeping the descent at idle thrust and with no speed brakes usage.

Figure IV-2 depicts the vertical and lateral profiles of scenario 1 in a simplified way, where an aircraft is approaching a given airport where only one arrival route, corresponding to the published route, is available (i.e., one distance to go). The neutral and powered time windows at the metering fix down-linked to the air traffic control (ATC) are shown in the figure for a given distance $D_{\text{published}}$. The TOD for the earliest neutral trajectory is further (or closer to the metering fix) than the TOD for the latest neutral trajectory, as aircraft can fly at higher speeds during the cruise phase. As it will be seen in Section IV.3, the TOD for the earliest and latest powered trajectories is typically further from the landing runway than those of the neutral trajectories, as aircraft can fly at altitudes different from the cruise altitude where faster and lower speeds are achievable, respectively (see also Figure IV-5).

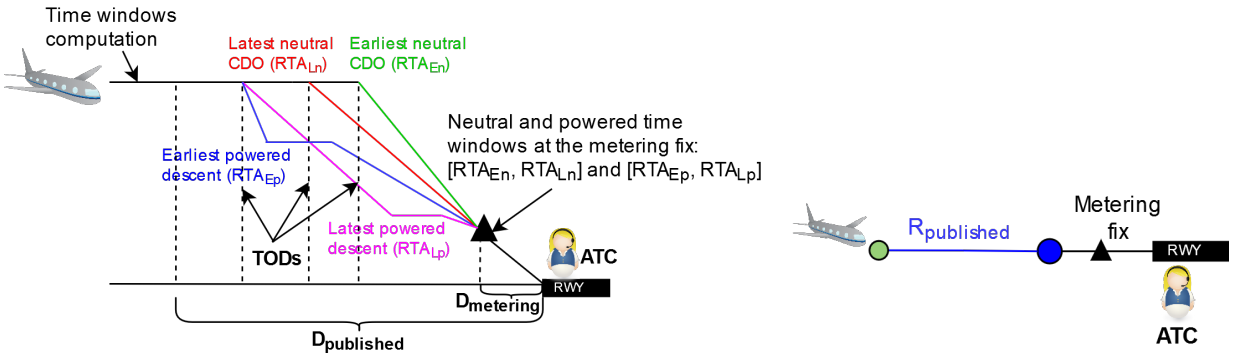

(a) Vertical profile (b) Lateral profile

Figure IV-2: *Scenario 1 - Powered descents flying the published route (procedure)*

The vertical and lateral profiles of scenario 2 are depicted in a simplified way in Figure IV-3. In this case, it is assumed that ATC could negotiate with the aircraft the assignment of a longer or shorter route, different from the published route $R_{\text{published}}$ (with an associated distance $D_{\text{published}}$). In order to illustrate this, a finite set of available arrival routes—$R_0, ..., R_n$, with associated distances to go $D_0, ..., D_n$—are defined. In this chapter, the arrival route is considered to be pre-negotiated before the TOD, as discussed by Sáez *et al.* (2020b), so the FMS could know the remaining distance to go when the RTA is assigned at the metering fix.

Finally, in both scenarios, the distance from the metering fix—where the RTA is assigned—to the runway ($D_{metering}$ in Figure IV-3) remains the same.

IV.2.2 RTA Assignment or Update in Descent

In the previous section, it was assumed the aircraft was still in the cruise phase when the ATCO uplinked the RTA. However, in real operations, this RTA could also be assigned or updated when the aircraft is already descending. This is particularly common for small TMAs, where the communication with the ATC might start later.

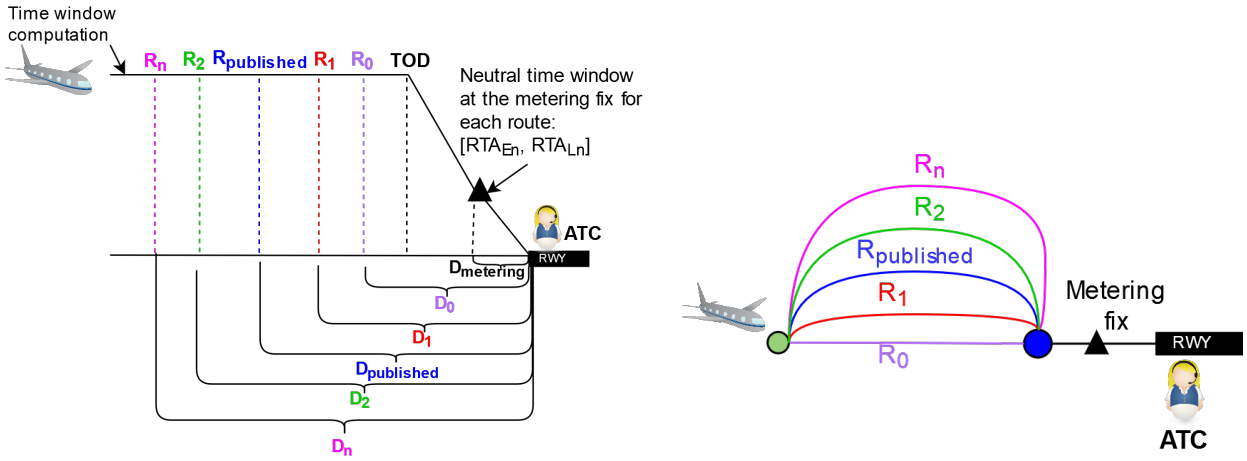

(a) Vertical profile (b) Lateral profile

Figure IV-3: *Scenario 2 - Neutral CDO flying longer/shorter predefined (up-linked) routes*

For any given route (as depicted in Figure IV-4)—with an associated distance to go (D_i)—and cruise altitude (h_{cruise}), the aircraft computes its time window at the metering fix ($t\_window_{initial}$). In such a case, in order to arrive at different times at the metering fix, the aircraft could adapt its trajectory both during the remaining part of the cruise phase and during the whole descent, leading to large time windows. On the other hand, once the aircraft starts the descent, it is no longer possible to adapt the trajectory during the cruise phase. Still, as reported by Dalmau & Prats (2017b), the time window at the metering fix is not negligible at this point (even for neutral CDOs). However, the lower the altitude, the shorter the time window ($t\_window_1, ..., t\_window_n$). Furthermore, the aircraft energy state (altitude and speed conditions) also affects the size of this time window.

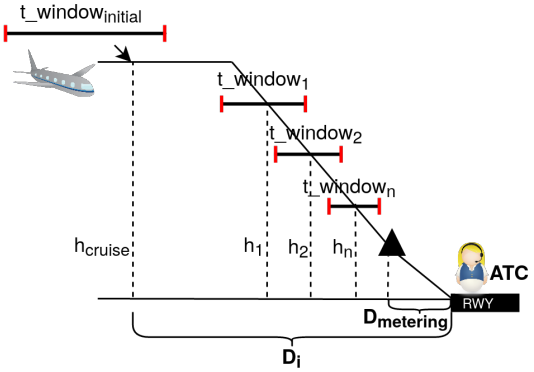

Figure IV-4: *Time windows for already initiated descents*

If the ATCO updates the RTA at the metering fix while the aircraft is already descending, the aircraft could still adapt its trajectory—and follow the published route—providing this RTA falls within the powered time window. Furthermore, it would still be possible to fly an energy-neutral CDO along a shorter or longer route in order to fulfill this RTA. However, in this case, the aircraft could not use additional thrust nor speed brakes to adapt the trajectory. This is different from the previous situation (for RTAs notified in cruise), where even in the neutral case, the aircraft, while still in the cruise phase, could still use thrust, speed brakes and/or modify the TOD in order to comply with the RTA.

IV.3 Experimental Setup

This section presents the experimental setup used to illustrate the CONOPs and methodology proposed in this chapter. The generic models introduced in Section II.1 are particularized in Section IV.3.1. Analogously, the generic optimal control problem stated in Section II.2.1 is particularized in Section IV.3.2 with specific cost function and constraints. Finally, the experiments performed in this chapter are described in Section IV.3.3, where the several independent variables considered in the sensitivity study are detailed.

IV.3.1 Models

The models presented in Section II.1 are particularized below for the experiment conducted in this chapter.

IV.3.1.1 Aircraft Dynamics Model

A variant of the γ-*command* model described by Eq. (III.4) was implemented in the trajectory planner. Different from typical formulations, the independent variable in this problem is the distance to go (s) and not the time (Dalmau *et al.*, 2019b). The selection of s as the independent variable is driven by the fact that during an ideal CDO, with no intervention from ATC except for the assignment of the RTA, the aircraft will follow a "closed route", and therefore the remaining distance to go will be always known by the FMS. In addition, this formulation replicates how constraints are defined in the current operational environment, thereby enabling more precise modeling of the constraints.

In the distance-based γ-*command* model, the state vector is $\vec{x} = [t, v, h, m]$, which is composed of time, true airspeed (TAS), geometric altitude and mass; the control vector $\vec{u} = [\gamma, T, \beta]$ is composed of the aerodynamic flight path angle, engine thrust, and speed brakes deflection. The flight path angle is the control that is used by the aircraft to modulate energy (i.e., exchange potential energy for kinetic energy and vice-versa), whereas thrust and speed brakes are used to add and remove energy from the system, respectively. The dynamics of $\vec{x}$ are expressed by the following system of ordinary differential equations (ODEs):

$$\begin{aligned}
\frac{\mathrm{d}t}{\mathrm{d}s} &= t' = \frac{1}{v\cos\gamma + w_s(h)} \\
\frac{\mathrm{d}v}{\mathrm{d}s} &= v' = \left(\frac{T - D(v,h,\gamma)}{m}) - g\sin\gamma\right)\frac{1}{v\cos\gamma + w_s(h)} \\
\frac{\mathrm{d}h}{\mathrm{d}s} &= h' = \frac{v\sin\gamma}{v\cos\gamma + w_s(h)} \\
\frac{\mathrm{d}m}{\mathrm{d}s} &= m' = \frac{-q(v,h,T)}{v\cos\gamma + w_s(h)}.
\end{aligned} \tag{IV.1}$$

Finally, w_x was neglected in this experiment, as the effect of the cross-wind on the ground speed is orders of magnitude below that of the longitudinal wind.

IV.3.1.2 Aircraft Performance Model

The base of aircraft data (BADA) v4 aircraft performance model (APM) was adopted for the experiments conducted in this chapter, like in Chapter III. However, in this case, the contribution of the speedbrakes was also taken into account. This contribution is modeled as an extra linear term $C_{D_\beta}\beta$ in the generic BADA v4 drag coefficient model, where C_{D_β} is a coefficient representing the increase in drag coefficient for unit of speed brakes deflection (equal to 0.03 in BADA v4).

IV.3.1.3 Weather Model

This study aimed to be as generic as possible. Accordingly, the international standard atmosphere (ISA) model, established to provide a common reference for temperature and pressure, was considered to represent the normalized temperature θ and pressure δ as a function of h through Eqs. (II.7) and (II.8), respectively. Then, the normalized density was computed assuming the perfect gas law relationship with Eq. (II.9).

With the same rationale, the empirical Hellman model defined by Eq. (II.10) was used to represent the wind speed as a function of h. The parameters of this empirical model were particularized as follows: $\alpha = 1/7$, which is the typical value for neutral stability conditions (Kaltschmitt *et al.*, 2007); h_r was set to 35,000 ft; and different values of w_r were analysed to assess the sensitivity of the fuel consumption to the longitudinal wind speed for the two strategies considered in this chapter (see Section IV.3.3 for the detailed list of case studies). In addition, the wind vector was assumed to point in the direction of the aircraft track (i.e., $w_s = |\vec{w}|$).

IV.3.2 Optimal Control Problem Formulation

The optimization process presented in this chapter is a multi-phase, constrained and non-linear optimal control problem, as described in Section II.2.1. This section particularizes the cost function and the dynamic, path algebraic and/or interior point constraints for each one of the phases composing the flight profile.

The dynamic constraints ($\vec{f}$) were particularized by the γ-*command* model given by Eq. (IV.1):

$$\vec{f}_j = \begin{bmatrix} 1 \\ \frac{T - D(v,h,\gamma)}{m} - g\sin\gamma \\ v\sin\gamma \\ -q(v,h,T) \end{bmatrix} \frac{1}{v\cos\gamma + w_s(h)}; \; j = 0, \ldots, P-1, \tag{IV.2}$$

where $D : \mathbb{R}^{n_x \times n_u} \to \mathbb{R}$ is the aerodynamic drag; g is the gravity acceleration and $q : \mathbb{R}^{n_x \times n_u} \to \mathbb{R}$ is the fuel flow.

Constraints are required to model the vertical profile. In order to accomplish that, the descent was divided in $P = 9$ different phases from the last part of cruise prior to the TOD until the runway, with associated phase-dependent path constraints, along with algebraic and/or interior-point constraints. The continuous optimal control problem is discretized into $N = 90$ time samples, with more time samples assigned to longer phases (e.g., Phase 1 , Descent above FL100). A higher number of time samples (shorter interval duration) results in a more accurate solution, but at the expense of a higher computational time. It should be noted that nominal flap/slat (and landing gear) transitions are also considered, which have been modeled as independent trajectory phases where the aerodynamic drag model of Eq. (IV.1) is changed accordingly.

Table IV-1 wraps up these phases and their associated constraints and time samples, where $M : \mathbb{R}^{n_x} \to \mathbb{R}$ is the Mach number (defined in Eq. (II.4)); $v_{CAS} : \mathbb{R}^{n_x} \to \mathbb{R}$ is the callibrated airspeed (CAS) (defined in Eq. (II.5)); MMO and VMO are the maximum operative Mach and CAS, respectively; GD is the green dot speed; h_{cruise} is the cruise altitude; V_{FE_1}, V_{FE_2}, V_{FE_3} and $V_{FE_{FULL}}$ correspond to the maximum flap-extended speeds, which are the highest speed permissible with wing flaps in configuration 1, 2, 3 and full, respectively; and V_{REF} is the landing reference speed.

The vertical profile defined in Table IV-1 considers a 250kt speed limitation below FL100, which is used in many TMAs. In addition, it is considered that the RTA is set at a hypothetical metering fix at an altitude of 3,000ft above aerodrome level (AAL). A hypothetical FAP—where the instrumental landing system (ILS) glide slope is intercepted—was defined at an altitude of

Table IV-1: *Phases and associated constraints from cruise phase to the runway for a generic arrival procedure*

Phase	N	$\vec{b}_j^{in}$	$\vec{b}_j^{eq}$	$\vec{\vartheta}_j^{in}$	$\vec{\vartheta}_j^{eq}$
0 (CRUISE)	15	$\begin{bmatrix} M - \text{MMO} \\ v_{CAS} - \text{VMO} \\ GD - v_{CAS} \end{bmatrix}$	$\begin{bmatrix} h - h_{cruise} \\ \gamma - 0.0° \end{bmatrix}$	-	-
1 (DESCENT ABOVE FL100)	30	$\begin{bmatrix} M - \text{MMO} \\ v_{CAS} - \text{VMO} \\ GD - v_{CAS} \end{bmatrix}$	-	$\begin{bmatrix} v_{CAS} - 250\,\text{kt} \\ GD - v_{CAS} \end{bmatrix}$	$\begin{bmatrix} h - 10,000\,\text{ft} \end{bmatrix}$
2 (DESCENT BELOW FL100)	15	$\begin{bmatrix} v_{CAS} - 250\,\text{kt} \\ GD - v_{CAS} \end{bmatrix}$	-	$\begin{bmatrix} v_{CAS} - V_{FE_1} \end{bmatrix}$	$\begin{bmatrix} h - 3,000\,\text{ft} \\ t - RTA \end{bmatrix}$
3 (CONF 1)	5	$\begin{bmatrix} v_{CAS} - V_{FE_1} \end{bmatrix}$	-	$\begin{bmatrix} v_{CAS} - V_{FE_2} \end{bmatrix}$	-
4 (CONF 2)	5	$\begin{bmatrix} v_{CAS} - V_{FE_2} \end{bmatrix}$	-	$\begin{bmatrix} v_{CAS} - V_{FE_3} \end{bmatrix}$	$\begin{bmatrix} h - 1,800\,\text{ft} \end{bmatrix}$
5 (CONF 3)	5	$\begin{bmatrix} v_{CAS} - V_{FE_3} \end{bmatrix}$	$\begin{bmatrix} \gamma - 3.0° \end{bmatrix}$	$\begin{bmatrix} v_{CAS} - V_{FE_3} \end{bmatrix}$	-
6 (CONF 3 GEAR DOWN)	5	$\begin{bmatrix} v_{CAS} - V_{FE_3} \end{bmatrix}$	$\begin{bmatrix} \gamma - 3.0° \end{bmatrix}$	$\begin{bmatrix} v_{CAS} - V_{FE_{FULL}} \end{bmatrix}$	-
7 (CONF FULL)	5	$\begin{bmatrix} v_{CAS} - V_{FE_{FULL}} \end{bmatrix}$	$\begin{bmatrix} \gamma - 3.0° \end{bmatrix}$	$\begin{bmatrix} v_{CAS} - V_{FE_{FULL}} \end{bmatrix}$	-
8 (LANDING)	5	$\begin{bmatrix} v_{CAS} - V_{FE_{FULL}} \end{bmatrix}$	$\begin{bmatrix} \gamma - 3.0° \end{bmatrix}$	-	$\begin{bmatrix} h - 50\,\text{ft} \\ v_{CAS} - V_{REF} \end{bmatrix}$

1,800 ft AAL, at the end of phase 4. From phase 5 on, the aircraft follows a trajectory with a constant flight path angle equal to -3 degrees.

While the phases defined in Table IV-1 may work for the great majority of conventional aircraft models, the values for some of the constraints of these phases may differ depending on the aircraft. For instance, the values for MMO and VMO are aircraft model dependent, as well as the values for the maximum flap-extended speeds.

The values for VMO, MMO and flap speeds are obtained from the BADA v4 global parameters file for a specific aircraft model. Furthermore, additional thrust and the use of speed brakes (T and β, respectively) are only allowed for powered descents, while T_{idle} and q_{idle} are imposed all along the descent down to the FAP for neutral trajectories. For the remainder of the descent, for both neutral and powered descents, the aircraft thrust T is left free between T_{idle} and T_{max}, which is also a function of M, τ and p. Thus, the aircraft can keep a reasonable deceleration rate while flying the glide slope. In such conditions, the nominal fuel flow (q) is computed as a function of T, M, τ and p. Finally, for already initiated descents, the first phase, which corresponds to the cruise phase, is not considered when generating the trajectory.

Phase-independent path constraints on the controls (i.e., applying all along the descent) are also considered, aiming to ensure that the maximum and minimum descent gradients, thrust and speed brakes are not exceeded:

$$\vec{b}_j^{in} = \begin{bmatrix} \gamma \\ \gamma_{min} - \gamma \\ T_{min}(v,h) - T \\ T - T_{max}(v,h) \\ \beta \\ \beta - 1.0 \end{bmatrix}; j = 0, \ldots, P-1, \tag{IV.3}$$

where γ_{min} is the minimum descent gradient, while $\beta = 0$ and $\beta = 1$ indicate that speed brakes are retracted and fully extended, respectively.

The following terminal constraints are enforced at the end of the trajectory:

$$\vec{\psi} = \begin{bmatrix} v_{CAS}(v,h) - v_{CAS_F} \\ h - h_F \end{bmatrix}, \tag{IV.4}$$

where v_{CAS_F} and h_F are the CAS and altitude at the landing runway threshold, respectively. In the experiments conducted in this chapter, the values chosen were the following: $h_F = 50$ ft and $v_{CAS_F} = V_{REF}$.

Since the flight time is fixed by the RTA, the goal is to minimize the fuel consumption for the remaining descent. Therefore, the stage cost is:

$$\pi_j(v,h,T,\gamma) = \frac{q(v,h,T)}{v\cos\gamma + w(h)}; \; j = 0, \ldots, P-1. \tag{IV.5}$$

It should be noted that in this application example, no terminal cost is considered (i.e., $\phi_j = 0$ for $j = 0, \ldots, P-1$). Furthermore, a fourth-order Runge-Kutta scheme is used to obtain $\vec{F}_j$ and Π_j from $\vec{f}_j$ and π_j, respectively.

In this chapter, the non-linear programming (NLP) problem was formulated by using CasADi (Andersson *et al.*, 2018)[1], a symbolic framework for automatic differentiation and numeric non-linear optimization, and solved by using the sequential quadratic programming (SQP) algorithm implemented by sparse nonlinear optimiser (SNOPT) NLP solver (Gill *et al.*, 2005). Furthermore, the soft-constraint method was implemented to recover feasibility (Section II.2.5.1).

IV.3.2.1 Earliest and Latest Trajectories

For illustrative purposes, Figure IV-5 depicts the earliest and latest neutral (i.e., neutral CDOs) and powered (i.e., powered descents) trajectories. The evolution of altitude and speed as a function of the remaining distance to the runway is shown and, for all cases, the distance to go is 180 NM.

In the earliest neutral case (Figure IV-5(a)), the aircraft accelerates to MMO in the cruise phase, before reaching the TOD. After the TOD, the aircraft descents at a constant Mach equal to MMO, which implies an increase of the CAS. Then, when reaching VMO, the descent continues at this maximum speed down to FL100, where a deceleration is performed to comply with the 250 kt speed limit on CAS. The trajectory optimizer proposes to achieve this deceleration by means of a level-off at FL100—which was not enforced as any additional constraint in the vertical profile—while the aircraft is still flying an energy-neutral trajectory.

Figure IV-5(b), in turn, shows the latest neutral trajectory, which slows down to the minimum allowed speed—green dot speed (GD)—before the TOD, while the aircraft is still in cruise. This

[1] https://github.com/casadi/casadi/wiki

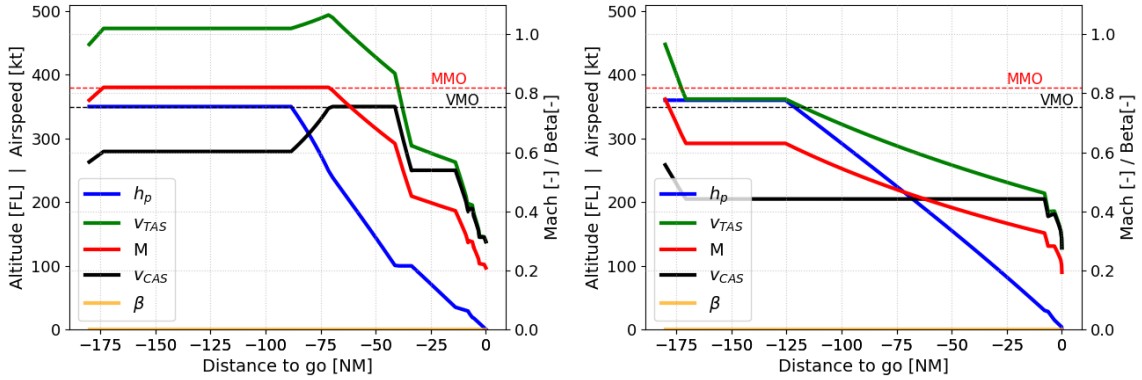

(a) Earliest neutral CDO

(b) Latest neutral CDO

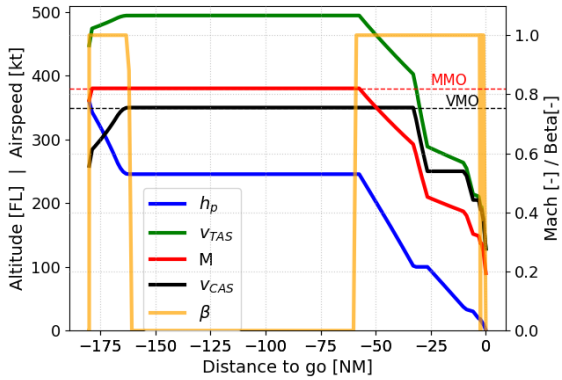

(c) Earliest powered descent

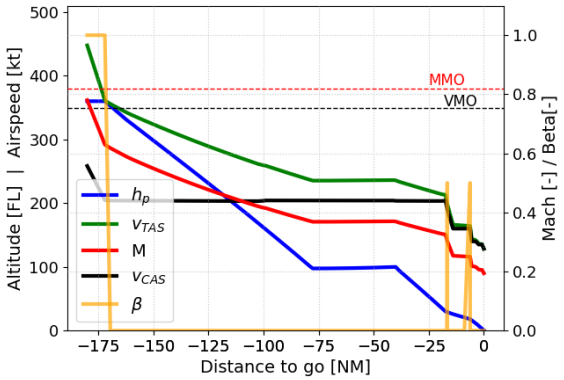

(d) Latest powered descent

Figure IV-5: *Illustrative example for earliest and latest trajectories (representative narrow-body-jet aircraft, no wind, 90% maximum landing weight (MLW))*

speed is maintained during the cruise phase and most of the descent, until few nautical miles before arriving at the runway, where another deceleration is performed. Furthermore, the TOD for the latest neutral trajectory is further from the runway, which means the aircraft starts to descend earlier than in the earliest case.

As expected, the results for the powered trajectories are different, as the energy of the aircraft can be increased or decreased by means of additional thrust and speed brakes usage. In both earliest/latest cases, the descent starts before than in the neutral cases. The earliest powered trajectory (Figure IV-5(c)) consists in descending as fast as possible to the altitude where both VMO and MMO are attained, maximizing, in this way, the TAS. In order to expedite this initial descent, speed brakes are used in order to increase drag and, therefore, the rate of descent. Then, the altitude and speed are kept constant until a deceleration is performed to comply with the FL100 speed limit. Speed brakes are also used in this second descent, again with the objective to achieve the highest possible rate of descent and, consequently, maximizing the amount of time the aircraft is flying at this intermediate altitude where the TAS is maximum.

In the latest powered case (Figure IV-5(d)), a descent at the maximum descent gradient is performed in order to release potential energy as fast as possible, which means a reduction in the TAS. In addition, at the beginning of the trajectory, speed brakes are also deployed in order to decrease the speed of the aircraft as fast as possible until the GD is reached. When generating the latest powered trajectory, the trajectory optimizer tries to minimize the TAS in order to arrive at the runway as late as possible. In general, for a given constant CAS value, the lower the altitude, the

lower the TAS. Therefore, depending on how the phases are defined, the optimizer could compute a trajectory which, after reaching a CAS equal to the GD, would continue descending in order to minimize the TAS. As a result, the aircraft could end up flying at a very low altitude even when it is still far from the runway. In order to avoid this kind of trajectories, additional constraints were added when defining the vertical profile to make it closer to real operations. Basically, two constraints were defined in order to ensure the aircraft remains at an operational altitude during the descent: first, aircraft are not allowed to fly below FL130 before being at a distance of at least 100NM from the runway; second, aircraft cannot descend to altitudes lower than FL100 before reaching a distance of at least 40NM from the runway.

Not only the latest powered trajectory could risk not being compliant with the air traffic operational requirements, but also the earliest one, and maybe as well the neutral trajectories. In the earliest powered trajectory, the aircraft descends to an intermediate cruise altitude[2] in order to maximize the TAS. First of all, it is not clear whether it would be operationally sound for a flight not subject to any emergency to fly at its speed limit for such a long time. Furthermore, this MMO/VMO crossover altitude usually lies around FL250, which might risk aircraft entering ATC sectors located in lower altitudes that might not expect those aircraft. Similarly, in the earliest neutral case, maximum operating speeds are also used for a long time. Finally, the use of the speed brakes at some points of the trajectory might also be undesired from the point of view of the pilots, passenger comfort, etc. In the powered trajectories, they are used not only for increasing the rate of descent, but also for decelerating.

The trajectories and constraints presented herein are the ones used for the experiments conducted in this chapter. However, in the future, it will be necessary to discuss with the stakeholders involved (ATCOs and pilots) which will be the requirements needed for each kind of trajectory. The trajectory computation framework presented in this chapter is generic and flexible enough to add new constraints on these profiles and, in a real world application, these additional constraints would be included in the vertical profiles used by the trajectory optimizer.

IV.3.3 Case Studies

In this chapter, the sensitivity of the proposed solution to several parameters is analyzed, as shown in Table IV-2. First of all, a baseline case study is defined. A representative narrow-body-jet aircraft belonging to the medium aircraft category according to the international civil aviation organization (ICAO) wake turbulence aircraft categorization (SKYbrary, 2020a) is chosen for this study. The following assumptions are also considered: a cruise altitude of FL350, a mass equal to 90% of the MLW and no wind. Then, only one parameter at a time was changed in order to study its effect on the results.

Table IV-2: *Design matrix for the experiment*

Independent variable	Negative variation	Baseline case study	Positive variation
Cruise altitude [FL]	320, 330, 340	350	360, 370, 380
Wind speed [kt]	-60, -40, -20	0	20, 40, 60
Mass [% MLW]	80	90	100
a/c type	Light	Medium	Heavy
RTA assignment altitude [FL]	200, 250, 300	350 (cruise altitude)	-

For all experiments except for the last one (RTA assignment altitude), it is assumed that the aircraft is in the cruise phase and at a distance of 180NM from the runway. At this point, the

[2]Technically speaking, this altitude corresponds to the *crossover altitude* for MMO and VMO

energy-neutral time window at the metering fix is computed. In addition to this time window, the optimal descent trajectory (i.e., minimizing fuel) is also computed. This trajectory is used to obtain the optimal time of arrival at the metering fix, corresponding to the ETA at that fix. Next, several experiments are run for a series of RTAs located outside the energy-neutral time window and inside the powered time window. In total, for the sensitivity study, 10 RTAs later than the latest neutral time of arrival for the baseline case study are defined, evenly spaced within the available powered time window.

As explained in Section IV.2.1, two strategies are considered in this chapter to allow the aircraft fulfill an RTA outside the neutral window: flying powered descents along the published route; or flying neutral CDOs along shorter or longer predefined routes. For the first strategy, the distance to go is 180NM and the vertical profile is defined in such a way that both additional thrust and speed brakes usage are allowed. For the second strategy, the distance to go corresponds to the minimum distance that would enable the aircraft to fulfill the RTA by flying an energy-neutral trajectory. The fuel consumption for both strategies is computed and compared, in order to see how it evolves depending on how far the RTA is defined with respect to the ETA for each trajectory. It is important to highlight the fact that the fuel consumption is computed for the whole trajectory, including both the last of part of the cruise prior to the descent and the descent itself.

For the last parameter analyzed in the sensitivity study (RTA-assignment altitude), it is assumed that the aircraft is already descending when it receives the RTA (see Section IV.2.2). The objective in this case is to study how the aircraft fulfills the RTA as a function of its altitude—and, consequently, distance to go—when receiving the RTA. In order to do this study, the aircraft conditions when it is already descending (e.g., altitude, speed, distance to go and time) are required. For this purpose, a reference neutral trajectory assuming the baseline case study conditions is generated. In addition, an RTA at the middle of the energy-neutral time window is enforced. Therefore, the aircraft will have more flexibility to adapt its trajectory in order to fulfill the updated RTA when already descending. From this profile, and for each of the altitudes shown in the design matrix (i.e., FL200, FL250 and FL300), the distance to go, speed and time are obtained. These parameters are used as initial conditions when generating the trajectories.

IV.4 Results

This section presents the results obtained in this chapter. First, the results for the baseline case study comparing the strategies considered in this chapter are shown in Section IV.4.1. Then, the results obtained for the sensitivity study are presented in Sections IV.4.2 to IV.4.6, classified according to the independent variable subject to study. It is important to remark that in the plots of these sections, the y-axis corresponds to the difference of fuel consumption obtained when flying neutral CDOs along longer/shorter routes with respect to the fuel consumption obtained when flying powered descents along the published route.

It is important to highlight the fact that, in some of the plots in the following sections, sometimes not all RTAs defined in the baseline case study are achievable by all trajectories when performing the sensitivity study. For instance, when considering different cruise altitudes (Section IV.4.2), not all the RTAs that can be achieved for a cruise altitude of FL350 (i.e., baseline case study) can be achieved for a cruise altitude of, for instance, FL320. In this case, in order to compare the fuel consumption for the same RTAs, the RTAs located outside the energy-neutral time window that are not common to all cases are discarded. As a result, in the particular case where the effect of the cruise altitude is assessed, results for 8 out of 10 RTAs are shown in the end (Figure IV-7).

IV.4.1 Results for Baseline Case Study

Figure IV-6 shows, for the baseline case study conditions, the fuel consumption for the two strategies compared in this chapter when an RTA different from the aircraft's ETA is assigned.

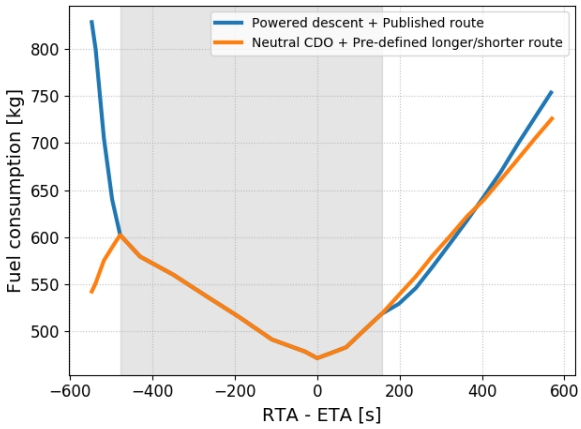

Figure IV-6: *Baseline case study: results for the whole powered time window*

Figure IV-6 leads to several interesting conclusions. First of all, for RTAs lying in the energy-neutral time window (the shaded area in the graph), both strategies show the same behavior in terms of fuel consumption. This is the expected result, as in both cases the aircraft performs an energy-neutral CDO and the route length remains the same. Furthermore, the lowest fuel consumption is achieved at the ETA (0 in the x-axis), corresponding to the arrival time for the optimal trajectory where fuel was minimized.

On the other hand, for RTAs outside the energy-neutral time window and before the ETA, flying powered descents along the published route leads to a higher fuel consumption than flying neutral CDOs along a different—in this case shorter—route. In the powered case, the aircraft flies at very high speeds and at very low altitudes (around FL250, see Figure IV-5(c)), leading to a very high fuel consumption. However, only one small decrease on the arrival time is achieved.

For RTAs later than the ETA and outside the energy-neutral time window, both strategies lead to an increase of fuel consumption the further the RTA is located with respect to the ETA. However, a slightly different behavior is observed for each strategy. At the beginning, for RTAs closer to the latest neutral time of arrival, flying neutral CDOs along a longer route—which means flying for a longer time in cruise—leads to a higher fuel consumption than flying powered descents along the published route. However, for later RTAs, flying powered descents increases the fuel consumption of the flight, as the aircraft remains for a longer time at low altitudes (Figure IV-5(d)). At the end, for the latest RTA, the fuel consumption in this case is higher than that obtained with neutral CDOs (around 30kg more), even if the distance flown is shorter. Although one might think that the difference in Figure IV-6 is not very significant, it is also true that the plot scale can lead to misleading conclusions. A better view of the fuel consumption behavior after the ETA can be observed, for instance, in the red line of Figures IV-7(a) and IV-7(b), where the absolute and relative difference between both strategies, respectively, is depicted.

For the baseline case study, RTAs before and after the ETA have been tested, in order to show the results in the whole powered window. As previously discussed in this section, for RTAs in the neutral time window, the fuel consumption is equal for both strategies. In addition, before the earliest neutral time of arrival, flying neutral CDOs means to always fly shorter routes in order to fulfill the RTA, which always leads to a lower fuel consumption. While these results are quite obvious, for RTAs after the latest neutral time of arrival, the fuel consumption behavior is not obvious and depends on several factors. The following sections present a sensitivity analysis

to assess the effect of several parameters in this region, as well as to find out whether the behavior observed in the baseline case study after the latest neutral time of arrival is the same or not depending on the parameter studied.

IV.4.2 Effect of Cruise Altitude

In order to study the effect of the final cruise altitude (i.e. altitude at the TOD), 6 different values were chosen, plus the altitude of the baseline case study. Figure IV-7 shows the evolution of the difference in fuel consumption for the two strategies compared in this chapter as a function of the cruise altitude and the assigned RTA.

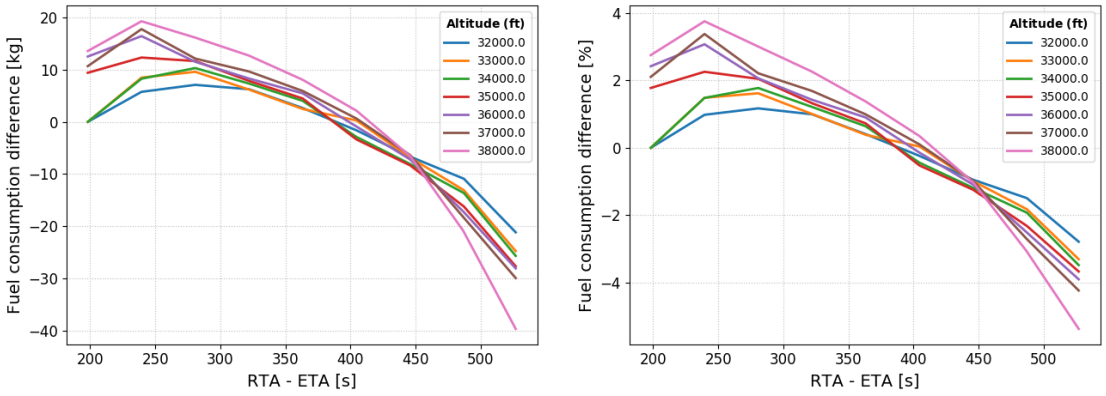

(a) Absolute difference (b) Relative difference

Figure IV-7: *Sensitivity of fuel consumption differences to cruise altitude*

In general, the behavior for each altitude individually is quite similar to that observed in the baseline case study: for RTAs close to the ETA, a lower fuel consumption is obtained when flying powered descents along the published route, while for RTAs farther from the ETA, the behavior is the opposite.

For RTAs far from the ETA, the higher the altitude, the higher the difference in fuel consumption, presumably due to the fact that the optimum cruise altitude for the aircraft model and mass considered in this study lies around 40,000 ft, as shown as well previously by Dalmau & Prats (2015). As a result, when flying neutral CDOs along a longer route, a more efficient flight can be achieved at higher cruise altitudes, leading to a higher difference in fuel consumption with respect to powered descents along the published route. At an RTA of approximately 450s from the ETA, the fuel consumption achieved with powered CDOs along the published route increases at a bigger rate the higher the altitude, increasing the difference between both strategies.

On the other hand, for RTAs closer to the ETA, the difference in the distance to go for both strategies is lower, almost equal in some cases. In this case, for higher cruise altitudes, aircraft can cover part of this distance while already descending. However, for lower cruise altitudes, aircraft have to stay for a longer time at inefficient constant altitudes, leading to an increase in the fuel consumption. As a result, for RTAs close to the ETA, the higher the altitude the lower the fuel consumption achieved with powered descents along the published route. For instance, for a cruise altitude of 38,000 ft, a maximum difference of approximately 20kg (almost a 4%) is obtained at an RTA of 240s from the ETA. Moreover, a minimum difference of almost -40kg (more than a -5%) is obtained for the latest RTA. On the other hand, maximum and minimum differences of 7kg and -21kg, respectively, are obtained for an altitude of 32,000 ft.

IV.4.3 Effect of Longitudinal Wind

Different values for w_r (the known wind speed at h_r, see Eq. (II.10)) were chosen to study the effect of the longitudinal wind on the results. The wind direction in all cases matches the track followed by the aircraft. Furthermore, negative values of wind speed correspond to headwind, while positive values correspond to tailwind. Results are shown in Figure IV-8.

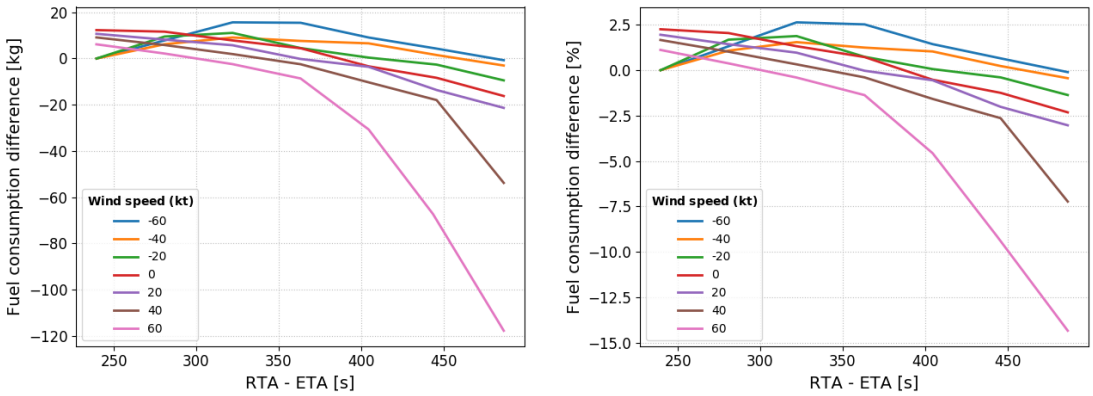

(a) Absolute difference (b) Relative difference

Figure IV-8: *Sensitivity of fuel consumption differences to longitudinal wind*

In general, if there is headwind, the difference between the two strategies compared in this chapter is less than if there is tailwind. For the headwind cases plus the baseline case (with no wind), the difference between strategies increases for RTAs close to the ETA, being more beneficial to fly powered descents along the published route. However, at an RTA of approximately 315s from the ETA, the difference decreases and, at the latest RTA, flying neutral CDOs along a longer route represents a slight advantage with respect to flying powered descents along the published route.

For the tailwind cases, the behavior is different. For RTAs close to the ETA, flying powered descents along the published route is a better option in terms of fuel consumption. However, from that moment on, the difference between both strategies decreases the later the RTA. For the latest considered RTA, the situation becomes the opposite, specially for the case with 60kt of tailwind. Flying neutral CDOs along longer routes means a reduction of 20kg (2.5%), 55kg (7.5%) and 120kg (15%) for wind speeds of 20kt, 40kt and 60kt, respectively.

When there is tailwind and for the strategy consisting of flying powered descents along the published route, aircraft need to descend to lower altitudes in order to minimize the effect of the wind—which is stronger at higher altitudes—and, thus, reduce the TAS. For earlier RTAs, the difference between strategies is not very significant, as it is not necessary to descend to very low altitudes to achieve the assigned RTA when flying powered descents along the published route, leading to a lower efficiency loss. Furthermore, when flying neutral CDOs, the route is only stretched by a little amount in order to fulfill the RTA. Still, at this point, flying an energy-neutral CDO along a longer route leads to a higher fuel consumption. However, for later RTAs, the aircraft needs to descend to very low altitudes in order to fulfill the time constraint when flying powered descents along the published route, which drastically increases the fuel consumption. On the other hand, when flying neutral CDOs, the route has to be stretched by a higher amount, increasing the distance flown in cruise. Still, the fuel consumed when flying neutral CDOs along a longer route—involving a longer cruise—is lower than the fuel consumed when flying powered descents at very low altitudes.

For the headwind case, in order to arrive at later RTAs, the TAS can be reduced either by staying at cruise, where the headwind is stronger, or by descending to lower altitudes, as lower

TAS values can be achieved at low altitudes. However, the lower the altitude, the weaker the headwind, which means that the TAS would be higher. Conversely, the higher the altitude, the higher the TAS. For early RTAs, the fuel consumption for neutral CDOs along a longer route is higher, as the aircraft remains at relatively high altitudes in both strategies. However, for later RTAs, the situation is the opposite: flying powered descents along the published route leads to a higher fuel consumption. Still, this difference is not very high if compared with the tailwind case, as aircraft do not need to descend to very low altitudes in order to fulfill the RTA.

IV.4.4 Effect of Aircraft Mass

Three aircraft masses have been considered in this study, defined as a percentage of the MLW. The evolution of the fuel consumption difference between both strategies, depicted in Figure IV-9, is similar for the three masses tested, and similar to that observed in the baseline case study. In this case, the difference between both strategies increases until an RTA between 230s and 275s from the ETA. From that moment on, the difference decreases, as the fuel consumption for powered descents along the published route increases at a bigger rate. For the latest RTA, the fuel consumption for powered descents along the published route is higher, resulting in a difference between both strategies of approximately 39kg, 27kg and 22kg for a percentage of MLW equal to 80%, 90% and 100%, respectively.

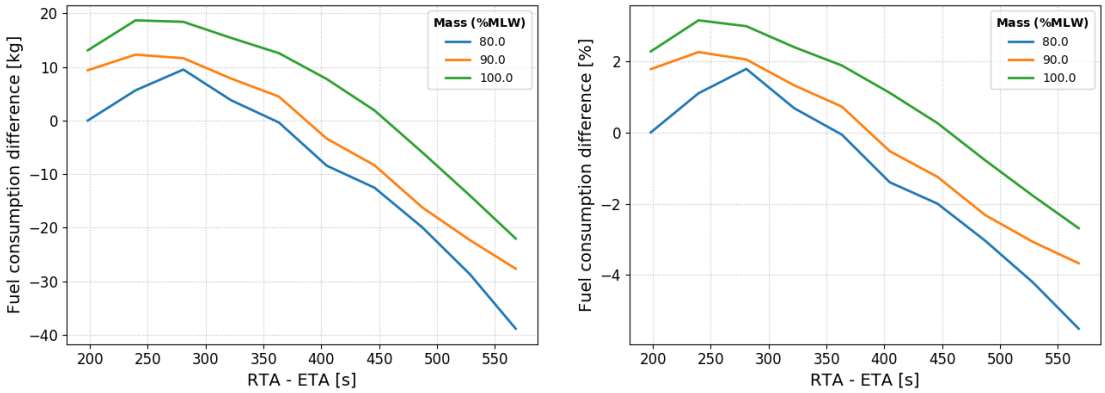

(a) Absolute difference (b) Relative difference

Figure IV-9: *Sensitivity of fuel consumption differences to aircraft mass*

The lower the mass, the lower the required altitude needed to fulfill the RTA when flying powered descents along the published route. As a result, the lower the mass, the higher the fuel consumption obtained by following this strategy. Similarly, the farther the RTA is from the ETA, the lower the altitude needed to fulfill the RTA when flying powered descents along the published route, which increases even more—specially for the lowest mass—the difference in fuel consumption with respect to flying neutral CDOs along longer predefined routes.

IV.4.5 Effect of Aircraft Type

In order to assess the effect of the aircraft model in the results, three representative aircraft models belonging to different wake turbulence aircraft categories as defined by ICAO (SKYbrary, 2020a) were chosen: light, medium (corresponding to the baseline case study) and heavy. As shown in Figure IV-10, very different behaviors can be observed between the three aircraft models.

For RTAs close to the ETA, the medium aircraft consumes a lower quantity of fuel by flying powered descents along the published route, being the maximum difference between both strate-

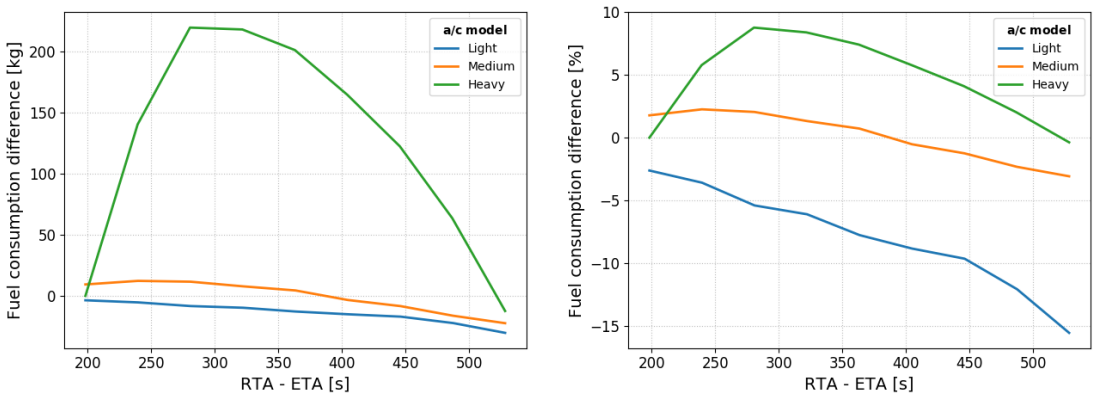

(a) Absolute difference (b) Relative difference

Figure IV-10: *Sensitivity of fuel consumption differences to aircraft type*

gies 15kg at an RTA of 240s from the ETA. However, for RTAs later than approximately 400s from the ETA, the situation is the opposite: the fuel consumption for powered descents becomes higher than that obtained with neutral CDOs along longer routes.

Regarding the heavy aircraft, almost for all RTAs, flying powered descents along the published route consumes a lower quantity of fuel. The maximum difference is found at an RTA of approximately 275s from the ETA, where a fuel consumption difference of 220kg is obtained. From that point on, the difference between both strategies starts to decrease; for the latest RTA, the difference is almost 0.

Finally, for the light aircraft, conversely to the heavy aircraft behavior, flying neutral CDOs along longer routes always leads to a lower fuel consumption. A maximum difference between both strategies of approximately 35kg for the latest RTA is obtained, representing a 15% reduction in fuel consumption.

IV.4.6 Effect of RTA Assignment for already Initiated Descents

When assigning an RTA to an aircraft that is already descending, the resulting time window at the metering fix is reduced by a big rate, both for neutral CDOs and powered descents. Yet, it could still be significant, as reported by Dalmau & Prats (2017b); and, as expected, it increases the higher the altitude at which the RTA is assigned. Furthermore, the difference between the latest neutral and latest powered times of arrival at the metering fix is much lower than in the other cases, when the aircraft is still in the cruise phase.

In order to assess such a kind of scenario, three different altitudes were chosen, which correspond to the altitudes at which the aircraft would receive the RTA while already descending. In addition, as indicated in Section IV.3.3, a reference neutral trajectory was used—with an RTA assigned at the middle of the energy-neutral time window—from which the aircraft conditions (e.g. speed, distance to go and time) at the designated altitude were obtained. Results are shown in Figure IV-11.

It can be observed that the results for the baseline case study are not shown in Figure IV-11. This is due to the fact that all RTAs in the powered time window in this case are achievable with an energy-neutral CDO when the aircraft is in the baseline conditions. As a result, there is no difference between both strategies.

Still, the differences between each case are not very significant. It is important to remark the fact that the aircraft, specially if it flies an energy-neutral CDO, does not have a lot of flexibility

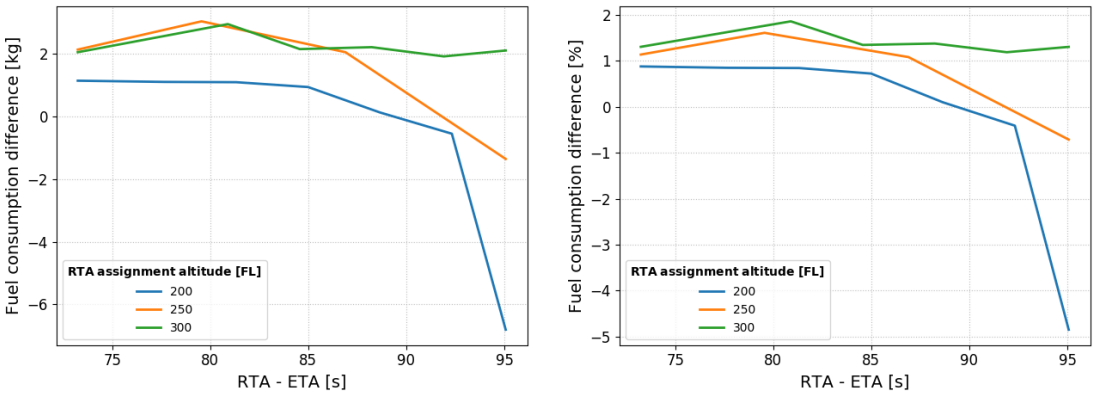

(a) Absolute difference (b) Relative difference

Figure IV-11: *Sensitivity of fuel consumption differences to RTA assignment altitude*

when it comes to fulfill an RTA outside the energy-neutral time window. Even if the route is stretched, very late RTAs cannot be achieved. In the previous cases, when the aircraft was in the cruise phase, the TOD could be adapted in order to achieve different times of arrival at the metering fix. As a result, a higher number of RTAs in the powered window where achievable. Conversely, in this case, the aircraft can only achieve different times of arrival by adapting the profile by means of the elevator. In the end, when flying neutral CDOs along a longer route, the distance to go can only be increased by a little quantity (up to 5NM) to achieve feasible trajectories fulfilling the RTA.

In general, the lower the flight level (FL) at which the RTA is assigned, the highest the difference between both strategies for late RTAs. The results are similar if the RTA is assigned at FL200 or FL250. For early RTAs, flying neutral CDOs along a longer route is less efficient and, for later RTAs, the situation is the opposite: powered descents along the published route leads to a higher fuel consumption. Finally, if the RTA is assigned at FL300, flying neutral CDOs along a longer route is always less efficient no matter the value of the RTA. Still, the values obtained for each case are very low. As it has been aforementioned, routes are stretched by a very low quantity in order to fulfill the RTA with neutral CDOs, which does not lead to a high increase in fuel consumption. Moreover, the latest RTA in this case is only located at approximately 20 seconds from the first RTA. Regarding powered descents, the lower the altitude the less efficient the trajectories, leading to a higher difference in fuel consumption between strategies, specially in the FL200 case.

IV.5 Discussion

This chapter compared the fuel consumption of two strategies that aircraft could follow when they are assigned an RTA outside their energy-neutral time window: flying powered descents along the published route or flying neutral CDOs along shorter or longer predefined routes. Results for RTAs earlier than the ETA, as expected, show that flying neutral CDOs—which involves flying shortcuts to fulfill the RTA—always represent an advantage with respect to flying powered descents along the published route. When the RTA is assigned later than the ETA, however, different behaviors are observed, which depend on different factors such as the aircraft model or the current wind. For instance, in a tailwind scenario—except if the assigned RTA is very close to the ETA—stretching the route (and fly neutral CDOs) will always increase the efficiency of the operation. Similarly, light aircraft will also benefit from being assigned longer predefined routes, while for heavy aircraft it will be better to fly powered descents along the published route.

In all case studies it was assumed that the aircraft was following a straight route. However, depending on the scenario, the aircraft will be required to follow different courses during the arrival procedure, which would affect the results. Moreover, results were computed assuming the aircraft was following always the shortest—non-published and predefined by the ATCO—possible route when an energy-neutral CDO was enforced. Nevertheless, in a real application, usually a fixed number of predefined routes (i.e., distances to go) will be available, so not always the shortest route will be an option. Furthermore, different distances to go might allow the fulfillment of the same RTA so, depending on the scenario, it might be better to choose a longer route in order to ease the scheduling the arrival traffic. Still, in this chapter, the objective was to obtain the results for the best possible conditions in terms of available distances to go. Then, in a real application, the computations presented herein should be adapted to take into account the available routes that might be predefined by the ATCO in the arrival procedure.

The work presented in this chapter could complement and mitigate the limitations of the work presented in Chapters V and VI, which focus on sequencing and merging traffic in TMA. When it is not possible to schedule all aircraft by flying energy-neutral CDOs along the published route, maybe shortening/stretching the route or flying powered descents (along the published route) could help to accommodate all traffic while keeping separation among all aircraft.

This chapter gives a clear understanding of aircraft performance and behavior in a scenario where the ATC needs to assign an RTA outside the energy-neutral time window of the arriving aircraft. Consequently, the results obtained in this chapter could be valuable towards the definition of a ground-support tool to help ATC to manage more efficiently arriving traffic. This aligns with the TBO paradigm, where advanced synchronization mechanisms between ground and airborne tools are expected.

Hem de morir a temps, no vegetar, [...] confosos en la multitud que creix, sense ordre ni mesura, cap a un destí de rusc o de formiguer.
[We must die in time, not vegetate, [...] confused in the crowd that grows, without order or measure, towards a hive or anthill.]

— Salvador Espriu

V

Enabling CDOs in Trombone Sequencing and Merging Procedures

Tromboning is an interim strategy to sequence and merge arrival traffic in terminal maneuvering areas (TMAs) that lies in between full four-dimensional (4D) negotiated trajectories and open-loop vectoring. It consists in a trombone-shape area navigation (RNAV) procedure consisting of a set of parallel legs composed of multiple waypoints, in which air traffic control officers (ATCOs) may give a shortcut (depending on the traffic) to the next leg. Figure V-1 shows a simplified tromboning procedure, with two entry points (EP_a and EP_b) for two different traffic flows. Aircraft are supposed to fly the full route (black lines in the figure) unless the ATCO gives a shortcut at some of the waypoints. In such a case, aircraft would be able to fly one of the red-dashed trombone shortcuts depicted in the figure, which would suppose a reduction in the total distance flown. Currently, trombone procedures are used in several European airports, such as Munich and Frankfurt airports, in Germany, or Warsaw Chopin airport, in Poland. Recently, tromboning procedures have been implemented also in Barcelona-El Prat airport.

In Chapter III, it was shown how neutral continuous descent operations (CDOs), which involve the use of idle thrust and no speed brakes usage, lead to a significant reduction in the fuel

This chapter is based on the following publications:

- Sáez, R., Prats, X., Polishchuk, T. & Polishchuk, V.. 2020. Traffic synchronization in terminal airspace to enable continuous descent operations in trombone sequencing and merging procedures: An implementation study for Frankfurt airport. *Transportation Research Part C: Emerging Technologies*. **121**. D.O.I: 10.1016/j.trc.2020.102875.
- Sáez, R., Dalmau, R. & Prats, X.. 2018 (Sept.). Optimal assignment of 4D close-loop instructions to enable CDOs in dense TMAs. *In: IEEE/AIAA 37th Digital Avionics Systems Conference (DASC)*. London, UK: IEEE.

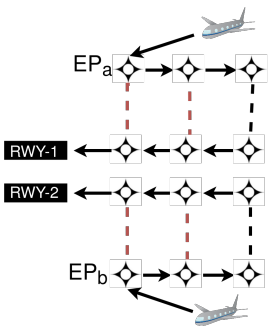

Figure V-1: *Simplified diagram of a tromboning procedure*

consumption during a descent. However, this kind of trajectories involve a lower flexibility if compared with powered descents, as the achievable time window at the metering fix is smaller (as discussed in Chapter IV). Moreover, although not negligible, there is a smaller margin to adapt the trajectory once the descent has started. Still, neutral CDOs bring a lot of environmental benefits, which motivated their use in the experiments conducted in this chapter.

In this chapter, the current tromboning paradigm is enhanced with a 4D trajectory negotiation and synchronization process with the aim to enable the highest number of neutral CDOs; and to maximize runway throughput. Currently, tromboning shortcuts are assigned by the air traffic control (ATC) via open-loop instructions, limiting the use of CDOs. Furthermore, in many cases, as depicted in Figure V-2, the ATCs issues open-loop instructions leading the arrival aircraft through routes not matching the arrival procedures and/or tromboning shortcuts defined in the arrival charts. Conversely, in this chapter, it is assumed that a required time of arrival (RTA) and a shortcut of the trombone procedure will be negotiated (i.e., closed-loop instruction) way before the top of descent (TOD) in order to derive a 4D conflict-free trajectory throughout the whole descent following the published arrival route.

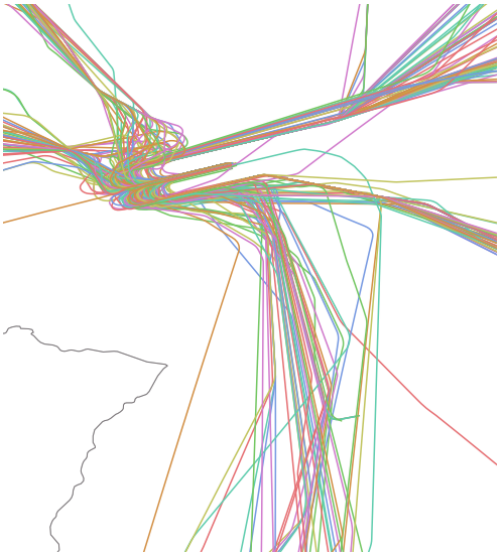

Figure V-2: *Arrival traffic on September 14th, 2018 in Frankfurt airport obtained from OpenSky (The OpenSky Network, 2019) automatic dependent surveillance-broadcast (ADS-B) trajectories*

Besides improving current operations in the short-mid term, the methodology presented in this chapter could become a technical enabler towards extended arrival managers (E-AMANs) or advanced 4D trajectory synchronization technologies in line with the trajectory based operations (TBO) paradigm.

V.1 State of the Art

Besides tromboning, point merge (depicted in Figure V-3) represents also an interim strategy that lies in between full 4D negotiated trajectories and open-loop vectoring. Both methodologies have proven successful to maximize runway throughput, reduce ATCO workload and enhance significantly the aircraft crew situational awareness, since the predictability of the trajectory improves.

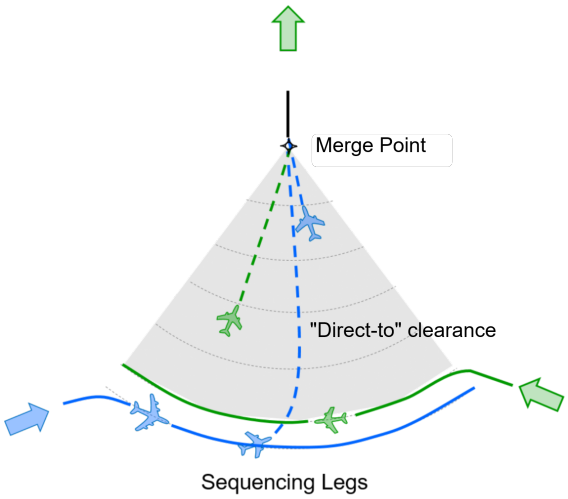

Figure V-3: *Simplified diagram of a point merge procedure (Eurocontrol, 2018b)*

In a point merge arrival, aircraft fly sequencing legs at a constant altitude (typically between FL90 and FL110), until "direct-to" clearance is given to a merge point, used for traffic integration (Ivanescu *et al.*, 2009; Boursier *et al.*, 2007). Its environmental benefits, however, are limited to altitudes below the sequencing leg altitude, since the remaining distance is known with certainty only after the "direct-to" clearance has been issued. Thus, even if the CDO were initiated at the cruise level, it would be interrupted to maintain level flight while following the sequencing leg before cleared to the merge point, leading to an increase in fuel burn while leveling off at relatively low altitudes.

Regarding tromboning, Sprong *et al.* (2005) demonstrated how this kind of procedures reduce lateral dispersion, time flown and distance flown, while at the same time allow arriving flights to remain at higher altitudes. In addition, Schultz *et al.* (2012) took advantage of the Frankfurt trombone procedure in order to study the management of uncertainty caused by trajectory prediction errors, seeking more automation in the management of arrival traffic.

Several studies have proposed arrival schedulers with RTAs to manage all the incoming traffic; however, they assumed fixed arrival routes (Sadovsky & Windhorst, 2019) or they did not necessarily enforce the use of CDOs (Zelinksi & Jung, 2015; Sadovsky & Windhorst, 2019). Dalmau *et al.* (2017) proposed a concept consisting of separating, sequencing and merging traffic by negotiating RTAs and shortcuts between aircraft and ATC before starting the descent. Results showed that, for a given RTA, several shortcuts could be assigned such that the RTA fits into the feasible time window.

To the best of our knowledge, no other works analyzed a high-demand scenario with real traffic, in which aircraft fly neutral CDOs from cruise level to a given metering fix by following a real trombone procedure (with pre-negotiated shortcuts) in which separation is ensured at all waypoints.

V.2 Concept of Operations

This section details the concept of operations (CONOPs) proposed in this chapter, in which an aircraft scheduling and synchronization problem in TMA without open-loop instructions is solved by taking advantage of the tromboning philosophy. Figure V-4 depicts a simplified scenario used to illustrate the problem addressed in this chapter.

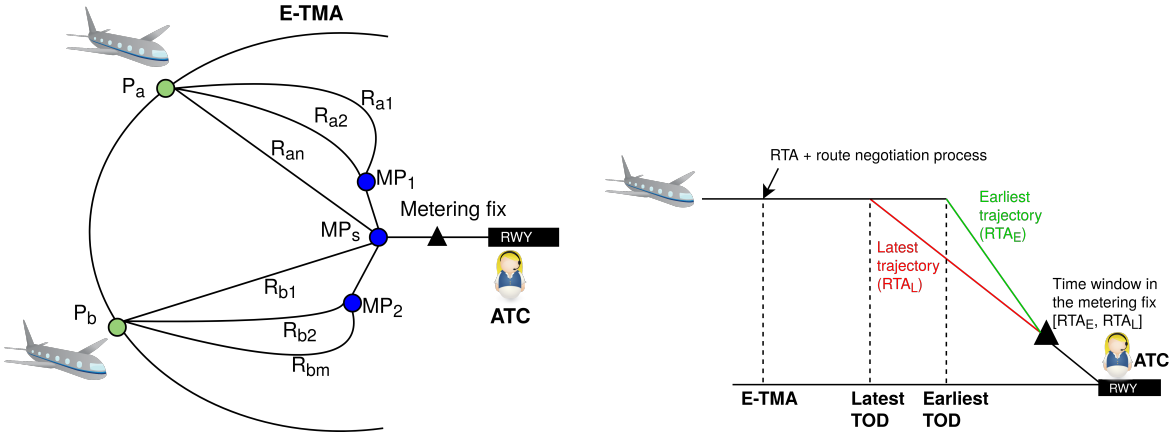

(a) Lateral perspective (b) Vertical perspective

Figure V-4: *CONOPs: trajectories*

Let us assume several aircraft have planned to land in a given airport divided into N traffic flows of one or more aircraft each, entering an extended terminal maneuvering area (E-TMA) through several entry points (P_a and P_b in this case). In this chapter, the E-TMA nomenclature is used to emphasize the fact that the aircraft are still in the en-route phase of the flight when the sequencing requirements in the TMA are negotiated, which will include a revision of the trajectory's TOD. In the majority of conventional TMAs, however, this would not be possible. TMAs are areas of controlled airspace surrounding the airport, designed to efficiently manage all the incoming and departing traffic. The size of a TMA depends on the level of traffic for which it is designed, so it will be bigger for airports with high traffic loads and smaller for airports with low traffic loads. In the case of small airports, it might even be designed up to altitudes below the TOD of the majority of flights, which would mean that aircraft would be already descending. On the other hand, for big airports the aircraft may still be in cruise when entering the TMA; however, in most cases, there would not be enough time to efficiently negotiate the sequencing requirements with the ATC. In Europe, for instance, for some big airports such as Barcelona, the TMA horizontal limits are defined by the border with neighboring countries (in this case, by the border with France), leading to a loss of efficiency.

For each entry point, there are several available routes an aircraft could fly. These traffic flows could merge at several merging points (MP_1...MP_s), until they all meet at the metering fix, which is the point where the RTA will be assigned.

Once the aircraft enter the E-TMA, they start an RTA and route negotiation/synchronization process with the ATCO (or ground-automated system), as shown in Figure V-5. First of all, aircraft are requested to compute their arrival time window in the metering fix, which is the difference between the earliest and the latest time of arrival at that fix (RTA_E and RTA_L), which are assumed to be computed by the flight management system (FMS) of the different incoming aircraft by considering the earliest and latest trajectories (Figure V-4(b))[1]. In addition, the aircraft FMS downlink

[1]The TOD for the earliest trajectory is further (or closer to the metering fix) than the TOD for the latest trajectory, as aircraft can fly at higher speeds during the cruise phase (Figure V-10).

to the ATCO the aircraft estimated time of arrival (ETA) and a set of finite profiles within the available time window (computed by the FMS too). In this chapter, a profile has to be understood as the resulting descent trajectory when combining the assignment of an RTA and a route choice in the tromboning procedure. It should be noted that, while the earliest and latest times of arrival at the metering fix will mainly depend on aircraft performance, flight envelope and weather conditions; the ETA at the same fix will be obtained after computing the optimal descent trajectory for that particular flight, subject to airline and crew policies, such as the cost index (CI) setting for that particular flight. It is worth highlighting the fact that the profiles are computed by on-board systems (such as an FMS), and not by ground systems, thus improving the accuracy of the generated trajectories as aircraft systems have access to much more accurate aircraft performance data.

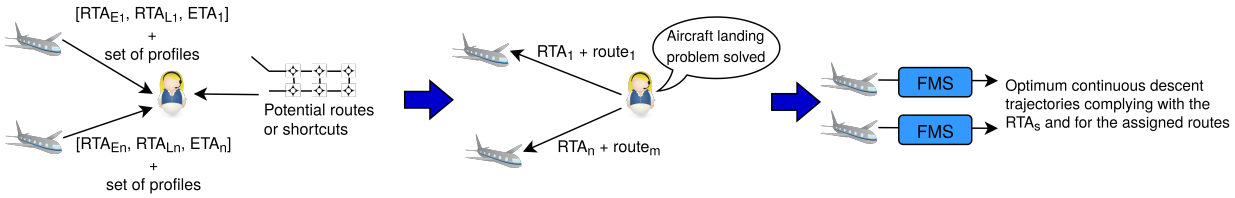

Figure V-5: *CONOPs: RTA and route negotiation process*

After receiving all the profiles and analyzing the potential routes for each aircraft, ATCOs (with the help of an automated ground system) can solve the aircraft landing problem. They assign a profile (i.e. an RTA within each aircraft feasible time window and a route in the arrival procedure) to each aircraft that ensures a safe separation between aircraft throughout the whole arrival procedure (no matter how many routes and merging points) and which minimizes the deviation with respect to the aircraft ETA at the metering fix. The objective is that the aircraft know this information while still in cruise, just after entering the E-TMA. Therefore, the FMS onboard can compute the neutral trajectory (i.e. idle thrust and no speebrakes usage) that complies with the RTA and follows the requested route by the ATCO .

One interesting matter is the width of the time window in the metering fix, which depends on several factors, e.g. the aircraft performance, weather conditions, etc. However, there are two factors that could be changed in order to obtain wider or shorter time windows. The first one is the type of descent being considered. Neutral CDOs assume idle thrust and no speed brakes usage throughout the descent, and are the ones considered in this chapter. Then, powered descents allow the use of thrust and speed brakes, supposing a higher flexibility with respect to neutral CDOs, which leads to wider time windows, but at the expense of increasing the fuel burn and/or noise nuisance.

The other influential factor is related to the time when the RTA and route assignment are notified to the aircraft. If the ATCO sends this information when the aircraft enters the E-TMA while it is still in cruise, the time window will be wider than if the RTA and route are assigned while the aircraft is already descending. While in cruise, the aircraft could accelerate or decelerate to achieve earlier or later times of arrival. Furthermore, the position of the TOD can be changed too. Several studies have dealt with the assignment of RTAs (and the quantification of the feasible time window) when the aircraft is still in cruise, well before the TOD. The work presented by Takeichi & Inami (2010) quantified the feasible time window that could be achieved by either enabling the addition (resp. omission) of waypoints to stretch (resp. reduce) the flight path length, or adjusting the duration of the cruise phase. However, as it has been aforementioned, ATCOs could potentially assign or update previously assigned RTAs while the aircraft is already descending. This is addressed by Dalmau & Prats (2017b), where it is shown that the available time window allowing to update the RTA while still executing a CDO at idle thrust is in some cases still significant.

Ideally, the RTA and route negotiation/synchronization process should be done as soon as aircraft enter the E-TMA. However, this would be feasible only if the flight sequence is generated

fast enough so that aircraft know the profiles they have been assigned before reaching the TOD. Otherwise, the E-TMA size should be extended or the communication between the aircraft and the ATC should be established before the E-TMA, with enough look-ahead time to make the required computations.

V.3 Methodology

The goal of the aircraft landing problem considered in this chapter is to schedule the arrival traffic to the E-TMA by assigning one profile to each aircraft a. This involves assigning both RTAs at the metering fix and routes to all incoming traffic. Each RTA must fit within the corresponding feasible time window for each particular aircraft and, together with the route assignment, a time separation between aircraft must be ensured through the whole descent. As commented before, this feasible time window, together with the ETA at the metering fix ETA_a, is assumed to be computed by the FMS of each aircraft and down-linked, as input, to the aircraft landing scheduler.

In this chapter, the arrival time window in the metering fix is discretized. This leads to a finite set of candidate descent profiles per aircraft, which are also computed by the FMS and down-linked to the aircraft landing scheduler. The process followed in order to solve the aircraft landing problem and, thus, to obtain an optimal profile assignment, is shown in Figure V-6 and detailed below:

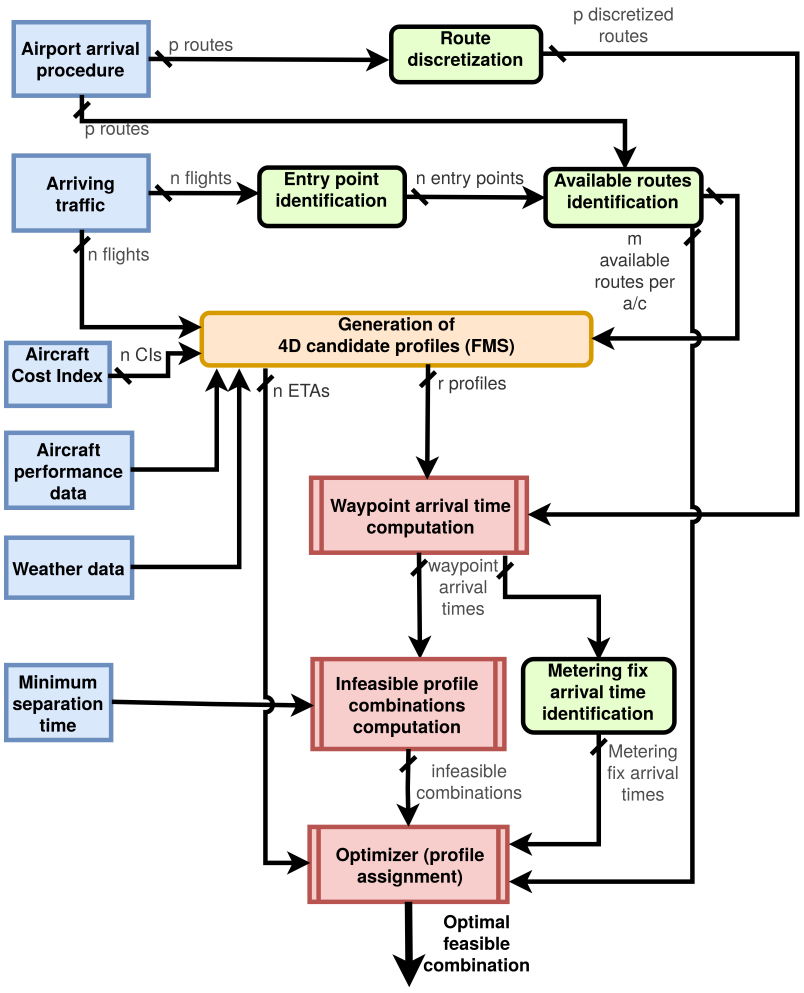

Figure V-6: *Profile assignment process*

1. The possible routes for each aircraft arriving to the destination airport are obtained from the arrival and approach charts published by the corresponding country's AIP (aeronautical information publication). Each route is discretized in a finite number of segments, so that new (intermediate) waypoints are added to the procedure.

2. By observing the arriving traffic and the airport arrival procedure the entry points for each incoming aircraft are obtained, which are those corresponding to the moment the aircraft enters the E-TMA. As soon as aircraft enter this area, the RTA and route negotiation process starts.

3. The FMS of each aircraft computes a set of candidate profiles. These profiles are computed per route and thus, the arrival time windows at the metering fix (for each aircraft and possible route) are obtained.

4. The ETA at the metering fix is also computed by each arriving aircraft FMS according to the CI set for that particular flight.

5. The arrival times per profile at different waypoints are computed by the FMS, by using all the waypoints generated when discretizing the available routes per aircraft.

6. Infeasible profile combinations are computed on the ground. This involves checking if a minimum time separation is ensured at all waypoints of the procedure between all the aircraft for a given combination of aircraft and profile. Algorithm V.1 shows the pseudo-code used to find these infeasible profile combinations by brute force.

7. The ETA per aircraft, and also the set of possible RTAs at the metering fix (one per profile), together with the infeasible combinations are used as an input to the optimizer. The solution of the aircraft landing problem is the profile-to-aircraft assignments for all aircraft that minimizes a given cost function. The details of this optimization problem are given below.

Algorithm V.1: *Pseudo-code for finding infeasible profile combinations*

```
Define sep. time                                   ▷ f is flight, wp waypoint and r route
for f_1 and f_2 in flights do
    for wp_1 in waypoints flown by f_1 and f_2 do
        for r_1 in routes flown by f_1 and containing wp_1 do
            for r_2 in routes flown by f_2 and containing wp_1 do
                if abs((wp_1 arrival time of f_1 using r_1) - (wp_1 arrival time of f_2 using
  r_2)) ≤ sep.time then
                    Save infeasible combination
                else
                    Save feasible combination
```

There are several approaches in the literature focusing on formulating and solving the aircraft landing problem. Regarding its formulation, mixed integer programming (MIP) is the preferred option by most (if not the totality) of the authors. The problem formulation and the number of variables and constraints involved may vary depending on the airport infrastructure, the runways and routes considered or the number of aircraft to be scheduled. More complex formulations are needed for more complex scenarios, as well as more advanced strategies to solve the problems. Beasley *et al.* (2000) presented the classical MIP formulation for the aircraft landing problem. This formulation sets the basis for some of the future works developed on that topic, such as the job shop formulation presented by Benheikh *et al.* (2009).

In order to solve the aircraft landing problem, some authors propose to use ant colony algorithms (Beasley *et al.*, 2011), while others just rely on commercial solvers like CPLEX, which solves

integer linear problems using either primal or dual variants of the simplex method or the barrier interior point method (Vadlamani & Seyedmohsen, 2014; Samà *et al.*, 2014). In this chapter, the aircraft landing problem is modeled with a mixed integer linear programming (MILP) formulation. The problem formulation is quite simple, as the aircraft profiles are precomputed and are used as the input to the problem. This approach has been chosen mainly because it always outputs optimal solutions. The resulting problem instances corresponding to the real operational scenarios are of relatively small size and are solved in reasonable time using a commercial (CPLEX) solver, as detailed in Section V.5.

Let $\mathcal{A}$ be the set containing all aircraft scheduled to land at the airport during a certain period of time. Then, let $\mathcal{P}_a$ be the set containing all possible vertical and speed profiles (a finite number of profiles per available route) that can be flown by a given aircraft a (i.e. one set per aircraft), which are computed by each aircraft FMS. Finally, let $\mathcal{I}$ be the set containing aircraft-profile pairs (e.g. $((a_i, p_k), (a_j, p_r))$) representing the incompatibilities between profiles, meaning that there will be a loss of time separation between aircraft a_i and a_j if aircraft a_i flies profile p_k and aircraft a_j flies profile p_r. The required time of arrival at the metering fix $\text{RTA}_{a,p}$ is a known value and corresponds to the arrival time at the metering fix for each profile an aircraft can fly.

Let $x_{a,p}$ be the binary decision variables defined as follows:

$$x_{a,p} = \begin{cases} 1, & \text{if aircraft } a \text{ flies profile } p \\ 0, & \text{otherwise.} \end{cases} \tag{V.1}$$

Where $a \in \mathcal{A}$ and $p \in \mathcal{P}_a$.

The constraints of the problem are shown in Eqs. (V.2) and (V.3). Eq. (V.2) ensures that if there are incompatibilities between two aircraft flying two profiles, at most one aircraft will be allowed to fly its profile. Otherwise, there would be a loss of separation. On the other hand, Eq. (V.3) ensures that all aircraft will fly only one profile.

$$x_{a_i,p_k} + x_{a_j,p_r} \leq 1, \quad \forall a_i, a_j \in \mathcal{A},\ \forall p_k \in \mathcal{P}_{a_i},\ \forall p_r \in \mathcal{P}_{a_j} \mid ((a_i, p_k), (a_j, p_r)) \in \mathcal{I} \tag{V.2}$$

$$\sum_{p \in \mathcal{P}_a} x_{a,p} = 1, \quad \forall a \in \mathcal{A}. \tag{V.3}$$

The solution of the aircraft landing problem could be feasible or infeasible depending on the complexity of the scenario. For those feasible scenarios, there may exist many distinct solutions such that all the constraints of the problem are satisfied; namely, each aircraft is assigned one profile compatible with the profiles assigned to all the other aircraft, and an RTA within the feasible time window for that aircraft.

In this chapter, it is considered that the RTA at the metering fix should be as close as possible to the ETA at that fix for each particular flight (ETA_a), assuming that the cost of the (flight) operation is minimized. Thus, the objective function J of the optimization problem formulated in this section is the following:

$$\min \quad J := \sum_{a \in \mathcal{A}} \sum_{p \in \mathcal{P}_a} x_{a,p} \cdot |\text{RTA}_{a,p} - \text{ETA}_a|. \tag{V.4}$$

Aircraft arriving before or later than the ETA are penalized in the same way, so it is assumed that any absolute value of time deviation is detrimental for the arriving aircraft.

Below it is proven that the above-defined problem is NP-hard, which justifies attacking it with an integer program. To show the hardness, it is reduced from independent set (IS)—a classical NP-hard problem. An instance of IS is specified by a graph G and an integer k; the question is whether G has an independent set of size k (an independent set is a set of vertices no two of which are connected by an edge). In Figure V-7(a) a graph G with 5 vertices is depicted, where the IS (in black) contains 3 vertices.

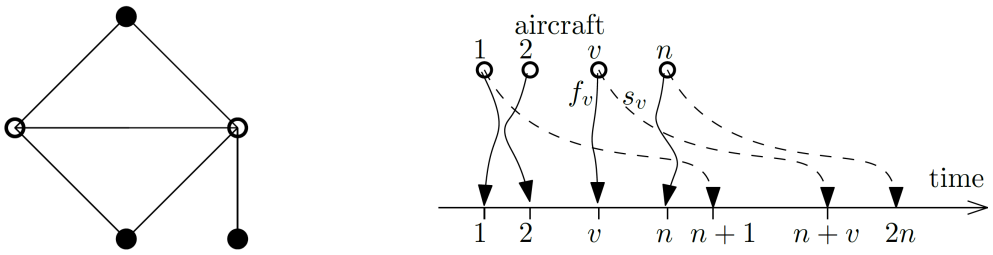

(a) Graph G with IS (in black)

(b) Vertices 1 and 2 are connected by an edge in G and hence their fast profiles cannot be used simultaneously

Figure V-7: *Independent Set (IS) diagrams*

Given an instance of IS, an instance of the problem is produced as follows. There will be an aircraft for every vertex in G; the aircraft and the vertices are identified with integers from 1 to n, where n is the number of the vertices (and hence the aircraft). Every aircraft v will have two profiles: a *fast* profile f_v and a *slow* profile s_v. If v follows the fast profile, then the aircraft arrives at time v; if v follows s_v, then it arrives at time $n + v$ (Figure V-7(b)). When creating the profiles, the following rules are adhered: if vertices u, v are connected by an edge in G, then using the fast profiles f_u, f_v together will lead to separation loss between aircraft u and v. On the contrary, any slow profile does not conflict with any other profile (slow or fast), i.e., using any slow profile is possible irrespective of what profiles are chosen for all other aircraft.

Finally, the ETA of aircraft v is set to v. That is, if all aircraft follow fast profiles, the objective function is 0. More generally, the objective function is equal to $(n - k)n$ if and only if exactly k aircraft follow fast profiles (because n is added to the objective function for every aircraft following slow profiles). But the set of aircraft following fast profiles corresponds to an independent set in G. Hence, G has an independent set of size k if and only if the objective function in our problem is at most $(n - k)n$. Since the optimization problem is NP-hard, it is non-convex (a convex problem could be solved in polynomial time).

V.4 Experimental Setup

This section presents the experimental setup used to illustrate the CONOPs and methodology proposed in this chapter, where all incoming aircraft are assigned the shortest possible route, allowing them to attain an RTA at the metering fix as close as possible to their ETA and without incurring a time separation loss with the surrounding traffic. Frankfurt's airport trombone procedure has been chosen for this study. A hypothetical E-TMA of 250 NM of radius is defined around the airport. In addition, the current standard terminal arrival routes (STARs) are extended with a straight line from the first waypoint of each STAR to the aircraft entry points to the E-TMA. As soon as they enter the E-TMA, aircraft are assigned an RTA and a route (after pre-negotiation with the ATCO). Then, they are assumed to fly the extended STAR, after which they start the trombone procedure to follow the assigned route. In this chapter, the aircraft landing problem was formulated in the general algebraic modelling system (GAMS) software suite, and solved with

the CPLEX solver.

Section V.4.1 presents the scenario. Then, the generic models introduced in Section II.1 are particularized in Section V.4.2. Analogously, the generic optimal control problem stated in Section II.2.1 is particularized in Section V.4.3 with specific cost function and constraints. Finally, the case studies are presented in Section V.4.4.

V.4.1 Scenario

Frankfurt airport was selected as the scenario for the experiment performed in this chapter. It is by far the busiest airport in Germany as well as the fourth busiest in Europe. This airport is provided with four runways, of which three are disposed parallel in east-west direction and one in north-south direction. During normal operation, the two outer parallel runways (07L/25R and 07R/25L) are used for arrivals and the north-south runway (18-36) and the central parallel runway (07C/25C) for departures. In this chapter, the GPS/FMS RNAV 25L/C/R transition to final approach (i.e. west configuration) is used, which is a trombone procedure, assuming aircraft could land either in 25L (i.e. north) or 25R (i.e. south) runways.

Figure V-8 shows this procedure. Note that the altitude in the last segment of the trombone procedure (waypoints from DF426 to DF422 and waypoints from DF626 to DF622 for north and south arrivals, respectively) is different, being 4,000 ft for south arrivals and 5,000 ft for north arrivals. Therefore, in the final segment aircraft are separated vertically by 1,000 ft.

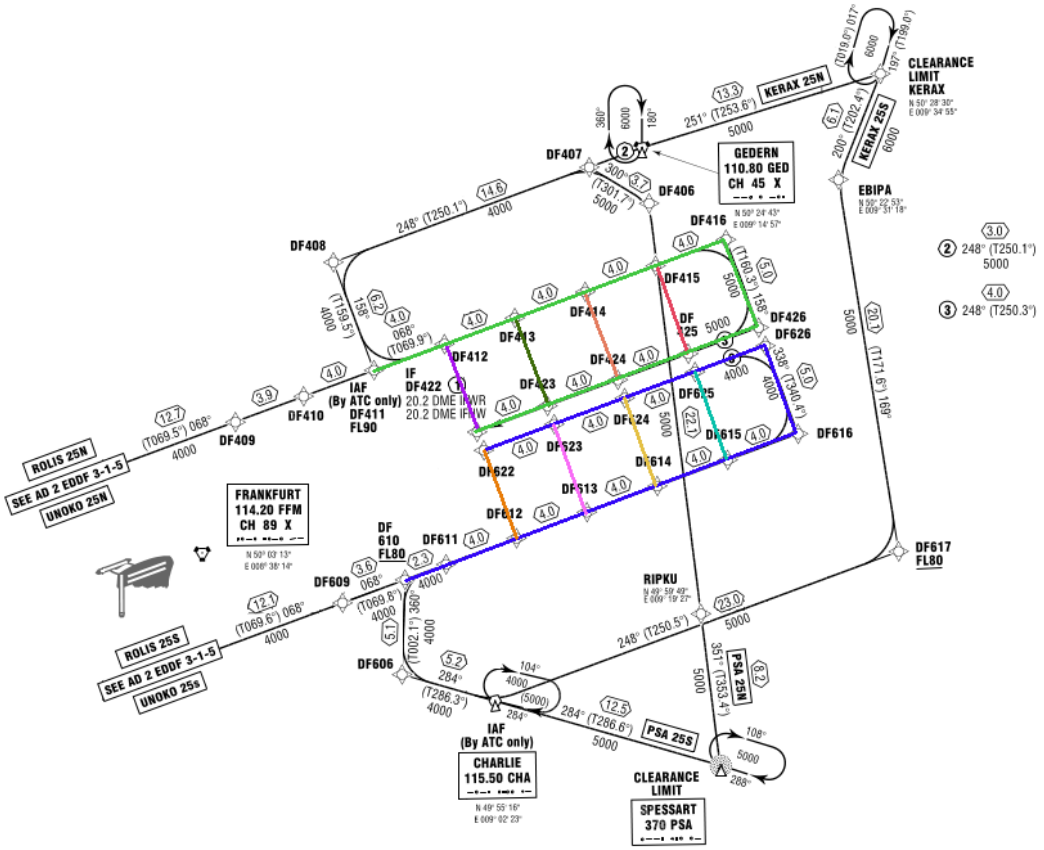

Figure V-8: *Frankfurt am Main Airport (EDDF) GPS/FMS RNAV 25L/C/R Tromboning (Eurocontrol, 2018a)*

Besides the tromboning, STARs are also used. There are 7 STAR entry points in Frankfurt airport. PSA, ROLIS, UNOKO and KERAX are shown in Figure V-8. EMPAX, ASPAT and PETIX

STARs all converge in PSA, from where they continue the PSA STAR. In addition, each entry point allows the aircraft to fly the arrival procedure to both the north or the south runway (e.g. KERAX 25S and PSA25S lead to runway 25L; and KERAX 25N and PSA25N lead to runway 25R). The tromboning common part for all entry points starts at waypoint DF411 for the north runway (colored in green in Figure V-8) and at DF610 for the south runway (colored in blue in Figure V-8). From these points on, the ATCO could potentially give a shortcut at any of the regularly spaced waypoints, depending on the volume of traffic. Thus, for each entry point there are only 5 possible routes, as it is only possible to assign 5 shortcuts in the trombone. For the north runway arrivals, the shortcuts are given in waypoints from DF412 to DF416 (both included), and for the south runway arrivals in waypoints from DF612 to DF616 (both included). The tromboning ends at the intermediate fix (IF) of the approach, which is the waypoint DF422 for the north and DF622 for the south runways, respectively.

Table V-1 shows all potential tromboning routes for north and south runway arrivals, identified with different colors as in Figure V-8. Route numbers from 01 to 05 correspond to arrivals to the north runway while route numbers from 06 to 10 correspond to arrivals to the south runway. The higher the route number the shortest the route (for north and south, respectively). In this table, the distance for each tromboning route is also given. For instance, for route 08, corresponding to the south case, a shortcut is given at DF614 towards DF624, skipping the waypoints from DF615 to DF625 and reducing by 16 NM the total distance flown. Finally, the metering fix for each runway has been set to the respective intermediate fixes (DF422 and DF622).

Table V-1: *Potential routes for Frankfurt trombone procedure (North and South cases)*

ID	Waypoint sequence	Distance [NM]
01	DF411-...-DF416-DF426-...-DF422	41
02	DF411-...-DF415-DF425-...-DF422	33
03	DF411-...-DF414-DF424-...-DF422	25
04	DF411-...-DF413-DF423-DF422	17
05	DF411-DF412-DF422	9
06	DF610-...-DF616-DF626-...-DF622	43.3
07	DF610-...-DF615-DF625-...-DF622	35.3
08	DF610-...-DF614-DF624-...-DF622	27.3
09	DF610-...-DF613-DF623-DF622	19.3
10	DF610-...-DF612-DF622	11.3

V.4.2 Models

For all the experiments conducted in this chapter, the aircraft dynamics model, performance model and weather model were identical to those used in Chapter III (Section III.3.1). A point-mass model reduced to a γ-*command* model was considered, as well as the base of aircraft data (BADA) v4 aircraft performance model (APM). The weather data was obtained from gridded binary (GRIB) formatted files; more specifically, for each arriving flight, the GRIB file corresponding to its entry point at the E-TMA time was used.

V.4.3 Optimal Control Problem Formulation

In this chapter, the optimal control problem considered was identical to the one presented in Chapter III (Section III.3.2). In real life, the trajectories generated by solving this optimal control problem would be generated by an advanced functionality of the FMS of each aircraft, equipped with

the RTA functionality.

The initial state of the aircraft, consisting of the cruise altitude, cruise speed and distance to go in the E-TMA entry point, was obtained directly from an historical-flight database, as detailed in Section V.4.4. The final state considered was set to a speed equal to the green dot speed (GD), an altitude equal to 2,000 feet and a distance to go equal to 0 NM.

As an example, Figure V-9 shows several optimal speed profiles for an Airbus A320 Neo and for several CIs (i.e. RTAs), in international standard atmosphere (ISA) conditions and no wind. A distance to go of 378 NM, a cruise true airspeed (TAS) of 430 kt and a cruise altitude at FL360 were used as initial conditions for the generation of these illustrative trajectories. The initial time (t_0) was set at 17:01:31 and the final state was defined assuming a distance to go of 0 NM, a final altitude of 2,000 ft and a final airspeed equal to the GD[2].

The *bang-singular-bang* behavior described in Section II.2.2 can be observed in these speed profiles, with a non-singular arc from the time when the descent starts (t_{TOD} in Figure V-9) to the singular arc and a final non-singular arc from the singular arc to the final time at the metering fix (t_f in Figure V-9). It can be observed how the optimal speed profiles lie in between the boundaries delimited by $v_{CAS,min}$ and MMO/VMO, as enforced by Eq. (III.8). Also note that since these maximum and minimum speeds are given in terms of callibrated airspeed (CAS) and Mach, the corresponding TAS changes with altitude. The earlier the RTA, the closer the speed profile is to the MMO/VMO bound and, on the other hand, the later the RTA, the closer the speed profile is to the $v_{CAS_{min}}$ line. Therefore, the speed profiles corresponding to the earliest and latest trajectories (purple and cyan lines, respectively) try to match as soon as possible the MMO/VMO and $v_{CAS,min}$ speed profiles, respectively.

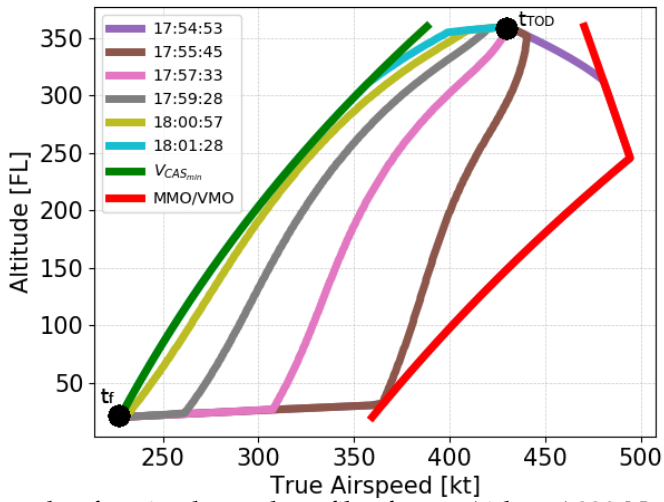

Figure V-9: *Example of optimal speed profiles for an Airbus A320 Neo and several required times of arrival in ISA and no wind conditions*

Figure V-10 shows the evolution of the aircraft pressure altitude (h_p) and speed (i.e., TAS, CAS, and M), as a function of the remaining distance to the metering fix, for the earliest (17:54:53) and latest (18:01:28) trajectories corresponding to the illustrative flight presented before. Note that the y-left axis is used to represent both altitude and airspeed. In this study, the cruise speed is kept constant to the originally planned speed, optimizing only the descent trajectory. In Figure V-10(a) it is observed how the aircraft accelerates to the MMO right after the TOD. This descent at constant Mach implies an increase of the CAS and, when reaching the VMO, the descent continues at this

[2]For the Airbus A320 Neo, the GD is the minimum operating speed in managed mode and clean configuration, being approximately the best lift-to-drag ratio speed.

maximum speed. Few nautical miles before the metering fix a quick deceleration is observed in order to fulfill the speed constraint at this fix. Figure V-10(b), in turn, shows the latest trajectory, which slows down to $v_{CAS,min}$ right after the TOD.

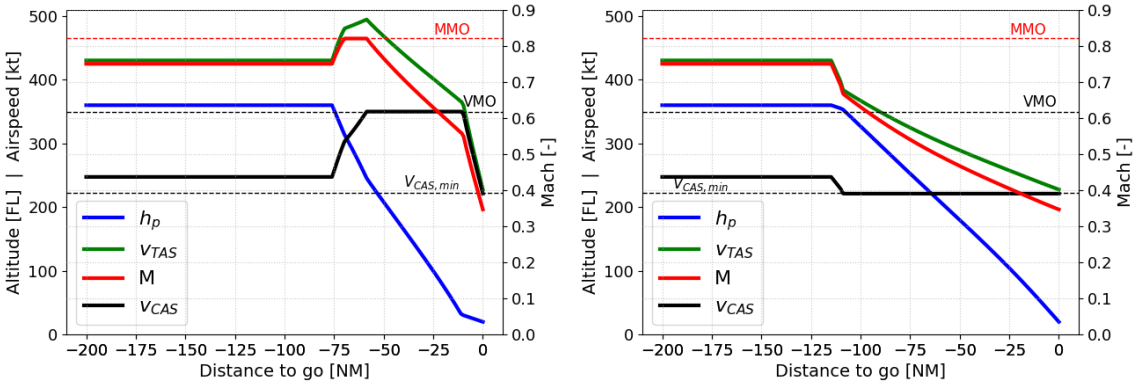

(a) Earliest trajectory (RTA = 17:54:53)

(b) Latest trajectory (RTA = 18:01:28)

Figure V-10: *Illustrative earliest and latest trajectories for an A320 Neo in ISA and no wind conditions*

For the earliest trajectory, a CI equal to 999 kg/min was used, while for the latest trajectory the CI was set to 0 kg/min. It is important to remark the fact that, in reality, aircraft could fly with a slightly negative cost index, thus leading to later times of arrival than those obtained when flying with a cost index equal to 0 (as considered in this chapter). In such a case, aircraft would be flying at a range of speeds between the lowest selectable speed (VLS) and the maximum lift-to-drag ratio speed. However, these speeds are hardly ever chosen by aircraft crew in normal operations. In such a case, aircraft would be flying at unstable speeds (in the 2nd regime of the power curve or region of reversed command) and, although this is manageable by the auto-pilot, it usually involves undesired continuous actions on the aircraft throttle in order to keep the requested speed.

V.4.4 Case Studies

The assessment has been performed by using flight traffic data from August 10th, 2017. This data was obtained from Eurocontrol's demand data repository (DDR) (Eurocontrol, 2017), which contains historical trajectory data (M3 format). In that day, there were 731 flights (divided into 52 aircraft types) arriving at Frankfurt airport; the demand per hour, in Coordinated Universal Time (UTC), is shown in Figure V-11.

Section V.4.4.1 presents the baseline case studies. Then, Section V.4.4.2 focuses on the discretization of the available routes in Frankfurt airport and the computation of the profiles. Finally, Section V.4.4.3 details a set of enhancements added to the scenario analyzed in this chapter.

V.4.4.1 Baseline Case Studies

In this chapter, three time periods of the day of study are selected to validate the proposed algorithm, which represent three different traffic situations (they are highlighted in different colors in Figure V-11). They correspond to the three baseline case studies:

- High-traffic case study (red): from 17 to 18 UTC
- Medium-traffic case study (yellow): from 07 to 08 UTC

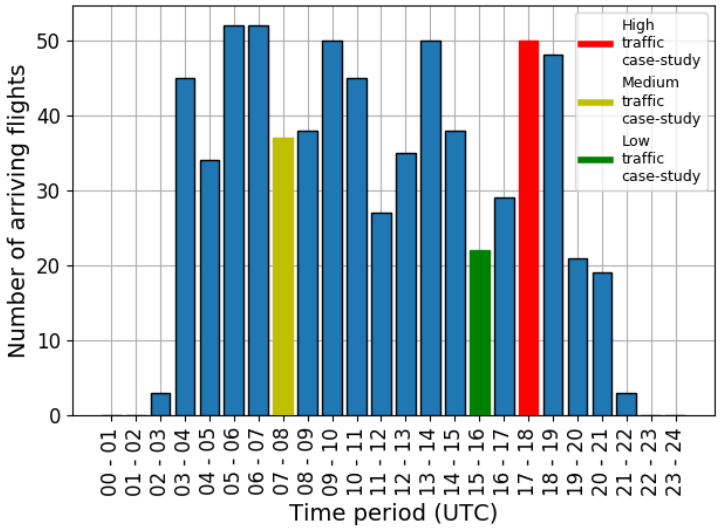

Figure V-11: *Frankfurt airport demand per hour on August 10th, 2017. The 3 case studies are highlighted.*

- Low-traffic case study (green): from 15 to 16 UTC

For all case studies, a separation between aircraft has to be ensured in order to maintain the safety of the operation. The separation will be defined by taking into account the wake turbulence categorization proposed by the international civil aviation organization (ICAO) (SKYbrary, 2020a), which classifies aircraft into three categories depending on their maximum take-off mass. In this chapter, the minimum time separation between aircraft that ICAO proposes according to that categorization (ICAO, 2016) will be used: 180 seconds of time separation will be considered for light aircraft following medium or heavy aircraft, while 120 seconds will be considered otherwise. During the day chosen for the experiment, there were 184 heavy aircraft, 544 medium aircraft and 2 light aircraft (17 heavy, 52 medium and 2 light different aircraft types among all the arriving traffic). The distribution of aircraft in the case studies chosen was the following:

- High-traffic case study: 5 heavy and 45 medium aircraft (4 heavy and 9 medium different aircraft types)
- Medium-traffic case study: 9 heavy and 28 medium aircraft (7 heavy and 9 medium different aircraft types)
- Low-traffic case study: 6 heavy and 16 medium aircraft (5 heavy and 10 medium different aircraft types)

As it has been mentioned in Section V.4.1, a separation of 1,000ft between north and south arrivals is ensured in the final segment of the tromboning. However, in this chapter, neutral CDOs are assumed, which means that this vertical separation is not necessarily ensured. Therefore, it would be considered that the runways are not independent and that a lateral separation should also be ensured between north and south arrivals in the final segment. This means that, for instance, it would not be possible that two aircraft are at the same time at waypoints DF424 and DF624 (Figure V-8).

V.4.4.2 Profiles Computation

All routes that can be found in the Frankfurt airport arrival and approach charts were discretized in 5-NM-length segments. Then, 10 profiles were generated per available route an aircraft could

fly, with RTAs equally spaced in time in the available time window at the metering fix. This means that if the time window at the metering fix for a given aircraft flying a given route was, for instance, equal to nine minutes, there would be one profile per minute (both the earliest and latest arrival times to the metering fix are included). This is illustrated in Figure V-12, where p stands for profile (e.g. $p1$ is profile 1). RTA_E and RTA_L are the earliest and latest times of arrival at the metering fix for a given route, respectively.

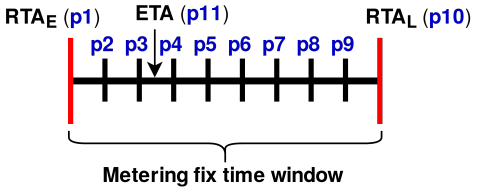

Figure V-12: *Time window and candidate profiles for a given route*

It is worth noting that this time window (defined as the difference between the earliest and latest arrival times to the metering fix) is computed per available route. Therefore, the final time window or "absolute" time window for each aircraft used in the scheduling algorithm will be given as the difference between the earliest time of arrival for the shortest route and the latest time of arrival for the longest route.

Finally, an extra profile was generated and added to the set of profiles, which corresponds to the desired trajectory by the airline that gives the ETA at the metering fix. In this chapter, the shortest route per aircraft was considered to compute this ETA, along with the speed (and time) profiles extracted from the DDR data.

V.4.4.3 Model Enhancements

Besides performing the profile assignment for the three baseline case studies defined in Section V.4.4.1, six additional enhancements were added to the scenario analyzed in this chapter. In case of infeasible scenarios, in which not all aircraft can be scheduled, these enhancements could help to improve the results.

- **Additional shortcuts**: in the current Frankfurt trombone procedure there are 10 available shortcuts per STAR entry point, 5 for the north and 5 for the south (more details in Section V.4.1). The number of shortcuts could also be modified in order to add more possible routes for the incoming aircraft. In this case, three waypoints are added between waypoints DF407 and DF408, which suppose three new shortcuts, as shown in Figure V-13.

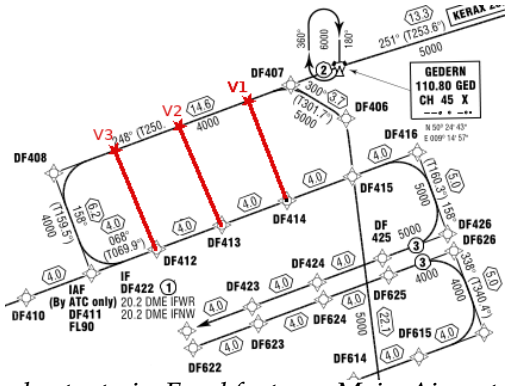

Figure V-13: *Three new shortcuts in Frankfurt am Main Airport (EDDF) GPS/FMS RNAV 25L/C/R trombone procedure (source: German AIP)*

- **Entry time**: the arrival time to the E-TMA is manually modified for all incoming aircraft, seeking to improve the output of the aircraft landing problem (i.e. to maximize the number of neutral CDOs while ensuring a safe separation between aircraft). Two additional case studies are considered, one with a maximum variation of $\pm$ 2 minutes in the entry time and another one with a maximum variation of $\pm$ 5 minutes. For instance, in the $\pm$ 2 minutes case, if an aircraft was expected to arrive at 10:00 at the E-TMA, it is assumed that it could also arrive at 9:58 and 10:02. In a real situation, this change in the entry time could be achieved during the en-route phase. As shown in previous works, these modifications in the entry time are feasible. From the results obtained by Delgado & Prats (2012), it can be concluded that, for typical CIs between 30 kg/min and 100 kg/min, aircraft can gain/lose between 1.2 seconds/NM and 4 seconds/NM. Therefore, assuming a cruise length of between 75 NM and 250 NM aircraft would be able to arrive 5 minutes earlier or later to the E-TMA entry point. These values depend on several factors, like the aircraft type or the cruise flight level. Furthermore, the wind can also affect the amount of time that can be gained/lost during cruise (Delgado & Prats, 2013).

- **Fairness in the delay assignment**: the cost function used in the aircraft landing problem defined in Eq. (V.4) does not consider any equity between flights when assigning delay. Therefore, a new cost function was defined in order to assign delays moderately across all flights, instead of unevenly to one particular flight (Bertsimas & Patterson, 1998). The total delay is raised to a given coefficient (1+ϵ) (with ϵ slightly greater than 0) as follows:

$$\min \quad J := \sum_{a \in \mathcal{A}} \sum_{p \in \mathcal{P}_a} x_{a,p} \cdot \left(|\mathrm{RTA}_{a,p} - \mathrm{ETA}_a|\right)^{(1+\epsilon)} \tag{V.5}$$

  This is just a preliminary approach toward the consideration of fairness in the delay assignment; in future work it is planned to explore more fairness strategies.

- **Time separation**: in the baseline case studies, RTAs are assumed to be met with a 100% of accuracy. However, this is not the case in actual operations, as perturbations during flight may introduce errors in meeting the RTA. However, Prats *et al.* (2017) showed that RTAs can be achieved with errors lower than 10 seconds at the final approach point, while a good RTA accuracy can be maintained too in presence of significant wind prediction errors (Dalmau *et al.*, 2016). Further guidance improvements were proposed by Dalmau *et al.* (2019a), showing even better results in terms of RTA accuracy for neutral trajectories (using only energy modulation). All these works endorse the assumption that RTAs can be achieved with high levels of accuracy, thus enabling robust neutral CDOs . Still, inaccuracies will be always present, so based on the aforementioned results, another case will be analyzed, in which the minimum time separation between the arriving aircraft is increased by 20 seconds. This corresponds to the worst case scenario if an accuracy of 10 seconds in the RTA is assumed: if considering two aircraft with their corresponding RTAs separated by 120 seconds, the worst situation would be the one in which the leading aircraft is arriving at the metering fix 10 seconds later than its RTA and the trailing aircraft arrives 10 seconds earlier.

- **Independent runways**: independent runways are assumed in this enhancement, which means that during the final segment of the tromboning a vertical separation is supposed to be maintained between the north and south arrivals. As a result, it is no longer necessary to maintain a lateral separation between traffic arriving to different runways in the final segment of the tromboning. This assumption is endorsed by Fricke *et al.* (2015), in which it is described that, for any given flight, a *vertical CDO corridor* can be defined, in which all the flyable CDOs are contained. However, not all these CDOs would be optimal from an efficiency point of view. Still, the definition of these corridors would be useful to apply the

methodology described in this chapter for a procedure with independent runways. By applying altitude restrictions in the corridors it would be possible to force the aircraft to fly those trajectories that ensure a vertical separation in the final segment of the tromboning. This may lead to fly sub-optimal CDOs , but it would keep the safety of the operation.

V.5 Results

This section presents the results obtained after simulating the scenario and case studies described in Section V.4. Section V.5.1 presents an analysis of the time window for all case studies. Then, Section V.5.2 analyzes the results obtained for the baseline case studies, while more details are given in Section V.5.3. It is shown that not all aircraft can be scheduled in all three baseline case studies, mainly due to high traffic density in the medium and high-traffic case studies and the fact that only neutral CDOs are assumed. Better results are presented in Section V.5.4, showing how by changing some parameters (Section V.4.4.3) it is possible to increase the number of neutral CDOs with a safe separation in the medium and high-traffic case studies. Regarding computational times, the set of profiles was generated in around 5 minutes per aircraft. Then, the incompatible profiles were found in 10 to 30 minutes (depending on the volume of traffic) and finally, the optimizer (the MILP formulation) took between 1 and 5 minutes (depending on the volume of traffic) to find the optimal feasible profile combination. All computations were made in a laptop computer running Ubuntu 18.04 LTS, with 16GB of RAM memory and an Intel(TM) Core(R) i7-7500U @ 2.70GHz processor. While these computational times might seem high, they are enough to generate the flight arriving sequence. However, in this case, aircraft might need to establish the communication with the ATC before entering the E-TMA, so that the RTA and the route are assigned before the optimal TOD. Another option would be to extend the E-TMA size in order to perform the required computations while the aircraft is in cruise before the TOD, but inside the E-TMA.

V.5.1 Time Windows Analysis

As detailed in Section V.4.4.2, 11 profiles are computed per available route an aircraft can potentially fly, being the "absolute" time window the difference between the earliest time of arrival for the shortest route and the latest time of arrival for the longest route. The time window is affected by the aircraft model, and by the entry point, which will determine the potential routes an aircraft could fly.

Figure V-14 shows the time window value distribution for the three traffic case studies. As it can be observed, the median value for all case studies is very similar, around 650 seconds ($\approx$ 10 minutes). Maximum values of up to 1000 seconds ($\approx$ 16 minutes) are observed in the high-traffic case study, while the minimum value, found in the medium-traffic case, is 200 seconds ($\approx$ 3 minutes).

For illustrative purposes, Figure V-15 shows the time windows at the metering fix for all available routes of an Airbus A320 Neo flying the EMPAX arrival procedure. The time in the x-axis corresponds to the time flown from the E-TMA entry point—while the aircraft is still in cruise—until the metering fix. For every route, time windows are about 6 to 7 minutes, being the total time window in the metering fix (i.e. the difference between the earliest and latest times of arrival considering all routes) around 15 minutes. It can be observed how several routes could be chosen to attain the same RTA, although in some cases this would mean not flying with the optimum speed profile.

The computation of the vertical and speed profiles is of high importance for the work pre-

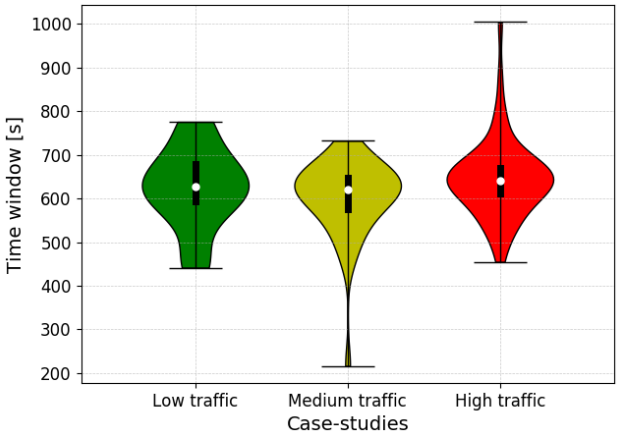

Figure V-14: *Time windows for the baseline case of the 3 traffic case studies*

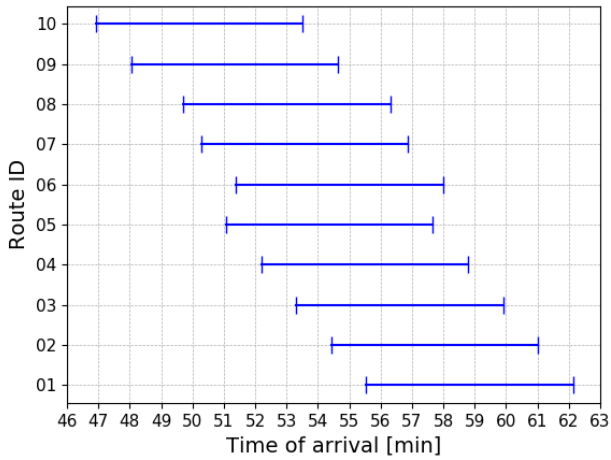

Figure V-15: *Time windows for the available routes of an A320 Neo flying the EMPAX arrival procedure*

sented in this chapter, as it allows to know the earliest and latest times of arrival to the metering fix and, therefore, the feasible time window for each distance to go corresponding to a trombone shortcut. Figure V-10 in Section V.4.3 showed the earliest and the latest trajectories for the same A320 Neo used to generate the time windows of Figure V-15, which flew the Frankfurt EMPAX arrival procedure. The earliest case corresponds to route 10 of the arrival procedure and the latest case to route 01 (Table V-1).

V.5.2 Profile Assignment Results

Table V-2 shows the percentage of aircraft successfully scheduled for the three traffic case studies. As it can be observed, only for the low-traffic case study all aircraft can be scheduled. While the number of aircraft in the low-traffic case study is 22, in the time periods corresponding to the medium and high-traffic case studies (7-8 UTC and 17-18 UTC, respectively) there were 37 and 50 aircraft arriving at Frankfurt airport.

As the traffic density increases, it becomes more difficult to schedule all aircraft with the current trombone procedure and entry times. The number of aircraft merging in the several waypoints of the procedure increases, and time separation cannot be ensured throughout the descent

Table V-2: *Percentage of aircraft scheduled per case study*

Case study	Number of aircraft (in 1h)	% aircraft scheduled
Low traffic	22	100%
Medium traffic	37	84%
High traffic	50	68%

for any combination of route and RTA at the metering fix.

At this point, it is worth recalling that all the trajectories being considered in this chapter are neutral CDOs with idle thrust and no speed brakes usage, so the time windows in the metering fix are smaller than those that can be achieved with powered descents (where thrust and speed brakes are allowed). Therefore, there is not much flexibility regarding the arrival time in the metering fix, which makes the aircraft scheduling process more challenging. In a real situation, all traffic that cannot be accommodated with neutral CDOs would eventually be sequenced by giving RTAs requiring thrust/speedbrakes or even level-offs (so, *breaking* the CDO). The optimal solution for these case studies where not all aircraft can fly a neutral CDO is an interesting research problem that will be assessed in future work. The purpose of the work presented in this chapter is to show that the proposed CONOPs already allows to fly neutral CDOs to a very significant percentage of the incoming traffic.

Finally, only 11 profiles per aircraft and route are considered in this chapter. Perhaps a finer discretization could help to potentially find more feasible profiles.

Figure V-16 shows the delay distribution (i.e the difference between the RTA and ETA) for the three baseline case studies, by taking into consideration only those aircraft that were successfully scheduled. The low-traffic case study shows relatively low delay values, where most of the aircraft scheduled are landing close to their ETA. On the other hand, the medium and high-traffic case studies show a different behavior, where a large number of aircraft is assigned a high delay in order to sequence all traffic. Still, in both cases the maximum delay remains below 650 seconds ($\approx$ 11 minutes). This is understandable as the value of maximum delay that could be achieved is strictly related to the value of the time window: it is impossible for an aircraft to have a higher delay than its time window width. Both the medium and high-traffic case studies show a similar distribution (with a slightly higher dispersion in the high-traffic case). However, although the percentage of aircraft scheduled is higher in the medium case, it represents almost the same number of aircraft than in the high case (31 and 34 aircraft respecitvely). This leads to the conclusion that similar results would be obtained if the traffic density kept increasing: the distribution would be similar but the percentage of aircraft scheduled would decrease.

Figure V-17 shows the extra distance flown for the three baseline case studies and for the two versions of the cost function: with and without considering fairness in the delay assignment.

When possible, the scheduling algorithm tries to assign the shortest route to the aircraft. This is well illustrated in the low-traffic case study, where 11 aircraft (half of the aircraft sample during that hour) are assigned the shortest possible route. In the medium-traffic case study, more shortcuts are used in order to maintain separation, and the extra distance flown increases. This is more obvious in the high-traffic case study, where only one third of aircraft are assigned the shortest possible route, while the rest are assigned longer shortcuts.

V.5.3 Detailed Results for the Baseline Case Studies

Table V-3 shows all aircraft arriving in Frankfurt airport for the low-traffic case study, the totality of which were successfully scheduled with the solution proposed in this chapter. The DDR flight id, the STAR entry point and the ETA for the incoming traffic are given. Furthermore, the route

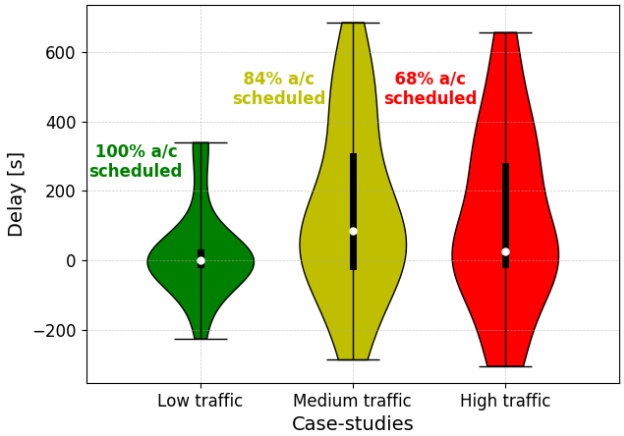

Figure V-16: *Delays for the baseline case of the 3 traffic case studies*

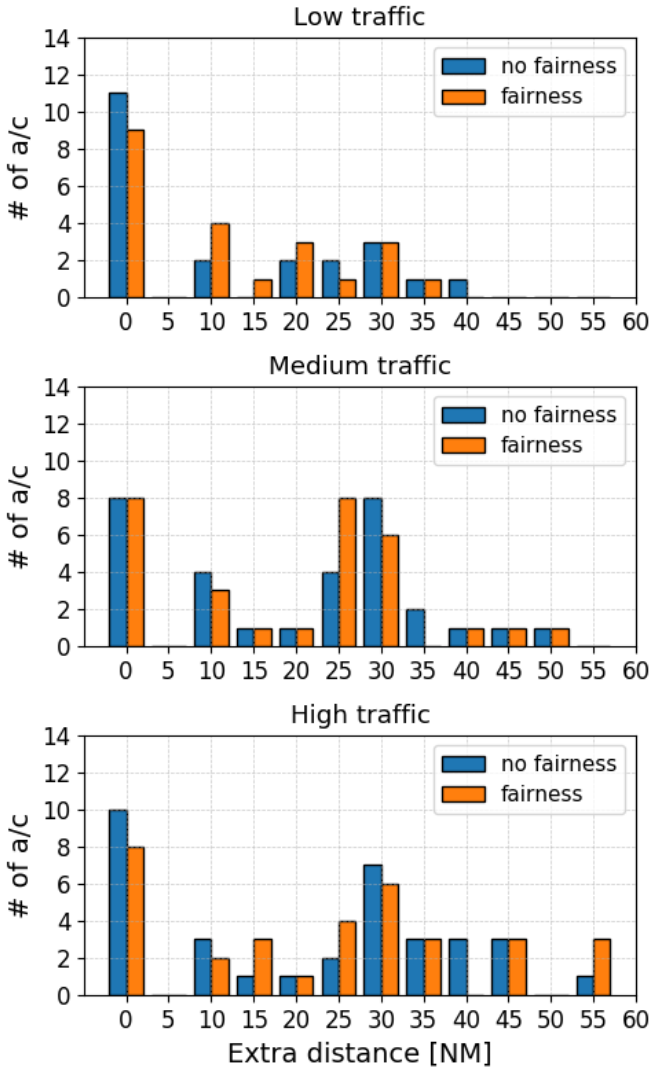

Figure V-17: *Extra distance flown for the baseline case of the 3 traffic case studies*

and RTA assigned to each aircraft are shown (i.e. profile), as well as the corresponding delay when flying that profile.

Table V-3: *Results for the low-traffic baseline case study*

Flight ID	Entry point	Route	ETA (UTC)	RTA (UTC)	Delay (sec.)
209912693	ASPAT	08	14:57:13	14:55:49	-84
209903832	KERAX	05	14:57:58	14:57:58	0
209922177	UNOKO	10	14:59:41	15:00:28	47
209923238	UNOKO	05	15:04:23	15:04:23	0
209909575	UNOKO	05	15:10:58	15:10:58	0
209903416	KERAX	01	15:13:56	15:13:29	-27
209918608	ASPAT	07	15:17:44	15:15:36	-128
209919516	EMPAX	10	15:17:57	15:17:57	0
209920805	UNOKO	05	15:20:27	15:20:27	0
209922757	KERAX	05	15:25:17	15:25:17	0
209921846	EMPAX	10	15:29:59	15:29:59	0
209923949	KERAX	04	15:40:44	15:40:33	-11
209921936	KERAX	04	15:46:35	15:42:50	-225
209920383	PSA	04	15:45:08	15:44:56	-12
209919813	KERAX	05	15:47:47	15:47:47	0
209920720	ASPAT	05	15:48:37	15:50:10	93
209922778	EMPAX	10	15:46:37	15:52:18	341
209923810	UNOKO	06	15:48:50	15:54:29	339
209924354	KERAX	10	15:53:14	15:56:40	206
209924874	ASPAT	08	16:03:45	16:02:21	-84
209921663	EMPAX	05	16:04:39	16:04:34	-5
209924577	UNOKO	10	16:05:47	16:06:40	53

As it can be observed in Table V-3, the "delay" for some aircraft is negative, which means they are assigned an RTA before the ETA. In average, the delay for the low-traffic case study is 75 seconds, while the maximum absolute delay is 341 seconds (almost 6 minutes). Overall, these delay values are relatively low.

Another interesting matter is the actual routes assignment. Depending on the entry point, one of the runways (i.e. north or south) would be more desirable for the incoming aircraft, as it would mean flying a shorter route. For aircraft starting the arrival procedure in KERAX, ROLIS and UNOKO route 05 is the shortest one, while for aircraft starting in PSA, ASPAT, PETIX or EMPAX route 10 would be the shortest one (Figure V-8). Table V-3 shows how half of the aircraft are assigned the shortest possible route (either 10 or 05 depending on the entry point). The rest are assigned shortcuts that increase the total distance flown, as shown in Figure V-17. Finally, tables V-4 and V-5 show the results for the aircraft successfully scheduled in the medium and high-traffic baseline case studies, respectively.

V.5.4 Model Enhancement Results

As it has been explained in Section V.5.2, the 100% of the incoming traffic was only scheduled for the low-traffic case study, while losses of separation were found in the medium and high-traffic case studies that were not possible to solve with neutral CDOs and the available set of routes. This section analyzes the effect of changing certain parameters, as explained in Section V.4.4.3. These are the availability of additional tromboning shortcuts, the entry time distribution, the fairness strategy and the time separation. Table V-6 shows the percentage of aircraft scheduled, average delay and maximum delay per case study.

Figure V-18(a) shows the delay distribution for all the case studies and for all the enhancements made to the model except for the time separation analysis, which is shown in Figure V-18(b).

Table V-4: *Results for the medium-traffic baseline case study*

Flight ID	Entry point	Route	ETA (UTC)	RTA (UTC)	Delay (sec.)
209901616	UNOKO	03	06:56:38	06:56:04	-34
209905972	UNOKO	05	06:58:13	06:58:13	0
209905861	KERAX	09	06:59:20	07:00:14	54
209907338	UNOKO	10	07:08:50	07:04:38	-252
209906369	ASPAT	10	07:10:12	07:07:15	-177
209904895	KERAX	01	07:11:24	07:09:20	-124
209901977	KERAX	04	07:16:16	07:11:31	-285
209906786	UNOKO	05	07:13:34	07:13:34	0
209901604	UNOKO	10	07:16:06	07:15:37	-29
209907498	PSA	06	07:16:22	07:17:43	81
209907734	KERAX	05	07:20:59	07:20:16	-43
209908172	KERAX	02	07:20:17	07:22:21	124
209906547	PSA	04	07:17:31	07:24:48	437
209901559	UNOKO	09	07:25:06	07:26:50	104
209907708	UNOKO	07	07:24:24	07:29:05	281
209905137	EMPAX	05	07:24:05	07:31:46	461
209907807	KERAX	07	07:23:43	07:33:47	604
209905625	EMPAX	08	07:28:23	07:35:49	446
209908418	KERAX	10	07:36:40	07:38:05	85
209907380	UNOKO	04	07:39:08	07:40:06	58
209906733	EMPAX	06	07:40:17	07:42:12	115
209903091	PSA	07	07:46:30	07:44:52	-98
209902050	UNOKO	05	07:41:37	07:46:54	317
209900481	UNOKO	01	07:45:32	07:49:08	216
209907033	ASPAT	05	07:47:57	07:51:32	215
209907121	EMPAX	05	07:44:16	07:53:46	570
209908891	ASPAT	05	07:52:24	07:55:47	203
209907163	UNOKO	06	07:46:25	07:57:50	685
209906791	PSA	09	07:52:13	07:59:57	464
209909054	KERAX	08	08:03:03	08:02:55	-8
209909126	UNOKO	10	08:04:19	08:04:58	39

Table V-5: *Results for the high-traffic baseline case study*

Flight ID	Entry point	Route	ETA (UTC)	RTA (UTC)	Delay (sec.)
209921147	KERAX	04	16:54:05	16:49:01	-304
209905779	KERAX	04	16:54:52	16:51:42	-190
209924440	KERAX	05	16:53:43	16:53:43	0
209916195	ASPAT	10	16:55:44	16:55:44	0
209914280	KERAX	05	16:58:49	16:58:49	0
209904774	KERAX	01	17:06:36	17:06:39	3
209924901	ASPAT	08	17:13:18	17:08:43	-275
209925944	KERAX	04	17:15:05	17:11:02	-243
209906722	KERAX	05	17:13:35	17:13:13	-22
209923488	UNOKO	01	17:10:34	17:15:21	287
209926911	EMPAX	10	17:17:41	17:17:41	0
209979722	ASPAT	03	17:13:53	17:19:41	348
209921346	KERAX	05	17:23:39	17:23:39	0
209926920	PSA	03	17:18:44	17:25:41	417
209926853	KERAX	08	17:17:55	17:28:24	629
209926587	ASPAT	07	17:30:58	17:31:26	28
209927424	KERAX	03	17:35:32	17:34:06	-86
209927718	KERAX	05	17:36:52	17:36:52	0
209927556	EMPAX	07	17:35:07	17:38:55	228
209924578	KERAX	09	17:31:38	17:40:56	558
209926663	UNOKO	06	17:32:37	17:43:34	657
209927152	PSA	05	17:41:59	17:46:05	246
209924673	UNOKO	01	17:48:32	17:48:13	-19
209926303	UNOKO	10	17:45:58	17:50:14	256
209927974	KERAX	05	17:56:58	17:52:17	-281
209927560	KERAX	06	17:47:42	17:54:57	435
209924999	ASPAT	04	17:56:05	17:57:13	68
209925224	PETIX	04	17:53:08	17:59:48	400
209928111	ASPAT	05	17:59:00	18:02:26	206
209925155	PETIX	05	18:01:48	18:05:34	226
209927507	UNOKO	06	18:01:54	18:08:00	366
209927876	UNOKO	10	18:16:42	18:16:19	-23
209927762	APSAT	04	18:18:02	18:18:23	21
209928341	PSA	05	18:19:22	18:20:58	96

As it can be observed, the number of aircraft successfully scheduled increases in those case studies where there is a change in the entry time. Dispersion also decreases, and delay is reduced. However, in the high-traffic case study it is still not possible to schedule the totality of the aircraft, even with a variation in the entry time of $\pm$ 5 minutes there is still one aircraft that cannot be scheduled. The traffic order at the entry point is a very significant factor when scheduling the aircraft and in this case it was impossible to keep a minimum time separation between this remaining aircraft and the rest of the arriving traffic if neutral CDOs were flown. However, flying powered descents could help in this case. Nonetheless, it is worth noting the fact that by slightly modifying the entry time of the arriving aircraft it is possible to greatly increase the number of neutral CDOs that can be flown, even with high traffic loads.

Regarding those case studies where additional shortcuts are added to the tromboning, although it is true that the delay is slightly reduced, it is not enough to ensure the minimum time separation between all aircraft throughout the procedure when the traffic density is high.

When fairness is considered, it can be observed that in all case studies the average delay increases. In the low and high-traffic case studies, the maximum delay remains almost the same, while in the medium-traffic case study it decreases approximately by 1 minute.

In general, due to the modification of the cost function, aircraft with a higher delay than

Table V-6: *Model enhancement results*

Traffic case study	Enhancement case	% a/c scheduled	Avg. delay (seconds)	Max. delay (seconds)
Low	baseline	100%	75	341
Low	$\pm 2'$	100%	58	234
Low	$\pm 5'$	100%	53	296
Low	additional shortcuts	100%	70	355
Low	Fairness	100%	89	340
Low	$t_{sep} + 20s$	100%	113	556
Low	indep. runways	100%	29	259
Medium	baseline	84%	213	685
Medium	$\pm 2'$	100%	142	721
Medium	$\pm 5'$	100%	101	488
Medium	additional shortcuts	84%	209	685
Medium	Fairness	84%	222	622
Medium	$t_{sep} + 20s$	71%	123	364
Medium	indep. runways	84%	64	317
High	baseline	68%	203	657
High	$\pm 2'$	76%	77	277
High	$\pm 5'$	98%	137	488
High	additional shortcuts	68%	150	558
High	Fairness	68%	222	657
High	$t_{sep} + 20s$	60%	142	389
High	indep. runways	72%	99	643

average have now a lower delay, while aircraft that had a very low delay have now experienced some increase in the delay. However, some of the aircraft still have the same assigned delay due to the separation constraint; one such example is the aircraft which was assigned the highest delay in the high-traffic case study; as it can be seen in Table V-6, the maximum delay for the high-traffic case study is the same in both cases.

Figure V-17 shows the extra distance flown by the aircraft to meet the assigned RTA with and without fairness considered in the delay assignment. It can be observed how some of the aircraft that before were assigned the shortest route (extra distance equal to 0 NM) are now assigned longer routes. For instance, in the low-traffic case study, the number of aircraft flying the shortest route is decreased by 2. On the other hand, some of the aircraft that were assigned longer routes before the modification, are flying shorter ones now, like the aircraft that was flying 40 extra NM in the low-traffic case study, which is no longer present in that distance range.

When considering changes in the minimum time separation between aircraft, big variations can be observed in both the number of aircraft scheduled and the average and maximum delay values (Table V-6). In the low-traffic case study, the number of aircraft scheduled remains 100%; however, having a higher time separation translates into a higher delay dispersion, with both higher maximum and average delays (Figure V-18(b)).

For the medium and high-traffic case studies, the situation is different, as not all aircraft are scheduled. The higher the time separation the lower the number of aircraft scheduled. In both case studies, it can be observed that the delay decreases when the minimum separation is higher. When the separation increases, less aircraft can be scheduled and those which end up being scheduled require lower delays, as they can use the "room" left by the non-scheduled aircraft. However, the entry time distribution may have a big effect in this case. Furthermore, the delay dispersion decreases.

Finally, if independent runways are considered, the results greatly improve, with lower average and maximum delays for all case studies (Table V-6, Figure V-18(b)). However, the number of aircraft scheduled remains almost equal for all case studies, with a slight increase in the high-

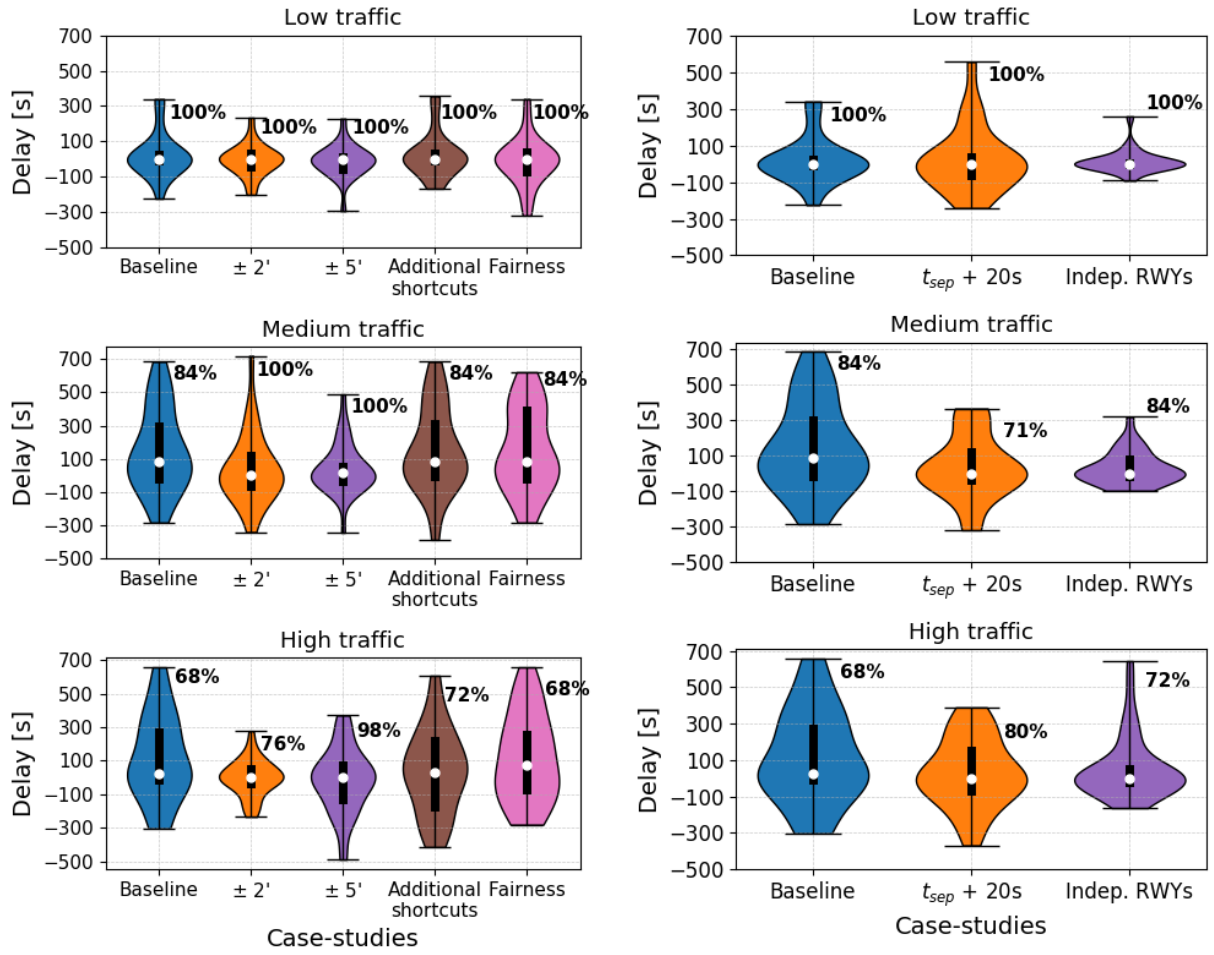

(a) Different entry time, additional shortcuts and fairness in the delay assignment

(b) Different time separation and independent runways

Figure V-18: *Delay distribution and percentage of aircraft scheduled for each case study and for different model enhancements*

traffic case study. Once again, it can be concluded that the traffic order at the entry point has a big effect in the number of aircraft that can be scheduled.

V.6 Discussion

This chapter proposed to sequence traffic in the TMA by means of 4D negotiated closed-loop instructions, based on current tromboning procedures, enabling aircraft to fly CDOs from cruise level to a given metering fix. Results show that, after assigning RTAs and routes to every arriving aircraft when still in cruise, it is possible to ensure that a high percentage of them will perform neutral CDOs (with idle thrust and no speed brakes usage), guaranteeing at the same time a safe separation between aircraft throughout the whole descent.

In the work presented in this chapter, the objective was to maximize the number of aircraft performing neutral CDOs. However, this kind of operations involve aircraft having a more limited time window in the metering fix than in powered descents (where both thrust and speed brakes usage is allowed). As a result, the scheduling process becomes more challenging. Furthermore, the aircraft entry distribution is also a key factor affecting the feasibility of the solution proposed.

Better distributions where aircraft arrive with enough separation at the entry points would represent an increase in the number of neutral CDOs performed and, therefore, an improvement in the efficiency of the operations.

While the CONOPs proposed in this chapter works properly for low-traffic scenarios, it could be concluded that, in some cases, in airports or time periods with high traffic loads, it might be necessary to reformulate it. Basically, it would be worth investigating the possibility of establishing the communication between the arriving aircraft and the ATC even before arriving at the E-TMA. As it has been shown, gaining or losing 5 minutes in the en-route phase, before entering the E-TMA, would avoid a lot of separation losses. Furthermore, other conflicts could also be avoided by gaining or losing time during the cruise section between the E-TMA entry point and the TOD, which could be achieved by increasing the size of the E-TMA.

Finally, due to the current computational times, the communication between the aircraft and the ATC might need to be established before the E-TMA too. Nonetheless, in this chapter the results were generated with a very simple prototype; there are several ways in which it could be improved: several tasks could be parallelized, a more efficient code could be written and a more powerful computer or server could be used.

The CONOPs proposed in this chapter should be understood as an "interim" solution between the current tactical operations and more futuristic and strategic approaches to the same problem with the TBO concepts deployed to its limits. In this chapter, the objective was to take advantage of advanced arrival and approach procedures currently in operation (such as tromboning) while maximizing the number of neutral CDOs performed, by negotiating a route and an RTA at a given metering fix. However, it would be very challenging or even impossible to deploy this solution in other types of procedures, such as STARs with very restrictive speed and altitude constraints or procedures that usually rely on intensive tactical radar vectoring. In these cases, neutral CDOs would be infeasible and the CONOPs presented in this chapter would not be viable. Furthermore, the solution presented in this chapter could also be useful to set an air traffic management (ATM) performance ambition in current arrival procedures (as well as highlighting possible limitations), as it shows the best that can be done from the point of view of flight efficiency (as arrival aircraft fly energy-neutral CDOs).

In the specific case of the STARs with very restrictive constraints, it is assumed that in a future TBO environment some of these constraints could be removed in favor of RTAs in several waypoints for both arriving and departing traffic that would also allow the use of neutral CDOs (Vilardaga & Prats, 2015). Furthermore, aircraft not equipped with the RTA technology could not benefit from the solution proposed in this chapter and they should be given vector instructions from the ATC. However, in a fully-deployed TBO environment, it is reasonable to assume that (almost) all aircraft would be equipped with this functionality.

The solution proposed aligns with the TBO concept, where more detailed data is expected to be shared by aircraft and airlines, such as the extended projected profile (EPP) or more detailed aircraft intents downlinked. Thus, it is expected to become a technical enabler towards future arrival manager (AMAN) systems, providing more automated and enhanced ground support to ATCOs and allowing flights to perform more efficient descents. In this context, a series of operational concepts and technologies required to support future arrival management was proposed by Itoh *et al.* (2017). In order to exchange the data between ground and air specified in the CONOPs (Section V.2), current AMAN systems, as explained by Itoh *et al.* (2017), need to face several technical challenges. For instance, future AMANs should be able to exchange 4D trajectories and handle possible updates of this trajectory. Furthermore, all information should be shared as adequate structures in order to compute efficient arrival schedules via system-wide information management (SWIM) networks.

In this chapter, aircraft had a predefined number of arrival routes which were pre-negotiated

with the ATC, corresponding to the tromboning shortcuts. Next chapter goes one step further, and presents a CONOPs and methodology to generate arrival routes that automatically adapt to the current traffic demand and that are also pre-negotiated with the ATC.

He aquí, hoy por hoy, todo lo que ambiciono: ser un comparsa en la inmensa comedia de la humanidad; y concluido mi papel de hacer bulto, meterme entre bastidores sin que me silben ni me aplaudan, sin que nadie se dé cuenta siquiera de mi salida.
[Here I am, at present, and everything that I aspire to is to be an extra in the immense comedy of humanity; and once my role of making up the numbers is finished, getting behind the scenes without being whistled or applauded, without anyone even noticing my departure.]

— Gustavo Adolfo Bécquer

VI

Enabling CDOs in Dynamic Arrival Routes in Terminal Airspace

Ensuring separation in standard terminal arrival routes (STARs) represents a very demanding task for the air traffic control officers (ATCOs), who could face situations with very high workload for extended periods of time. Thus, automation tools are often needed in high-traffic-demand scenarios in order to help them ensure the necessary separation along the arrival routes and, especially, at the merge points.

In this context, Chapter V presented an interim solution towards a full trajectory based operations (TBO) concept, where the current tromboning sequencing and merging paradigm—which is based on open-loop instructions to assign the shortcuts—was enhanced with a four-dimensional

This chapter is based on the following publications:

- Sáez, R., Polishchuk, T., Schmidt, C., Hardell, H., Smetanová, L., Polishchuk, V. & Prats, X.. 2021. Automated Sequencing and Merging with Dynamic Aircraft Arrival Routes and Speed Management for Continuous Descent Operations. Submitted to *Transportation Research Part C: Emerging Technologies*.
- Polishchuk, T., Polishchuk, V., Schmidt, C., Sáez, R., Prats, X., Hardell, H. & Smetanová, L.. 2020 (Dec.). How to achieve CDOs for all aircraft: automated separation in TMAs - enabling flexible entry times and accounting for wake turbulence categories. *In: 10th SESAR Innovation Days (SIDS)*. Virtual event: SESAR JU.
- Sáez, R., Prats, X., Polishchuk, T., Polishchuk, V. & Schmidt, C.. 2020. Automation for separation with continuous descent operations: dynamic aircraft arrival routes. *Journal of Air Transportation*. **28(4)**, 144–154. D.O.I: 10.2514/1.D0176.
- Sáez, R., Prats, X., Polishchuk, T., Polishchuk, V. & Schmidt, C.. 2019 (Jun). Automation for separation with continuous descent operations: dynamic aircraft arrival routes. *In: 13th USA/Europe Air Traffic Management Research & Development Seminar*. Vienna, Austria: FAA/EUROCONTROL.

(4D) trajectory negotiation and synchronization process—where the tromboning shortcuts were pre-negotiated before the top of descent (TOD)—with the aim of maximizing continuous descent operations (CDOs) and where separation was ensured throughout the arrival and approach procedures. However, tromboning procedures have a limited number of predefined routes and, depending on the traffic demand, the available routes might be sub-optimal.

This chapter presents an optimization framework to automatically generate aircraft arrival routes in terminal airspace at a tactical level; these routes are computed for periods of time from 30 minutes to 1 hour and assigned to incoming traffic. Furthermore, the generated arrival routes guarantee temporal separation, automatically adapt to the current traffic demand and enable the use of CDOs for all the arriving aircraft. The framework has the potential to serve as a ground-support tool for ATCOs, which will both reduce their workload and the environmental impact of the operations.

This chapter proposes a mixed integer programming (MIP)-based approach for the generation of optimized arrival routes to enable CDOs for all arriving aircraft. Aircraft are assumed to arrive within a time window at the terminal maneuvering area (TMA) entry point, which could be achieved by adjusting the speed during the en-route phase. This chapter also formulates and provides a detailed explanation of the concept of operations (CONOPs) to show the applicability of the optimization framework in the current air traffic operations system. In addition, the methodology presented in this chapter is applied to different scenarios with different traffic levels and distributions. Furthermore, this chapter assesses the sensitivity of the proposed solution to the size of the entry point time window, as well as the effect that different traffic mixes have on the optimized arrival routes. By testing this variety of scenarios under several conditions, the aim is to capture the benefits of the proposed concept in terminal airspace operations by comparing it with the current static arrival routes paradigm.

Besides improving the efficiency of current operations in terminal airspace, the methodology presented in this chapter could become a technical enabler towards an extended arrival manager (E-AMAN) with enhanced capabilities, in which the sequencing horizon would be extended into the en-route sector and airport's arrival management information will be shared with upstream sectors in real time by using a system-wide information management (SWIM) service. Similarly, the proposed solution could also become a technical enabler towards an advanced 4D trajectory synchronization in line with the TBO paradigm.

VI.1 State of the Art

Turn-constrained route planning for just a single path was considered by Krozel *et al.* (2006). Similarly, Zhou *et al.* (2014) generated individual routes in a TMA by taking into account the current weather. Then, Visser & Wijnen (2001) generated single routes—where the focus was on the optimization of a single trajectory, but without considering the interactions with other aircraft in the vicinity—in order to minimize the noise impact. However, none of these authors considered any temporal component in their models: the routes were generated without taking into account the effect that real traffic—which involves having constraints in the separation between aircraft—could have in the generation of the arrival routes.

More recently, Chevalier, J. (2020) proposed a simulated annealing approach to generate arrival trees in a TMA. However, while MIP methods (the one used in this chapter) are an exact approach, meta-heuristic methods like simulated annealing are not. As a result, in general, better—probably optimal—results will be obtained with MIP, but at the expense of higher computational times.

The scheduling of traffic along arrival routes was considered by Choi *et al.* (2010), who

showed how throughput can be increased in congested terminal airspace by using scheduling algorithms different than the traditional first-come-first-served (FCFS) approach. In addition, other authors studied sequencing models based on alternative graph formulations (Adacher *et al.*, 2003). Similarly, Le Ny & Pappas (2011) used mixed integer geometric programming to determine the optimal arrival order of aircraft at a metering fix in a stream-merging scenario. The merging of traffic flows was also studied by Michelin *et al.* (2011), who did the optimization of the aircraft trajectories merging at a given fix in two steps in order to ensure a sufficient separation between the arrival flows. More recently, Samà *et al.* (2019) presented various approaches to integrate several modelling features in the aircraft scheduling problem—both for take-off and landing operations—with the aim of minimizing, for instance, the total travel time or the maximum delay. However, the location of merge points or constraints like the limit on a turn angle were not considered by any of these works.

Differently from Dalmau & Prats (2016), who studied speed variation for airborne delay to adjust the controlled time of arrival (CTA) of one flight, in this chapter paths adjustment to coordinate the merge of multiple aircraft trajectories are used. Furthermore, the idea of assigning not only routes, but also times, is applied similarly in a non-aviation context, in dynamic vehicle routing (Bertsimas & Van Ryzin, 1991) and dynamic scheduling (Ouelhadj & Petrovic, 2008).

Last but not least, noise also plays an important role in the generation of both arrival and departure routes in TMA, and extensive research has been made in the past decades about this topic (Visser & Wijnen, 2001; Prats, 2010; Ho-Huu *et al.*, 2020). For instance, Ho-Huu *et al.* (2020) proposed a multilevel optimization framework to design departure routes. The approach was divided in two steps: first, both noise impact and fuel consumption were taken into account in order to obtain a set of optimal routes; then, routes from this set were selected and the departing flights were distributed among these routes.

VI.2 Concept of Operations

This section focuses on the CONOPs proposed in this chapter. Section VI.2.1 describes the CONOPs, while Section VI.2.2 provides a discussion regarding the applicability of this CONOPs as a technical enabler for several air traffic operations solutions. Furthermore, several factors directly affecting this CONOPs are enumerated.

VI.2.1 Concept of Operations: General Description

Figure VI-1 depicts a simplified scenario used to illustrate the problem addressed in this chapter. Let us assume that several aircraft have planned to land in a given airport. The strategy proposed to safely bring these aircraft from the cruise phase until the runway by following a CDO is managed, in a general way, in the following regions:

1. **Pre-sequencing area**: the communication between ATCOs and aircraft is established in the pre-sequencing horizon, where the sequencing requirements are negotiated: a required time of arrival (RTA) at the dynamic-trajectories horizon and a specific route in the dynamic-trajectories area. Aircraft follow the published routes in this pre-sequencing area, but in order to meet the negotiated RTA, can adapt their speed, vertical profile and, to some extent, even the route—by stretching or shortening, within some bounds, the route followed in the pre-sequencing area.

2. **Dynamic-trajectories area**: in this area, arrival routes linking each of the entry points with the runway will be dynamically generated by the ATCO ground-support system. Aircraft

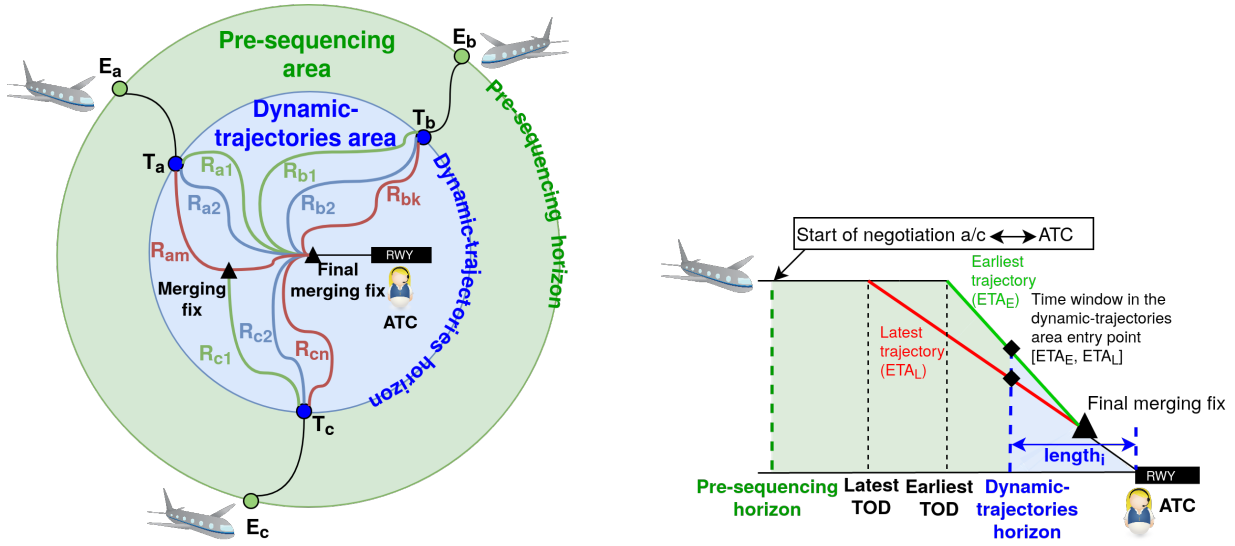

(a) Lateral perspective: Pre-sequencing and dynamic-trajectories areas and potential routes in dynamic-trajectories area

(b) Vertical profile for a given route length inside the dynamic-trajectories area

Figure VI-1: *Concept of operations: trajectories*

are requested to follow these routes, which may merge in some intermediate merging fixes.

3. **Final merging fix**: all traffic flows will eventually merge at the final merging fix, from where they will proceed to the landing runway.

A more detailed explanation of this CONOPs is given in the remainder of this section. The aim is to better describe the interactions and roles of both aircraft and ATCOs in the pre-sequencing and dynamic-trajectories areas, as well as the function of these areas.

As it has been aforementioned, the arriving traffic flows enter the pre-sequencing area through several entry points, located in the pre-sequencing horizon (E_a, E_b and E_c in Figure VI-1(a)). Once the aircraft enter the pre-sequencing area, they follow the published route until the entry point of the dynamic-trajectories area, located in the dynamic-trajectories horizon (T_a, T_b and T_c in Figure VI-1(a)). At the same time, they initiate an RTA-and-route-negotiation/synchronization process with the ATCO (or ground-automated system), as shown in Figure VI-2.

This RTA-negotiation/synchronization process starts with the aircraft being requested to compute an estimated time of arrival (ETA)—as well as the 4D trajectory complying with this ETA—at the entry point of the dynamic-trajectories area for a given set of predefined route lengths inside this area. In order to do that, aircraft have to compute, first, the time window at the dynamic-trajectories horizon. This time window is the difference between the earliest and the latest time of arrival at a given fix (in this case, the entry point of the dynamic-trajectories area), corresponding to ETA_E and ETA_L in Figures VI-1(b) and VI-2. These times of arrival depend on aircraft performance, flight envelope and weather conditions, and are assumed to be computed by the flight management system (FMS) of the different incoming aircraft by considering the earliest and latest trajectories (while following the published routes joining the two horizons).

Once all time windows—of aircraft arriving within a limited time interval—are computed, the aircraft FMS selects a feasible ETA at the dynamic-trajectories horizon. The proposed method to do this selection is explained in Section VI.3. Once the ETA is selected, aircraft compute and downlink a set of 4D profiles (i.e., descent trajectories complying with a specific ETA at the dynamic-trajectories horizon and flying a given route length within the dynamic-trajectories area)

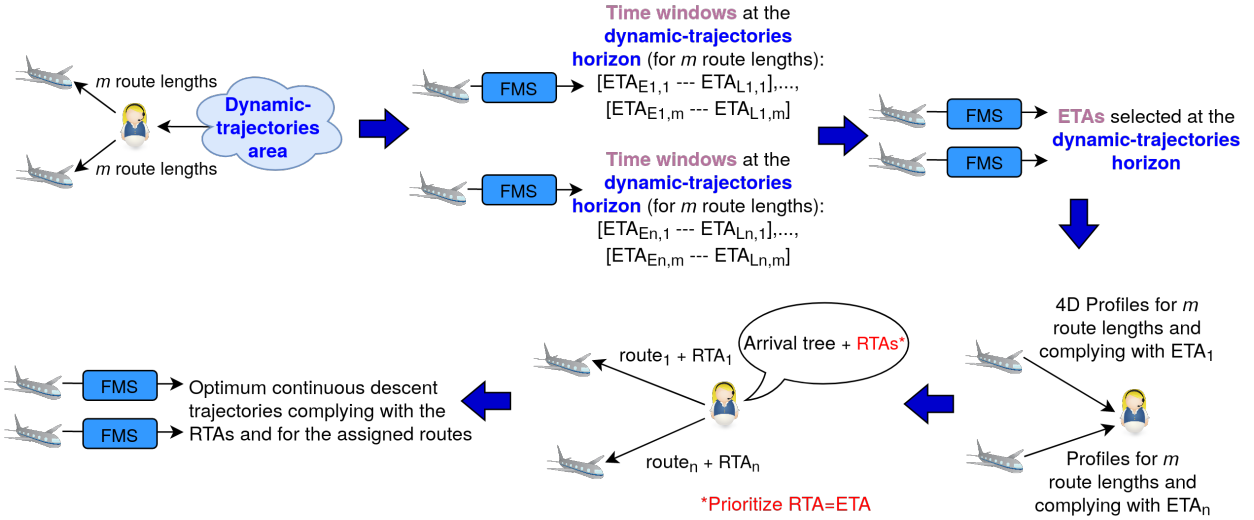

Figure VI-2: *Concept of operations: RTA and route negotiation process for n aircraft and m routes*

to the ATCO.

The automated system on-ground, after receiving all the 4D profiles, assigns, first, an RTA[1] at the dynamic-trajectories horizon. This RTA, if possible, will be equal to the ETA. Then, the automated system on-ground generates an optimal arrival tree in the dynamic-trajectories area, which is composed of a single arrival route from each of the entry points of this area to the final merging fix. As a result, each aircraft are assigned a single 4D profile to execute (with a final route length chosen from the predefined set of lengths inside the dynamic-trajectories area).

While an RTA equal to the ETA might work for low to average traffic scenarios, it might not be enough for more congested airspaces surrounding larger airports Sáez *et al.* (2020a). As the traffic increases, the separation between aircraft at the dynamic-trajectories horizon is reduced, and the generation of the arrival tree becomes more challenging. Not only the amount of traffic could be a problem, but also the arrival distribution at the dynamic-trajectories horizon. In general, it is not desirable that large aircraft clusters arrive in a short period of time, as it might be impossible to schedule them effectively and safely. Furthermore, some aircraft arrival distributions, which *a priori* might seem good and easy to schedule, in the end might lead to an infeasible scenario where it is impossible to schedule all arrival traffic. Even if the entry times at the dynamic-trajectories horizon for each aircraft are safely separated, when taking the dynamic-trajectories area as a whole (i.e., by taking into account all its entry points), it might be impossible to generate an arrival tree that safely schedules all arriving aircraft. This *goodness* in the arrival distribution is indeed a very interesting topic and will be investigated in future work.

To be able to schedule all arriving aircraft even in the most challenging scenarios, the following process is proposed: first, ATCOs, when communicating with the aircraft in the pre-sequencing horizon, could request them to gain or lose a given amount of time in the pre-sequencing area. Thus, as depicted in Figure VI-2, ATCOs, when generating the arrival tree, may eventually assign an RTA different from each aircraft's ETA. As it will be shown in Section VI.5, by requesting aircraft to arrive a few minutes earlier or later at the dynamic-trajectories horizon, the scheduling of the arrival traffic could be enhanced and applied in dense traffic scenarios. This time could be gained/lost in the pre-sequencing area.

The generated arrival tree will change during the day (new time intervals will be considered), as it will automatically adapt to the actual traffic demand. The objective is that the aircraft know

[1]If the aircraft FMS is not equipped with the RTA capability, speed advisories will be given instead

the RTA at the dynamic-trajectories horizon and the current arrival-tree configuration (and, thus, the distance to go) while still in cruise, somewhere in the pre-sequencing area. Therefore, the FMS on-board (with RTA capabilities) can compute a neutral descent trajectory (i.e., idle thrust and no speebrakes usage) that complies with the RTA and follows the corresponding route of the optimal arrival tree requested by the ATCO. Consequently, the flight sequence should be generated fast enough within the distance between the pre-sequencing horizon and the dynamic-trajectories horizon, with the aim of ensuring aircraft know the profiles they have been assigned before reaching the top of descent (TOD).

Furthermore, the distance between horizons is also affected by the amount of time to be gained/lost in the pre-sequencing area. Delgado & Prats (2012) showed that for typical cost index (CI) values between 30 kg/min and 100 kg/min, aircraft can gain or lose between 1.2 seconds/NM and 4 seconds/NM by managing their speed. For instance, if the worst-case scenario is considered—1.2 seconds/NM—and a pre-sequencing horizon located at 250NM from the dynamic-trajectories horizon, aircraft would be able to gain/lose up to 5 minutes in the pre-sequencing area. As it will be shown in Section VI.4, these are the conditions considered in the case studies defined in this chapter. The amount of time that can be gained/lost in the pre-sequencing area depends on various factors, such as the aircraft model or the cruise flight level. In addition, the effects of wind should also be considered (Delgado & Prats, 2013). Finally, another option to even gain/lose a higher amount of time would be to shorten/stretch the path in the pre-sequencing area. However, this strategy has been left out of the scope of this chapter.

Similarly, the location of the dynamic-trajectories horizon could also be modified depending on several factors. The farther the horizon is located, the larger the dynamic-trajectories area, which would allow the ATCOs to generate a set of dynamic arrival routes in a larger region. Consequently, arriving aircraft would be sequenced in optimal arrival routes from an earlier stage. However, a larger dynamic-trajectories area comes at the expense of a higher computational load. As a result, the time needed for the RTA-and-route-negotiation/synchronization process would increase, which would ultimately have an effect on the location of the pre-sequencing horizon too.

VI.2.2 Concept of Operations: Technical Discussion

The work presented in this chapter focuses only on the trajectory plan generated by the FMS. Therefore, it is out of the scope of this chapter studying how this plan will be flown by the aircraft, which is the task of the guidance system of the FMS. Once the trajectory plan is generated, this system will be responsible of adapting the aircraft trajectory in order to meet the assigned RTA and minimize uncertainty. For instance, a guidance system like the one proposed by Garrido-López *et al.* (2009) could be used to minimize wind uncertainties by combining elevator and throttle actuations to control ground speed and efficiently match a prescribed ground speed law, thus, improving the predictability of the operation.

In this CONOPs, aircraft trajectories are computed by on-board systems (such as an FMS), and not by ground-based systems. This improves the accuracy of the generated trajectories as aircraft systems have access to much more accurate aircraft performance data. This aligns with the initial four-dimensional (i4D) concept, which will be integrated as a new feature in current FMSs. With i4D, the aircraft FMS will be able to downlink the whole 4D trajectory flight plan with the associated predictions—e.g. predicted aircraft weight, as well as the predicted horizontal and vertical speed—of up to 128 waypoints, so called extended projected profile (EPP)(Bronsvoort *et al.*, 2016), via automatic dependent surveillance-contract (ADS-C). Similarly, the FMS will also be able to receive a direct up-link of air traffic control (ATC) clearances upon crew confirmation. Such data-link enhancements will provide seamless exchanges that are key to the success of i4D operations. Furthermore, another key element of i4D operations is also to improve trajectory predictions using time constraints, being the assignment of RTAs a key criterion for pilots to follow.

The trajectories computed by the FMS are used to obtain the arrival time window at the dynamic-trajectories horizon. However, this window is not something fixed and depends on several factors, such as aircraft performance, weather conditions, etc. Specifically, there are two main factors that could be changed in order to modify the width of the time window. The first one is related to the type of descent performed. Neutral CDOs are the trajectory type considered in this chapter, which involve descents with idle thrust and no speed brakes. On the other hand, powered descents could also be considered, allowing both the use of thrust and speed brakes, which leads to wider time windows, but at the expense of increasing the fuel burn and/or noise nuisance.

The other factor affecting the width of the time window is related to the moment the available route lengths are notified to the aircraft. Since the RTA negotiation will begin (at the earliest) at the pre-sequencing horizon, the arrival time window will be wider the further this horizon is from the dynamic-trajectories horizon. Besides this distance to the RTA metering point, also the window width will be much wider if the aircraft has not yet initiated the descent: while in cruise, not only the aircraft could easily accelerate or decelerate to achieve earlier or later times of arrival, but it could also adapt the position of the TOD. Several studies have dealt with the assignment of RTAs (and the quantification of the feasible time window) when the aircraft is still in cruise, well before the TOD. For instance, in Takeichi & Inami (2010), the authors quantified the feasible time window that could be achieved by either adding or omitting waypoints in order to stretch or reduce the flight-path length. Once the descent has already started, ATCOs could still assign (or update) RTAs, but the possibilities to fly neutral CDOs are reduced. This situation was addressed by Dalmau & Prats (2017b), who showed that noticeable time windows are still possible while aircraft are already flying a neutral CDO.

The solution presented in this chapter is expected to be a technical enabler towards an E-AMAN (SESAR JU, 2019b) with enhanced capabilities. The aim of E-AMAN is to alleviate pressure in the terminal airspace by allowing to sequence arrival traffic much earlier than is currently the case. The current AMAN horizon is extended from the airspace close to the airport to further upstream, thus, allowing a smoother traffic management, where information is shared with upstream sectors in real time by using a SWIM service. In this chapter, the pre-sequencing horizon would correspond to the E-AMAN horizon. Furthermore, the capabilities of E-AMAN are enhanced by introducing an additional region surrounding the airport (i.e., the dynamic-trajectories area), which would be similar to the current TMAs—where arrival routes are static—but with additional functions and a variable size. In the proposed CONOPs, as discussed in Section VI.2.1, routes inside this region would be in constant evolution, automatically adapting to the current traffic demand (which would be divided into several time intervals). Previous authors considering aircraft scheduling and E-AMAN algorithms under the TBO concept include Toratani *et al.* (2018) and Toratani (2019), who focused on optimizing simultaneously the aircraft arrival sequence and the trajectory. However, to the best of our knowledge, no current work considers the generation of dynamic arrival routes together with E-AMAN algorithms.

As detailed in this section, the proposed solution aligns with some of the key concepts and technologies defined by single european sky ATM research (SESAR) and it could be applied with existing aircraft equipment. However, there are some concepts which are still under development or deployment, which may mean that still not all aircraft (and airports) have the required functionalities to make the proposed solution work. Furthermore, aircraft with old systems onboard—for instance, an aircraft FMS without the RTA functionality—may also cause a problem for the application of the solution presented in this chapter.

VI.3 Methodology

This section describes the workflow of the system (depicted in Figure VI-3) and gives an overview of the methodology followed. The proposed system consists of the following steps:

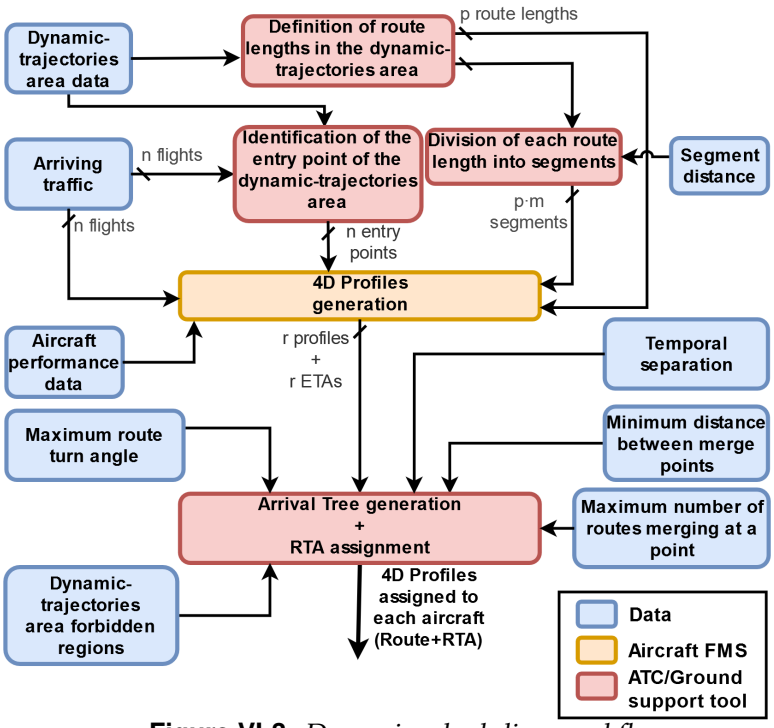

Figure VI-3: *Dynamic scheduling workflow*

1. **Entry points identification:** from each arriving aircraft's trajectory, the entry points to the pre-sequencing and dynamic-trajectories area are identified—which should be static and published in the corresponding aeronautical information publication (AIP). As soon as aircraft enter the pre-sequencing area, the RTA-and-route-negotiation process starts.

2. **Definition of route lengths in the dynamic-trajectories area:** in this area, no static routes are published, so it is the task of the ATCO (with the help of a ground support tool) to dynamically generate the arrival routes. In order to ensure the traffic can be properly managed by the ATCO and/or ground support tool, and in order to ensure the routes are flyable by the aircraft (and the pilot), it can be considered that the number of potential routes in the dynamic-trajectories area is finite. Furthermore, the departing traffic, potential obstacles and other kind of limitations, such as separation constraints, could also limit the number of potential arrival routes. Thus, as depicted in Figure VI-1(a), an aircraft entering the dynamic-trajectories area through point T_a could follow any single route out of m (finite) potential routes until the final merging fix. As a result, the ground support tool defines a finite number of route lengths. Then, each route is divided into several fixed distance segments.

3. **Generation of earliest and latest trajectories + ETA computation at the dynamic-trajectories horizon:** the ATCO requests from each arriving aircraft an ETA at the dynamic-trajectories horizon, as well as the 4D profile complying with this ETA. Aircraft compute, first, their corresponding neutral time window at the entry point of the dynamic-trajectories area for each route length inside this area. The aircraft FMS accesses the current aircraft performance data and computes the earliest and latest neutral trajectories (i.e., neutral CDO) for each route length. Then, the FMS selects an ETA within the neutral time window and downlinks it to the ATCO, together with the 4D profile for each available route length and

complying with this ETA. Furthermore, the time required to cover each segment of the corresponding route is also downlinked to the ATCO. The ETA selection is done as follows: let us assume m route lengths are defined inside the dynamic-trajectories area, depicted as D_1, D_2, D_3, and D_m in Figure VI-4. For each route length, the earliest and latest trajectories are computed in order to obtain a time window at the dynamic-trajectories horizon. Some of the possible times of arrival are shared by trajectories corresponding to different route lengths, corresponding to the purple time interval in Figure VI-4. The idea is that each aircraft FMS selects an ETA at the center of this interval, which will be attainable by the aircraft no matter which route is chosen. In case there are no feasible (i.e., overlapping) sets of arrival times common to all route lengths, longer lengths are discarded first. Thus, longer route options are removed from the set of potential routes until there is an overlap where a feasible ETA can be selected.

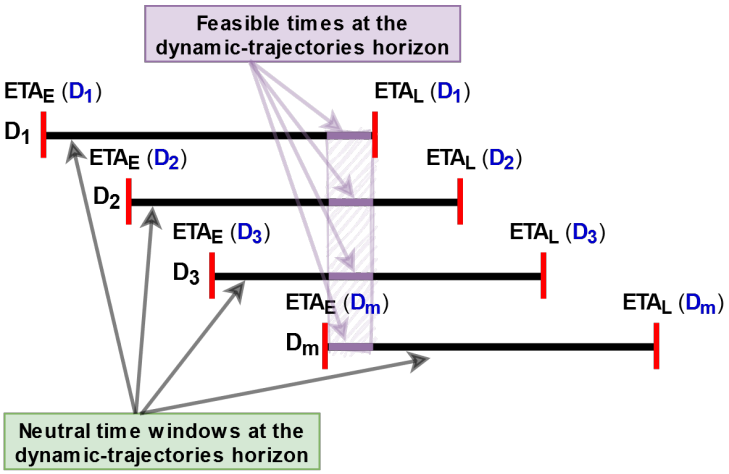

Figure VI-4: *Feasible times at the dynamic-trajectories horizon for profiles corresponding to different route lengths inside the dynamic-trajectories area*

4. **Generation of the arrival tree and RTA assignment**: the ATCO, supported by a ground tool, generates an arrival tree in the dynamic-trajectories area—which takes into account a set of operational constraints—and then assigns to each aircraft an RTA at the dynamic-trajectories horizon. While preferably the assigned RTA would be equal to the ETA, for scenarios with a larger amount of traffic, aircraft might be requested to arrive a few minutes earlier or later at the dynamic-trajectories horizon. Consequently, ATCOs will consider an offset in the time window, thus shifting the time windows depicted in Figure VI-4 to earlier or later times. In such a case, an RTA different from the ETA would be assigned, which would involve aircraft adjusting both the speed and the vertical profile in order to meet the RTA. As discussed in Section VI.2.1, this time will be gained/lost by the aircraft in the pre-sequencing area.

Section VI.4.2 presents the models and optimal control problem formulation used to generate the (optimal) trajectories for the validation scenarios of this chapter (simulated traffic), based on the semi-analytic trajectory optimization approach presented in Section II.2.2. The underlying computations and theory behind step 3 of this section are explained (corresponding to the yellow box of Figure VI-3—*4D profiles generation*). In real life, these trajectories would be generated by an advanced functionality of the FMS of each aircraft, equipped with the RTA functionality. Two examples of trajectories that can be obtained with the semi-analytic trajectory optimizer were shown in Figure V-10 (Chapter V).

Appendix A presents the grid-based MIP formulation used to generate the optimal arrival tree that complies with all the operational constraints that will be described hereafter. This work

is based on the framework developed by Dahlberg *et al.* (2018), which was improved for the experiments conducted in this chapter. For computing the arrival trees, the dynamic-trajectories area is overlaid with a square grid, and both axis-aligned and diagonal edges are used as possible components of the arrival tree. This yields a discrete set of possible lengths of any entry-point-runway path (from the shortest grid-path from entry point to runway to the longest edge-disjoint grid path from entry point to runway). In particular, an upper bound on these paths is imposed. For these discrete paths length, the corresponding neutral CDOs are computed by solving the optimal control problem presented in Section VI.4.2.

The computation of arrival trees—which have the runway as their root and the entry points as their leaves—is built by using a MIP formulation. Then, the speed profiles obtained from the CDOs are an input to the MIP. Moreover, aircraft following the computed path along the arrival tree from the entry point to the runway are temporally separated. Furthermore, it is also ensured that each aircraft uses the speed profile that corresponds to the route length of the entry-point-runway path of the computed tree. By using further constraints, the following operational constraints $1-4$ are enforced:

1. *Temporal separation of all aircraft along the routes:* each pair of aircraft (with the leading and trailing aircraft being of wake-turbulence category A and B, respectively) that shares a given subroute is separated by a temporal distance of at least $\sigma_{A,B}$ along this subroute. Thus, if all aircraft comply with the planned time of arrival at the entry point of the dynamic-trajectories area, they will be safely separated along the arrival routes.

2. *Limitation of the number of routes merging at a point:* ATCOs need to give heightened attention to merge points of routes. Thus, traffic complexity around the merges should be as low as possible (Prete *et al.*, 2008). It is assumed that at most 2 routes can merge at a point in the dynamic-trajectories area.

3. *Merge points separation:* operational constraint 2 could be circumvented by placing merge points arbitrarily close to each other. As a result, this would still result in a very small zone with a very high traffic complexity in terms of many merging routes. Thus, the requirement of a minimum distance between any two merge points—which needs to be larger than a given distance threshold L (Prete *et al.*, 2008)—is added.

4. *No sharp turns:* because of aircraft dynamics and limitations in the bank angle—which usually does not exceed 30 degrees for most aircraft under nominal conditions for reasons such as safety and passenger comfort—there is a limit on the turn angle for each arrival route. Consequently, any turn from a route segment to the consecutive route segment must be larger than a given minimum track change angle θ.

5. *Obstacle avoidance:* a set of regions (e.g., no-fly zones, noise-sensitive areas, etc.) could be marked so that the generated routes do not pass over them.

VI.4 Experimental Setup

This section presents the experimental setup used to illustrate the CONOPs and methodology proposed in this chapter. Stockholm-Arlanda airport TMA has been chosen for this study so, from now on, and for the sake of simplicity, the dynamic-trajectories area will be referred as the TMA. A hypothetical pre-sequencing area of $250\,\mathrm{NM}$ of radius was defined around the airport. As soon as aircraft enter the pre-sequencing area, and after a pre-negotiation with the ATCO, RTAs at the TMA entry points and routes along the optimal arrival tree are assigned. In this scenario, aircraft

are assumed to fly straight to the TMA entry point, after which they follow the assigned route inside the TMA.

The scenario is introduced in Section VI.4.1, where Arlanda airport and its available runway configurations—as well as its current TMA—are described. Then, the generic models introduced in Section II.1, as well as the generic optimal control problem stated in Section II.2.1, are particularized in Section VI.4.2. Section VI.4.3 details the input parameters used for the MIP, while Section VI.4.4 focuses on the trajectory generation: the required input parameters and the set of profiles generated are detailed. Finally, Section VI.4.5 details the set of experiments carried out in this chapter. Furthermore, details are given regarding the analysis performed to assess the sensitivity of the proposed solution to several parameters.

VI.4.1 Scenario

Stockholm-Arlanda airport was selected as the scenario for the experiment performed in this chapter. The airport has three runways: Runway 1 (01L/19R), Runway 2 (08/26) and Runway 3 (01R/19L). Runways 1 and 3 are parallel runways that can be operated independently of one another and, when used at the same time, allow the airport to handle simultaneous take offs and landings.

Arlanda arriving and departing traffic is managed in the Stockholm TMA. Currently, there are 4 TMA entry points in Arlanda, corresponding to the 4 STAR starting points: HMR (north), XILAN (east), NILUG (south) and ELTOK (west). These points are shown in Figure VI-5(a), which corresponds to the area navigation (RNAV) STAR for runway 26.

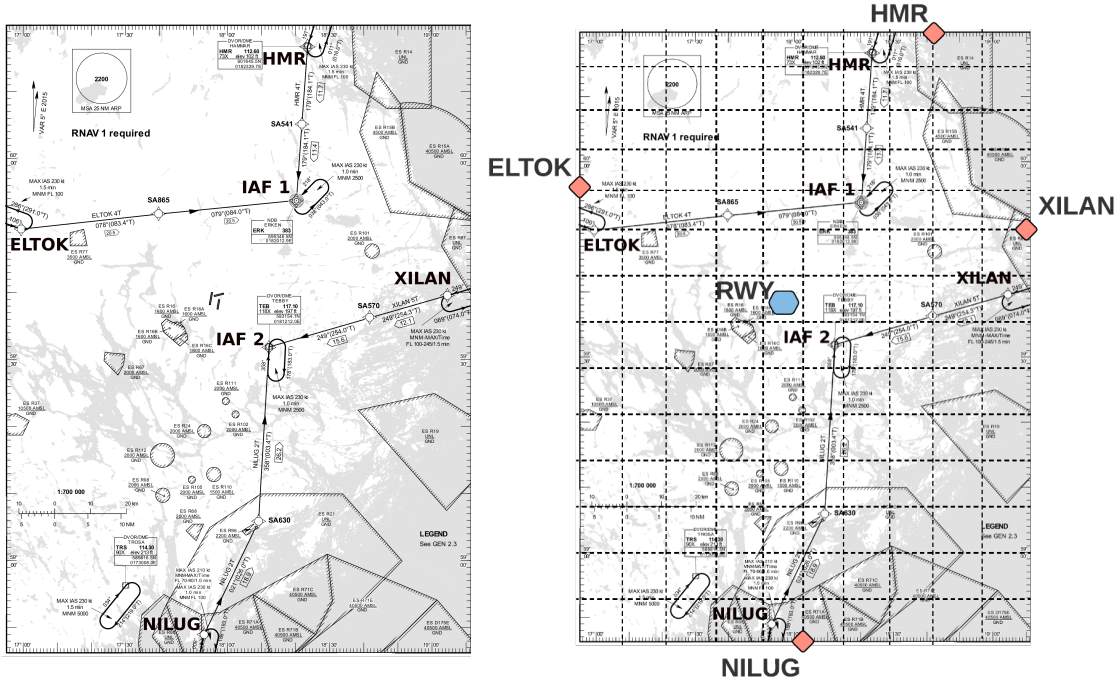

(a) Arlanda RNAV(DME/DME or GNSS) STAR for RWY 26 and TMA entry points (source: Swedish AIP)

(b) 15x11 grid over Arlanda TMA

Figure VI-5: *Overlaying Arlanda TMA with a 15x11 grid*

VI.4.2 Models and Optimal Control Problem Formulation

For all the experiments conducted in this chapter, the aircraft dynamics model, performance model and optimal control problem were identical to those used in Chapter III, with some minor changes as described hereafter.

The initial state of the aircraft, consisting of the cruise altitude and cruise speed, is obtained directly from an historical-flight database (as detailed in Section VI.4.4) in the position where the aircraft enter the pre-sequencing area. In addition, the corresponding entry point to the TMA is identified from each aircraft's trajectory. The terminal constraints considered in the optimal control problem are the following: the final speed, v_f, corresponds to the V_{F1} speed, which is the speed at which flaps/slats configuration 1 is typically deployed; the final altitude, h_f, is equal to the altitude of a hypothetical final approach point (FAP), which would correspond to roughly 2,000 feet; and the distance to go, s_f, corresponds to the the distance to the FAP, which depends on the route length. The final merging fix in the proposed CONOPs (Section VI.2) would be located at a given distance prior to the FAP.

This study aimed to be as generic as possible. Accordingly, the international standard atmosphere (ISA) model, established to provide a common reference for temperature and pressure, was considered to represent the normalized temperature θ and pressure δ as a function of h through Eqs. (II.7) and (II.8), respectively. Then, the normalized density was computed assuming the perfect gas law relationship with Eq. (II.9).

In the experiment performed in this chapter, calm wind conditions were considered. Thus, $w_s = w_x = w_h = 0$.

VI.4.3 MIP Configuration Parameters

Since the objective of this chapter is to generate an optimal arrival tree that adapts to the current aircraft demand, none of the STARs designed for Arlanda (such as the one shown in Figure VI-5(a)) was considered. However, the location of the TMA entry points is required, from where each of the routes that make up the arrival tree will start.

The TMA of Stockholm-Arlanda airport is overlaid with a 15x11 grid (Figure VI-5(b)), which automatically ensures a separation of about 6NM (corresponding to parameter L, described in Appendix A). Using finer grids would make the problem computationally too expensive.

Apart from the location of the TMA entry points and the grid used to overlay Arlanda's TMA, the following input parameters needed to setup the framework have been set:

- **Runway orientation and location**: in this chapter, single-runway operations were assumed. Using parallel runways is supported by the framework immediately, as the runway location is snapped to the closest grid point. If an airport has several, non-parallel runways, a merge tree per runway could be computed, imposing constraints on how the trees may interact (e.g., on intersections). However, this functionality is not yet implemented in the current version of the framework.
- **Aircraft time at the TMA entry point**: for each arriving aircraft, an entry time at the TMA entry point is required, corresponding to the ETA selected by each aircraft FMS.
- **Aircraft speed profile**: for each arriving aircraft, the corresponding speed profile for different route lengths is required. With these speed profiles, the framework is aware of the time spent by each aircraft to cover each TMA segment.
- **Temporal separation (as a function of aircraft category)**: a separation between aircraft has to be ensured in order to maintain the safety of the operation. The separation will be defined by taking into account the wake turbulence categorization proposed by international

civil aviation organization (ICAO) (SKYbrary, 2020b), which classifies aircraft into three categories depending on their maximum take-off mass. In this chapter, the minimum time separation between aircraft that ICAO proposes according to that categorization (ICAO, 2016) will be used: 3 minutes of time separation will be considered for light aircraft following medium or heavy aircraft, while 2 minutes of time separation will be considered otherwise. As reported in a recent project (Flache, 2018), wake turbulence effects could even be noticeable during the cruise phase of flight, so it is important to ensure this separation in the whole TMA in order to avoid potential wake turbulence hazards.

- **Number of differing edges (U)**: as defined in Appendix A, the parameter U is used in the MIP formulation to ensure a consistency in terms of number of differing edges between arrival trees during consecutive time periods (a small sensitivity study of the resulting trees for several U parameter values was conducted by Hardell *et al.* (2020b)). Depending on the experiment, and as shown in table VI-1, the value for U has been set to either 20 or 30.
- **Minimum angle of outgoing edge (θ)**: as detailed in Section VI.3 and Appendix A, in order to avoid sharp turns in the arrival routes, a minimum angle θ for each outgoing edge is needed. For all the experiments, the value for θ has been set to 135 degrees.
- **Time-window offset at the TMA entry point**: a time-window offset at the TMA entry point is defined, which will be different for each experiment, as detailed in Section VI.4.5.
- **Parameter to obtain a convex combination of the paths lengths and tree weight (β)**: this parameter is set to 0.1 in all experiments in order to prioritize the minimization of the sum of paths lengths.

VI.4.4 Trajectory Input Data and Profiles Computation

The flight-traffic data needed to carry out the experiments was mainly obtained from the OpenSky Network (The OpenSky Network, 2019). This network contains raw-trajectory data stored in a large historical database, which is obtained thanks to the automatic dependent surveillance-broadcast (ADS-B) technology, as commented in Chapter III. Two types of data-sets are available in OpenSky: OpenSky states vectors, which provide a very-high-resolution data of the actual flown trajectory, and OpenSky tracks, which contain a subset of the recordings from the states data. OpenSky states was the preferred database for the experiments due to its higher resolution, as reported in Chapter III. However, there were two flights used in the experiments which lacked an ADS-B transponder. Thus, there was no data available in OpenSky. For those specific cases, data from Eurocontrol's demand data repository (DDR) (Eurocontrol, 2017) was used, which is less accurate than OpenSky, especially in areas close to the airport, as reported in Chapter III.

For any given flight, the number of trajectories generated depends on the the number of possible routes the aircraft can fly. In this case, route lengths within the TMA from 30 NM (corresponding to the minimum route length within the grid) to 108 NM are considered, with each route split into several segments of constant length equal to 6 NM. For instance, a 30 NM route inside the TMA would be split into 5 segments (i.e. [0-6, 6-12, ..., 24-30]). The set of route lengths in this experiment were chosen according to the grid size (as described in Section VI.4.3). The lower bound stems directly from the grid (it is not possible to have route lengths lower than 30 NM from any of the entry points to the runway). The upper bound could also be derived from the grid (no path from any entry point to the runway can use any edge twice). However, this is far from a realistic upper bound and a smaller upper bound was imposed, which still allows for feasible solutions. That is, an upper bound was chosen, such that an arrival tree can be computed fulfilling all constraints using route lengths in the interval [lower bound, upper bound] (which would not be possible for an upper bound equal to the lower bound), but that is significantly smaller than the upper bound that can be directly identified from the grid.

First, as detailed in Section VI.3, earliest and latest trajectories are computed in order to obtain the time window at the TMA entry point. In total, 28 trajectories per flight were computed (i.e. 14 possible route lengths ranging from 30 NM to 108NM for both earliest and latest cases). Then, once each aircraft computes its ETA, 14 trajectories per aircraft and for each route length ensuring the same arrival time (i.e., the ETA) at the TMA entry point were generated. As indicated in Section VI.3, in case the same ETA was not achievable for all route lengths, longer routes were discarded first.

VI.4.5 Case Studies

Table VI-1 details all the experiments carried out in this chapter. The case studies are named after the corresponding amount of arriving traffic during the day and time chosen (i.e. low, average and high).

Table VI-1: *Design matrix for the experiments*

Case study	Day & Time	Runway	Number of aircraft	Time-window offset (minutes)	Traffic mix (% light a/c)	Number of differing edges (U)
Low-traffic	29/12/2018 - 11h to 12h	01L	8	$\pm 0, \pm 1$	0	-
Average-traffic	04/10/2017 - 15h to 16h	19R	22	$\pm 0, \pm 1$	0	20
				± 2	0 20	20
				± 3	0, 20	20
				± 4	20	20
High-traffic	16/05/2018 - 05h to 06h	01L	30	$\pm 0, \pm 2$	0	20
				$\pm 1, \pm 3, \pm 4$	0	30
				± 5	0, 20	20

This chapter mainly studies the sensitivity of the proposed solution to 3 parameters:

- **Number of arriving aircraft**: three different case studies are analyzed with different amounts of traffic.
- **Entry-time-window offset**: for each case study, different entry-time-window offsets are assumed. As detailed in Section VI.2.1, gaining/losing time in the pre-sequencing area to achieve different entry times at the TMA entry point could help to schedule aircraft even in the most challenging scenarios. Discrete time-window offsets are used, so, for instance, an offset of ± 3 minutes would represent that the arriving traffic could arrive to the entry point of the dynamic-trajectories area 3, 2 or 1 minutes earlier or later than the original time of arrival.
- **Traffic mix**: for the average and high-traffic case studies, a given number of randomly chosen aircraft was replaced with a light aircraft type. The model chosen was an Embraer EMB-500 Phenom 100 (E50P).

As it can be seen in Table VI-1, not all parameters are tested for all case studies. For instance, in the low-traffic case study, only an entry point time-window offset of $\pm$ 1 minutes is tested (apart from the case where no deviation in the entry time is considered). As it will be shown in the results (Section VI.5), experiments have been performed until the minimum length tree has been obtained. Therefore, in the particular case of the low-traffic case study, it did not make sense to simulate the results for larger time-window offsets as the minimum length tree was already obtained when considering an offset of $\pm$ 1 minutes. Larger offsets would lead to the same results.

Regarding the analysis of different traffic mixes, it was decided to only study the effects of replacing a 20% of the arriving aircraft with light aircraft. The aim was to study how the framework deals with different kinds of aircraft types and the effect it has on the resulting trees. However, it was decided not to study further cases (with different numbers of light aircraft) due to the low applicability that such kind of study would have in real operations. In major airports such as Arlanda, the ratio of light aircraft per day is usually between 1% and 3%. Even in airports with a less uniform traffic mix, like Palma de Mallorca airport, the ratio of light aircraft during a day hardly surpasses 5%. On the other hand, airports with a higher ratio of light aircraft are usually small aerodromes with a low amount of traffic, where the proposed solution would not be worth applying to. Therefore, in this chapter, the aim is just to study the theoretical limits of the proposed framework in a scenario with a significant number of light aircraft.

Finally, for the average and high-traffic case studies, the corresponding 1-hour-period was divided into 2 half-an-hour-periods. As a result, two arrival trees were generated for each case study. In order to ensure a smooth transition between trees, different values of the parameter U were used.

VI.5 Results

This section presents and analyzes the results of the experiments described in Table VI-1 (Section VI.4.5). For the sake of simplicity, in this section, the entry point of the dynamic-trajectories area, which in this case corresponds to the Stockholm TMA, will be referred simply as the *entry point*.

VI.5.1 Computational Effort

The MIP was solved by using the Gurobi optimization solver installed on a powerful Tetralith server National Supercomputer Centre (2019), utilizing Intel HNS2600BPB computer nodes with 32 CPU cores, 384 GB, provided by the Swedish National Infrastructure for Computing (SNIC). The computational time required to generate the arrival trees varies from 1.58 hours for the low-traffic case study to 40.9 hours for the high-traffic case study with light traffic. One of the main issues when running the simulation was the memory usage, specially for the case studies with a higher amount of traffic, in which the memory usage reached values of 89% and sometimes even went up to a 99%.

Currently, the computational times obtained with the proposed framework may limit its application in real operations, except for low traffic loads. The arrival management problem is very dynamic, and fast computational times are usually required in order to ensure the success of the operations. There are several factors affecting the computational load of the route-optimization framework. Firstly, the size of the dynamic-trajectories area and, consequently, the size of the grid, has an important impact on it. In this case, it was decided to define an area that fitted the Stockholm TMA. However, smaller areas could be chosen in order to speed up the process. In addition, the computational time is also affected by the fact that only neutral CDOs are considered—which involve a smaller time window—and by the amount and distribution of the arrival traffic. In both cases, ATCOs are eventually forced to request the aircraft to gain/lose a specific amount of time in the pre-sequencing area in order to find feasible solutions. As a result, the route-optimization framework has to deal with a larger number of potential solutions (i.e., more times of arrival for each arriving aircraft at the entry point), which slows down the computation of the arrival tree.

For the high and medium-traffic case studies, two trees were generated for the 1-hour period, in order to obtain solutions that adapt better to the current traffic situation and in order to speed up the process. In the future, it may be worth trying to generate arrival trees for even smaller

periods of time, so that the framework has to work with a lower amount of arrival traffic. In addition, working with smaller time horizons could help to generate trees that adapt better to the current traffic situation. However, continuous switches between the trees are undesirable from an ATCO point of view. Therefore, in future work, we are planning to do a trade-off analysis to find out which would be the optimum time horizon to generate the arrival trees depending on the current traffic situation. While there are several factors dramatically increasing the computational load of the proposed framework, in this chapter, the results were generated with a very simple prototype. A more efficient code could be written to speed up the process, or more powerful solvers could be used. Furthermore, it would be worth investigating other approaches, like the one proposed by Chevalier, J. (2020), which provides a sub-optimal solution but could potentially accelerate the generation of the arrival tree while working with the same CONOPs.

VI.5.2 Arrival Trees and Summary of Results

Table VI-2 shows the number of aircraft scheduled and the sum of paths lengths of the resulting arrival tree for each case study. Note that in the low-traffic case study only one arrival tree was generated for the whole-hour period.

Table VI-2: *Results summary*

Case study	Time-window offset (minutes)	Traffic mix (% light a/c)	Number of aircraft scheduled (#a/c 1st 30′ / #a/c 2nd 30′)	Sum of paths lengths [NM] (Lentgh 1st 30′ / Length 2nd 30′)
Low-traffic (8 aircraft)	± 0	0	8	220.22
	± 1	0	8	216.68
Average-traffic (22 aircraft)	± 0	0	10/5	224.92/216.68
	± 1	0	13/6	213.14/216.68
	± 2	0	14/8	220.22/213.14
	± 2	20	12/8	216.68/213.14
	± 3	0	14/8	213.14/213.14
	± 3	20	13/8	220.22/213.14
	± 4	20	14/8	220.22/213.14
High-traffic (30 aircraft)	± 0	0	8/10	246.16/242.62
	± 1	0	11/11	243.78/227.3
	± 2	0	13/13	227.3/220.22
	± 3	0	14/13	230.84/220.22
	± 4	0	14/14	230.84/214.33
	± 5	0	15/15	230.84/220.22
	± 5	20	13/12	230.84/220.22

The lower the traffic, the easier is to schedule the totality of the arriving aircraft. However, as the traffic increases, the number of potential solutions is reduced and, ultimately, it is necessary to ask the aircraft to gain or lose a given amount of time in the pre-sequencing area in order to be able to succeed in the scheduling. Figure VI-6 shows the effect of the entry-time-window offset on the percentage of aircraft scheduled and on the difference, for each case study, between the obtained sum of paths lengths and the minimum sum of paths lengths.

In the average-traffic case study, a time-window offset of at least ± 2 minutes is needed to schedule all aircraft, while in the high-traffic case study the required offset is ± 5 minutes. On the other hand, in the low-traffic case study, there is no need for the arriving aircraft to gain or lose time in the pre-sequencing area, as all aircraft can be scheduled by taking into account the original times of arrival. Once all aircraft are scheduled for a specific case study, it is possible to further increase the time-window offset to reduce the total sum of paths lengths. For instance, in the average-traffic case study, if the time-window offset is increased from ± 2 minutes to ± 3 minutes, the sum of paths lengths is reduced. Similarly, the sum of paths lengths is reduced by

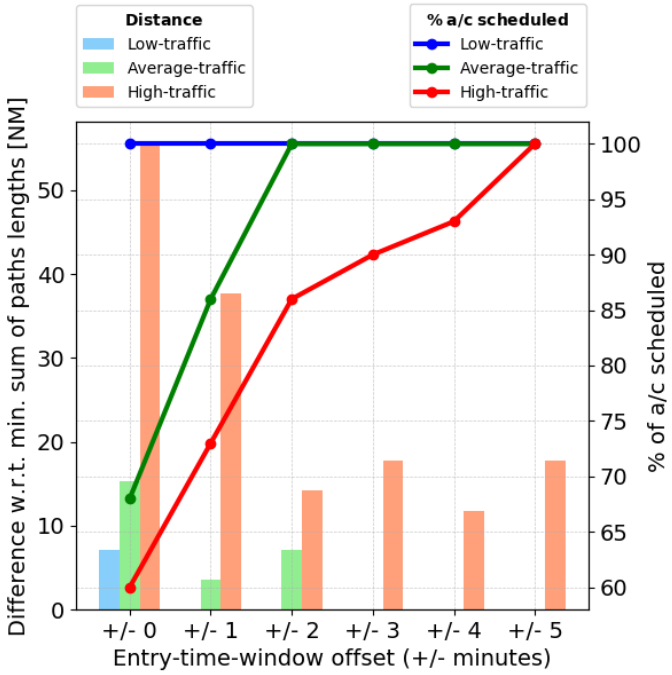

Figure VI-6: *Entry-time-window offset effect on the number of aircraft scheduled and on the sum of paths lengths for each case study (0% light aircraft)*

approximately 8NM in the low-traffic case study if an offset of ± 1 minute is considered. The route-optimization framework generates a shorter arrival tree because the aircraft arrival time at the TMA entry point is flexible, which results in a larger set of feasible solutions (and the minimum objective value over a superset cannot be larger than that over the original set). However, it is not evident whether it would be better for the aircraft to consider larger time-window offsets—which would involve gaining or losing more time in the pre-sequencing area, with the consequence of flying further from the optimum speed—or to fly a longer route but with a lower deviation with respect to the original time of arrival at the entry point. Both strategies have the potential to increase or reduce the fuel consumption of the flights and the final decision might depend on the specific scenario.

While in the average and low-traffic case studies it is possible—with a sufficiently large time-window offset—to schedule all aircraft and to obtain an arrival tree with the shortest possible paths, in the high-traffic case study this is impossible. As it can be observed in Figure VI-6, although the difference with respect to the minimum sum of paths lengths is reduced as the time-window offset increases, even with an offset of ± 5 minutes the resulting arrival tree is around 18NM longer than the shortest arrival tree.

Another interesting matter is the entry time deviation requested for each aircraft. As discussed in Section VI.4.5, this value depends on the considered time-window offset. For instance, for an offset of ± 3 minutes, the route-optimization framework considers that the arriving aircraft can gain or lose 1, 2 or 3 minutes in the pre-sequencing area. Figures VI-7(a) and VI-7(b) depict the distribution of the requested entry time deviation per aircraft. Figure VI-7(a) focuses on the effect of the amount of traffic, depicting the results for the low, average and high-traffic case studies when an time-window offset of ± 5 minutes is considered. On the other hand, Figure VI-7(b) focuses on the high-traffic case study, but by showing the results for different offsets.

For the low-traffic case study all aircraft can be scheduled by considering no deviation at the entry point. Conversely, in the average-traffic case study this is not possible, and a time-window offset of ± 2 minutes is necessary to schedule all traffic. As it can be observed in Figure VI-7(a), most of the aircraft are requested to gain or lose 1 or 2 minutes in the pre-sequencing area in that

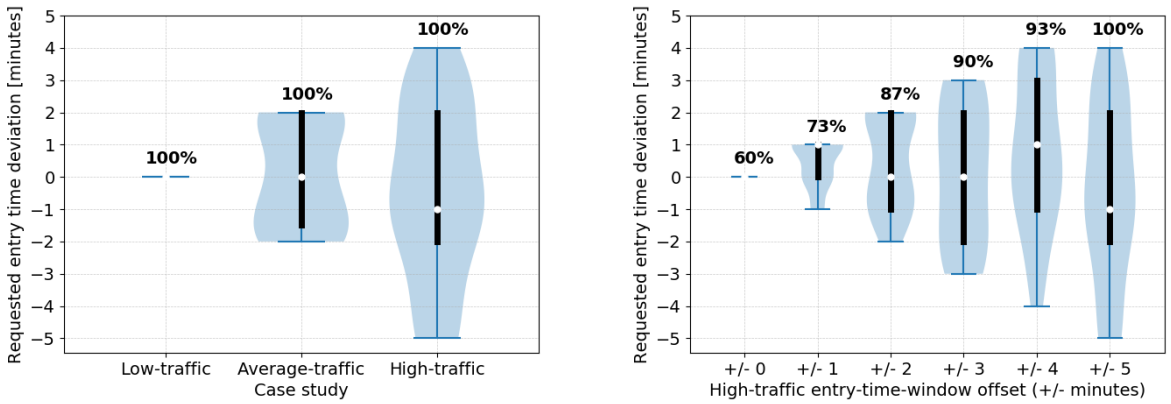

(a) Entry time deviation per aircraft with an entry-time-window offset of +/- 5 minutes for each case study

(b) High-traffic case study: requested entry time deviation distribution + percentage of aircraft scheduled (as a function of the entry-time-window offset)

Figure VI-7: *Results of the entry time deviation*

case, while a few of them can still arrive at the entry point at their original time of arrival. On the other hand, in the high-traffic case study, where a time-window offset of ± 5 minutes is needed to schedule all traffic, the majority of aircraft are requested to gain or lose a time in the ± 2 minutes range. Still, some aircraft are also requested to gain a larger amount of time (i.e. 3 and 4 minutes) and some of them are even requested to lose 5 minutes. As a result, all aircraft can be safely scheduled.

Figure VI-7(b) shows the different entry time deviations requested depending on the considered time-window offset for the high-traffic case study. In general, and whenever it is allowed, most of the aircraft are requested to gain/lose a time in the ± 2 minutes range. While only a time-window offset of ± 5 minutes allows to automatically schedule all aircraft, it is also true that the largest variation in the number of aircraft scheduled is observed from an offset of ± 0 to ± 2 minutes, where 26 out of 30 can be scheduled (i.e., 87% of the total aircraft). Then, considering larger offsets slightly increases the number of aircraft scheduled. In this particular case it is possible to find a reasonable time-window offset to schedule all aircraft (i.e., ± 5 minutes); however, if that was not possible, or if a very big offset was needed, those aircraft that were impossible to schedule could be managed manually by the ATCO via the assignment of vector instructions. Furthermore, powered descents could be considered in order to ease the scheduling of the most conflicting aircraft, as they offer more flexibility than neutral CDOs, as reported in Chapter IV. In such a situation, there would be an efficiency loss, but, still, all of the aircraft could be scheduled.

Regarding the results for different traffic mixes, it can be observed that, as expected, having a significant ratio of light aircraft in the arrival traffic complicates the task of the route-optimization framework. Larger time-windows offsets have to be considered in order to be able to schedule all aircraft. In the average-traffic case study, an offset of ± 4 minutes is required, while only an offset of ± 2 minutes was needed to schedule all aircraft when considering the original arrival distribution without light aircraft. On the other hand, in the high-traffic case study, it was not possible to schedule all aircraft even with a time-window offset of ± 5 minutes. Still, as discussed in Section VI.4.5, the aim when testing different traffic mixes was to assess how the proposed framework handled such a situation; however, from an operational point of view, this is not representative enough, as in major airports the ratio of light aircraft per day is usually between 1% and 3%.

The resulting arrival trees generated by the route-optimization framework for the average-traffic case study are depicted in Figure VI-8.

Arrival trees for the given 1-hour-period and for several entry-time-window offsets are pre-

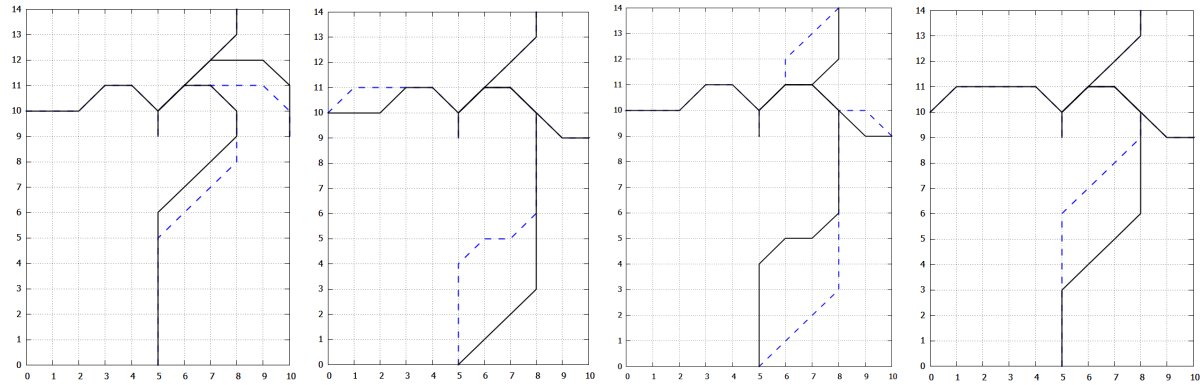

(a) ± 0 (15 of 22 a/c scheduled) (b) ± 1 (19 of 22 a/c scheduled) (c) ± 2 (22 of 22 a/c scheduled) (d) ± 3 (22 of 22 a/c scheduled)

Figure VI-8: *Arrival trees as a function of the entry-time-window offset for the average-traffic case study (0% light aircraft)*

sented. As discussed in Section VI.4.5, two trees are generated for each 1-hour-period; in Figure VI-8, black paths correspond to the first arrival tree and blue paths correspond to the second arrival tree, while the paths that are common to both trees are black. In this particular case, arrival trees from no time-window offset to an offset of ± 3 minutes are presented, where minimum route lengths are achieved. Figures VI-9 and VI-10 show the resulting arrival trees as a function of the entry-time-window offset for the high and low-traffic case studies, respectively.

It is important to highlight the fact that the trees depicted in Figures VI-8, VI-9 and VI-10 correspond to the output of the route optimization framework. Thus, in some situations, it could happen that the trees obtained are not optimal from an operational point view, even if the cost function defined in Section A.1 is minimized. For instance, for the average-traffic case study with a time-window offset of ± 3 minutes (Figure VI-8(d)), the route-optimization framework proposes to change the shape of the tree for the second half an hour period. However, the second tree (blue path) has the same length as the first tree (black path). Furthermore, only the route from the southern entry point is affected. Therefore, from an ATCO point of view (in order to reduce the workload), it would be better to have the same arrival tree for the whole 1-hour period. Thus, a post-processing would be needed in this kind of situations in order to obtain such a solution. Another option would be to alter the value of U, which is the parameter of the MIP formulation used to ensure a consistency in terms of number of differing edges between arrival trees during consecutive time periods. Smaller values than the ones used in the experiments could be used in order to obtain the same tree. However, how this "small" value of U is found should be done through a binary search, which is not a fast process.

On the other hand, noise could also have an effect on the final shape of the arrival tree. For instance, let us assume a scenario where the route coming from the south in the first tree (in Figure VI-8(d)) overflies a populated area; in such a case, maybe it would be better to keep the tree as it is now in order to minimize the noise effects over populated regions (assuming the southern route of the second tree avoids these regions). Similarly, it might be also better to keep 2 trees in order to increase noise dispersion and, thus, minimize aircraft noise impact on communities around an airport (Ho-Huu *et al.*, 2020). The effect of noise is indeed a very interesting topic and will be investigated in future work.

VI.5.3 Evaluation of Arrival Sequencing

The optimized solutions obtained guarantee separation at any point of the TMA with the chosen separation parameter $\sigma_{A,B}$. The benefits provided by this approach were evaluated by using

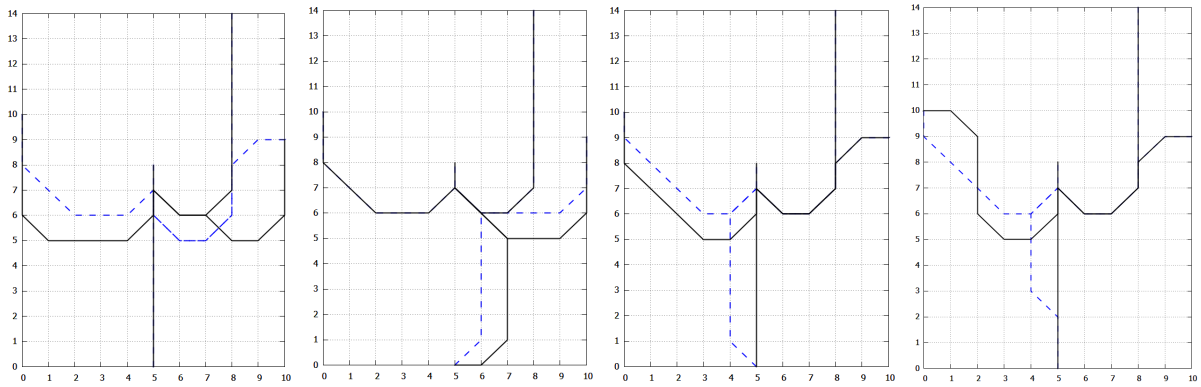

(a) ± 0 (18 of 30 a/c scheduled) (b) ± 1 (22 of 30 a/c scheduled) (c) ± 2 (26 of 30 a/c scheduled) (d) ± 3 (27 of 30 a/c scheduled)

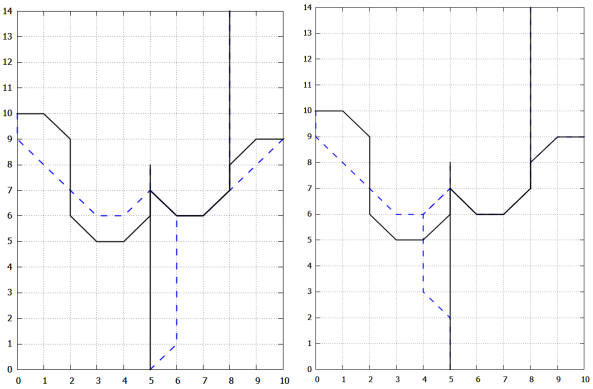

(e) ± 4 (28 of 30 a/c scheduled) (f) ± 5 (30 of 30 a/c scheduled)

Figure VI-9: *Arrival trees as a function of the entry-time-window offset for the high-traffic case study (0% light aircraft)*

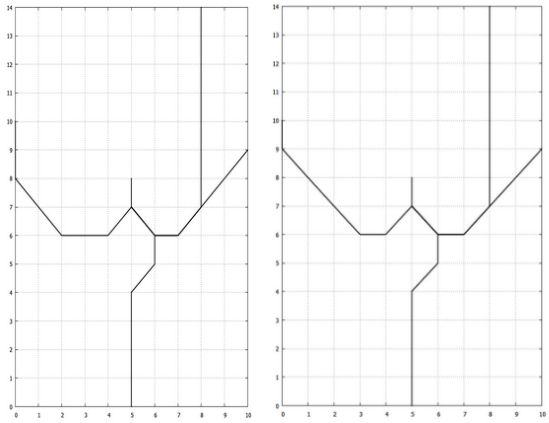

(a) ± 0 (8 of 8 a/c scheduled) (b) ± 1 (8 of 8 a/c scheduled)

Figure VI-10: *Arrival trees as a function of the entry-time-window offset for the low-traffic case study (0% light aircraft)*

a set of key performance indicators (KPIs) recently proposed by Eurocontrol Experimental Centre (Christien *et al.*, 2019), with several adjustments to the proposed methodology, as detailed by Smetanová (2020):

- **Minimum time to final (ttf):** the minimum ttf is defined as the minimum time it takes an aircraft to fly from its current position to the final approach point. The minimum ttf is computed as the minimum time needed from any point within a grid cell to the final approach point along any of the aircraft trajectories passing through the cell.
- **Spacing deviation:** the spacing of an arriving aircraft pair at time t is defined as the difference between the respective minimum times to final. The spacing deviation (sd) is computed for pairs of leading and trailing aircraft at time t; it captures the aircraft's mutual position in time. It is calculated using Equation (VI.1):

$$\text{ttf}(\text{trailer}(t)) - \text{ttf}(\text{leader}(t - s_{rwy})), \tag{VI.1}$$

  where s_{rwy} is the temporal separation at the runway.

  The spacing deviation reflects information about the control error, which is the accuracy of spacing around the airport.
- **Sequence pressure:** the sequence pressure for an aircraft at time t corresponds to the number of aircraft sharing the same minimum time to final within a given time window; it reflects the density of aircraft. It is calculated for each aircraft at any time of its presence within the TMA in discrete time steps. A window of 2 minutes—the minimum separation requirement in the optimization framework—was chosen.

Figure VI-11 depicts the actual and optimized routes (i.e., optimal arrival tree) for each case study. Additionally, several heat maps are generated in order to depict the minimum time to final (ttf) for each case. Table VI-3 shows the minimum, maximum, average and standard deviation values for the minimum time to final, as well as for the spacing deviation (sd) and sequence pressure (sp) key performance indicators.

Table VI-3: *Minimum time to final (ttf), spacing deviation (sd) and sequence pressure (sp): Min/Max/Average/Standard deviation*

Case study	Actual ttf [sec.]	Optimal ttf [sec.]	Actual sd [sec.]	Optimal sd [sec.]	Actual sp [# a/c]	Optimal sp [# a/c]
Low-traffic	0/836/456/215	0/660/332/162	-203/152/0.62/73.18	0/240/36.73/57.21	1/2/1.15/0.36	1/1/1/0
Average-traffic	0/1073/807/400	0/1140/607/292	-236/249/2.89/64.72	-300/360/11.25/117.22	1/4/1.33/0.55	1/2/1.04/0.19
High-traffic	0/986/494/228	0/660/331/161	-328/338/-2.86/86.25	-300/300/16.42/69.45	1/4/1.38/0.65	1/1/1/0

In general, the shape of the optimal arrival tree is similar to that of the actual arrival routes. However, in the optimal arrival tree, there is only one arrival route per entry point, while in the actual case aircraft follow several routes from each of the entry points; actually, it seems that there are more than only 4 entry points to the TMA in the actual case. This is due to the fact that in reality ATCOs might need to give vector instructions in order to be able to schedule all aircraft. On the other hand, in the optimal arrival tree, the arrival routes automatically ensure that a separation is already maintained between the arriving aircraft. Therefore, there is no need for vectoring and, consequently, there is a lower route dispersion leading to a lower amount of airspace used.

In the optimal case, there is a higher situational awareness by both the ATCO and the flight crew. ATCOs, when aircraft are in the pre-sequencing horizon, up-link an RTA at the TMA entry point and an arrival route from the optimal arrival tree. Thus, the flight crew already knows which route they should follow in the TMA (Figures VI-11(b), VI-11(f), VI-11(j)), and the FMS on board can optimize the descent trajectory accordingly. This is quite different from the current situation, where neither the flight crew nor the ATCO know the arrival route that will be followed inside the TMA. This is specially remarkable in very congested scenarios, where many vector instructions might be needed in order to safely schedule all traffic (Figures VI-11(a), VI-11(e), VI-11(i)).

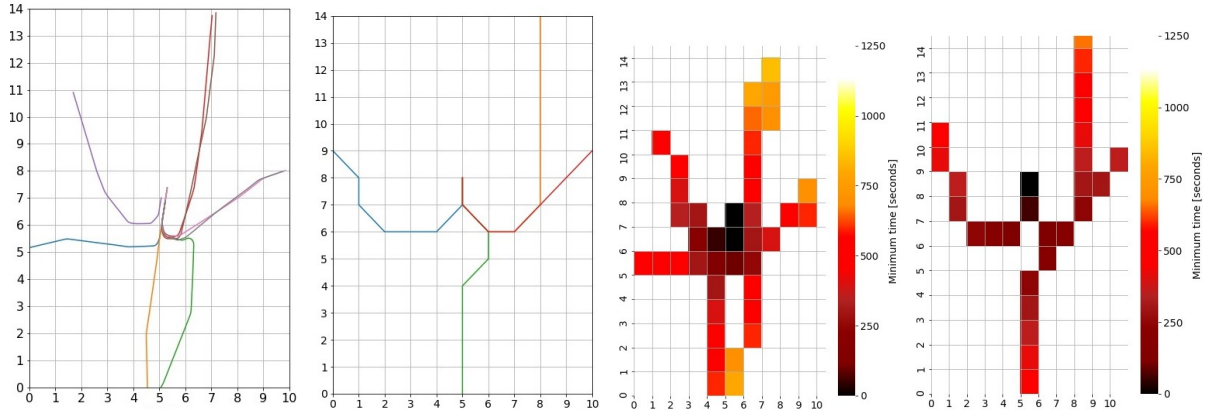

(a) Low-traffic: actual arrival routes (b) Low-traffic: optimized arrival routes (c) Low-traffic: actual minimum time to final (d) Low-traffic: optimized minimum time to final

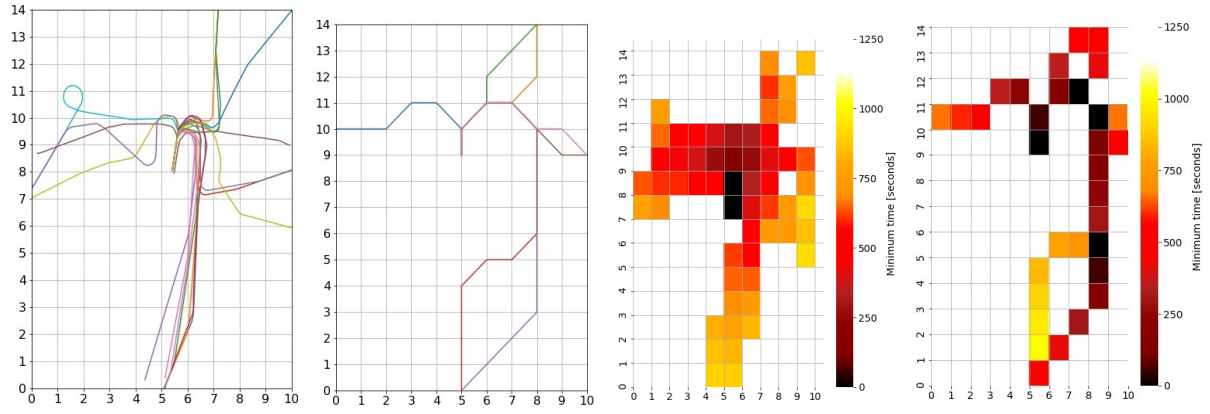

(e) Average-traffic: actual arrival routes (f) Average-traffic: optimized arrival routes (g) Average-traffic: actual minimum time to final (h) Average-traffic: optimized minimum time to final

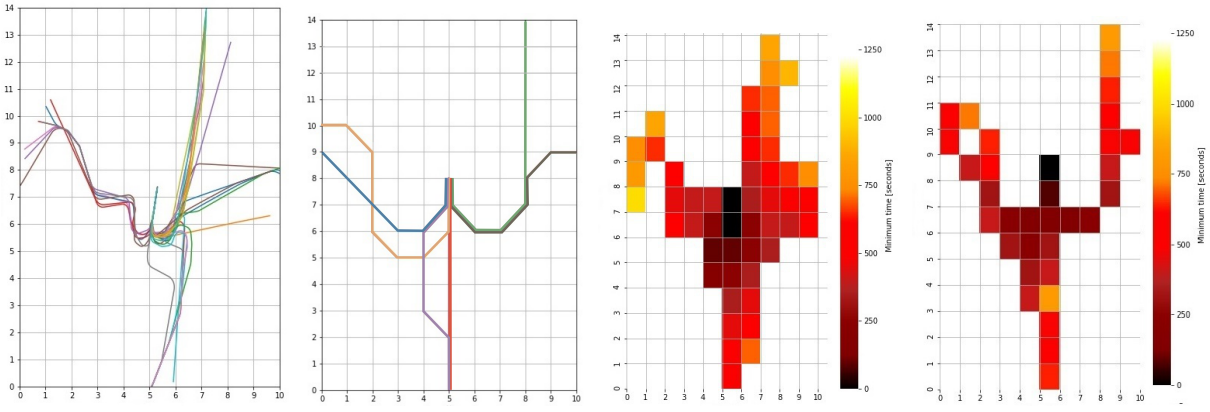

(i) High-traffic: actual arrival routes (j) High-traffic: optimized arrival routes (k) High-traffic: actual minimum time to final (l) High-traffic: optimized minimum time to final

Figure VI-11: *Actual flown trajectories vs. optimized trajectories for low, average and high-traffic case studies: arrival routes and minimum time to final*

Regarding the minimum time to final, in all three case studies lower average values are obtained in the optimal case, with a reduction in comparison to the actual case of between 2 and 3 minutes, depending on the case study. However, in the average-traffic case study, the maximum value is higher than that of the actual case, around 300 seconds more. Still, the proposed solution provides a lower average value. Furthermore, it is important to remark that in this chapter all aircraft were scheduled by assuming neutral CDOs so, even if in some cases longer routes

are generated—which may lead to higher ttf values—the overall efficiency of the operations is improved.

The results for the spacing deviation and sequence pressure analysis are shown in Figure VI-12. For the low and high-traffic case studies, shorter intervals (i.e., difference between the maximum and minimum values) for the spacing deviation are obtained with the proposed solution, which means that, on average, for an arriving aircraft pair at time t, the difference between their respective minimum times to final is lower. On the other hand, in the average-traffic case study, longer intervals are obtained in the optimized case. Another important metric to analyze is the maximum width of the 90th quantile, which quantifies the spread of the 90% confidence interval and is shown in turquoise in Figures VI-12(c), VI-12(d), VI-12(g), VI-12(h), VI-12(k) and VI-12(l). For both the low and average-traffic case studies a lower width of the 90th quantile is observed for the optimized case in comparison with the actual case; 211/120 and 387/363 seconds, respectively. On the other hand, in the high-traffic case study, the value obtained in the real case is 427 seconds, which is lower than the width of the 90th quantile for the optimized case, which is 537 seconds.

Regarding the sequence pressure, in all case studies the proposed solution provides lower values than the actual case. For a window size of 120 seconds, in both the low and high-traffic case studies the minimum, maximum and average sequence pressure obtained with the proposed solution is equal to 1, while in the average-traffic case study the maximum value is equal to 2. In that case, that means that up to two aircraft intended to arrive at the same time (± 2 minutes), which might indicate a potential separation problem. However, as shown by Hardell *et al.* (2020a), this is not always the case and the fact of having sequence pressure values equal to 3 does not always necessarily indicate a separation violation problem. Regarding the actual case, sequence pressure maximum values up to 4 are obtained. This metric clearly uncovers the benefits of the proposed approach, which noticeably lowers the sequence pressure not only at the runway, but also at all points in the TMA. As a result, ATCOs would need to spend less time resolving potential separation problems to smooth the scheduling process of the arrival traffic.

VI.5.4 Vertical and Lateral Efficiency

In order to assess the benefits of the proposed solution, the vertical efficiency for the different case studies was analyzed, where a comparison was made between the vertical profiles of the actual flown trajectories—which follow the STARs inside the TMA—and the corresponding flights flying neutral CDOs and following the assigned route of the arrival tree. As mentioned in Section VI.4.4, most of the data for the actual trajectories was obtained from the OpenSky Network, with the exception of two aircraft whose data was obtained from Eurocontrol's DDR.

Because DDR data is sparser, the information about the vertical profiles is not as detailed as in OpenSky states data. On the other hand, OpenSky states data is very dense. Thus, in order to speed up the computations, the selected dataset was sparsified by using every third recording, which reflects aircraft position every three seconds and results in less fluctuations. The data also contains erroneous position records, as well as false altitude records, which were filtered out. Data from DDR was used unfiltered.

In order to compare the vertical profiles of the actual flown trajectories with the corresponding flights flying neutral CDOs, the actual trajectories were cut at the same altitude as the end of the CDOs. Since only the vertical profiles inside the TMA were compared, the starting point of the trajectory was defined as the point where the aircraft entered the Stockholm TMA.

The difference in distance flown inside the TMA between the actual trajectories and the trajectories following a CDO was also studied, as well as the time spent in the TMA. The definition of the start and the end of the trajectory was identical to the one used for the vertical profiles. The distance between each recording was computed based on the latitude and longitude coordinates

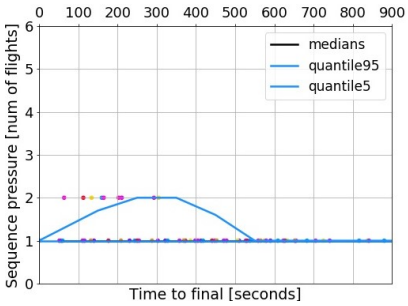

(a) Low-traffic: actual sequence pressure

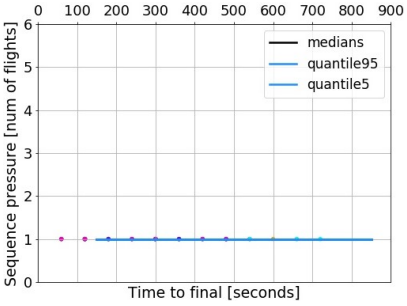

(b) Low-traffic: optimized sequence pressure

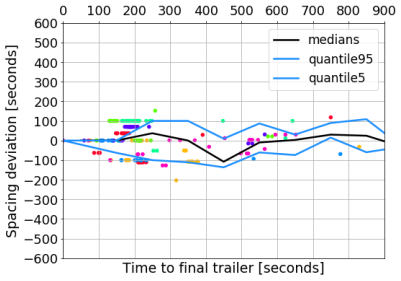

(c) Low-traffic: actual spacing deviation

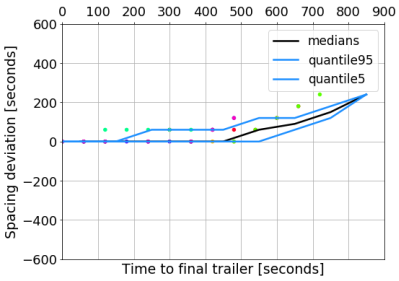

(d) Low-traffic: optimized spacing deviation

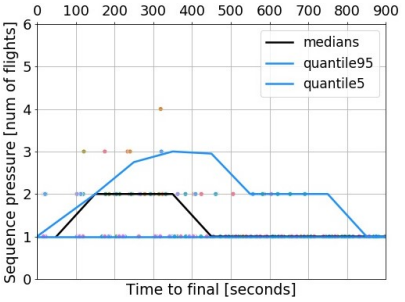

(e) Average-traffic: actual sequence pressure

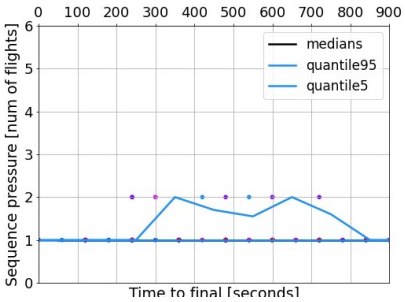

(f) Average-traffic: optimized sequence pressure

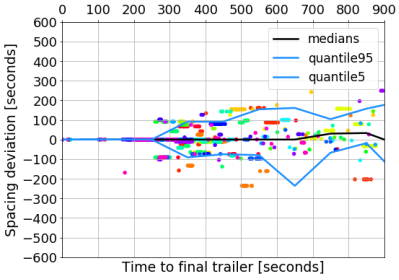

(g) Average-traffic: actual spacing deviation

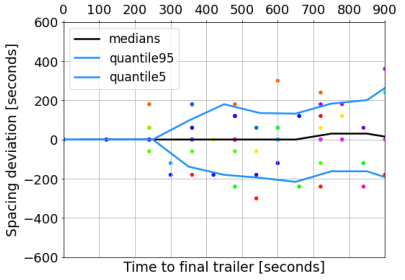

(h) Average-traffic: optimized spacing deviation

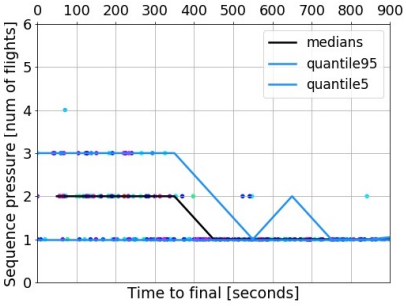

(i) High-traffic: actual sequence pressure

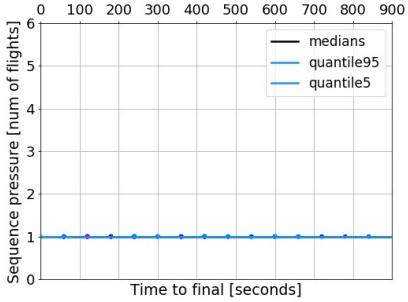

(j) High-traffic: optimized sequence pressure

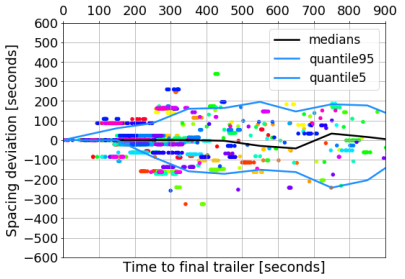

(k) High-traffic: actual spacing deviation

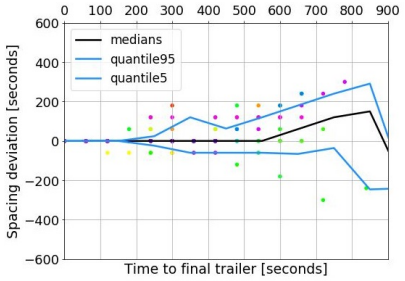

(l) High-traffic: optimized spacing deviation

Figure VI-12: *Actual trajectories vs. optimized trajectories for low, average and high-traffic case studies: sequence pressure and spacing deviation*

provided in OpenSky and DDR data.

A comparison of the vertical profiles inside the TMA is shown in Figure VI-13. As expected, some of the actual flown trajectories follow very inefficient descent profiles with several steps at

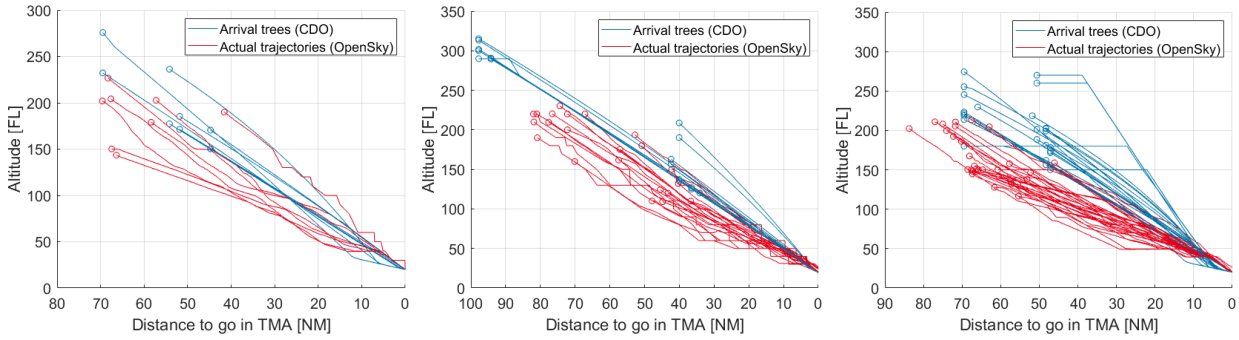

(a) Low-traffic (b) Average-traffic (c) High-traffic

Figure VI-13: *Vertical profiles for the different traffic case studies*

constant altitude; some of them are even performed at very low altitudes, which has an adverse effect on fuel consumption. On the other hand, CDOs allow the aircraft to follow a more continuous descent path, without intermediate steps at constant altitude when following the arrival route. Furthermore, when flying CDOs, aircraft tend to start the descent later, meaning that their top of descent is usually closer to the final point of the trajectory. As a result, aircraft flying CDOs usually enter the TMA at a higher altitude, thus, improving the flight efficiency. Finally, in the high-traffic case study (Figure VI-13(c)), it can be observed that there are several optimized trajectories that enter the TMA at very low cruise altitudes, at FL270 or even at FL150. These trajectories correspond either to short flights, where there is no time for the aircraft to reach a higher cruise altitude, or to turboprop aircraft, which tend to fly at lower cruise altitudes.

Table VI-4 shows the average distance and time spent by the arriving aircraft in TMA for both actual trajectories and CDOs. Then, Figure VI-14 depicts the individual values for each arriving aircraft.

Table VI-4: *CDOs vs actual flown trajectories: Distance and time in TMA*

Case study	CDOs average distance in TMA [NM]	Actual trajectories average distance in TMA [NM]	CDOs average time in TMA [minutes]	Actual trajectories average time in TMA [minutes]
Low-traffic	55.06	56.66	8.5	12.13
Average-traffic	62.63	61.68	17.14	13.76
High-traffic	57.32	65.3	9.33	15.12

While better results are obtained for the low and high-traffic case studies—with a reduction in the average distance and time spent in TMA of 1.6 NM/3.6 minutes and 8 NM/5.8 minutes, respectively—worse results are obtained for the average-traffic case study—where, in average, an increase of approximately 1 NM and 3.5 minutes spent in TMA are obtained with the proposed solution.

While the proposed solution does not ensure a reduction in the distance and time spent in TMA in all cases, it is also true that only neutral CDOs are considered in all case studies. In such a situation, the route-optimization framework—whose task is to optimize the scheduling of the arrival traffic by providing an automated separation in time and space—needs to generate, in some cases, arrival trees with longer routes than those flown in the actual case. For the actual flown trajectories, it can be observed that CDOs are not flown and trajectories follow in some cases step-down approaches. Shorter paths might be considered in some cases, but at the expense of flying less efficient vertical profiles.

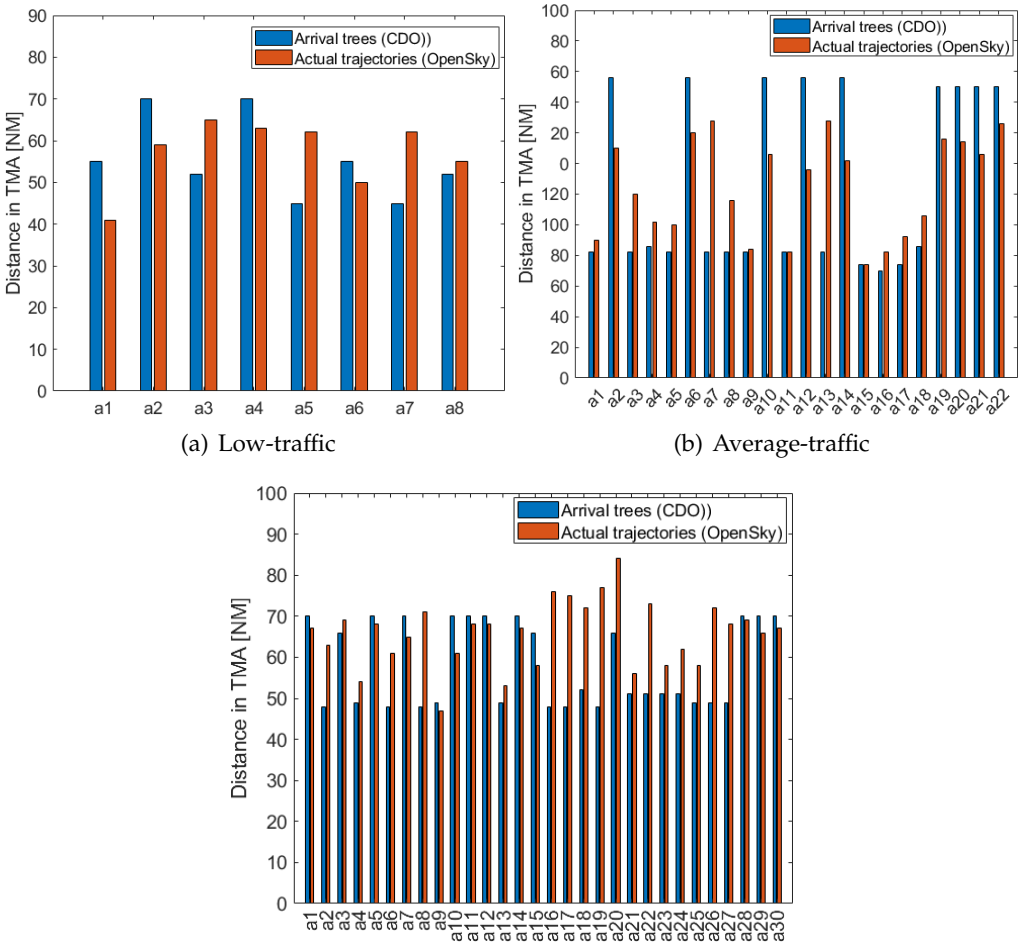

(a) Low-traffic

(b) Average-traffic

(c) High-traffic

Figure VI-14: *Distance in TMA for the different traffic case studies*

VI.6 Discussion

This chapter proposed to schedule arrival traffic by means of two different areas surrounding the airport. In the pre-sequencing area, a 4D-traffic-negotiation/synchronization process is performed between the ATCO and the arriving aircraft. The outcome of this process, which is managed by a ground-based tool, is a set of optimal arrival routes (i.e., arrival tree) inside the dynamic-trajectories area, as well as the assignment of an RTA at the entry point of this area for each arriving aircraft. The proposed solution adapts to the current traffic demand, allows the aircraft to fly CDOs and ensures a safe separation between aircraft throughout the arrival procedure.

The approach presented in this chapter has the potential to both reduce the environmental impact of aircraft operations and the workload of ATCOs. However, there are several factors to be considered that may limit the benefits of the proposed solution. The arrival traffic amount and distribution greatly affect the outcome of the route-optimization framework. Although it was shown that a solution can always be found, even in the scenarios with a high amount of traffic, it is also true that in such cases aircraft are requested to gain/lose more time in the pre-sequencing area. As a result, the computational time needed for generating the optimal arrival tree drastically increases. In addition, the use of neutral CDOs (idle thrust and no speed brakes usage allowed) was enforced for all aircraft, with the consequent reduction in each aircraft's arrival time window when compared with powered descents (where both thrust and speed brakes usage is allowed). Hence, it takes a longer time for the route-optimization framework to find a solution. Finally, the size of the dynamic-trajectories area, where the optimal arrival tree is generated, could also affect

the computational load of the framework. In this chapter, it was decided to define this area in such a way that it fitted the current Stockholm TMA. A smaller area would potentially speed up the generation of the arrival tree, while larger areas would have the opposite effect. The size of the dynamic-trajectories area (and the pre-sequencing area) is indeed a very interesting topic and will be investigated in future work.

While a solution is always found by the route-optimization framework, the computational time in some cases is too high. A more efficient code could be written or other approaches—like the one proposed by Chevalier, J. (2020), which provides a sub-optimal solution—could be investigated to speed up the computations. In future work, it is planned to integrate wind to the proposed solution, which might involve computing a higher number of trajectories (where wind is considered when generating the CDO).

The CONOPs proposed in this chapter replaces the current STAR paradigm—where routes are static and not designed to meet the requirements of the arriving traffic—with a dynamic generation of arrival routes that increases the efficiency and safety of operations while keeping the same levels of capacity. The proposed solution aligns with the TBO concept, and is expected to become a technical enabler towards an E-AMAN with enhanced capabilities, where the sequencing horizon would be extended into the en-route sector, thus improving the situational awareness of both the flight crew and the ATCO. Furthermore, airport's arrival management information would be shared with upstream sectors in real time by using a SWIM service.

You need people like me so you can point your [...] fingers and say, "that's the bad guy." So... what that make you? Good? You're not good. You just know how to hide, how to lie. Me, I don't have that problem. Me, I always tell the truth. Even when I lie. So say good night to the bad guy!

—Al Pacino (*Scarface*)

VII

Concluding Remarks

Despite the desirable growth of the global economy, the higher volume of air traffic has also increased the environmental impact of aviation. The introduction of more fuel-efficient trajectories, however, comes at the expense of a reduction on capacity due to the higher diversity of trajectories that need to be handled by the air traffic control officers (ATCOs). Continuous descent operations (CDOs) with controlled times of arrival (CTAs) were identified as a potential solution to maintain capacity at acceptable levels, or even increasing it, while simultaneously allowing fuel-efficient descents. The introduction of this kind of flight operations, however, will require the modernization of both ground and airborne systems, where higher levels of automation and information sharing are expected among all the involved actors in the air traffic management (ATM) system. The main objective of this PhD thesis was the development of methodologies to efficiently schedule arrival aircraft flying environmentally friendly descents in terminal airspace, together with concept of operations (CONOPs) aligned with the trajectory based operations (TBO) paradigm.

During this work, some questions arose that were assessed and some of them are still open and could be topics of further research. A brief summary and conclusions of the achieved results, as well as hints on the possible directions for future work, are presented in the following sections.

VII.1 Summary of Contributions

The main contributions of this PhD thesis are summarized as follows:

- A trajectory optimization framework for the generation of aircraft descent trajectories was defined in Chapter II. This framework includes the formulation of a generic optimal con-

trol problem to generate optimal trajectory plans taking into account any aircraft dynamics, aircraft performance model (APM) and weather model as well as any number of flight phases, constraints and cost function. Mainly two approaches were identified to solve the optimal control problem: a semi-analytic approach, used to tackle simpler optimal control problems—where, among other simplifications, cruise speed is assumed to be constant, the flight path angle is the only control variable of the problem and required times of arrival (RTAs) can only be achieved by brute force—and direct multiple-shooting methods, targeting more complex non-linear programming (NLP) optimization problems. Furthermore, several recommendations to face the most common issues that one could encounter when implementing non-linear optimization algorithms were also provided.

- Several performance indicators (PIs) were used in Chapter III to assess the efficiency of arrival operations in the terminal maneuvering area (TMA) of Stockholm-Arlanda airport for year 2018. For that purpose, two data sources were used: OpenSky Network automatic dependent surveillance-broadcast (ADS-B) data (tracks and states) and Eurocontrol demand data repository (DDR) data. It was concluded that OpenSky states—with a previous filtering of the data for removing outliers—are more accurate than DDR data for efficiency assessments within the TMA, as they led to more realistic results when comparing the benefits, in terms of fuel consumption, of flying energy-neutral CDOs. By generating the CDOs with the trajectory optimization framework presented in Chapter II, fuel savings of up to 30% were achieved.

- In Chapter IV, two strategies were compared in a scenario where the ATCO assigns a CTA outside the energy-neutral time window (for an aircraft flying along the published route): flying energy-neutral CDOs along shorter/longer predefined routes vs. flying powered descents along the published route. Results for CTAs earlier than the estimated time of arrival (ETA), as expected, show that flying neutral CDOs—which involves flying shorter predefined routes to fulfill the CTA—always represent a lower fuel consumption with respect to flying powered descents along the published route. When the CTA is assigned later than the ETA, however, different behaviors are observed, which depend on different factors such as the aircraft model or the current wind. In a tailwind scenario—except if the assigned CTA is very close to the ETA—stretching the route (and fly energy-neutral CDOs) will always increase the efficiency of the operation. Similarly, light aircraft will also benefit from being assigned longer predefined routes, while for heavy aircraft it will be better to fly powered descents along the published route. The results obtained for the analysis presented in Chapter IV are expected to be valuable towards the definition of a ground-support tool to help air traffic control (ATC) to manage more efficiently arriving traffic under the TBO paradigm.

- Chapter V focused on the definition of a CONOPs and methodology to schedule arrival traffic in the TMA by means of four-dimensional (4D) closed-loop instructions, where a route and a RTA at a given metering fix were negotiated at the extended terminal maneuvering area (E-TMA) entry point. For that purpose, the trombone procedure of Frankfurt airport was used. Results show that, after assigning RTAs and routes to every arriving aircraft when still in cruise, it is possible to ensure that a high percentage of them will perform energy-neutral CDOs, guaranteeing at the same time a safe separation between aircraft throughout the whole descent. While the CONOPs proposed in this chapter works properly for low-traffic scenarios, it could be concluded that, in some cases, in airports or time periods with high traffic loads, it might be necessary to reformulate it. Establishing the communication between the arriving aircraft and the ATC even before arriving at the E-TMA—in order to request arrival aircraft to gain or lose a given amount of time in the en-route phase, before entering the E-TMA—could potentially avoid a lot of separation losses. Furthermore, conflicts could also be avoided by gaining or losing time during the cruise section between the E-TMA entry point and the top of descent (TOD), which would involve, depending on the

scenario, an extension of the E-TMA size. Finally, the aircraft entry distribution is also a key factor affecting the feasibility of the solution proposed. Better distributions where aircraft arrive with enough separation at the E-TMA entry points would represent an increase in the number of energy-neutral CDOs performed and, therefore, an improvement in the efficiency of the operations. The solution presented in Chapter V is expected to become a technical enabler towards future arrival manager (AMAN) systems, providing more automated and enhanced ground support to ATCOs and allowing flights to perform more efficient descents.

- By assuming a more futuristic scenario with TBO deployed to its limits, another contribution of this PhD thesis was to propose a CONOPs and develop a methodology to schedule arrival traffic by means of dynamic arrival routes within terminal airspace, thus, shifting away from the current standard terminal arrival route (STAR) paradigm. This work was presented in Chapter VI. Two areas were defined around the airport: (1) the dynamic-trajectories area, where arrival routes enabling energy-neutral CDOs are generated and automatically adapt to the current traffic demand; and (2) a pre-sequencing area, where an RTA at the dynamic-trajectories horizon and a specific route in the dynamic-trajectories area are negotiated between the arrival aircraft and the ATCO. The approach presented in Chapter VI has the potential to both reduce the environmental impact of aircraft operations and the workload of ATCOs, reducing route dispersion and improving the predictability of the operations. However, similarly to Chapter V, the arrival traffic amount and distribution greatly affect the outcome of the route-optimization framework. Furthermore, although a solution was always found, the computational times were very high for some case studies, which might limit the application of this solution in real scenarios. Still, there is margin to further optimize the framework, and other strategies different from mixed integer programming (MIP) might speed up the route-generation process. Ultimately, the solution presented in Chapter VI is expected to become a technical enabler towards an extended arrival manager (E-AMAN) with enhanced capabilities, where the sequencing horizon would be extended into the en-route sector, thus improving the situational awareness of both the flight crew and the ATCO.

VII.2 Future Research

During this PhD thesis new questions and research lines arose. Taking advantage of the trajectory optimization framework that has been developed, several work items that deserve further research and/or resources have been identified. The following elements could potentially help to increase the technology readiness level (TRL) of the solutions proposed:

- A higher number of scenarios (e.g., different airports or arrival traffic characteristics) should be tested in the future to validate the solutions proposed in Chapters V and VI focusing, respectively, in scheduling traffic in trombone procedures and in scheduling traffic by means of arrival routes automatically adapting to the traffic demand. This would allow to obtain statistically significant results.
- When generating the dynamic arrival routes in the experiments conducted in Chapter VI, no wind was considered in the computations. In the future, in order to obtain more realistic results, wind should be integrated in both the route-optimization framework and when generating the CDOs that are input to the framework.
- In some of the case studies considered in Chapters V and VI, it was impossible to schedule all the arrival traffic. One potential solution to that problem could be to allow the aircraft to fly also powered descents. Furthermore, the cost function could be adapted in order to

minimize the number of aircraft flying this kind of descents, as they are less efficient than energy-neutral CDOs.

- In the fuel consumption comparison between energy-neutral CDOs and powered descents presented in Chapter IV, only a straight route was considered. In future work, it would be worth obtaining new results for more realistic scenarios, where aircraft could fly real arrival procedures from the cruise level to the runway threshold.
- In all the experiments considered in this PhD thesis, only aircraft arrivals were considered. However, depending on the scenario, departures could also have an effect on the obtained results. In general, issuing vector instructions to departures would be the preferred solution in the majority of cases, as these instructions are not as detrimental for the climb operations as it is the case with descents. In addition, it might be necessary to ensure separation in certain waypoints where arrivals and departures cross. Therefore, in the future, a scenario considering both arrivals and departures could be investigated in order to check the effect that climb operations could have on the efficiency of the descents operations.
- The results obtained in Chapters V and VI depend heavily on the arrival distribution. In the future, it would be interesting to propose metrics to measure this "goodness" of the arrival traffic distribution.
- Shifting away from the current STAR paradigm where ATCOs issue open-loop instructions, in Chapters V and VI arrival traffic was scheduled by means of closed-loop instructions in a trombone procedure and in a dynamic-arrival-route scenario, respectively. These three methods (i.e., aircraft scheduling in trombone procedures, dynamic arrival routes and STARs) could be compared in the future by assuming a common scenario (i.e., same airport and same arrival traffic amount and distribution).
- The workload of the ATCOs could be included in the future via a task load model integrated in the experiments tackled in Chapters V and VI, with the aim of better enabling a comparability of the developed solutions from the point of view of the ATCOs.

Свобода не в том, чтоб не сдерживать себя, а в том, чтоб владеть собой.
[Freedom is not in restraining but in controlling yourself.]
— Фёдор Михайлович Достоевский [Fyódor Mikháylovich Dostoyévskiy]

A

Grid-Based MIP Formulation

The proposed MIP formulation is based on the MIP developed by Dahlberg *et al.* (2018), which was improved for the experiments conducted in this chapter. Dahlberg *et al.* (2018) made the simplified assumption that traversing a single edge takes u time units for all aircraft (independent of aircraft type and distance to runway). Then, Sáez *et al.* (2020a) considered aircraft with different speeds, and, in particular, the speed profile given by a CDO for the specific aircraft type.

In both papers, a uniform separation value was used, that is, any pair of consecutive aircraft needs to be separated by σ time units. In this MIP formulation, the wake-turbulence categories of the leading and trailing are taken into account into account, that is, a uniform separation of σ is no longer used, but a temporal separation $\sigma_{A,B}$ that depends on the categories A and B of the leading and trailing aircraft, respectively. A flexibility of the arrival time at the entry point of the dynamic-trajectories area is also introduced.

Subsections A.1, A.2 and A.3 start with a review of the prior proposed MIP-formulation for static optimal STAR merge trees (Andersson *et al.*, 2016). Subsection A.4 presents auxiliary constraints to prevent crossings, using a uniform temporal separation of σ (Dahlberg *et al.*, 2018), as detailed in A.5. Then, the integration of different speed profiles is described in Subsection A.6. In particular, the speed profiles that stem from CDOs for the different aircraft will be used, see Section VI.4.2 (Chapter VI) for details of their computation. Subsection A.7, concludes the presentation of prior constraints and show largest possible consistency of trees from two consecutive time periods can be enforced. Subsection A.8, presents the required formulation to allow aircraft to arrive at their entry point of the dynamic-trajectories area within a time window (from which any arrival time may be picked) instead of forcing them to arrive at a specific time. This flexibility enables scheduling more aircraft flying CDOs. Subsection A.9, introduces the temporal separation based on the wake turbulent categories of the aircraft. Finally, Subsection A.10 presents the

complete MIP for better readability.

The input consists of the position of entry points to the dynamic-trajectories area; the location and direction of the runway; arrival time (within a given time window T), arrival entry point, and aircraft type for all aircraft. It was decided to use the position of the runway for the experiments of this work although, in general, as described in the CONOPs in Section VI.2, the final merging fix position should be considered instead. The aim is to output an arrival tree that merges traffic from the entries to the runway such that all aircraft are separated at all points of the arrival routes. The tree has the entries as leaves and the runway as the root (here the notation is slightly abused twice, as directed trees are usually called arborescences, and these are usually directed from leaves to root). Aircraft are assumed to fly according to their optimal continuous descent speed profile for the route length of the entry point-runway path along the tree. These speed profiles are computed separately, and provided as input to the MIP in the form of different speed profiles for different arrival route lengths.

A.1 Tree Constraints and Objective Function

A discretization is used: the dynamic-trajectories area is overlaid with a square grid, and the location of both entry points and runway are snapped to the grid. The set of (snapped) entry points are denoted by $\mathcal{P}$, and the (snapped) runway by r. The threshold L is used as side length of grid pixels, hence, operational Constraint 3 is fulfilled with any path in the grid. Every grid node is connected to its 8 neighbors (where $N(i)$ denotes set of neighbors of i, including i), resulting in a bidirectional graph $G = (V, E)$: for any two adjacent vertices i and j, both edges (i, j) and (j, i) are included in E; exceptions are the entry points (they do not have incoming edges) and r (it does not have outgoing edges). Let ℓ_{ij} denote the length of an edge $(i, j) \in E$. Let G be a grid of size $q \times n$.

In case operational Constraint 5 is used, the edges from the region that the routes may not pass from the edge set E are deleted (as the arrival tree is built from grid edges no route will then cross any obstacle).

The underlying MIP formulation for static arrival routes (Andersson *et al.*, 2016) is based on the flow MIP formulation for Steiner trees (Wong, 1984; Goemans & Myung, 1993).

Binary decision variables x_e that indicate whether the edge e participates in the arrival tree are used. Moreover, flow variables are also used: f_e gives the flow on edge $e = (i, j)$ (i.e., the flow from i to j). The constraints are given as follows:

$$\sum_{k:(k,i)\in E} f_{ki} - \sum_{j:(i,j)\in E} f_{ij} = \begin{cases} |\mathcal{P}| & i = r \\ -1 & i \in \mathcal{P} \\ 0 & i \in V \setminus \{\mathcal{P} \cup r\} \end{cases} \tag{A.1}$$

$$x_e \geq \frac{f_e}{Q} \quad \forall e \in E \tag{A.2}$$

$$f_e \geq 0 \quad \forall e \in E \tag{A.3}$$

$$x_e \in \{0, 1\} \; \forall e \in E \tag{A.4}$$

where Q is a large number (e.g., $Q = |\mathcal{P}|$).

Eq. (A.1) ensures that a flow of $|\mathcal{P}|$ reaches the runway r, a flow of 1 leaves every entry point, and in all other vertices of the graph the flow is conserved. Eq. (A.2) enforces edges with a positive flow to participate in the arrival route. The flow variables are non-negative (Eq. (A.3)), the edge variables are binary (Eq. (A.4)).

Eq. (A.1) could easily be adapted to allow minimization of the sum of trajectory lengths flown by all arriving aircraft. In that case, each path is counted as many times as it is used by aircraft (instead of minimizing the length of paths from entry points to the runway). Thus, the right-hand side of Eq. (A.1) is changed (and Q is increased accordingly).

Let w_b be the number of aircraft entering the dynamic-trajectories area via entry point $b \in \mathcal{P}$. Then, the new constraint is written as:

$$\sum_{k:(k,i)\in E} f_{ki} - \sum_{j:(i,j)\in E} f_{ij} = \begin{cases} \sum_{b\in\mathcal{P}} w_b & i = r \\ -w_i & i \in \mathcal{P} \\ 0 & i \in V \setminus \{\mathcal{P} \cup r\} \end{cases} \tag{A.5}$$

Two objective functions are considered: paths length and tree weight. These are given in Eqs. (A.6) and (A.7), respectively:

$$\min \quad \sum_{e\in E} \ell_e f_e \tag{A.6}$$

$$\min \quad \sum_{e\in E} \ell_e x_e \tag{A.7}$$

For this work, convex combinations of these objective functions are considered, that is:

$$\min \quad \beta \sum_{e\in E} \ell_e x_e + (1-\beta) \sum_{e\in E} \ell_e f_e \tag{A.8}$$

A.2 Degree Constraints

Eqs. (A.1)-(A.4) are standard MIP-constraints for a MinCostFlow Steiner tree formulation, (A.5) allows to weigh different paths in the resulting tree differently. However, further equations to enforce the operational constraints presented in Section VI.3 need to be added.

For operational Constraint 2, it is required that no more than two routes merge at any point, that is, the in- and out-degree of every vertex is restricted: the out-degree is at most 1 and the maximum in-degree is 2:

$$\sum_{k:(k,i)\in E} x_{ki} \leq 2 \quad \forall i \in V \setminus \{\mathcal{P} \cup r\} \tag{A.9}$$

$$\sum_{j:(i,j)\in E} x_{ij} \leq 1 \quad \forall i \in V \setminus \{\mathcal{P} \cup r\} \tag{A.10}$$

$$\sum_{k:(k,r)\in E} x_{kr} = 1 \tag{A.11}$$

$$\sum_{j:(i,j)\in E} x_{ij} = 1 \quad \forall i \in \mathcal{P} \tag{A.12}$$

Eq. (A.11) enforces one ingoing edge for the runway r, Eq. (A.12) guarantees that each entry point has one outgoing edge. For all other vertices, Eq. (A.9) yields the maximum indegree of 2 and Eq. (A.10) results in the maximum out-degree of 1.

A.3 Turn angle Constraints

The next operational constraint from Section VI.3 is Constraint 4: sharp turns must be avoided. Thus, it is enforced that if edge $e = (i, j)$ is used in the arrival tree, all outgoing edges at j must form an angle of at least θ with e.

Let Γ_e be the set of all outgoing edges from j that form an angle $\leq \theta$ with e, i.e., $\Gamma_e = \{(j, k) : \measuredangle ijk \leq \theta, (j, k) \in E\}$, and let $c_e = |\Gamma_e|$.

$$c_e x_e + \sum_{f \in \Gamma_e} x_f \leq c_e \quad \forall e \in E \tag{A.13}$$

By Eq. (A.13), either of these elements could be used: edge x_e—which sets the left-hand side to c_e, the upper bound provided by the right-hand side, and prohibits the use of any other edge in Γ_e—any subset of the edges in Γ_e. See Figure A-1 for an example.

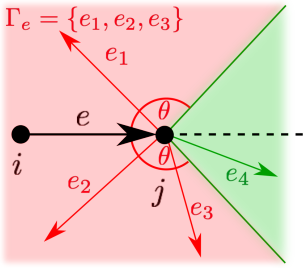

Figure A-1: *Limited turn: if edge $e = (i, j)$ is used, only edges within the green region are allowed, that is, edges with an angle of at least θ with e. If edges in the light red region, Γ_e, are used, x_e must be set to zero. Here: $\Gamma_e = \{e_1, e_2, e_3\}, e_4 \notin \Gamma_e$.*

A.4 Auxilliary Constraints to Prevent Crossings

When only the length of the arrival tree is minimized, but no constraint on temporal separation is integrated, no route crossings arise: uncrossing the routes would always shorten them by triangle inequality. However, the aim is to integrate temporal separation constraints, hence, possible route crossings should be taken into account.

While such route crossings at vertices are prevented by the degree constraints in Subsection A.2 (at least in-degree and out-degree of 2 each would be needed), routes crossing within a grid square may still be encountered, so auxiliary constraints are added to prevent this behavior.

Let V' be defined as the set of all grid nodes without those which belong to the last column and last row of the grid, that is, $V' = V \setminus \{\text{last row}\} \setminus \{\text{last column}\}$. Then, Eq. (A.14) is used to prevent crossings.

$$\begin{aligned} &x_{i,i+1+n} + x_{i+1+n,i} + x_{i+n,i+1} + x_{i+1,i+n} && \leq 1 \\ &\forall i \in V' \setminus \{\mathcal{P} \cup r\} : i+1+n, i+n, i+1 \notin \{\mathcal{P} \cup r\} \end{aligned} \tag{A.14}$$

Remember that entry points have no incoming edges. Hence, if one of the grid points in the considered grid square is an entry point, one of the four edges considered in Eq. (A.14) does not exist. Thus, Eqs. (A.15)-(A.18) are added. Figure A-2 illustrates the four cases depending on the location of the entry point.

$$x_{i,i+1+n} + x_{i+n,i+1} + x_{i+1,i+n} \leq 1 \; \forall i \in \mathcal{P} \tag{A.15}$$
$$x_{i,i+1+n} + x_{i+1+n,i} + x_{i+1,i+n} \leq 1 \; \forall i : i+1 \in \mathcal{P} \tag{A.16}$$
$$x_{i,i+1+n} + x_{i+n+1,i} + x_{i+n,i+1} \leq 1 \; \forall i : i+n \in \mathcal{P} \tag{A.17}$$
$$x_{i+1+n,i} + x_{i+n,i+1} + x_{i+1,i+n} \leq 1 \; \forall i : i+n+1 \in \mathcal{P} \tag{A.18}$$

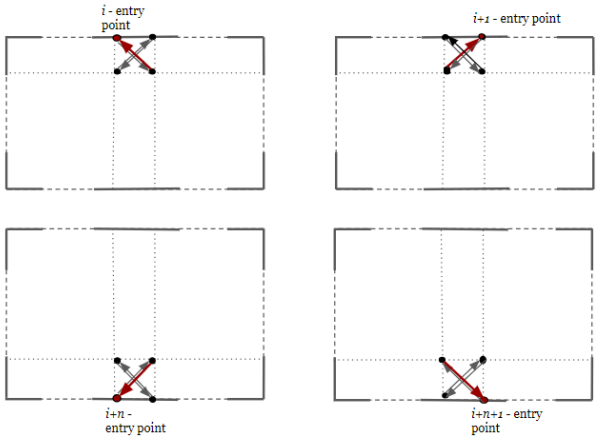

Figure A-2: *Four cases with entry point (marked in red) in a grid square: missing edges are shown in red. The figures in order refer to Eqs. (A.15), (A.16), (A.17) and (A.18), respectively.*

A.5 Integration of Temporal Separation

So far, the proposed MIP can compute an optimal (static) arrival tree (according to objective function (A.8)). This subsection, recapitulates the temporal separation described by Dahlberg *et al.* (2018). The assumption by the authors was that traversing any edge for any aircraft took a unit time of u. It was also assumed that the time of arrival at the entry point of the dynamic-trajectories area is fixed for all aircraft: aircraft a arrives at entry point $b \in \mathcal{P}$ at time t_a^b. New variables that keep track of where aircraft are located at what time are introduced: binary variables $y_{a,j,t}$ that indicate whether aircraft a occupies vertex j at time t.

Additionally, apart from the indicator x_e for an edge e participating in the routes, indicators $x_{e,b}$ for the edge e participating in the route from entry point b to the runway (for all entry points $b \in \mathcal{P}$) are introduced. The variables $x_{e,b}$ are set by using Eqs. (A.19)-(A.22):

$$x_{e,b} \leq x_e \; \forall b \in \mathcal{P}, \forall e \in E \tag{A.19}$$
$$\sum_{j:(b,j)\in E} x_{(b,j),b} = 1 \quad \forall b \in \mathcal{P} \tag{A.20}$$
$$\sum_{j:(j,r)\in E} x_{(j,r),b} = 1 \quad \forall b \in \mathcal{P} \tag{A.21}$$
$$\sum_{i:(i,j)\in E} x_{(i,j),b} - \sum_{k:(j,k)\in E} x_{(j,k),b} = 0 \quad \forall j \in V \setminus \{\mathcal{P} \cup r\}, \; \forall b \in \mathcal{P} \tag{A.22}$$

With this, the new variables $y_{a,j,t}$ can be set. Let $\mathcal{A}_b$ be the set of all aircraft arriving at entry point $b \in \mathcal{P}$, and $\mathcal{A} = \cup_{b\in\mathcal{P}} \mathcal{A}_b$. Moreover let $T = \{0, \ldots, \overline{T}\}$ be the considered time window.

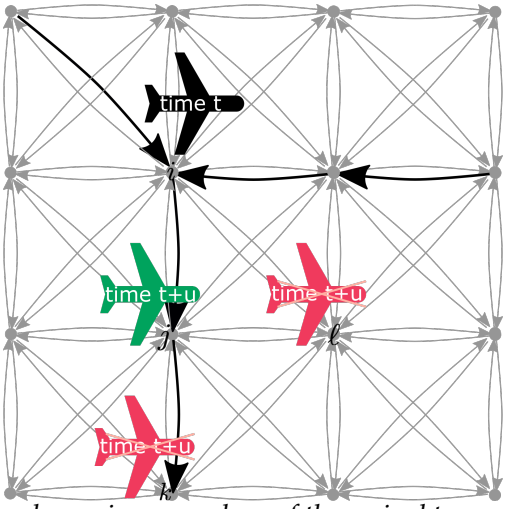

Figure A-3: *Grid edges are shown in gray, edges of the arrival tree are shown in black. From its location at i at time t, the black aircraft a can reach the green position at j at time $t+u$, the red positions cannot be reached: ℓ is not on any path, and for k there is $x_{j,k} = 1$, but a is not at j at time t.*

Aircraft a arrives at entry point b at time t_a^b, hence, with Eq. (A.23), $y_{a,b,t_a^b} = 1$ is set. Moreover, several of the y-variables can be set to zero: whenever it is known that an aircraft cannot occupy the vertex at all or not at certain points in time. It is ensured that an aircraft that does not arrive at entry point b will occupy b at no point in time with Eq. (A.24), and it is enforced that an aircraft a arriving at b occupies b only at t_a^b using Eq. (A.25). Finally, in Eq. (A.26), the y-variables and the $x_{e,b}$ are combined: any aircraft a can occupy a vertex j at any time t only if there exists an ingoing edge for j, that is, if j is located on a route. Thus, if j is a grid vertex but does not lie on any route, no aircraft a will occupy it at any time.

$$y_{a,b,t_a^b} = 1 \quad \forall b \in \mathcal{P}, \forall a \in \mathcal{A}_b \tag{A.23}$$

$$y_{a,b,t} = 0 \quad \forall b \in \mathcal{P}, \forall a \in \mathcal{A} \setminus \mathcal{A}_b, \forall t \in T \tag{A.24}$$

$$y_{a,b,t} = 0 \quad \forall b \in \mathcal{P}, \forall a \in \mathcal{A}_b, \forall t \in T \setminus \{t_a^b\} \tag{A.25}$$

$$y_{a,j,t} \leq \sum_{\substack{k \in V: \\ (k,j) \in E}} x_{(k,j)} \quad \forall b \in \mathcal{P}, \forall a \in \mathcal{A}, \forall j \in V \setminus \mathcal{P}, \forall t \in T \tag{A.26}$$

Then, the information on the times at which a arrives at nodes along the route from b to the runway is forwarded. Eqs. (A.23)-(A.25) only set the variable $y_{a,j,t}$ for entry points, it is still needed to set the variable for all the other vertices along the arrival tree (Eq. (A.26) only enforces that for vertices that are not located on the arrival tree the y-variable will be equal to zero at all times and for all aircraft).

An aircraft a can reach vertex k at time $t+u$ ($y_{a,k,t+u} = 1$) only by traversing an edge from another vertex j to vertex k (which takes u time units by assumption). Hence, a must have occupied some vertex j at time t ($y_{a,j,t} = 1$), such that the edge (j,k) exists in the path from b. If no such edge (j,k) exists, or if a did not occupy any such vertex at time t ($y_{a,j,t} = 0 \; \forall j$ for which edge (j,k) exists in the path from b), a cannot reach k at $t+u$, and $y_{a,k,t+u} = 0$ is set; see Figure A-3.

The forwarding of the temporal information on the aircraft along each arrival route can be formulated as:

$$\sum_{j:(j,k)\in E} x_{(j,k),b} \times y_{a,j,t} = y_{a,k,t+u}$$
$$\forall b \in \mathcal{P}, \forall a \in \mathcal{A}_b, \forall k \in V \setminus \mathcal{P}, \forall t \in \{0,\dots,\overline{T}-u\} \tag{A.27}$$

However, Eq. (A.27) is not a linear constraint (two binary variables are multiplied), which cannot be added to the MIP. Hence, a new binary variable $z_{a,j,k,b,t}$ is defined as the product of $x_{(j,k),b}$ and $y_{a,j,t}$ by using Eqs. (A.28)-(A.30):

$$z_{a,j,k,b,t} \leq x_{(j,k),b} \quad \forall a \in \mathcal{A}, \forall j,k \in V, \forall b \in \mathcal{P}, \forall t \in \{0,\dots,\overline{T}-u\} \tag{A.28}$$
$$z_{a,j,k,b,t} \leq y_{a,j,t} \quad \forall a \in \mathcal{A}, \forall j,k \in V, \forall b \in \mathcal{P}, \forall t \in \{0,\dots,\overline{T}-u\} \tag{A.29}$$
$$z_{a,j,k,b,t} \geq x_{(j,k),b} - (1 - y_{a,j,t}) \quad \forall a \in \mathcal{A}, \forall j,k \in V, \forall b \in \mathcal{P}, \forall t \in \{0,\dots,\overline{T}-u\} \tag{A.30}$$

Using the auxiliary variables $z_{a,j,k,b,t}$, Eq. (A.27) can be reformulated as a linear constraint:

$$\sum_{j:(j,k)\in E} z_{a,j,k,b,t} - y_{a,k,t+u} = 0$$
$$\forall b \in \mathcal{P}, \forall a \in \mathcal{A}_b, \forall k \in V \setminus \mathcal{P}, \forall t \in \{0,\dots,\overline{T}-u\} \tag{A.31}$$

Finally, it is ensured that temporal separation between any pair of aircraft along the routes is kept: a minimum temporal separation of σ time units between all aircraft at all vertices is required:

$$\sum_{\tau=t}^{t+\sigma-1} \sum_{a\in\mathcal{A}} y_{a,j,\tau} \leq 1 \quad \forall j \in V, \forall t \in \{0,\dots,\overline{T}-\sigma+1\} \tag{A.32}$$

A.6 Integration of Different Speed Profiles for Aircraft

In order to transfer the proposed approach to a real-world scenario different aircraft types are distinguished, considering their optimal continuous descent speed profile for different route lengths. Thus, the assumption that traversing any edge takes u time units for all aircraft is no longer a valid assumption.

For each aircraft a, a set of speed profiles is given, $\mathcal{S}(a)$, which contains speed profiles, p, of different lengths (that is, the speed profile is optimized for different route lengths). See Section VI.4.2 (Chapter VI) for the computation of these speed profiles. The speed profile determines the time to cover the first, second..., and subsequent segments of the route. So, for each aircraft a, $S(a)$ has speed profiles for routes of length (minimum number of edges in an entry-point-runway path)$\times L$ to (maximum number of edges in an edge-disjoint entry-point-runway path)$\times L$. Then, it is needed to be ensured that on an entry-point-runway path with X edges, a uses the speed profile p for a route of length $X \times L$. Here, is is assumed that the time to cover the n-th segment of the route is constant, that is, the time is independent of the grid-edge that actually constitutes that segment in the arrival tree. This assumption is valid due to the fact that no wind is considered in the case-studies analyzed in this work (Section VI.4.5).

So far, binary variables $y_{a,j,t}$ were used to indicate whether aircraft a occupies vertex j at time t. This is no longer enough to keep track of the aircraft's location: the evolution of the time to cover a segment depends on the number of segments covered in the route until the current vertex—a profile p has a time for covering the first edge, another for covering the second edge, etc. Thus, it is not necessary to know which profile p is used, but what is the edge number along the route (which will be deduced by counting how many vertices lie before the vertex along the route). Hence, $y_{a,j,t}$ is substituted by binary variables $y_{a,j,p,n,t}$ that indicate whether aircraft a using speed profile p occupies the n-th vertex (on a route from b) j at time t.

Let λ be an upper bound on the number of vertices in any path, $\mathcal{L} = \{1, \ldots, \lambda\}$. Eqs. (A.23)-(A.26) are substituted by (and the set of constraints that set variables to zero are extended):

$$\sum_{p \in \mathcal{S}(a)} y_{a,b,p,1,t_a^b} = 1 \quad \forall b \in \mathcal{P}, \forall a \in \mathcal{A}_b \tag{A.33}$$

$$y_{a,b,p,k,t_a^b} = 0 \quad \forall b \in \mathcal{P}, \forall a \in \mathcal{A}_b, \forall p \in \mathcal{S}(a), \forall k \neq 1 \in \mathcal{L} \tag{A.34}$$

$$y_{a,b,p,1,t} = 0 \quad \forall b \in \mathcal{P}, \forall a \in \mathcal{A}_b, \forall p \in \mathcal{S}(a), \forall t \in T \setminus \{t_a^b\} \tag{A.35}$$

$$y_{a,b',p,k,t} = 0 \quad \forall b' \neq b \in \mathcal{P}, \forall a \in \mathcal{A}_b, \forall p \in \mathcal{S}(a), \forall k \in \mathcal{L}, \forall t \in T \tag{A.36}$$

$$y_{a',b,p,1,t_a^b} = 0 \quad \forall b \in \mathcal{P}, \forall a' \neq a \in \mathcal{A}_b, \forall p \in \mathcal{S}(a) \tag{A.37}$$

$$y_{a,j,p,k,t} \leq \sum_{\substack{i \in V: \\ (i,j) \in E}} x_{(i,j)} \quad \forall j \in V \setminus \mathcal{P}, \forall a \in \mathcal{A}, \forall p \in \mathcal{S}(a), \forall k \in \mathcal{L}, \forall t \in T \tag{A.38}$$

$$y_{a,j,p,1,t} = 0 \quad j \in V \setminus \mathcal{P}, \forall a \in \mathcal{A}, \forall p \in \mathcal{S}(a), \forall t \in T \tag{A.39}$$

$$\sum_{p \in \mathcal{S}(a)} y_{a,j,p,k,t} \leq 1 \quad j \in V, \forall a \in \mathcal{A}, \forall k \in \mathcal{L}, \forall t \in T \tag{A.40}$$

Finally, it is needed to ensure that on an entry-point-runway path with X edges, a uses the speed profile p for a route of length $X \times L$. First, a variable $\ell(b)$ that gives the length of the path from entry point to runway in the arrival tree is introduced—where, instead of the physical length of the path, the number of grid edges is counted:

$$\ell(b) = \textstyle\sum_{(i,j) \in E} x_{(i,j),b} \quad \forall b \in \mathcal{P} \tag{A.41}$$

Then, the aim is that for each aircraft a arriving at entry point b, the speed profile of length $\ell(b)$ is picked from $\mathcal{S}(a)$. If $\ell(b)$ would be a parameter, it could simply be stated $y_{a,b,\ell(b),1,t_a^b} = 1$ and $y_{a,b,p,1,t_a^b} = 0 \; \forall p \neq \ell(b)$. However, $\ell(b)$ is a variable and it is not possible to use it as an index of another variable. Consequently, two auxiliary binary variables $\psi_{b,a,p}$ and $\phi_{b,a,p}$ are introduced to achieve the desired result. It is ensured that:

$$\psi_{b,a,p}=\begin{cases}0 & p=\ell(b)\\ 1 & p\neq\ell(b)\end{cases} \quad \forall b\in\mathcal{P},\forall a\in\mathcal{A}_b,\forall p\in\mathcal{S}(a) \tag{A.42}$$

Then the following is set:

$$y_{a,b,p,1,t_a^b}=1-\psi_{b,a,p} \quad \forall b\in\mathcal{P},\forall a\in\mathcal{A}_b,\forall p\in\mathcal{S}(a) \tag{A.43}$$

Together with Eq. (A.33) this ensures that for at least one profile (and exactly for the one of the correct length) the variable y is set to one.

Eq. (A.42) is enforced by adding Eqs. (A.44)-(A.47) to the MIP:

$$-\psi_{b,a,p}\leq(\ell(b)-p+\frac{1}{2})/\lambda+\lambda\cdot\phi_{b,a,p} \quad \forall b\in\mathcal{P},\forall a\in\mathcal{A}_b,\forall p\in\mathcal{S}(a) \tag{A.44}$$

$$\psi_{b,a,p}\leq-\ell(b)+p+\frac{1}{2}+\lambda\cdot\phi_{b,a,p} \quad \forall b\in\mathcal{P},\forall a\in\mathcal{A}_b,\forall p\in\mathcal{S}(a) \tag{A.45}$$

$$\psi_{b,a,p}\leq(\ell(b)-p)+\frac{1}{2}+\lambda(1-\phi_{b,a,p}) \quad \forall b\in\mathcal{P},\forall a\in\mathcal{A}_b,\forall p\in\mathcal{S}(a) \tag{A.46}$$

$$-\psi_{b,a,p}\leq(-\ell(b)+p+\frac{1}{2})/\lambda+\lambda(1-\phi_{b,a,p}) \quad \forall b'\neq b\in\mathcal{P},\forall a\in\mathcal{A}_b,\forall p\in\mathcal{S}(a) \tag{A.47}$$

Finally, a reformulation of the constraints used to forward the information about when an aircraft arrives at which vertex along the arrival route is needed: Eqs. (A.28)-(A.30) and (A.31). Instead of the binary variable $z_{a,j,k,b,t}$ being the product of $x_{(j,k),b}$ and $y_{a,j,t}$, two new indices are introduced and the binary variables $z_{a,j,i,b,p,k,t}$ are used: they represent the product of $x_{(j,i),b}$ and $y_{a,j,p,k,t}$. Let $u_{a,p,k}$ be the time that aircraft a using speed profile p needs to cover segment number k on its route from entry point to runway. Eqs. (A.28)-(A.30) are substituted by Eqs. (A.48)-(A.50).

$$z_{a,j,i,b,p,k,t-u_{a,p,k}}\leq x_{(j,i),b} \quad \forall b\in\mathcal{P},\forall a\in\mathcal{A}_b,\forall(j,i)\in E,\forall k\in\mathcal{L},\forall t\in\{u_{a,p,k}+1,\ldots,\overline{T}+1\} \tag{A.48}$$

$$z_{a,j,i,b,p,k,t-u_{a,p,k}}\leq y_{a,j,p,k,t-u_{a,p,k}} \quad \forall b\in\mathcal{P},\forall a\in\mathcal{A}_b,\forall(j,i)\in E,\forall k\in\mathcal{L},\forall t\in\{u_{a,p,k}+1,\ldots,\overline{T}+1\} \tag{A.49}$$

$$z_{a,j,i,b,p,k,t-u_{a,p,k}}\geq x_{(j,k),b}-(1-y_{a,j,p,k,t-u_{a,p,k}}) \quad \forall b\in\mathcal{P},\forall a\in\mathcal{A}_b,\forall(j,i)\in E,\forall k\in\mathcal{L},\forall t\in\{u_{a,p,k}+1,\ldots,\overline{T}+1\} \tag{A.50}$$

The new version of Eq. (A.31) is:

$$\sum_{j:(j,i)\in E} z_{a,j,i,b,k,t-u_{a,p,k}}-y_{a,i,p,k+1,t}=0 \quad \forall b\in\mathcal{P},\forall a\in\mathcal{A}_b,\forall p\in\mathcal{S}(a),\forall k\in\mathcal{L},\ \forall i\in V\setminus\mathcal{P},\forall t\in\{u_{a,p,k}+1,\ldots,\overline{T}\} \tag{A.51}$$

A uniform minimum temporal separation of σ time units between all pairs of consecutive aircraft at all vertices is still used. To enforce this separation, Eq. (A.52) is added:

$$\begin{aligned} \sum_{\tau=t}^{t+\sigma-1} \sum_{a\in\mathcal{A}} \sum_{p\in\mathcal{S}(a)} \sum_{k\in\mathcal{L}} y_{a,j,p,k,\tau} \quad &\leq 1 \\ \forall j \in V, \forall t \in \{0,\ldots,\overline{T}-\sigma+1\} \quad & \end{aligned} \tag{A.52}$$

A.7 Consistency between Trees of Different Time Periods

The arrival trees are optimized for the currently arriving aircraft. Certain traffic might require longer arrival paths than traffic at other times. Hence, the arrival tree should be recomputed frequently to adapt to the aircraft currently moving in the dynamic-trajectories area. However, trees for consecutive time periods should potentially not differ too much. Here, consistency in terms of number of different edges used for the routes in the trees is measured.

Let x_{ij} and x_{ij}^{old} denote the edge indicator variable for the current and previous period, respectively. A new variable, ax_{ij}, is defined, which determines $|x_{ij} - x_{ij}^{old}|$ in Eqs. (A.53)-(A.54), and then the number of differing edges in Eq. (A.55) is limited by parameter U:

$$ax_{ij} \leq x_{ij} - x_{ij}^{old} \quad \forall (j,i) \in E \tag{A.53}$$

$$ax_{ij} \leq x_{ij}^{old} - x_{ij} \quad \forall (j,i) \in E \tag{A.54}$$

$$\sum_{(i,j)\in E} ax_{ij} \leq U \tag{A.55}$$

A.8 Flexibility at the Entry Points of the dynamic-trajectories area

This Subsection and Subsection A.9 introduce the new constraints. First, flexibility at the entry points of the dynamic-trajectories area is allowed. When two aircraft arriving consecutively at the same entry point undercut the required temporal separation at the entry point, this yields infeasibility already at the entry point, and they cannot be scheduled. On the other hand, the aim is to schedule as many arriving aircraft with a CDO profile as possible. In order to ensure that, a deviation from the planned time at the entry points of the dynamic-trajectories area is allowed. That is, to schedule even such aircraft, instead of requiring that aircraft a arrives at its entry point b at the given time t_a^b (Eq. (A.33)), it is allowed for it to arrive in the time window $[t_a^{b,1}, t_a^{b,2}]$. Thus, it is needed to substitute Eqs. (A.33)-(A.35) and Eq. (A.42) by Eqs. (A.56), (A.57), (A.58) and (A.59), and add Eq. (A.60), which ensures that aircraft a cannot be at any node before $t_a^{b,1}$. Eq. (A.56) ensures that for each aircraft a and its entry point b, exactly one speed profile p is chosen and the aircraft arrives at exactly one time in $[t_a^{b,1}, t_a^{b,2}]$. Eqs. (A.57), (A.58) set several of the y-variables to zero, and Eq. (A.59) ensures that for the speed profile of the correct length (the length $\ell(b)$ of the arrival path from b) y is set to 1.

$$\sum_{t=t_a^{b,1}}^{t_a^{b,2}} \sum_{p\in\mathcal{S}(a)} y_{a,b,p,1,t} = 1 \qquad \forall b \in \mathcal{P}, \forall a \in \mathcal{A}_b \tag{A.56}$$

$$y_{a,b,p,k,t} = 0 \qquad \forall b \in \mathcal{P}, \forall a \in \mathcal{A}_b, \forall p \in \mathcal{S}(a), \forall t \leq t_a^{b,1}, \forall k \neq 1 \in \mathcal{L} \tag{A.57}$$

$$y_{a,b,p,1,t_a^b} = 0 \qquad \forall b \in \mathcal{P}, \forall a \in \mathcal{A}_b, \forall p \in \mathcal{S}(a), \forall t \in T : t_a^{b,1} < t < t_a^{b,2} \tag{A.58}$$

$$\sum_{t=t_a^{b,1}}^{t_a^{b,2}} y_{a,b,p,1,t} = 1 - \psi_{b,a,p} \qquad \forall b \in \mathcal{P}, \forall a \in \mathcal{A}_b, \forall p \in \mathcal{S}(a) \tag{A.59}$$

$$y_{a,j,p,k,t} = 0 \qquad \forall b \in \mathcal{P}, \forall a \in \mathcal{A}_b, \forall p \in \mathcal{S}(a), \forall t < t_a^{b,1}, \forall k \in \mathcal{L} \tag{A.60}$$

A.9 Separation with Different Wake Turbulence Categories

Finally, separation criteria based on the wake turbulence categories of the leading and trailing aircraft is included (that is, there is a deviation from a uniform σ).

The aircraft categorization proposed by the international civil aviation organization (ICAO) is used: LIGHT (L), MEDIUM (M), HEAVY (H) (SUPER can easily be included in the proposed concept as well). Then, the following definitions are included to the MIP: $C_1 = \{\text{H,M}\}$, and $C_2 = \{\text{L}\}$. Let $\sigma_{A,B}$ be the temporal separation if the leading aircraft is of category A and the trailing aircraft is of category B.

Each aircraft a is an element of either set A or B. Then, $\Omega = \max \sigma_{A,B}$. If the leading and trailing aircraft are of two different ($A \neq B$) or the same category, it is enforced a temporal separation of $\sigma_{A,B}$ and $\sigma_{A,A}$ using a constraint of type (A.61) (and a constraint of type (A.62) if $\sigma_{A,B} \geq 2$) for all categories A, B and a constraint of type (A.63) (and a constraint of type (A.64) if $\sigma_{A,A} \geq 2$) for all categories A, respectively.

$$\sum_{a \in B} \sum_{p \in \mathcal{S}(a)} \sum_{k \in \mathcal{L}} \sum_{\tau=t}^{t+\sigma_{A,B}-1} y_{a,j,p,k,\tau} \leq \Omega - \Omega \cdot \sum_{a' \in A} \sum_{\substack{p' \in \\ \mathcal{S}(a')}} \sum_{k' \in \mathcal{L}} y_{a',j,p',k',t}$$
$$\forall j \in V, \forall t \in \{0, \ldots, \overline{T} - \sigma_{A,B} + 1\} \tag{A.61}$$

$$\sum_{a \in B} \sum_{p \in \mathcal{S}(a)} \sum_{k \in \mathcal{L}} \sum_{\tau=t}^{\overline{T}} y_{a,j,p,k,\tau} \leq \Omega - \Omega \cdot \sum_{a' \in A} \sum_{\substack{p' \in \\ \mathcal{S}(a')}} \sum_{k' \in \mathcal{L}} y_{a',j,p',k',t}$$
$$\forall j \in V, \forall t \in \{\overline{T} - \sigma_{A,B} + 2, \ldots, \overline{T}\} \tag{A.62}$$

$$\sum_{a \neq a' \in A} \sum_{p \in \mathcal{S}(a)} \sum_{k \in \mathcal{L}} \sum_{\tau=t}^{t+\sigma_{A,A}-1} y_{a,j,p,k,\tau} \leq \Omega - \Omega \cdot y_{a',j,p',k',t}$$
$$\forall a' \in A, \forall p' \in \mathcal{S}(a'), \forall j \in V, \forall t \in \{0, \ldots, \overline{T} - \sigma_{A,A} + 1\} \tag{A.63}$$

$$\sum_{a \neq a' \in A} \sum_{p \in \mathcal{S}(a)} \sum_{k \in \mathcal{L}} \sum_{\tau=t}^{\overline{T}} y_{a,j,p,k,\tau} \leq \Omega - \Omega \cdot y_{a',j,p',k',t}$$
$$\forall a' \in A, \forall p' \in \mathcal{S}(a'), \forall j \in V, \forall t \in \{\overline{T} - \sigma_{A,A} + 2, \ldots, \overline{T}\} \tag{A.64}$$

A.10 The Complete MIP

To enhance readability, the complete MIP is presented in the following set of equations. The variable ranges in the equations are not stated and the constraints for consistency between trees for consecutive time periods are used.

$$\min \quad \beta \sum_{e\in E} \ell_e x_e + (1-\beta) \sum_{e\in E} \ell_e f_e \tag{12}$$

$$s.t. \sum_{k:(k,i)\in E} f_{ki} - \sum_{j:(i,j)\in E} f_{ij} = \begin{cases} \sum_{b\in\mathcal{P}} w_b & i = r \\ -w_i & i \in \mathcal{P} \\ 0 & i \in V \setminus \{\mathcal{P} \cup r\} \end{cases} \tag{9}$$

$$x_e \geq \frac{f_e}{Q} \qquad \forall e \in E \tag{9}$$

$$\sum_{k:(k,i)\in E} x_{ki} \leq 2 \qquad \forall i \in V \setminus \{\mathcal{P} \cup r\} \tag{13}$$

$$\sum_{j:(i,j)\in E} x_{ij} \leq 1 \qquad \forall i \in V \setminus \{\mathcal{P} \cup r\} \tag{14}$$

$$\sum_{k:(k,r)\in E} x_{kr} = 1; \tag{15}$$

$$\sum_{j:(i,j)\in E} x_{ij} = 1 \qquad \forall i \in \mathcal{P} \tag{16}$$

$$c_e x_e + \sum_{f\in\Gamma_e} x_f \leq c_e \qquad \forall e \in E \tag{17}$$

$$x_{i,i+1+n} + x_{i+1+n,i} + x_{i+n,i+1} + x_{i+1,i+n} \leq 1 \qquad \forall i \in V' \setminus \{\mathcal{P} \cup r\} : i+1+n, i+n, i+1 \notin \{\mathcal{P} \cup r\} \tag{18}$$

$$x_{i,i+1+n} + x_{i+n,i+1} + x_{i+1,i+n} \leq 1 \qquad \forall i \in \mathcal{P} \tag{19}$$

$$x_{i,i+1+n} + x_{i+1+n,i} + x_{i+1,i+n} \leq 1 \qquad \forall i : i+1 \in \mathcal{P} \tag{20}$$

$$x_{i,i+1+n} + x_{i+n+1,i} + x_{i+n,i+1} \leq 1 \qquad \forall i : i+n \in \mathcal{P} \tag{21}$$

$$x_{i+1+n,i} + x_{i+n,i+1} + x_{i+1,i+n} \leq 1 \qquad \forall i : i+n+1 \in \mathcal{P} \tag{22}$$

$$x_{e,b} \leq x_e \qquad \forall b \in \mathcal{P}, \forall e \in E \tag{23}$$

$$\sum_{j:(b,j)\in E} x_{(b,j),b} = 1 \qquad \forall b \in \mathcal{P} \tag{24}$$

$$\sum_{j:(j,r)\in E} x_{(j,r),b} = 1 \qquad \forall b \in \mathcal{P} \tag{25}$$

$$\sum_{i:(i,j)\in E} x_{(i,j),b} - \sum_{k:(j,k)\in E} x_{(j,k),b} = 0 \qquad \forall j \in V \setminus \{\mathcal{P} \cup r\}, \forall b \in \mathcal{P} \tag{26}$$

$$\sum_{t=t_a^{b,1}}^{t_a^{b,2}} \sum_{p\in\mathcal{S}(a)} y_{a,b,p,1,t} = 1 \qquad \forall b \in \mathcal{P}, \forall a \in \mathcal{A}_b \tag{60}$$

$$y_{a,b,p,k,t} = 0 \qquad \forall b \in \mathcal{P}, \forall a \in \mathcal{A}_b, \forall p \in \mathcal{S}(a), \forall t \leq t_a^{b,1}, \forall k \neq 1 \in \mathcal{L} \tag{61}$$

$$y_{a,b,p,1,t_a^b} = 0 \qquad \forall b \in \mathcal{P}, \forall a \in \mathcal{A}_b, \forall p \in \mathcal{S}(a), t \in T : t_a^{b,1} < t < t_a^{b,2} \tag{62}$$

$$y_{a,b',p,k,t} = 0 \qquad \forall b' \neq b \in \mathcal{P}, \forall a \in \mathcal{A}_b, \forall p \in \mathcal{S}(a), \forall k \in \mathcal{L}, \forall t \in T \tag{40}$$

$$y_{a',b,p,1,t_a^b} = 0 \qquad \forall b \in \mathcal{P}, \forall a' \neq a \in \mathcal{A}_b, \forall p \in \mathcal{S}(a) \tag{41}$$

$$y_{a,j,p,k,t} \leq \sum_{\substack{i \in V: \\ (i,j) \in E}} x_{(i,j)} \qquad \forall j \in V \setminus \mathcal{P}, \forall a \in \mathcal{A}, \forall p \in \mathcal{S}(a), \forall k \in \mathcal{L}, \forall t \in T \quad (42)$$

$$y_{a,j,p,1,t} = 0 \qquad j \in V \setminus \mathcal{P}, \forall a \in \mathcal{A}, \forall p \in \mathcal{S}(a), \forall t \in T \quad (43)$$

$$\sum_{p \in \mathcal{S}(a)} y_{a,j,p,k,t} \leq 1 \qquad j \in V, \forall a \in \mathcal{A}, \forall k \in \mathcal{L}, \forall t \in T \quad (44)$$

$$\ell(b) = \sum_{(i,j) \in E} x_{(i,j),b} \qquad \forall b \in \mathcal{P} \quad (45)$$

$$\sum_{t=t_a^{b,1}}^{t_a^{b,2}} y_{a,b,p,1,t} = 1 - \psi_{b,a,p} \qquad \forall b \in \mathcal{P}, \forall a \in \mathcal{A}_b, \forall p \in \mathcal{S}(a) \quad (63)$$

$$y_{a,j,p,k,t} = 0 \qquad \forall b \in \mathcal{P}, \forall a \in \mathcal{A}_b, \forall p \in \mathcal{S}(a), \forall t < t_a^{b,1}, \forall k \in \mathcal{L} \quad (64)$$

$$-\psi_{b,a,p} \leq (\ell(b) - p + \frac{1}{2})/\lambda + \lambda \cdot \phi_{b,a,p} \qquad \forall b \in \mathcal{P}, \forall a \in \mathcal{A}_b, \forall p \in \mathcal{S}(a) \quad (48)$$

$$\psi_{b,a,p} \leq -\ell(b) + p + \frac{1}{2} + \lambda \cdot \phi_{b,a,p} \qquad \forall b \in \mathcal{P}, \forall a \in \mathcal{A}_b, \forall p \in \mathcal{S}(a) \quad (49)$$

$$\psi_{b,a,p} \leq (\ell(b) - p) + \frac{1}{2} + \lambda(1 - \phi_{b,a,p}) \qquad \forall b \in \mathcal{P}, \forall a \in \mathcal{A}_b, \forall p \in \mathcal{S}(a) \quad (50)$$

$$-\psi_{b,a,p} \leq (-\ell(b) + p + \frac{1}{2})/\lambda + \lambda(1 - \phi_{b,a,p}) \qquad \forall b' \neq b \in \mathcal{P}, \forall a \in \mathcal{A}_b, \forall p \in \mathcal{S}(a) \quad (51)$$

$$\sum_{a \in B} \sum_{p \in \mathcal{S}(a)} \sum_{k \in \mathcal{L}} \sum_{\tau=t}^{t+\sigma_{AB}-1} y_{a,j,p,k,\tau} \leq \Omega - \Omega \cdot \sum_{a' \in A} \sum_{\substack{p' \in \\ \mathcal{S}(a')}} \sum_{k' \in \mathcal{L}} y_{a',j,p',k',t} \qquad \forall j \in V, \forall t \in \{0, \ldots, \overline{T} - \sigma_{A,B} + 1\} \quad (65)$$

$$\sum_{a \in B} \sum_{p \in \mathcal{S}(a)} \sum_{k \in \mathcal{L}} \sum_{\tau=t}^{\overline{T}} y_{a,j,p,k,\tau} \leq \Omega - \Omega \cdot \sum_{a' \in A} \sum_{\substack{p' \in \\ \mathcal{S}(a')}} \sum_{k' \in \mathcal{L}} y_{a',j,p',k',t} \qquad \forall j \in V, \forall t \in \{\overline{T} - \sigma_{A,B} + 2, \ldots, \overline{T}\} \quad (66)$$

$$\sum_{a \neq a' \in A} \sum_{p \in \mathcal{S}(a)} \sum_{k \in \mathcal{L}} \sum_{\tau=t}^{t+\sigma_{AA}-1} y_{a,j,p,k,\tau} \leq \Omega - \Omega \cdot y_{a',j,p',k',t} \qquad \forall a' \in A, \forall p' \in \mathcal{S}(a'), \forall j \in V, \forall t \in \{0, \ldots, \overline{T} - \sigma_{A,A} + 1\} \quad (67)$$

$$\sum_{a \neq a' \in A} \sum_{p \in \mathcal{S}(a)} \sum_{k \in \mathcal{L}} \sum_{\tau=t}^{\overline{T}} y_{a,j,p,k,\tau} \leq \Omega - \Omega \cdot y_{a',j,p',k',t} \qquad \forall a' \in A, \forall p' \in \mathcal{S}(a'), \forall j \in V, \forall t \in \{\overline{T} - \sigma_{A,A} + 2, \ldots, \overline{T}\} \quad (68)$$

$$z_{a,j,i,b,p,k,t-u_{a,p,k}} \leq x_{(j,i),b} \qquad \forall b \in \mathcal{P}, \forall a \in \mathcal{A}_b, \forall (j,i) \in E, \forall k \in \mathcal{L}, \forall t \in \{u_{a,p,k}+1, \ldots, \overline{T}+1\} \quad (52)$$

$$z_{a,j,i,b,p,k,t-u_{a,p,k}} \leq y_{a,j,p,k,t-u_{a,p,k}} \qquad \forall b \in \mathcal{P}, \forall a \in \mathcal{A}_b, \forall (j,i) \in E, \forall k \in \mathcal{L}, \forall t \in \{u_{a,p,k}+1, \ldots, \overline{T}+1\} \quad (53)$$

$$z_{a,j,i,b,p,k,t-u_{a,p,k}} \geq x_{(j,k),b} - (1 - y_{a,j,p,k,t-u_{a,p,k}}) \qquad \forall b \in \mathcal{P}, \forall a \in \mathcal{A}_b, \forall (j,i) \in E, \forall k \in \mathcal{L}, \forall t \in \{u_{a,p,k}+1, \ldots, \overline{T}+1\} \quad (54)$$

$$\sum_{j:(j,i) \in E} z_{a,j,i,b,k,t-u_{a,p,k}} - y_{a,i,p,k+1,t} = 0 \qquad \forall b \in \mathcal{P}, \forall a \in \mathcal{A}_b, \forall p \in \mathcal{S}(a), \forall k \in \mathcal{L}, \forall i \in V \setminus \mathcal{P}, \forall t \in \{u_{a,p,k}+1, \ldots, \overline{T}\} \quad (55)$$

Bibliography

ADACHER, L., PACCIARELLI, D., & PRANZO, M. 2003 (May). *A Graph-Theoretical Model for the Aircraft Sequencing Problem*. Tech. rept. Università degli Studi Roma Tre, Dipartimento di Informatica e Automazione, Report n. RT-DIA-79-2003. 93

AIRBUS. 1998 (May). *Getting to grips with the cost index*. Tech. rept. Flight Operations Support & Line Assistance, Blagnac, France. 18

AIRBUS. 2002 (Dec). *Getting to grips with aircraft performance monitoring*. Tech. rept. Flight Operations Support & Line Assistance, Blagnac, France. 4

ALLAN, S.S., BEESLEY, J.A., EVANS, J.E., & GADDY, S.G. 2001. Analysis of Delay Causality at Newark International Airport. *In: 4th USA/Europe Air Traffic Management Research & Development Seminar*. Santa Fe, NM: FAA/EUROCONTROL. 34

ANDERSSON, J. 2013 (Oct). *A General-Purpose Software Framework for Dynamic Optimization*. Phd thesis, KU Leuven-Faculty of Engineering Science. 27

ANDERSSON, J.A.E., GILLIS, J., HORN, G., RAWLINGS, J.B., & DIEHL, M. 2018. CasADi – A software framework for nonlinear optimization and optimal control. *Mathematical Programming Computation*, **11**, 1–36. 53

ANDERSSON, T., POLISHCHUK, T., POLISHCHUK, V., & SCHMIDT, C. 2016. Automatic Design of Aircraft Arrival Routes with Limited Turning Angle. *In: 16th Workshop on Algorithmic Approaches for Transportation Modelling, Optimization, and Systems (ATMOS)*. Arhus, Denmark: OASIcs. 123, 124

BAI, Y. 2006. *Analysis of aircraft arrival delay and airport on-time performance*. Master thesis, Tongji University, China. 34

BEASLEY, J.E., KRISHNAMOORTHY, M., SHARAIHA, Y.M., & ABRAMSON, D. 2000. Scheduling aircraft landings – The static case. *Transportation Science*, **34**, 180–197. 71

BEASLEY, J.E., KRISHNAMOORTHY, M., SHARAIHA, Y.M., & ABRAMSON, D. 2011. Improved Ant Colony Algorithm to Solve the Aircraft Landing Problem. *International Journal of Computer Theory and Engineering*, **3**(2), 224–233. 71

BEATTY, R., HSU, R., BERRY, L., & ROME, J. 1999. Preliminary evaluation of flight delay propagation through an airline schedule. *Air Traffic Control Quarterly*, **7**(4), 259–270. 34

BENAVIDES, J.V., KANSEHIGE, J., SHARMA, S., PANDA, R., & STEGLINSKI, M. 2014. Implementation of a Trajectory Prediction Function for Trajectory Based Operations. *In: AIAA Atmospheric Flight Mechanics Conference*. Atlanta, GA, USA: AIAA. 11

BENHEIKH, G., BOUKACHOUR, J., EL HILALI, A.A., & EL KHOUKHI, F. 2009. Hybrid method for aircraft landing scheduling based on a Job Shop formulation. *International Journal of Computer Science and Network Security*, **9**(8), 78–88. 71

BERTSIMAS, D., & PATTERSON, S.S. 1998. The Air Traffic Flow Management Problem with Enroute Capacities. *Operations Research*, **46**(3), 406–422. 80

BERTSIMAS, D.J., & VAN RYZIN, G. 1991. A Stochastic and Dynamic Vehicle Routing Problem in the Euclidean Plane. *Operations Research*, **39**(4), 601–615. 93

BETTS, J.T. 2010. *Practical Methods for Optimal Control and Estimation Using Nonlinear Programming*. 2nd edn. Society for Industrial and Applied Mathematics (SIAM). 21, 27, 32

BETTS, J.T., & CRAMER, E.J. 1995. Application of direct transcription to commercial aircraft trajectory optimization. *Journal of Guidance, Control, and Dynamics*, **18**(1), 151–159. 2

BILIMORIA, K., SRIDHAR, B., CHATTERJI, G., SHETH, K., & GRABBE, S. 2000. FACET: Future ATM Concepts Evaluation Tool. *In: 3rd USA/Europe Air Traffic Management Research & Development Seminar*. Napoli, Italy: FAA/EUROCONTROL. 18

BOURSIER, L., FAVENNEC, B., HOFFMAN, E., TRZMIEL, A., VERGNE, F., & ZEGHAL, K. 2007. Merging Arrival Flows Without Heading Instructions. *In: 7th USA/Europe Air Traffic Management Research & Development Seminar*. Barcelona, Spain: FAA/EUROCONTROL. 67

BRONSVOORT, J. 2014. *Contributions to Trajectory Prediction Theory and its Application to Arrival Management for Air Traffic Control*. PhD Thesis, Department of Señales, Sistemas y Radiocumunicaciones-Technical University of Madrid (UPM), Madrid, Spain. 10

BRONSVOORT, J., MCDONALD, G., TORRES, S., PAGLIONE, M., YOUNG, C., HOCHWARTH, J., BOUCQUEY, J., & VILAPLANA, M. 2016. Role of Extended Projected Profile Down-Link to Achieve Trajectory Synchronisation in support of Trajectory Based Operations. *In: 16th Aviation Technology, Integration, and Operations Conference (ATIO)*. Washington, D.C., USA: AIAA. 96

BRYSON, A.E., & HO, Y.-C. 1975. *Applied Optimal Control : Optimization, Estimation, and Control*. New York, NY, USA: Taylor and Francis Group. 25, 27, 31

BYRD, R.H., LU, P., NOCEDAL, J., & ZHU, C. 1995. A Limited Memory Algorithm for Bound Constrained Optimization. *SIAM Journal on Scientific Computing*, **16**(5), 1190–1208. 30

BYRD, R.H., GOULD, N.I.M., NOCEDAL, J., & WALTZ, R.A. 2003. An algorithm for nonlinear optimization using linear programming and equality constrained subproblems. *Mathematical Programming*, **100**, 27–48. 30

CALLANTINE, J.T., KUPFER, M., MARTIN, L., & PREVOT, T. 2013. Simulations of Continuous Descent Operations with Arrival-Management Automation and mixed Flight-Dec Interval Management Equipage. *In: 10th USA/Europe Air Traffic Management Research & Development Seminar*. Chicago, IL, USA: FAA/EUROCONTROL. 9

CAO, Y., JIN, L., NGUYEN, N.V.P., LANDRY, S., SUN, D., & POST, J. 2014. Evaluation of fuel benefits Depending on Continuous Descent Approach Procedures. *Air Traffic Control Quarterly*, **22**(3), 251–275. 6

CASADO, E., GOODCHILD, C., & VILAPLANA, M. 2013. Sensitivity of Trajectory Prediction Accuracy to Aircraft Performance Uncertainty. *In: AIAA Infotech@Aerospace (I@A) Conference*. Boston, MA: AIAA. 22

CASADO MAGAÑA, E. J. 2016. *Trajectory Prediction Uncertainty Modelling for Air Traffic Management*. Phd thesis, University of Glasgow, Glasgow, UK. 12

CHATTERJI, G., SRIDHAR, B., & BILIMORIA, K. 1996. En-Route Flight Trajectory Prediction for Conflict Avoidance and Traffic Management. *In: Guidance, Navigation, and Control Conference*. San Diego,CA, USA: AIAA. 22

CHATTERJI, G.B. 2011. Fuel Burn Estimation Using Real Track Data. *In: 11th AIAA Aviation Technology, Integration, and Operations (ATIO) Conference*. Virginia Beach, VA, USA: AIAA. 34

CHEVALIER, J. 2020. *Departure and arrival route optimisation approaching big airports*. PhD Thesis, Institut de Mathématiques de Toulouse, Université Paul Sabatier, Toulouse, France. 92, 106, 117

CHOI, S., ROBINSON, J. E., MULFINGER, D. G., & CAPOZZI, B. J. 2010. Design of an optimal route structure using heuristics-based stochastic schedulers. *In: IEEE/AIAA 29th Digital Avionics Systems Conference (DASC)*. Salt Lake City, UT: IEEE. 92

CHRISTIEN, R., HOFFMAN, E., & ZEGHAL, K. 2019. Spacing and Pressure to Characterise Arrival Sequencing. *In: 13th USA/Europe Air Traffic Management Research & Development Seminar*. Vienna, Austria: FAA/EUROCONTROL. 110

CLARKE, J.-P., BENNETT, D., ELMER, K., FIRTH, J., HILB, R., HO, N., JOHNSON, S., LAU, S., REN, L., SENECHAL, D., SIZOV, N., SLATTERY, R., TONG, K.-O, WALTON, J., WILLGRUBER, A., & WILLIAMS, D. 2006 (Jan). *Development, Design, and Flight Test Evaluation of a Continuous Descent Approach Procedure for Nighttime Operation at Louisville International Airport*. Tech. rept. FAA PARTNER CDA Development Team. Report No. PARTNER-COE-2006-02. 3

CLARKE, J.-P., BROOKS, J., NAGLE, G., SCACCHIOLI, A., WHITE, W., & LIU, S.R. 2013. Optimized Profile Descent Arrivals at Los Angeles International Airport. *Journal of Aircraft*, **50**(2), 360–369. 3

CLARKE, J.-P.B., HO, N.T., REN, L., BROWN, J.A., ELMER, K.R., ZOU, K.F., HUNTING, C., MCGREGOR, D.L., SHIVASHANKARA, B.N., TONG, K.-O., WARREN, A.W., & WAT, J.K. 2004. Continuous descent approach: Design and flight test for Louisville international airport. *Journal of aircraft*, **41**(5), 1054–1066. 2, 3, 37

CLARKE, J.-P.B., BROOKS, J., REN, L., NAGLE, G., MCCLAIN, E., BOYCE, G., ALLERDICE, J., CHAMBERS, T., & ZONDERVAN, D. 2007. Flight Trials of CDA with Time-Based Metering at Atlanta International Airport. *In: Airline Group of the International Federation of Operational Research Societies (AGIFORS) Airline Operations*. 3

COPPENBARGER, R., LANIER, R., SWEET, D., & DORSKY, S. 2004. Design and Development of the En Route Descent Advisor (EDA) for Conflict-Free Arrival Metering. *In: AIAA Guidance, Navigation, and Control Conference and Exhibit*. Providence, RI, USA: AIAA. 7

COPPENBARGER, R.A., MEAD, R.W., & SWEET, D.N. 2009. Field Evaluation of the Tailored Arrivals Concept for Datalink-Enabled Continuous Descent Approach. *Journal of Aircraft*, **46**(4), 1200–1209. 7

COPPENBARGER, R.A., DYER, G., HAYASHI, M., LANIER, R.C., STELL, L.L., & SWEET, D. 2010. Development and Testing of Automation for Efficient Arrivals in Constrained Airspace. *In: 27th International Congress of the Aeronautical Sciences (ICAS)*. Nice, France: ICAS. ix, 7, 8

CORREIA, P.D. 2017. *Analysis of Vertical Flight Efficiency During Climb and Descent*. Master thesis, Técnico Lisboa. 34

DAHLBERG, J., GRANBERG, T. A., POLISHCHUK, T., SCHMIDT, C., & SEDOV, L. 2018. Capacity-Driven Automatic Design of Dynamic Aircraft Arrival Routes. *In: IEEE/AIAA 37th Digital Avionics Systems Conference (DASC)*. London, UK: IEEE. 13, 100, 123, 127

DALMAU, R. 2019. *Optimal trajectory management for aircraft descent operations subject to time constraints*. PhD Thesis, Department of Physics-Aerospace Division, Technical University of Catalonia (UPC), Castelldefels, Spain. ix, 5, 13, 18, 23

DALMAU, R., & PRATS, X. 2015. Fuel and time savings by flying continuous cruise climbs: Estimating the benefit pools for maximum range operations. *Transportation Research Part D: Transport and Environment*, **35**, 62–71. 2, 21, 58

DALMAU, R., & PRATS, X. 2016. Assessment of the feasible CTA windows for efficient spacing with energy-neutral CDO. *In: 7th International Conference on Research in Air Transportation (ICRAT)*. Philadelphia, PA: IEEE. 93

DALMAU, R., & PRATS, X. 2017a. Assessing the impact of relaxing cruise operations with a reduction of the minimum rate of climb and/or step climb heights. *Aerospace Science and Technology*, **70**(Nov), 461–470. 2

DALMAU, R., & PRATS, X. 2017b. Controlled time of arrival windows for already initiated energy-neutral continuous descent operations. *Transportation Research Part C: Emerging Technologies*, **85**(Dec), 334–347. 45, 49, 61, 69, 97

DALMAU, R., VERHOEVEN, R., DE GELDER, N., & PRATS, X. 2016. Performance comparison between TEMO and a typical FMS in presence of CTA and wind uncertainties. *In: IEEE/AIAA 35th Digital Avionics Systems Conference (DASC)*. Sacramento, CA, USA: IEEE. 80

DALMAU, R., ALENKA, J., & PRATS, X. 2017. Combining the assignment of pre-defined routes and RTAs to sequence and merge arrival traffic. *In: 17th AIAA Aviation Technology, Integration, and Operations Conference (ATIO)*. Denver, CO, USA: AIAA. 46, 67

DALMAU, R., PRATS, X., VERHOEVEN, R., BUSSINK, F., & HEESBEEN, B. 2019a. Comparison of Various Guidance Strategies to Achieve Time Constraints in Optimal Descents. *Journal of Guidance, Control, and Dynamics*, **42**(7), 1612–1621. 14, 80

DALMAU, R., PRATS, X., & BAXLEY, B. 2019b. Using wind observations from nearby aircraft to update the optimal descent trajectory in real-time. *In: 13th USA/Europe Air Traffic Management Research & Development Seminar*. Vienna (Austria): FAA/EUROCONTROL. 50

DE BOOR, C. 1972. On calculating with B-splines. *Journal of Approximation Theory*, **6**(1), 50–62. 21, 32, 38

DE JONG, P.M.A., DE GELDER, N., VERHOEVEN, R., BUSSINK, F.J.L., KOHRS, R., VAN PAASSEN, M.M., & MULDER, M. 2014. Time and Energy Management During Descent and Approach: Batch Simulation Study. *Journal of Aircraft*, **52**(1), 190–203. 38

DE LEEGE, A.M.P., IN'T VELD, A..C, MULDER, M., & VAN PAASSEN, M.M. 2009. Three-Degree Decelerating Approaches in High-Density Arrival Streams. *Journal of Aircraft*, **46**(5), 1681–1691. 6

DE PRINS, J., GÓMEZ, R., & MULDER, M. 2011. Towards Time-based Continuous Descent Operations with Mixed 4D FMS Equipage. *In: 11th AIAA Aviation Technology, Integration, and Operations (ATIO) Conference*. Virginia Beach, VA, USA: AIAA. 46

DE PRINS, J.L., SCHIPPERS, F.K.M., MULDER, M., VAN PAASSEN, M.M., IN'T VELD, A.C., & CLARKE, J.-P. 2007. Enhanced Self-Spacing Algorithm for Three-Degree Decelerating Approaches. *Journal of Guidance, Control, and Dynamics*, **30**(2), 576–590. 6, 9

DELGADO, L., & PRATS, X. 2012. En Route Speed Reduction Concept for Absorbing Air Traffic Flow Management Delays. *Journal of Aircraft*, **49**(1), 214–224. 80, 96

DELGADO, L., & PRATS, X. 2013. Effect of Wind on Operating-Cost-Based Cruise Speed Reduction for Delay Absorption. *IEEE Transactions on Intelligent Transportation Systems*, **14**(2), 918–927. 80, 96

ECMWF. 2021. *ERA5: data documentation*. https://confluence.ecmwf.int/display/CKB/ERA5%3A+data+documentation. Accessed: November 15, 2020. 23

ELMER, K.R. 2008. Tailored arrivals operations at SFO and expected environmental benefits. *In: 26th International Congress of the Aeronautical Sciences (ICAS) and 8th AIAA Aviation Technology, Integration, and Operations Conference (ATIO)*. Anchorage, AK, USA: AIAA. 7

ERKELENS, L. 2000. Research into new noise abatement procedures for the 21st century. *In: AIAA Guidance, Navigation, and Control Conference and Exhibit*. Denver, CO, USA: AIAA. 2

EUROCONTROL. 2017 (Sep). *DDR2 Reference Manual for General Users 2.9.4*. 35, 77, 103

EUROCONTROL. 2018a. *European AIS Database (EAD) Basic*. https://www.ead.eurocontrol.int/cms-eadbasic/opencms/en/login/ead-basic/. Accessed: March 2, 2018. x, 74

EUROCONTROL. 2018b. *Point Merge*. https://www.eurocontrol.int/concept/point-merge. Accessed: March 15, 2018. x, 67

EUROPEAN COMISSION. 2020. *Optimised Procedures and Techniques for Improvement of Approach and Landing (OPTIMAL)*. https://trimis.ec.europa.eu/project/optimised-procedures-and-techniques-improvement-approach-and-landing. Accessed: March 15, 2020. 3

FEDERAL AVIATION ADMINISTRATION. 2021a. *ADS-B: Interval Management (IM) Applications*. https://www.faa.gov/nextgen/programs/adsb/pilot/ima/. Accessed: April 22, 2019. 9

FEDERAL AVIATION ADMINISTRATION. 2021b. *Trajectory Based Operations (TBO)*. https://www.faa.gov/air_traffic/technology/tbo/. Accessed: February 15, 2021. 10

FLACHE, C. 2018. *The R-WAKE Project*. http://www.rwake-sesar2020.eu/. Accessed: November 20, 2020. 103

FORESTER, D.A, & DHARSSI, I. 1992. *The improvement of meteorological data for air traffic management purposes - stage 1*. Tech. rept. United Kingdom Meteorological Office, Bracknell, UK. 22

FRICKE, H., SEIβ, C., & HERRMANN, R. 2015. Fuel and Energy Benchmark Analysis of Continuous Descent Operations. *Air Traffic Control Quarterly*, **23**(1), 83–108. 7, 34, 80

GARRIDO-LÓPEZ, D., D'ALTO, L., & LEDESMA, R.G. 2009. A novel four-dimensional guidance for continuous descent approaches. *In: AIAA/IEEE 28th Digital Avionics Systems Conference (DASC)*. Orlando, FL, USA: IEEE. 96

GILL, P.E., MURRAY, W., & SAUNDERS, M.A. 2005. SNOPT: An SQP algorithm for large-scale constrained optimization. *Society for Industrial and Applied Mathematics (SIAM) Review*, **47**(1), 99–131. 30, 53

GOEMANS, M.X., & MYUNG, Y.-S. 1993. A catalog of steiner tree formulations. *Networks*, **23**(1), 19–28. 124

GWIGGNER, C., FUJITA, M., FUKUDA, Y., NAGAOKA, S., & NIKOLERIS, T. 2011. Trade-offs and Issues in Traffic Synchronization. *In: 9th USA/Europe Air Traffic Management Research & Development Seminar*. Berlin, Germany: FAA/EUROCONTROL. 12

HARDELL, H., POLISHCHUK, T., & SMETANOVÁ, L. 2020a. Fine-Grained Evaluation of Arrival Operations. *In: 10th SESAR Innovation Days (SIDs)*. Virtual: SESAR Joint Undertaking. 113

HARDELL, H., LEMETTI, A., POLISHCHUK, T., POLISHCHUK, V., VISHWANATH, B., & ROYO, E. 2020b. Morphing STARs vs drones and weather in TMA. *In: 9th International Conference for Research in Air Transportation (ICRAT)*. Virtual: FAA/EUROCONTROL. 103

HELLMANN, G. 1916. Über die Bewegung der Luft in den untersten Schichten der Atmosphäre. *Meteorol Z*, **34**, 273–285. 24

HELMKE, H., HANN, R., UEBBING-RUMKE, M., MÜLLER, D., & WITTKOWSKI, D. 2009. Time-Based Arrival Management for Dual Threshold Operation and Continuous Descent Approaches. *In: 8th USA/Europe Air Traffic Management Research & Development Seminar*. Napa, CA, USA: FAA/EUROCONTROL. 46

HO-HUU, V., HARTJES, S., PÉREZ-CASTÁN, J.A., VISSER, H.G., & CURRAN, R. 2020. A multilevel optimization approach to route design and flight allocation taking aircraft sequence and separation constraints into account. *Transportation Research Part C: Emerging Technologies*, **117**(Aug). 15, 93, 109

HULL, D.G. 2007. *Fundamentals of Airplane Flight Mechanics*. 1st edn. Springer-Verlag Berlin Heidelberg. 19

IACUS, S.M., NATALE, F., SANTAMARIA, C., SPYRATOS, S., & VESPE, M. 2020. Estimating and projecting air passenger traffic during the COVID-19 coronavirus outbreak and its socio-economic impact. *Safety Science*, **129**. 1

ICAO. 1993. *Manual of the ICAO Standard Atmosphere: Extended to 80 Kilometres (262500 Feet)-Doc 7488-CD*. Tech. rept. International Civil Aviation Organization (ICAO), Montréal, Québec, Canada. 22

ICAO. 2010. *Continuous Descent Operations (CDO) Manual-Doc 9931/AN/476*. Tech. rept. International Civil Aviation Organization (ICAO), Montréal, Québec, Canada. 7

ICAO. 2016. *Procedures for Air Navigation Services - Air Traffic Management - Doc 4444*. Montréal, Québec, Canada. 78, 103

ICAO. 2020. *KPI Overview*. https://www4.icao.int/ganpportal/ASBU/KPI. Accessed: August 29, 2019. 35

ITOH, E., & UEJIMA, K. 2013. Applying Flight-deck Interval Management based Continuous Descent Operation for Arrival Air Traffic to Tokyo International Airport. *In: 10th USA/Europe Air Traffic Management Research & Development Seminar*. Chicago, IL, USA: FAA/EUROCONTROL. 9

ITOH, E., BROWN, M., SENOGUCHI, A., WICKRAMASINGHE, N., & FUKUSHIMA, S. 2017. Future Arrival Management Collaborating with Trajectory-Based Operations. *Pages 137–156 of: Air Traffic Management Systems II*. Springer Japan. 89

ITOH, E., FUKUSHIMA, S., HIRABAYASHI, H., WICKRAMASINGHE, N.K., & TORATANI, D. 2018a. Evaluating Energy-Saving Arrivals of Wide-Body Passenger Aircraft via Flight-Simulator Experiments. *Journal of Aircraft*, **55**(6), 2427–2443. 7

ITOH, E., WICKRAMASINGHE, N.K., HIRABAYASHI, H., & FUKUSHIMA, S. 2018b. Feasibility study on fixed flight-path angle descent for wide-body passenger aircraft. *CEAS Aeronautical Journal*, **10**(2), 582–612. 7

IVANESCU, D., SHAW, C., TAMVACLIS, C., & KETTUNEN, T. 2009. Models of Air Traffic Merging Techniques: Evaluating Performance of Point Merge. *In: 9th AIAA Aviation Technology, Integration, and Operations (ATIO) Conference*. Hilton Head, SC, USA: AIAA. 67

IVANOV, N., PAVLOVIC, G., STRAUSS, A., STARITA, S., & FICHERT, F. 2017. *Coordinated Capacity Ordering and Trajectory Pricing for Better Performing ATM (COCTA) - Deliverable 2.2: Data Management Report*. Tech. rept. 35

JIN, L., CAO, Y., & SUN, D. 2013. Investigation of Potential Fuel Savings Due to Continuous-Descent Approach. *Journal of Aircraft*, **50**(3), 807–816. 4

JOHNSON, C., FERRANTE, J., & SHEPLEY, J. 2009. Human-In-The-Loop (HITL) Simulation and Analysis of Optimized Profile Descent (OPD) Operations at Atlanta. *In: 9th AIAA Aviation Technology, Integration, and Operations (ATIO) Conference*. Hilton Head, SC, USA: AIAA. 6

KALTSCHMITT, M., STREICHER, W., & WIESE, A. 2007. *Renewable Energy: Technology, Economics and Environment*. Springer-Verlag Berlin Heidelberg. 51

KHAN, Z., IDRIS, H., VIVONA, R., WOODS, S., & LANIER, R. 2009. Ground Automation Impact on Enabling Continuous Descent in High Density Operations. *In: 9th AIAA Aviation Technology, Integration, and Operations (ATIO) Conference*. Hilton Head, SC, USA: AIAA. 6

KROZEL, J., LEE, C., & MITCHELL, J.S.B. 2006. Turn-Constrained Route Planning for Avoiding Hazardous Weather. *Air Traffic Control Quarterly*, **14**(2). 92

KROZEL, J., PENNY, S., PRETE, J., & MITCHELL, J.S.B. 2007. Automated Route Generation for Avoiding Deterministic Weather in Transition Airspace. *Journal of Guidance, Control and Dynamics*, **30**(1), 144–153. 13

KUHN, H.W., & TUCKER, A.W. 1951. Nonlinear Programming. *In: 2nd Berkeley Symposium on Mathematical Statistics and Probability*. Berkeley, CA, USA: University of California Press. 30

LE NY, J., & PAPPAS, G.J. 2011. Joint Metering and Conflict Resolution in Air Traffic Control. *Journal of Guidance, Control and Dynamics*, **34**(5), 1507–1518. 93

LEMETTI, A., POLISHCHUK, T., SÁEZ, R., & PRATS, X. 2019a. Analysis of Weather Impact on Flight Efficiency for Stockholm Arlanda Airport Arrivals. *In: 6th ENRI International Workshop on ATM/CNS (EIWAC)*. Tokyo, Japan: ENRI. 43, 44

LEMETTI, A., POLISHCHUK, T., SÁEZ, R., & PRATS, X. 2019b. Evaluation of Flight Efficiency for Stockholm Arlanda Airport Arrivals. *In: IEEE/AIAA 38th Digital Avionics Systems Conference (DASC)*. San Diego, CA, USA: IEEE. 44

LIDEN, S. 1994. The Evolution of Flight Management Systems. *In: 13th AIAA/IEEE Digital Avionics Systems Conference (DASC)*. Phoenix, AZ, USA: IEEE. 17

LIN, C., & MORÉ, J. 1999. Newton's Method for Large Bound-Constrained Optimization Problems. *SIAM Journal on Optimization*, **9**(4), 1100–1127. 30

LOPEZ-LEONES, J., VILAPLANA, M.A., GALLO, E., NAVARRO, F.A., & QEREJETA, C. 2007. The Aircraft Intent Description Language: A key enabler for air-ground synchronization in Trajectory-Based Operations. *In: IEEE/AIAA 26th Digital Avionics Systems Conference (DASC)*. Dallas, TX, USA: IEEE. 11

MASSACHUSETTS INSTITUTE OF TECHNOLOGY. 2020. *Partnerhsip for Air Transportation Noise and Emission Reduction (PARTNER)*. http://partner.mit.edu/. Accessed: March 15, 2020. 3

MICHELIN, A., IDAN, M, & SPEYER, J.L. 2011. Merging of Air Traffic Flows. *Journal of Guidance, Control and Dynamics*, **34**(1), 13–28. 93

MONDOLONI, S., & ROZEN, N. 2020. Aircraft trajectory prediction and synchronization for air traffic management applications. *Progress in Aerospace Sciences*, **119**(Nov). 12

MOUILLET, V., NUIĆ, A., CASADO, E., & LÓPEZ-LEONÉS, J. 2018. Evaluation of the Applicability of a Modern Aircraft Performance Model to Trajectory Optimization. *In: 37th IEEE/AIAA Digital Avionics Systems Conference (DASC)*. London, UK: IEEE. 14, 21

MUYNCH, R.J., BOS, T., KUENZ, A., & TONER, S. 2012. Implementing time based CDA operations in medium-high density ATM environment. *In: 28th International Congress of the Aeronautical Sciences (ICAS)*. Brisbane, Australia: ICAS. 8, 10

NAGLE, G., SWEET, D., CARR, G., FELIPE, V., TRAPANI, A., COPPENBARGER, R., & HAYASHI, M. 2011. Human-in-the-Loop Simulation of Three-Dimensional Path Arrival Management with Trajectory Error. *In: 11th AIAA Aviation Technology, Integration, and Operations (ATIO) Conference*. Virginia Beach, VA, USA: AIAA. 7

NASA. 2021. *Technology Readiness Levels (TRLs)*. https://esto.nasa.gov/trl/. Accessed: Januray 25, 2021. 14

NATIONAL SUPERCOMPUTER CENTRE. 2019. *Tetralith*. https://www.nsc.liu.se/systems/tetralith/. Linköping University, Accessed: January 28, 2019. 105

NELSON, R.C. 1997. *Flight Stability and Automatic Control*. McGraw-Hill Education. 18

NIKOLERIS, T., CHATTERJI, G.B., & COPPENBARGER, R.A. 2016. Comparison of Fuel Consumption of Descent Trajectories Under Arrival Metering. *Journal of Aircraft*, **53**(6), 1853–1864. 46

NOAA. 2021. *Global Forecast System*. https://www.ncei.noaa.gov/products/weather-climate-models/global-forecast#. Accessed: February 15, 2018. 23

OBERHEID, H., TEMME, M.-M., KUENZ, A., MOLLWITZ, V., & HELMKE, H. 2008. Fuel Efficient and Noise-Reduced Approach Procedures. *In: German Aerospace Congress*. Darmstadt, Germany: German Aerospace Center (DLR). 9

OLIVE, X., GRIGNARD, J., DUBOT, T., & SAINT-LOT, J. 2018. Detecting Controllers' Actions in Past Mode S Data by Autoencoder-Based Anomaly Detection. *In: 8th SESAR Innovation Days (SIDs)*. Salzburg, Austria: SESAR Joint Undertaking. 34, 35

OUELHADJ, D., & PETROVIC, S. 2008. A survey of dynamic scheduling in manufacturing systems. *Journal of Scheduling*, **12**(417). 93

PARK, S.G., CLARKE, J.-P.B., FERON, E., & JIMENEZ, H. 2016. Encounter Rate Estimation of Continuous Descent Arrival Procedures in Terminal Area. *In: AIAA Guidance, Navigation, and Control Conference*. San Diego, CA, USA: AIAA. 6

PARK, S.G., DUTTA, P., & MENON, P.K. 2017. Optimal Trajectory Option Sets for In-Flight Climb-Descend Trajectory Negotiations. *In: 17th AIAA Aviation Technology, Integration, and Operations (ATIO) Conference*. Denver, CO, USA: AIAA. 25, 26

PAWELEK, A., LICHOTA, P., DALMAU, R., & PRATS, X. 2019. Fuel-Efficient Trajectories Traffic Synchronization. *Journal of Aircraft*, **56**(2), 481–492. 9, 46

PEETERS, S., & GUASTALLA, G. 2017 (Jan). *Analysis of vertical flight efficiency during climb and descent*. Tech. rept. Eurocontrol. Edition 00-04. 34, 36

PERFORMANCE REVIEW COMISSION. 2017. *Performance Review Report: An Assessment of Air Traffic Management in Europe during the Calendar Year 2017*. Tech. rept. Eurocontrol. 42

PERFORMANCE REVIEW COMISSION. 2018. *Performance Review Report: An Assessment of Air Traffic Management in Europe during the Calendar Year 2018*. Tech. rept. Eurocontrol. 34, 42

POLES, D., NUIC, A., & MOUILLET, V. 2010. Advanced aircraft performance modelling for ATM: Analysis of BADA model capabilities. *In: AIAA/IEEE 29th Digital Avionics Systems Conference (DASC)*. Salt Lake City, UT, USA: IEEE. 21

PRADEEP, P., & WEI, P. 2017. Predictability, variability and operational feasibility aspect of CDA. *In: 2017 IEEE Aerospace Conference*. Big Sky, MT, USA: IEEE. 6

PRATS, X. 2010 (Jan). *Contributions to the optimisation of aircraft noise abatement procedures*. PhD Thesis, Department of Physics-Aerospace Division, Technical University of Catalonia (UPC), Castelldefels, Spain. 27, 93

PRATS, X., VILARDAGA, S., ISANTA, R., BAS, I., & BIRLING, F. 2015. WEMSgen: A real-time weather modelling library for on-board trajectory optimisation and planning. *In: 34th IEEE/AIAA Digital Avionics Systems Conference (DASC)*. Prague, Czech Republic: IEEE. 32

PRATS, X., DALMAU, R., VERHOEVEN, R., & BUSSINK, F. 2017. Human-in-the-loop Performance Assessment of Optimized Descents with Time Constraints: Results from Full Motion Flight Simulation and a Flight Testing Campaign. *In: 12th USA/Europe Air Traffic Management Research & Development Seminar*. Seattle, WA, USA: FAA/EUROCONTROL. 80

PRATS, X., ARGÜI, I., NETJASOV, F., PAVLOVIC, G., & VIDOSAVLJEVIC, A. 2018a (Jul). *APACHE-Final project results report*. Tech. rept. 34

PRATS, X., BARRADO, C., NETJASOV, F., CRNOGORAC, D., PAVLOVIC, G., ARGÜI, I., & VIDOSAVLJEVIC, A. 2018b. Enhanced Indicators to Monitor ATM Performance in Europe. *In: 8th SESAR Innovation Days (SIDs)*. Salzburg, Austria: SESAR Joint Undertaking. 34

PRATS, X., DALMAU, R., & BARRADO, C. 2019. Identifying the Sources of Flight Inefficiency from Historical Aircraft Trajectories. *In: 13th USA/Europe Air Traffic Management Research & Development Seminar*. Vienna, Austria: FAA/EUROCONTROL. 34, 36

PRETE, J., KROZEL, J., MITCHELL, J., KIM, J., & ZOU, J. 2008. Flexible, Performance-Based Route Planning for Super-Dense Operations. *In: AIAA Guidance, Navigation and Control Conference and Exhibit*. Honolulu, HI, USA: AIAA. 100

REN, L., & CLARKE, J.-P.B. 2007. Separation Analysis Methodology for Designing Area Navigation Arrival Procedures. *Journal of Guidance Control and Dynamics*, **30**(5), 1319–1330. 5

REN, L., & CLARKE, J.-P.B. 2008. Flight-Test Evaluation of the Tool for Analysis of Separation and Throughput. *Journal of Guidance Control and Dynamics*, **45**(1), 323–332. 5

REYNOLDS, T., REN, L., CLARKE, J.-P., BURKE, A., & GREEN, M. 2005. History, Development and Analysis of Noise Abatement Arrival Procedures for UK Airports. *In: AIAA 5th Aviation Technology, Integration and Operations Conference (ATIO) and 16th Lighter-Than-Air Sys Tech. and Balloon Systems Conferences*. Arlington, VA, USA: AIAA. 3

RIEDEL, T., TAKAHASHI, M., ITOH, E., FROST, P., & FEUERLE, T. 2020. Pilot-Centered Evaluation of Flight-Deck Interval Management Control Laws Using an A320 Simulator. *Journal of Aircraft*, **57**(5), 974–984. 9

ROBERT, E., & DE SMEDT, D. 2013. Comparison of operational wind forecasts with recorded flight data. *In: 10th USA/Europe Air Traffic Management Research & Development Seminar*. Chicago, IL, USA: FAA/EUROCONTROL. 22

ROBINSON, J., & KAMGARPOUR, M. 2010. Benefits of Continuous Descent Operations in High-Density Terminal Airspace Under Scheduling Constraints. *In: 10th AIAA Aviation Technology, Integration, and Operations (ATIO) Conference*. Fort Worth, TX, USA: AIAA. 3, 4, 6

RYERSON, M.S., HANSEN, M., & BONN, J. 2014. Time to burn: Flight delay, terminal efficiency, and fuel consumption in the National Airspace System. *Transportation Research Part A: Policy and Practice*, **69**, 286–298. 34

SADOVSKY, A., & WINDHORST, R. 2019. A Scheduling Algorithm Compatible with a Distributed Management of Arrivals in the National Airspace System. *In: IEEE/AIAA 38th Digital Avionics Systems Conference (DASC)*. San Diego, CA, USA: IEEE. 67

SÁEZ, R., PRATS, X., POLISHCHUK, T., POLISHCHUK, V., & SCHMIDT, C. 2020a. Automation for Separation with CDOs: Dynamic Aircraft Arrival Routes. *Journal of Air Transportation*, **28**(4), 144–154. 95, 123

SÁEZ, R., PRATS, X., POLISHCHUK, T., & POLISHCHUK, V. 2020b. Traffic Synchronization in Terminal Airspace to Enable Continuous Descent Operations in Trombone Sequencing and Merging Procedures: An Implementation Study for Frankfurt Airport. *Transportation Research Part C: Emerging Technologies*, **121**. 48

SAMÀ, M., D'ARIANO, A., D'ARIANO, P., & PACCIARELLI, D. 2014. Optimal aircraft scheduling and routing at a terminal control area during disturbances. *Transportation Research Part C: Emerging Technologies*, **47**(1), 61–85. 72

SAMÀ, M., D'ARIANO, A., PALAGACHEV, K., & GERDTS, M. 2019. Integration methods for aircraft scheduling and trajectory optimization at a busy terminal manoeuvring area. *OR Spectrum*, **41**, 641–681. 93

SCHARL, J., BERGE, M.E., COATS, M.L., HARALDSDOTTIR, A., & SCHOEMIG, E. G. 2007. Modeling and Analysis of the 3D Path Arrival Management Concept. *In: AIAA Modeling and Simulation Technologies Conference and Exhibit*. Hilton Head, SC, USA: AIAA. 7

SCHULTZ, M., FRICKE, H., KUNZE, T., MUND, J., LÓPEZ-LEONÉS, J., GRABOW, C., DE PRINS, J., WIMMER, M., & KAPPERTZ, P. 2012. Uncertainty Handling and Trajectory Synchronization for the Automated Arrival Management. *In: 2nd SESAR Innovation Days (SIDs)*. Braunschweig, Germany: SESAR Joint Undertaking. 67

SCHÄFER, M., STROHMEIER, M., LENDERS, V., MARTINOVIC, I., & WILHELM, M. 2014. Bringing Up OpenSky: A large-scale ADS-B sensor network for research. *In: 13th International Symposium on Information Processing in Sensor Networks (IPSN)*. Berlin, Germany: IEEE. 35

SCOKAERT, P.O.M., & RAWLINGS, J.B. 1999. Feasibility issues in linear model predictive control. *AIChE Journal*, **45**(8), 1649–1659. 31

SENZIG, D.A., & FLEMING, G.G. 2009. Fuel consumption modeling in support of ATM environmental decision-making. *In: 8th USA/Europe Air Traffic Management Research & Development Seminar*. Napa, CA, USA: FAA/EUROCONTROL. 21

SENZIG, D.A., FLEMING, G.G, & IOVINELLI, R.J. 2009. Modeling of Terminal-Area Airplane Fuel Consumption. *Journal of Aircraft*, **46**(4), 1089–1093. 21

SERGEEVA, M., DELAHAYE, D., MANCEL, C., & VIDOSAVLJEVIC, A. 2017. Dynamic airspace configuration by genetic algorithm. *Journal of Traffic and Transportation Engineering (English Edition)*, **4**(3), 300–314. 2

SESAR JU. 2019a. *SESAR Concept of Operations (CONOPS 2019)*. Tech. rept. Single European Sky ATM Research (SESAR) Joint Undertaking. 11, 12

SESAR JU. 2019b. *SESAR Solutions Catalogue 2019*. Tech. rept. Single European Sky ATM Research (SESAR) Joint Undertaking. Luxembourg. 10, 97

SESAR JU. 2020. *European ATM Master Plan*. Tech. rept. Single European Sky ATM Research (SESAR) Joint Undertaking, Luxembourg. Edition 2020. 1, 2

SESAR JU. 2021. *Integrated local DCB processes*. https://www.sesarju.eu/sesar-solutions/integrated-local-dcb-processes. Accessed: March 25, 2021. 14

SKYBRARY. 2020a. *ICAO Wake Turbulence Category*. https://www.skybrary.aero/index.php/ICAO_Wake_Turbulence_Category. Accessed: December 5, 2020. 55, 60, 78

SKYBRARY. 2020b. *Mitigation of Wake Turbulence Hazard*. https://www.skybrary.aero/index.php/Mitigation_of_Wake_Turbulence_Hazard. Accessed: September, 26, 2020. 103

SLATER, G.L. 2009. Study on Variations in Vertical Profile for CDA Descents. *In: 9th AIAA Aviation Technology, Integration, and Operations (ATIO) Conference*. Hilton Head, SC, USA: AIAA. 22

SLATTERY, R., & ZHAO, Y. 1997. Trajectory Synthesis for Air Traffic Automation. *Journal of Guidance, Control, and Dynamics*, **20**(2), 232–238. 19

SMETANOVÁ, LUCIE. 2020. *Evaluation of Arrival Sequencing at Arlanda Airport*. Master thesis, Linköping University and Czech Techical University. 110

SOLER, M., OLIVARES, A., STAFFETTI, E., & ZAPATA, D. 2012. Framework for Aircraft Trajectory Planning Toward an Efficient Air Traffic Management. *Journal of Aircraft*, **49**(1), 341–348. 2

SOLER, M., OLIVARES, A., & STAFFETTI, E. 2015. Multiphase Optimal Control Framework for Commercial Aircraft Four-Dimensional Flight-Planning Problems. *Journal of Aircraft*, **52**(1), 247–286. 24

SOPJES, R., DE JONG, P., BORST, C., VAN PAASSEN, R., & MULDER, M. 2011. Continuous Descent Approaches with Variable Flight-Path Angles under Time Constraints. *In: AIAA Guidance, Navigation, and Control Conference*. Portland, OR, USA: AIAA. 6

SPINIELLI, E., KOELLE, R., BARKER, K., & KORBEY, N. 2018. Open Flight Trajectories for Reproducible ANS Performance Review. *In: 8th SESAR Innovation Days (SIDs)*. Salzburg, Austria: SESAR Joint Undertaking. 34

SPRONG, K.S, HALTLI, B.M, DEARMON, J.S., & BRADLEY, S. 2005. Improving Flight Efficiency through Terminal Area RNAV. *In: 6th USA/Europe Air Traffic Managament Research & Development Seminar*. Baltimore, MD, USA: FAA/EUROCONTROL. 67

SUBRAMANIAN, R., SABATINI, R., G. GARDI, A., & YIFANG, L. 2013. Novel Flight Management System for Real-Time 4-Dimensional Trajectory Based Operations. *In: AIAA Guidance, Navigation, and Control (GNC) Conference*. Boston, MA, USA: AIAA. 11

TAKEICHI, N., & INAMI, D. 2010. Arrival-Time Controllability of Tailored Arrival Subjected to Flight-Path Constraints. *Journal of Aircraft*, **47**(6), 2021–2029. 69, 97

THE OPENSKY NETWORK. 2019. *OpenSky Network*. https://opensky-network.org. Accessed: December 2, 2018. x, 35, 66, 103

THOMPSON, T., MILLER, B., MURPHY, C., AUGUSTINE, S., WHITEE, T., & SOUIHI, S. 2013. Environmental Impacts of Continuous-descent Operations in Paris and New York Regions. *In: 10th USA/Europe Air Traffic Management Research & Development Seminar*. Chicago, IL, USA: FAA/EUROCONTROL. 3

TORATANI, D. 2019. Application of merging optimization to an arrival manager algorithm considering trajectory-based operations. *Transportation Research Part C: Emerging Technologies*, **109**, 40–59. 10, 97

TORATANI, D., WICKRAMASINGHE, K.N., & ITOH, E. 2018. Study on the Arrival Manager Maximizing the Benefit of Four-Dimensional Trajectory Based Operations. *In: 31st congress of the international council of the aeronautical sciences (icas)*. Belo Horizonte, Brazil: ICAS. 10, 97

UEBBING-RUMKE, M., & TEMME, M.-M. 2011. Controller AIDS for Integrating Negotiated Continuous Descent Approaches into Conventional Landing Traffic. *In: 9th USA/Europe Air Traffic Management Research & Development Seminar*. Berlin, Germany: FAA/EUROCONTROL. 9

VADA, J., SLUPPHAUG, O., JOHANSEN, T.A., & FOSS, B.A. 2001. Linear MPC with optimal prioritized infeasibility handling: application, computational issues and stability. *Automatica*, **37**(11), 1835–1843. 31

VADLAMANI, S., & SEYEDMOHSEN, H. 2014. A novel heuristic approach for solving aircraft landing problem with single runway. *Journal of Air Transport Management*, **40**, 144–148. 72

VILARDAGA, S., & PRATS, X. 2015. Operating cost sensitivity to required time of arrival commands to ensure separation in optimal aircraft 4D trajectories. *Transportation Research Part C: Emerging Technologies*, **61**, 75–86. 46, 89

VISSER, H.G., & WIJNEN, R.A.A. 2001. Optimization of Noise Abatement Departure Trajectories. *Journal of Aircraft*, **38**(4), 620–627. 92, 93

WÄCHTER, A., & BIEGLER, L.T. 2006. On the implementation of an interior-point filter line-search algorithm for large-scale nonlinear programming. *Mathematical Programming*, **106**, 25–57. 30

WARREN, A., & TONG, K.-O. 2002. Development of continuous descent approach concepts for noise abatement. *In: IEEE/AIAA 21st Digital Avionics Systems Conference (DASC)*. Irvine, CA, USA: IEEE. 2

WAT, J., FOLLET, J., MEAD, R., BROWN, J., KOK, R., DIJKSTRA, F., & VERMEIJ, J. 2006. In Service Demonstration of Advanced Arrival Techniques at Schiphol Airport. *In: 6th AIAA Aviation Technology, Integration and Operations (ATIO) Conference*. Wichita, KS, USA: AIAA. 3

WILSON, I., & HAFNER, F. 2005. Benefit assessment of using continuous descent approaches at Atlanta. *In: 24th IEEE/AIAA Digital Avionics Systems Conference (DASC)*. Washington, D.C., USA: IEEE. 6

WONG, R.T. 1984. A dual ascent approach for steiner tree problems on a directed graph. *Mathematical Programming*, **28**, 271–287. 124

WUBBEN, F.J.M, & BUSINK, J.J. 2000. *Environmental Benefits of continuous descent approaches at Schiphol airport compared with conventional approach procedures*. Tech. rept. National Aerospace Laboratory (NLR). Report NLR-TP-2000-275. 34

WÜRTH, L., HANNEMANN, R., & MARQUARDT, W. 2009. Neighboring-extremal updates for nonlinear model-predictive control and dynamic real-time optimization. *Journal of Process Control*, **19**(8), 1277–1288. 30

ZELINKSI, S.J., & JUNG, J. 2015. Arrival Scheduling with Shortcut Path Options and Mixed Aircraft Performance. *In: 11th USA/Europe Air Traffic Management Research & Development Seminar*. Lisbon, Portugal: FAA/EUROCONTROL. 67

ZHOU, J., CAFIERI, S., DELAHAYE, D., & SBIHI, M. 2014. Optimization of Arrival and Departure Routes in Terminal Maneuvering Area. *In: 6th International Conference for Research in Air Transportation (ICRAT)*. Istanbul, Turkey: FAA/EUROCONTROL. 92